Þeistareykir Geothermal Area, Northern Iceland

3D Inversion of MT and TEM Data

Ragna Karlsdóttir
Arnar Már Vilhjálmsson
Knútur Árnason
Andemariam Teklesenbet Beyene

Prepared for Þeistareykir ehf.

ÍSOR-2012/046

ICELAND GEOSURVEY
Reykjavík: Orkugardur, Grensásvegur 9, 108 Reykjavík, Iceland - Tel.: 528 1500 - Fax: 528 1699
Akureyri: Rangárvellir, P.O. Box 30, 602 Akureyri, Iceland - Tel.: 528 1500 - Fax: 528 1599
isor@isor.is - www.isor.is

Report
Project no.: 700012

Þeistareykir Geothermal Area, Northern Iceland

3D Inversion of MT and TEM Data

Ragna Karlsdóttir
Arnar Már Vilhjálmsson
Knútur Árnason
Andemariam Teklesenbet Beyene

Prepared for Þeistareykir ehf.

ÍSOR-2012/046 October 2012

ÍSOR
ICELAND GEOSURVEY

Key page

Report no.	Date	Distribution
ÍSOR-2012/046	October 2012	☒ Open ☐ Closed

Report name / Main and subheadings	Number of copies
Þeistareykir Geothermal Area, Northern Iceland 3D Inversion of MT and TEM Data	10
	Number of pages 173 + CD
Authors	**Project manager**
Ragna Karlsdóttir, Arnar Már Vilhjálmsson, Knútur Árnason and Andemariam Teklesenbet Beyene	Magnús Ólafsson
Classification of report	**Project no.**
	700012

Prepared for

Þeistareykir ehf.

Cooperators

Abstract

A 3D inversion of TEM/MT resistivity data from Þeistareykir shows a conventional resistivity structure for a high temperature system, a low resistivity cap underlain by a high resistivity core. The low resistivity cap reaches surface at Þeistareykir/Bóndhólsskarð, where also the highest elevation of the high resistivity core is seen. Deep seated low resistivity body indicating the heat source of the geothermal system is present under Ketilfjall, extending from there towards north and north east. This is the most prominent low resistivity body at depth and it domes up under the southern part of Ketilfjall up to 2 km b.s.l. depth. Other low resistivity bodies are present at greater depths, under Stórihversmór and the south eastern part of Bæjarfjall. Two distinctive low resistivity bodies extend from the low resistivity cap in the northern part of the survey area down to 10 km depth b.s.l. It is tempting to connect these phenomena to the Húsavík Fracture Zone where it infiltrates with the Þeistareykir fissure swarm and even to crustal deformation detected in the area in 2007–2008.

Key words	ISBN-number
TEM/MT resistivity survey, resistivity structure of a high temperature system, deep seated low resistivity body, heat source, Húsavík Fracture Zone	
	Project manager's signature Magnús Ólafsson
	Reviewed by BS

Table of contents

List of figures

1 Introduction

For the last few decades, electrical resistivity methods have intermittently been used in the exploration of the Þeistareykir geothermal field, and have improved as the measuring and processing methods have evolved. The first survey was performed in the nineteen seventies into early eighties with DC methods (Schlumberger) (Grönvold and Karlsdóttir, 1975; Gíslason et al., 1984) and in 2004–2006 transient electromagnetic (TEM) soundings were performed by ÍSOR in the Þeistareykir and Gjástykki area (Karlsdóttir et al., 2006). According to the results of the TEM resistivity measurements, the Þeistareykir geothermal system covers an area of 45 km^2 surrounded by a low-resistivity cap (Figure 1) at a depth of 800–1000 m, but that is near the depth limit for TEM measurement penetration. Moreover, the TEM measurements revealed that the high-temperature system extends closest to the surface near Þeistareykir proper at Bóndhólsskarð but there are also indications of a geothermal up-flow beneath Stórahversmór. In their report, Karlsdóttir et al. (2006) proposed a magnetotelluric (MT) survey in the Þeistareykir area to resolve the resistivity at a greater depth than possible with TEM measurements. In 2007, KMS Technologies in cooperation with VGK Hönnun, presently Mannvit, conducted an AMT/MT (Audio Magnetic Telluric) survey at Þeistareykir for the energy company Þeistareykir ehf. (KMS Technologies, 2008), but the results of this survey will not be discussed in this report. After this study, additional MT measurements were proposed, and ISOR performed an MT/TEM survey of the area in 2009. 62 MT and 30 TEM soundings were performed and a joint 1D interpretation of the MT data along with the TEM data was done (Karlsdóttir and Vilhjálmsson, 2011). Resistivity irregularities close to the surface can cause static shift in the MT data (Sternberg et al., 1988; Árnason et al., 2010) but TEM does not suffer this problem. Joint inversion of TEM and MT at the same sounding site can correct for the static shift of the MT.

1D inversion of the MT measurements revealed a deep-seated low-resistivity layer under the whole survey area. In the southern part of the area the center of this low-resistivity layer is at a depth of 15 km but beneath Þeistareykir and in the northern part, the center is considerably shallower or at about 8 km depth. The low-resistivity layer domes up beneath the southern part of Ketilfjall where the upper boundary reaches 4–5 km depth below the surface. Low resistivity is seen extending downward from the deep low-resistivity layer under Ketilfjall and to the northwest of Ketilfjall but this has to be taken with caution as the resolution is very poor at that depth. In 2011 and 2012, 39 MT and 8 TEM soundings were added to the survey and are included in the 3D modeling.

3D inversion of electromagnetic data can give much more reliable and detailed results than inversion in terms of layered earth (1D inversion). Great improvements in computer technology and software development have made 3D inversion of MT data practical. In this report a 3D interpretation of the static shift corrected MT data will be displayed. In order to study the robustness of the results, the 3D inversion was done using three different initial models and the results are compared to the results of the joint 1D inversion of the TEM and MT data.

Knútur Árnason is the supervisor of the application of 3D inversion of resistivity data at ÍSOR. He supervised the preparations of MT data for the 3D inversion at Þeistareykir and ran the 3D inversion program. Andemariam Teklesenbet Beyene did some of the preparation of data for the 3D inversion and ran the 3D inversion program. Arnar Már Vilhjálmsson did part of the initial processing of the first MT data and wrote the technical part of the report. Ragna Karlsdóttir did the processing of the MT data as well as the joint inversion of the 1D model, the preparations of the MT data for the 3D inversion and wrote the report other than the technical part.

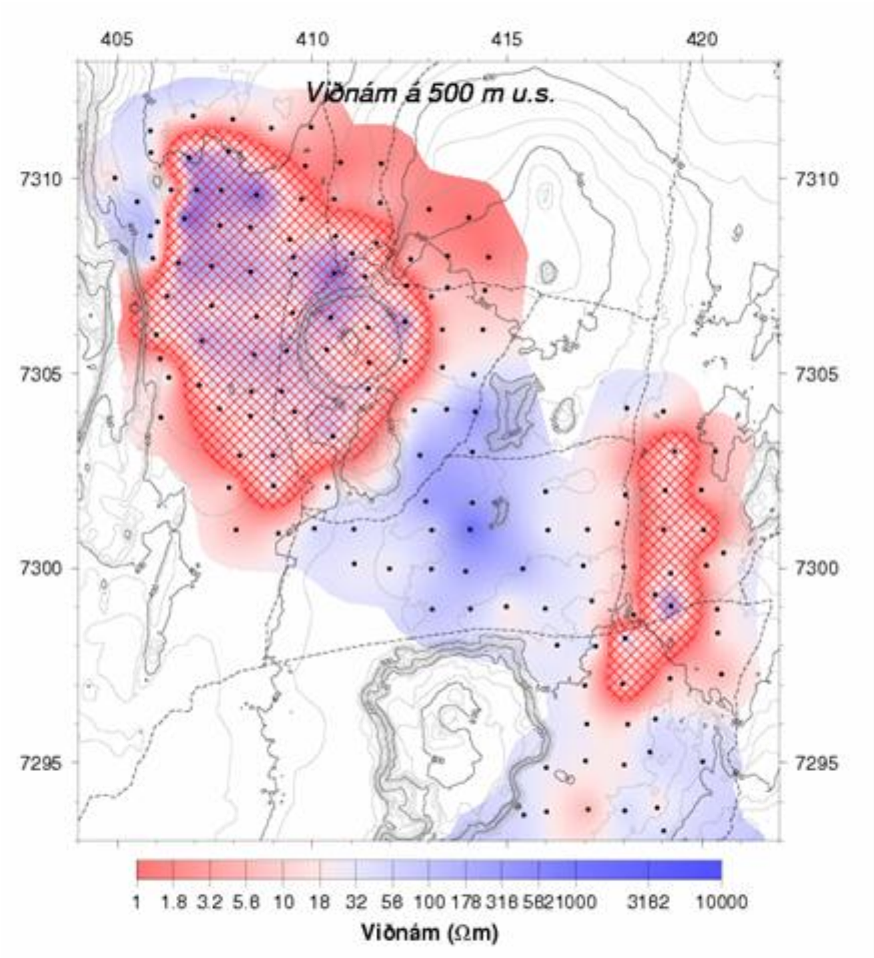

Figure 1. *Þeistareykir and Gjástykki geothermal fields. Resistivity at 500 m b.s.l.*

2 The resistivity survey

2.1 The role of resistivity surveying in geothermal exploration

The main factors influencing resistivity in rocks are water content, salinity and temperature of the fluid, and the type of alteration of the rocks due to geothermal activity. In essence, water-saturated rocks conduct electrical currents more readily than dry rocks and conductivity increases with increasing temperature up to about 300°C (Violay et al., 2010). Geothermal systems can be distinguished from the surroundings because the electrical conductivity (resistivity) of certain clay minerals (phyllosilicates, such as smectite) found in fractures in the rocks are strongly temperature dependent. The electrical resistivity of the rocks is only weakly influenced by the salinity of the fluid, unless the salinity is very high and approaches that of seawater (Flóvenz et al., 2005).

Surface resistivity surveys of high-temperature geothermal systems in the basaltic rocks of the volcanic zones of Iceland (and where the host rocks are volcanic) always seem to reveal basically the same resistivity structure which correlates to the distribution of alteration mineralogy. A low resistivity cap is observed on the outer and the upper margins of the reservoirs and is underlain by a more resistive core. Extensive comparison of this resistivity structure to well data has revealed a consistent correlation to the zones of dominant alteration minerals, where the low-resistivity cap coincides with the smectite-zeolite zone and the transition to the more resistive core occurs at the boundary, or within the mixed layer clay zone. Within the resistive core, chlorite and epidote are the dominant alteration minerals. The alteration mineralogy is, on the other hand, mostly predicted by temperature. This has the important consequence that, the resistivity structure can be interpreted directly in terms of temperature, if the alteration is in equilibrium with present formation temperature. The upper boundary of the low-resistivity cap is found where the temperature is in the range of 50–100°C and the transition to the resistive core occurs at temperatures in the range of 230–250°C (Árnason et al., 2000).

Figure 2. *Þeistareykir geothermal field.*

The resistivity reflects the alteration caused by the heating of the rocks and reflects the peak temperature experienced by the system, being it at the present or in the past. Thus, resistivity measurements reveal the alteration but do not indicate whether cooling has occurred after the alteration was formed because the resistivity profile only captures the alteration in the formation, irrespective of any later cooling of the system. The resistivity structure reflects the temperature, provided there is equilibrium between alteration and present temperature. In case of cooling the alteration may remain and the resistivity will reflect the temperature at which the alteration was formed. Whether the resistivity (and the alteration) indicates the present temperature of the system will only be confirmed by drilling.

Wherever MT measurements have been conducted in the volcanic zones in Iceland, a deep-seated low-resistivity layer is seen at a 10–15 km depth. The upper boundary (10 Ωm contact) of this low-resistivity layer arches up to a depth as shallow as 2–3 km beneath high-temperature geothermal systems, e.g., in the Krafla area. (Mortensen et al., 2009) As the low-resistivity layer is thought to reflect very high temperatures, it is interpreted as providing information about on upwelling of heat into geothermal systems. Plume-like low-resistivity anomalies in limited areas beneath the deep low-resistivity layer, as seen in TEM and MT measurements at Upptyppingar (Vilhjálmsson et al., 2008), also support the idea of active up-flow of hot material (magma?).

2.2 Data acquisition

The acquisition of the bulk of the TEM and MT data has been accounted for in a previous report on the joint 1D inversion (Karlsdóttir and Vilhjálmsson, 2011) and will only be briefly described here. ÍSOR performed an MT survey of the area in 2009–2011 followed by 1D interpretation of the MT data along with the existing TEM data. The survey was done in two periods, 62 MT soundings during summer 2009 and 25 MT soundings during summer 2011. Furthermore, 14 new MT soundings were performed in the summer of 2012 and two of the 2011 soundings were repeated. The total number of MT sites is therefore 101 and are shown in Figure 9 along with TEM sounding sites.

The MT instruments used in this campaign are from Phoenix Ltd. in Canada (MTU type) and can measure the MT signals in the range from 320 Hz up to DC. Four sets of MT equipment were used in the field work. One served as a base station for remote reference processing of the data and was located well away from the survey area. The other three MT units were operated in the investigation area, i.e. moved to a new location and installed every day for recording till the next day. Three of the MT units measure five components (E_x, E_y, H_x, H_y and H_z); the base station and two of the others. The forth station measures only the electric field, i.e. E_x, E_y. The two component unit is always set up close to a five component site (usually around 1 km away), and the magnetic field at that site used for the data processing. This approach is chosen if the magnetic field is almost identical at the two stations, valid for short distances. At each station, data were recorded for 16–22 hours.

In 2009 the reference station was set up at Hólasandur, approximately 20 km from Þeistareykir and in 2012 it was set up in Þrengsli in Hellisheiði, south Iceland, some 300 km away. In 2011, one of the 5 component MT instruments was out of order and no fixed base station was set up. Instead, an MT survey was conducted simultaneously in Þeistareykir and Námafjall and a 5 component station in one survey area was used as a reference for the other 5 component unit in the other survey area.

The MT method

The magnetotelluric method uses time variations of the Earth's magnetic field to investigate the resistivity structure of the earth. The time varying magnetic field represents electromagnetic waves that penetrate the earth. By measuring simultaneously the magnetic and electric field variations in the surface, which are coupled through Maxwell's equations, inference can be made about the subsurface resistivity.

The horizontal components of the electric and magnetic fields are determined by measuring voltage in short (~50 m) orthogonal grounded dipoles and induction in orthogonal induction coils, respectively (Figure 3). The field layout defines a co-ordinate system with one of the dipoles and one of the coils parallel to the x-axis, normally taken to be in magnetic N-S, and the other dipole and coil along the y-axis in magnetic E-W. The magnetic declination is 13 degrees west of north and hence the x-axis is oriented N13°W in the present survey.

The electrical dipoles consist of two non-polarizing electrodes (lead/lead-chloride in this case) connected to the data-logger by cables. The induction coils are normally buried to avoid them from shaking (in the wind) and picking up noise from the magnetic field. The vertical component of the magnetic field is usually also measured by a buried vertical induction coil.

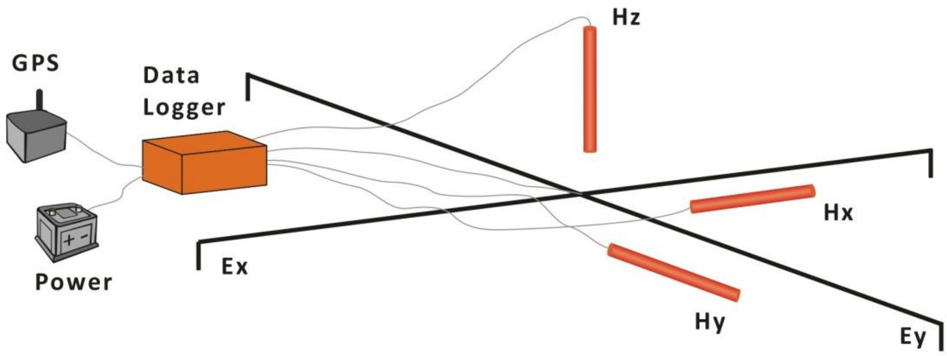

Figure 3. *A schematic picture of an MT equipment installation in the field.*

The electric and magnetic field variations are measured as a function of time or as time series. The time series are composed (a sum) of harmonic (sinusoidal) components of different periods (frequencies). Short period (high frequency) waves are attenuated at shallow depth and hence do not penetrate deep but the longer the period (lower the frequency) the deeper the waves probe into the earth. In the processing of the MT data the time series are sorted into different frequencies (by Fourier transformation) and the relation between the electric and magnetic fields give information about the resistivity at different depths. MT can therefore penetrate from shallow depths to the depth of several tens of kilometers.

2.3 Data processing

The measured MT time series are Fourier transformed into the frequency domain and the “best” solution that describes the relation between the electrical and magnetic field is found through the following equation:

$$\begin{bmatrix} E_x \\ E_y \end{bmatrix} = \begin{bmatrix} Z_{xx} & Z_{xy} \\ Z_{yx} & Z_{yy} \end{bmatrix} \begin{bmatrix} H_x \\ H_y \end{bmatrix}$$

or in matrix notation:

$$\vec{\boldsymbol{E}} = \boldsymbol{Z}\vec{\boldsymbol{H}}$$

where, $\vec{\boldsymbol{E}}$ and $\vec{\boldsymbol{H}}$ are the electrical and magnetic field vectors (in the frequency domain) and $\boldsymbol{Z}$ is a complex impedance tensor which contains information on the subsurface resistivity structure. Programs from Phoenix Geophysics (2005) were used to process the time series using a robust processing method technique (see e.g. Egbert and Booker, 1986) and for editing the results. The output was run through a program developed at ÍSOR, which calculates various MT parameters and produces the results in standard EDI file format (see SEG, 1991). The values of the impedance tensor elements depend on the resistivity structures below and around the site. For a homogeneous and 1D earth $Z_{xy} = -Z_{yx}$ and $Z_{xx} = Z_{yy} = 0$. For a 2D earth, i.e. resistivity varies with depth and in one horizontal direction, it is possible to rotate the coordinate system by mathematical means, such that $Z_{xx} = Z_{yy} = 0$, but $Z_{xy} \neq -Z_{yx}$. For a 3D earth all the impedance tensor elements are different.

From the impedances the apparent resistivity (ρ) and phases (θ) for each frequency are calculated according to

$$\rho_{xy} = 0.2T\left|Z_{xy}\right|^2;\ \theta_{xy} = \arg(Z_{xy})$$
$$\rho_{yx} = 0.2T\left|Z_{yx}\right|^2;\ \theta_{yx} = \arg(Z_{yx})$$

3 3D inversion

The 3D inversion was performed using the inversion program WSINV3DMT written by Prof. Weerachai Siripunvaraporn (Siripunvaraporn et al., 2005; Siripunvaraporn and Egbert, 2009). WSINV3DMT uses finite difference forward algorithm and utilizes a formulation of the inverse problem in the data-space rather than in the model-space. This reduces the dimensionality of the problem dramatically and makes 3D inversion of MT data attainable.

3D inversion of MT data is a highly underdetermined problem, i.e. the number of unknown resistivity values is much higher than the number of data values. In the present case the number of data points is 10504 (101 soundings x 26 periods x 4 real and imaginary off-diagonal tensor elements, see below) but the model has 151536 unknown resistivity values (in the 82 x 66 x 28 blocks, see below) or almost 14–15 times the number of data points. The inversion therefore needs to be regularized by imposing constraints on the model (mathematically this means to make the model parameters interdependent in such a way that the number of the actually free parameters is similar to the number of data values). This can be done by constraining the model parameters to vary smoothly. This is sometimes called minimum structure or Occam inversion (Constable et al., 1987). Another way of regularizing is to use so-called reference or "prior" models and constrain the model not to deviate too much from the prior model. Using a prior model also offers the possibility of fixing some of the model parameters to a priory known values. This option is used in the inversion here to take into account the very conductive Atlantic Ocean, approximately 25 km to the north of Þeistareykir. The inversion code used here uses a combination of these regularization methods and minimizes a weighted sum of the difference between measured data and calculated response, the roughness of the model and the deviation from the prior model. The user can adjust the smoothing criteria, but not the weight of the deviation from the prior model. This can prohibit the iteration process to fit of the measured data properly if that needs a model that deviates very much from the prior model. The data fit can, however, be further improved by restarting the iteration using the model that gave the best fit so far as both initial and prior model. This allows the inversion to deviate from the new prior model and towards a model that gives better data fit. In practice, the inversion is therefore run in steps, gradually relaxing the limitation of the prior model, until the data fit can no longer be improved.

WSINV3DMT assumes flat surface. This seems to be a limitation, but prior to the inversion, the MT data are corrected for static shift and this correction removes topographic effects in the data to a large extent. The inversion is performed for the complex off-diagonal elements of the MT impedance tensor, i.e. 4 numbers (2 real and 2 imaginary parts) for each period of each sounding. The misfit measure is the RMS misfit of the observed and calculated tensor elements, weighted by the variance of the measured values.

3.1 Data preparation

The processed MT data has the x-axis in true north. In the inversion program the measured data and the model are defined in an internal (local) coordinate system or grid. It is preferable to have one of the grid axis parallel to the dominant electric (resistivity) strike. According to strike analysis of the MT data (not shown in this report) the dominant electric strike is close to the geological strike of N15°E. The internal coordinate system of the model is therefore taken to have x-axis in N15°E and the y-axis in N105°E. The MT impedance tensors were therefore rotated by 28° to the internal system (i.e. 13° to correct for the magnetic declination and then 15° to match the geological strike).

The 3D inversion is performed for the MT tensor elements that may contain static shift. By assuming that the static shift is dominantly due to distortion of the electric field, the tensor can be static shift corrected by the equation:

$$\begin{bmatrix} Z^c{}_{xx} & Z^c{}_{xy} \\ Z^c{}_{yx} & Z^c{}_{yy} \end{bmatrix} = \begin{bmatrix} C_x & 0 \\ 0 & C_y \end{bmatrix} \begin{bmatrix} Z_{xx} & Z_{xy} \\ Z_{yx} & Z_{yy} \end{bmatrix} \quad ; \quad C_x = \sqrt{1/S_{xy}} \quad ; \quad C_y = \sqrt{1/S_{yx}}$$

where $\mathbf{Z}^c$ is the corrected and $\mathbf{Z}$ the uncorrected tensor. S_{xy} and S_{yx} are the shift multipliers for apparent resistivity of, respectively, xy and yx polarizations (Árnason et al., 2010). After the rotation of the soundings to the internal coordinate system, a joint 1D inversion was performed of the apparent resistivity and phase for both xy and yx polarizations and the nearby TEM sounding in order to determine the static shift multipliers.

The computational intensity in the inversion is directly proportional to the number of periods to be inverted for. The raw data generally contain 78 different periods ranging from about 0.003 s to 2940 s (0.0044 to 1449 s), with 13 periods per decade. To reduce the computation cost, the static shift corrected tensor was re-sampled at 26 periods equally spaced on log scale (five values per decade), from 0.0063 s to 631 s. This choice of periods is a "tradeoff" between computational cost on the one hand and resolution and depth of investigation on the other. For physical consistency, the MT tensor must be a smooth function of the logarithm of the period (Weidelt, 1972). Inverting for five periods per decade is generally considered to give enough resolution. The period range and the resistivity determine the depth range of exploration (the shorter the period and lower the resistivity, the shallower resistivity structures can be resolved and the longer the period and the higher the resistivity, the deeper structures can be resolved).

3.2 The model grid

The model grid is set out so that the dense part of the grid covers the main area of data coverage. The area of data coverage has gaps, with subareas with no MT soundings, even at critical areas. This has an explanation. MT surveys have been performed in a few batches by two different companies. It turned out that the whole Þeistareykir survey area had to be surveyed by the method used by ÍSOR to be used for the 3D inversion. This meant that ÍSOR recommended repeating of some of the MT soundings done by others. These recommendations have not fully been met by Þeistareykir ehf. and therefore there are still a few minor gaps in the survey area.

Before running the inversion with the 250 m grid in the inner part of the model, another mesh with 500 m grid pane spacing in the central area of the data coverage was also tested. Results showed that finer grid was preferable as well as a few extra soundings for better constraints of the model. A total of 23 MT and 11 TEM were recommended by ÍSOR but Þeistareykir ehf. accepted a total of 14 MT and 5 TEM, thereof two MT soundings were repeated from 2011. In addition, ÍSOR recorded two MT sounding at own expense in sites were TEM soundings were available.

The 3D model consists of resistivity cubes in a 3D grid mesh defining the internal coordinate system. The origin (centre) of the internal coordinate system is at the UTM (zone 28) coordinates (in km) 410.75E and 7308.00N (approximately at the centre of the area of interest and data coverage), and with x-axis positive towards N15°E and y-axis positive towards N105°E. The mesh has 83 vertical grid planes (two edges and 81 internal planes) in the x-direction (perpendicular to the x-axis) and 67 vertical (two edges and 65 internal planes) in the y-direction and 29 horizontal grid planes (surface, bottom and 27 horizontal internal planes). The grid is dense in the area of interest with grid plane spacing of 250 m in the area of the data coverage, that is in the range of

+/-7 km in the x-direction (SW-NE) and +/-5 km in the y-direction (NW-SE). Outside the dense area the grid spacing increases exponentially to the edges at +/-138,268 km and +/-136,268 km in the x- and y-directions, respectively. Figure 4 shows a horizontal slice of the central part of the model grid mesh and the location of the MT soundings in the grid. Red star shows the origin (middle point) of the grid. All resistivity cross sections are named with reference to their position in the grid and are named by distance from origin. A cross section, EW_N2000, refers to the EW cross section that is 2000 m to the north of origin point. Figure 5 shows a larger part of the model grid and the coastal line to the north.

The horizontal grid planes are likewise dense at shallow depth but eventually with exponentially increasing spacing to the bottom at the depth of 160,684 km. The shallowest layer thicknesses are 16, 26, 36, 50, 76, 100, 158, 200 m etc.

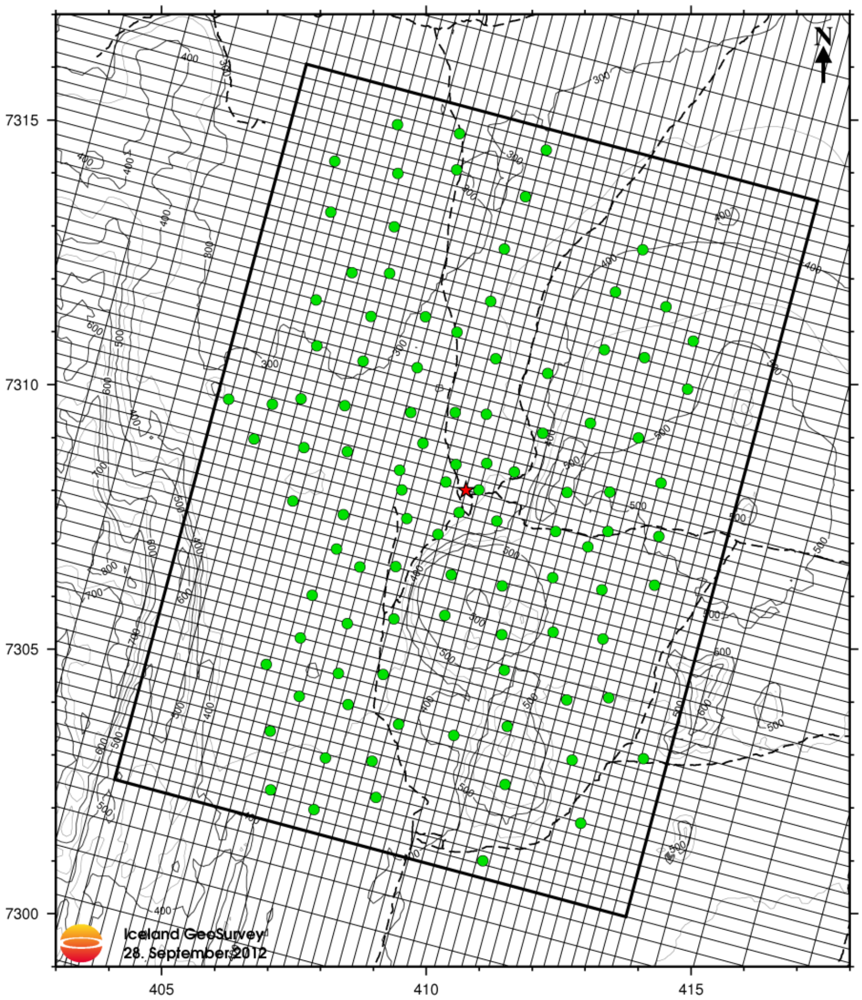

Figure 4. *The model grid with 250 m between the vertical planes. The heavy black line marks the area of interest (10 x 14 km). Red star shows the origin.*

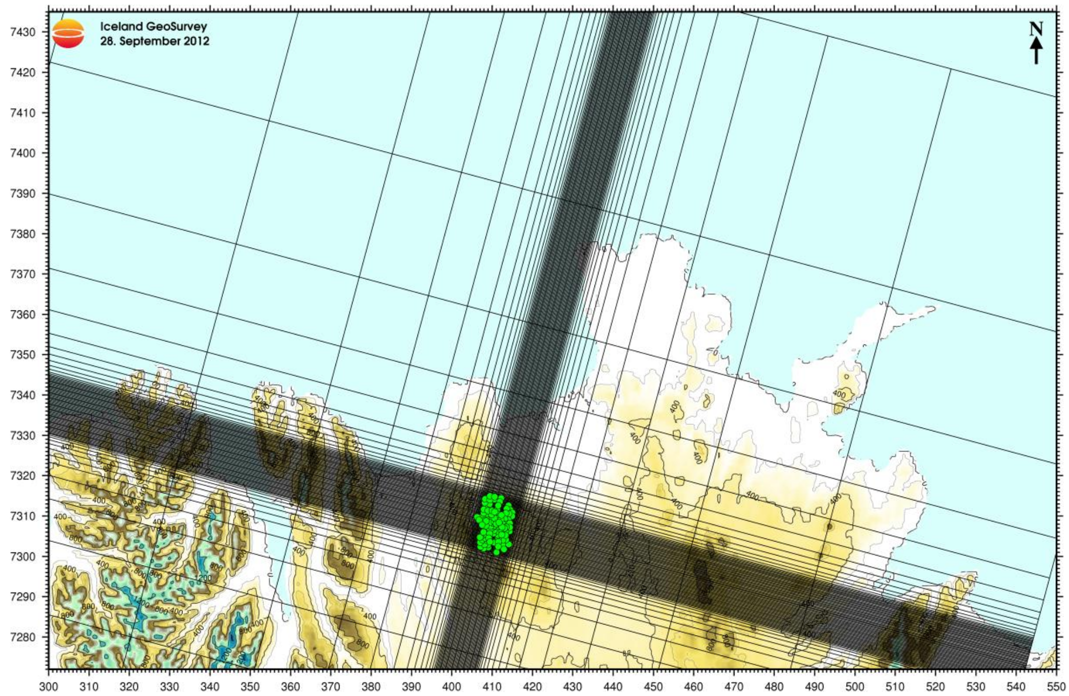

Figure 5. *The model grid. The dense grid, shown as grey shade, covers the survey area. MT soundings are marked as green dots*

3.3 Initial and prior models

As discussed earlier, 3D inversion of MT data is, in practical sense, a highly underdetermined problem. It was also mentioned that one of the ways to regularize the inversion is to use prior models and constrain the deviation of the actual model from the prior model. As a consequence of this the results depend on the prior model(s). The choice of prior models is therefore of great importance.

The optimal prior model is of course not known beforehand. Actually it should be the "best" model being looked for by the inversion. However, some important components of the model can, in some cases be assumed to be known a priory and even fixed in the inversion (see discussion above). In the case of the Þeistareykir area, the proximity of the sea (25 km) will probably not have a great influence but will be taken into account as it may have some impact in the MT data, at long periods. The sea has therefore to be taken into account in the inversion and the resistivity of the model cells in the sea were assigned the average resistivity of seawater (0.3 Ωm) and by a control file, the inversion was forced to keep it fixed.

In the inversion a "penalty function", which is a weighted sum of the data misfit, the roughness of the model and the deviation from the prior model, is minimized. This means that initially, the inversion process quickly adjusts the model to reduce severe misfit of the data. Later on, changes that would reduce the misfit are rejected because they make the model deviate too much from the prior model.

To investigate the influence of the initial model on the results, different results were investigated using three distinct initial models: (1) a model compiled from joint 1D inversion of individual TEM/MT sounding pairs (Karlsdóttir and Vilhjálmsson, 2011), (2) a homogeneous half-space with resistivity 100 Ωm and (3) a homogeneous half-space with resistivity 20 Ωm. Initially, the plan was to use only models (1) and (2), both with spacing of 250 m in the inner part of grid. However, as it turned out to be difficult to resolve the deeper structures in model (2) without deviating too much from the priory (initial) model, inversion with initial model (3) was launched. Grid spacing of 500 m in the central part was used for model (3) to save time. In all cases the sea is included in the model and kept fixed throughout the inversion

As for the prior models, they were in all cases initially taken to be identical to the initial model. When the iterations had adjusted the model somewhat to reduce the data misfit it was eventually prohibited to adjust the model further to reduce the misfit because it was starting to deviate considerably from the prior model. The iteration was then stopped (typically after 5 iterations steps) and restarted with the best model (in terms of the data fit) from the previous iteration as both initial and prior model. Then the iteration could improve the data fit by varying the model around the new prior model. This stepwise inversion (and relaxation of the prior model) was continued until the data fit could not be improved any more (2–6 times).

3.4 The inversion

The inversion program was executed using a parallel processing version of the WSINV3DMT code using the Message Passing Interface (MPI) parallel computing environment. It was executed on a 32 core computer with 132 GB memory. As stated above, the inversion was done using three different initial models (homogeneous 100 Ωm half-space in 250 m grid, homogeneous 20 Ωm half-space in 500 m grid and an initial model compiled from 1D inversion in 250 m grid). The limits of the prior model were stepwise relaxed (after 4–5 iterations in each step) as described above. Three steps were run for each initial model. The inversion is a very heavy computational task and each iteration with the 250 m grid spacing, took about 18 hours and the total computing time was more than 1000 hours.

The data misfit is defined as the RMS (Root-Mean-Square) of the difference between the measured and calculated values of the off diagonal tensor elements (real and imaginary parts), weighted by the variance of the measured values.

For the 100 Ωm (250 m grid) homogeneous half-space initial model, the initial RMS misfit was 30.8 and the final misfit was 2.20. For the 20 Ωm (500 m grid) homogeneous half-space initial model, the initial RMS misfit was 11.50 and the final misfit was 1.73. For the initial model compiled from the 1D in 250 m grid inversion the initial misfit was 4.96 and the lowest obtained misfit was 1.45. In all cases the measured data were fitted quite well.

A comparison of the (re-sampled) measured data for all the inverted soundings (presented as apparent resistivity and phase) and the calculated response of the final model from the 1D initial model is shown in Appendix 4

4 The 1D resistivity model

The 1D model derived from the MT survey only includes the MT soundings made by ÍSOR in 2009 as displayed in the 1D report (Karlsdóttir and Vilhjálmsson, 2011).

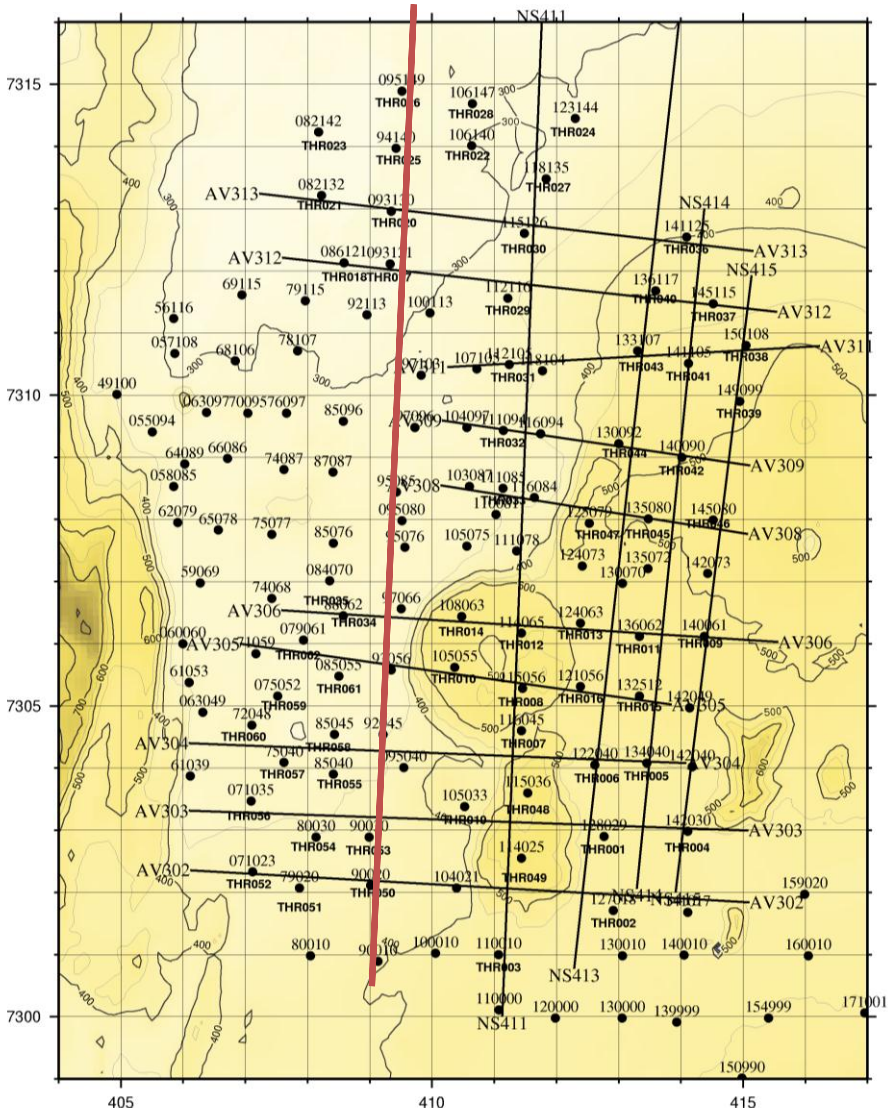

Figure 6. *MT soundings at Þeistareykir geothermal field and location of resistivity cross sections through the field from the 1D inversion report. Red line shows resistivity cross section (NS411) displayed on figure 7.*

The main conclusions from the 1D interpretation of the MT data are as follows:

- The TEM measurements of ÍSOR reveal a conventional resistivity configuration with a low-resistivity cap underlain by a high-resistivity core. In the north part of the survey area, the low-resistivity cap is reached at 800 m depth dipping northwards. This adds to the information from the 2004–2006 TEM survey (Karlsdóttir et al., 2006).

- The MT measurements by ÍSOR (see location on figure 6) show a deep-seated low-resistivity layer beneath the entire survey area with a centre near 15 km depth below the surface in the south part of the area see figure 7, a north south bound resistivity cross section through the geothermal system. Below Þeistareykir and in the north part of the survey area, the centre is considerably shallower or 8 km beneath the surface. It should be noted that the measurements by ÍSOR did not cover at that time the area with most geothermal activity at the surface or the borehole area. More soundings were added in this critical area in 2011 and 2012 by ÍSOR and they are included in the 3D inversions described in this report.
- The low-resistivity layer domes up below the southern part of Ketilfjall where the upper boundary of the layer is at 4 km depth. In the area northwest of Ketilfjall, the layer reaches 4–5 km depth below the surface. This is most evident in a resistivity map from 3000 m b.s.l. in Figure 8.

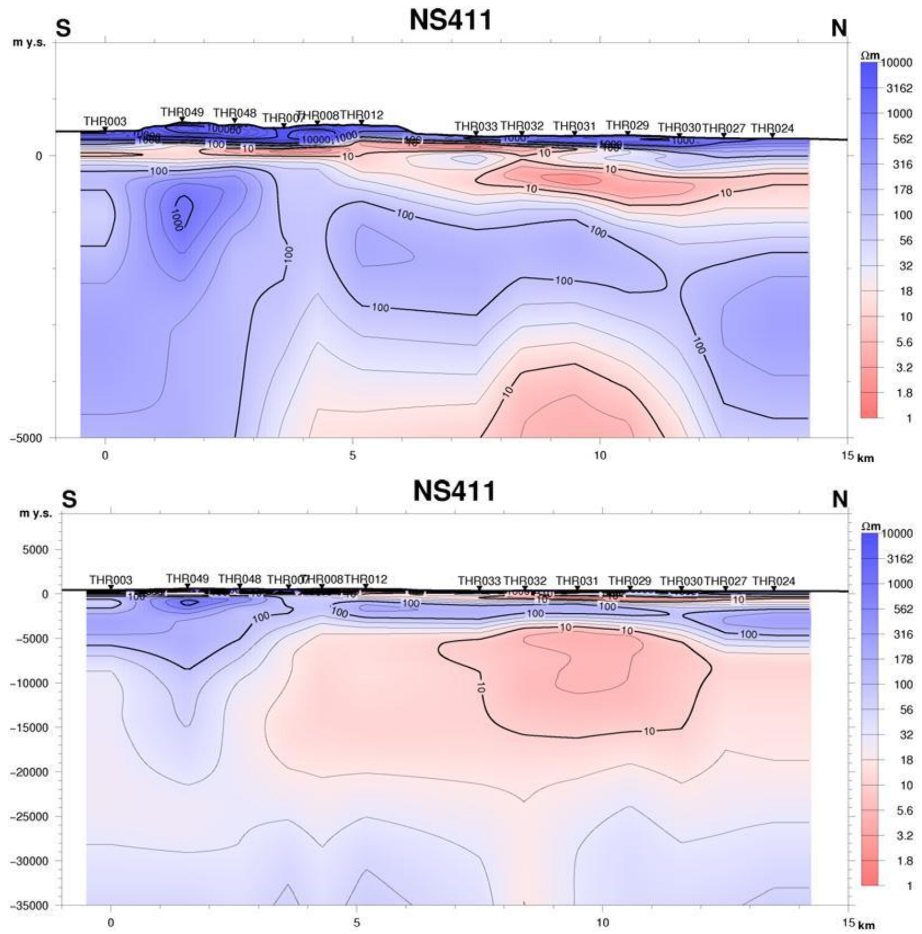

Figure 7. *Cross section 411 north-south. Resistivity down to 5 km b.s.l. (upper panel) and 35 km b.s.l. (lower panel) based on 1D interpretation of the MT/TEM data.*

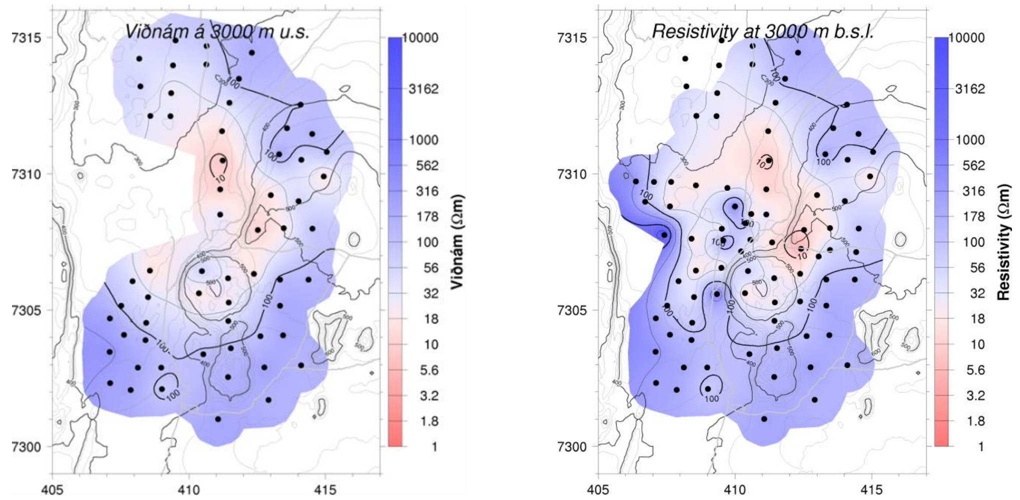

Figure 8. *Left: Resistivity at 3000 m b.s.l. according to the 1D report 2009. More MT soundings have been added to the survey since this map was drawn and the map to the right shows resistivity at 3000 m b.s.l. with all soundings included, except those from 2012.*

5 Presentation of the 3D model

Visual presentation of 3D resistivity models is not straightforward. The final models are presented here in two different ways, i.e., as a resistivity map (contour plot) for different elevations (depths) and as resistivity cross sections. Figure 9 shows the TEM/MT survey area and soundings used in the 3D inversion.

As mentioned earlier the 3D inversion is run with different input models. A model based on the 1D inversion results is considered as the most reliable input model. Then homogeneous half-space initial models with different initial resistivity values are run to put constraints on the model, especially artefacts that may be created by the 3D inversion in areas outside the area of data coverage.

As discussed above the 3D program assumes flat surface. The MT data were corrected for static shift prior to the inversion and this correction removes topographic effects in the data to a large extent. The resistivity models resulting from the inversion were elevation corrected, i.e. the depths below each model cell were converted to meters above sea level.

The outcome of the inversion for the initial model compiled from 1D inversion will be considered as the final results of the 3D inversion.

Smoothed resistivity maps from the elevation corrected models, showing the outcome of the inversion for the 1D initial model are presented at 24 different elevations in Appendix 1. Smoothed elevation corrected N-S (SW-NE parallel to the x-axis) and E-W (NW-SE oriented parallel to the y-axis) cross-sections, through the dense part of the model grid, from the 1D initial model are presented in:

- Appendix 2 (N-S cross sections)
- Appendix 3 (E-W cross sections)

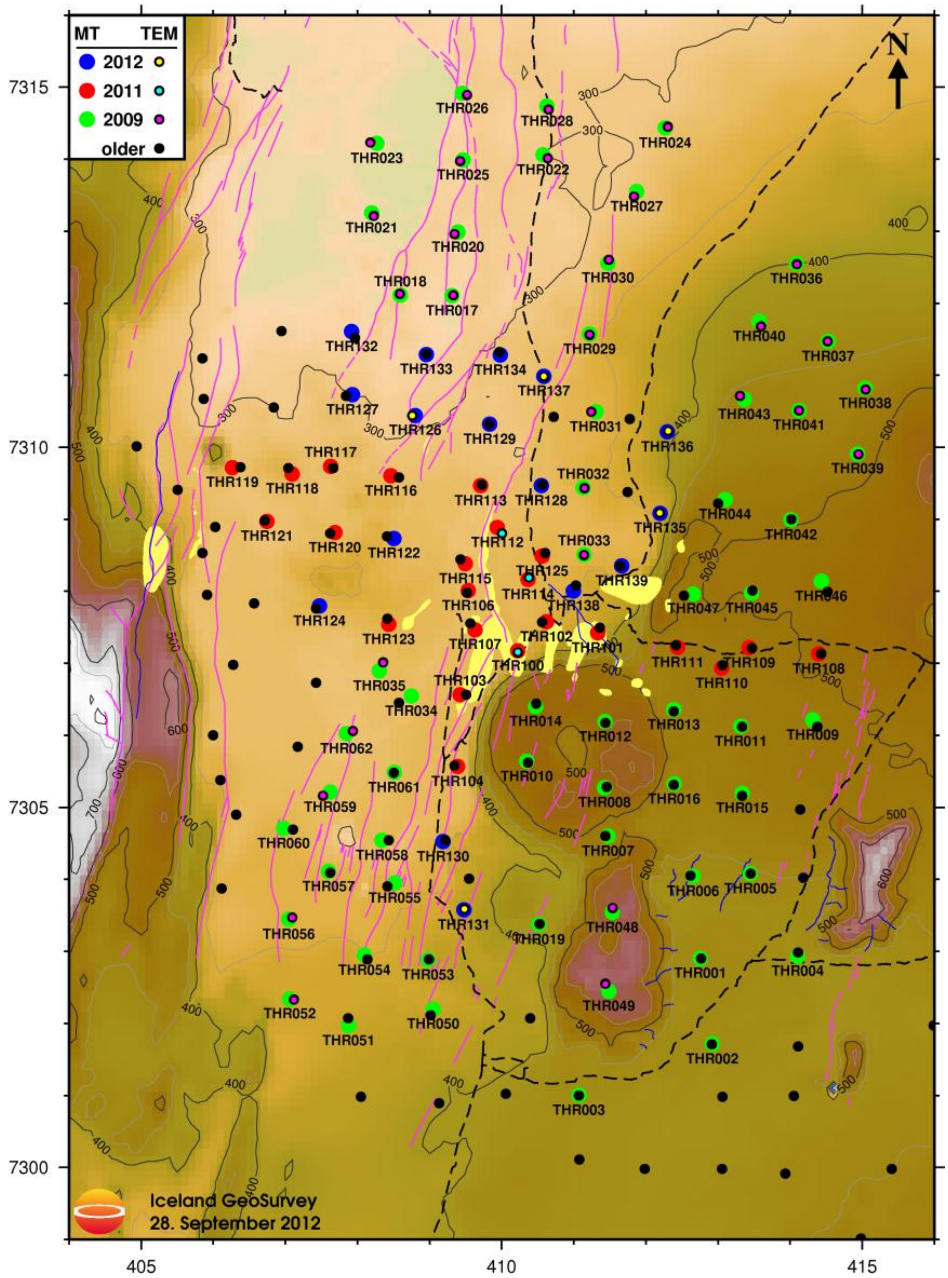

Figure 9. *MT and TEM soundings at Þeistareykir area. Colours of the dots indicate when the soundings were performed (see legend). Geothermal alteration at surface is marked with yellow and faults and fissures with magenta lines.*

6 Discussion of the 3D model

The main features of the 3D inversion based on the 1D input model, are as follows: A low resistivity cap; an underlying high resistivity core; low resistivity bodies at depth in the northern part and a deep seated low resistivity. This will be discussed in more details. Resistivity maps are displayed in Appendix 1 and resistivity cross sections are displayed in Appendices 2 and 3.

Names referred to in the discussion are displayed on the map on figure 10.

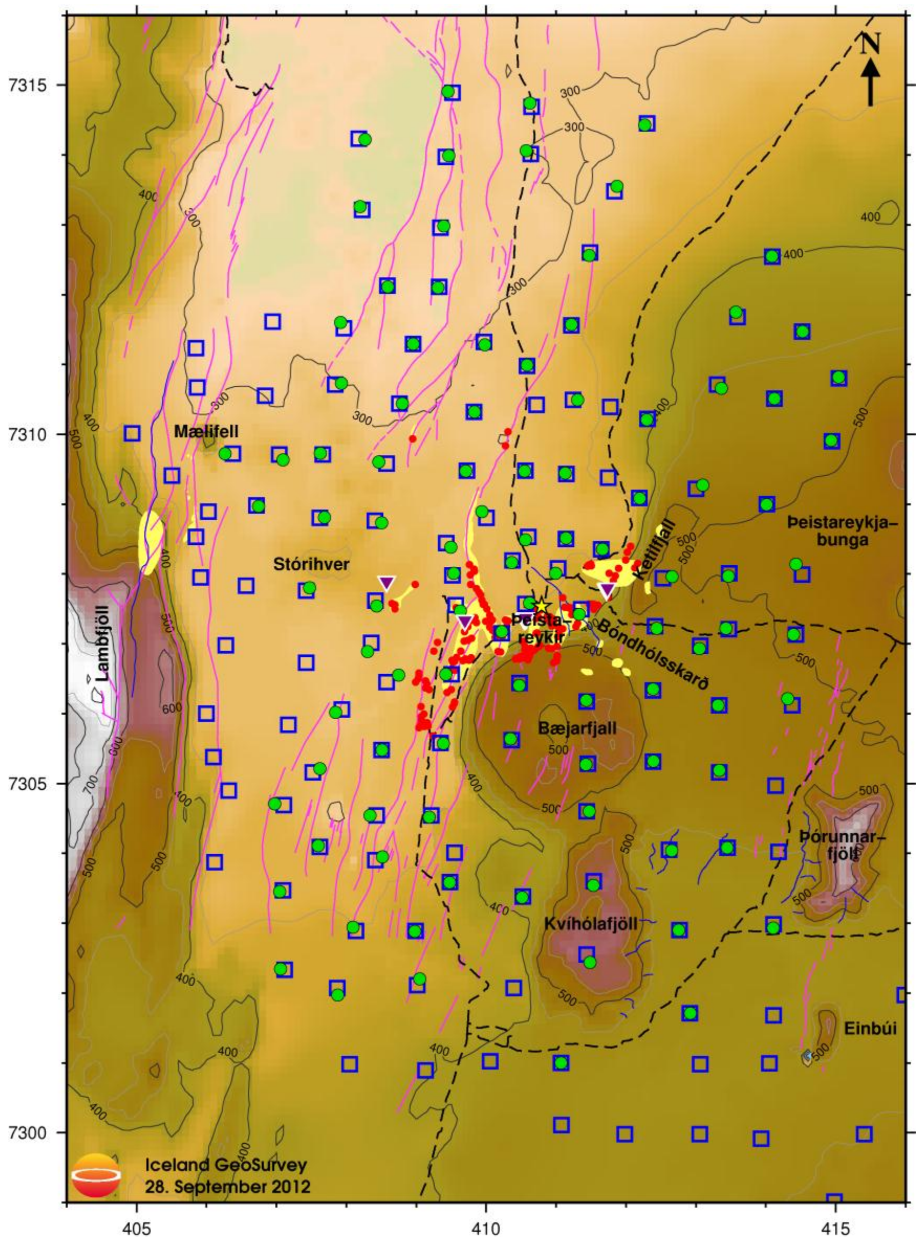

Figure 10. *An overview map of Þeistareykir area with names referred to in the text. Surface alteration zones are in yellow, faults and fissures as magenta lines and surface geothermal manifestations in red.*

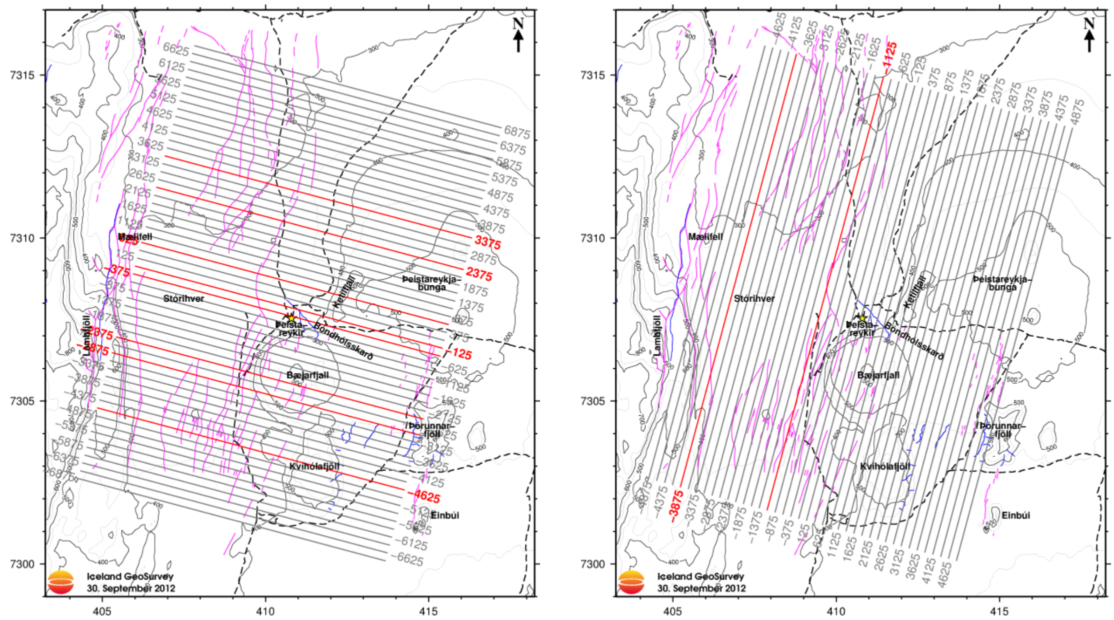

Figure 11. *The figure on the left shows EW bound resistivity cross sections and the one on right shows NS bound resistivity cross sections through the inner part of the 3D model. Cross sections discussed in the text are marked with red.*

6.1 The low resistivity cap and the underlying high resistivity core

Resistivity at 250 m a.s.l. (figure 12 and Appendix 1) reveals the top of the low resistivity cap at Þeistareykir and Bóndhólsskarð and how it extends from Ketilfjall to the south under the eastern flank of Bæjarfjall. The low resistivity at Þórunnarfjöll, to the southeast is to be disregarded due to lack of data coverage. In early TEM survey (Karlsdóttir et al., 2006), there is an indication of low resistivity at depth in the near vicinity of Þórunnarfjöll and Einbúi. Even though the 3D inversion may detect that low resistivity we will leave that out of our discussion as it is outside the area of good data coverage and the reliable model grid and hence out of the scope of this survey. The low resistivity in the south western part of the map is completely outside the area of data coverage and is therefore regarded as an artefact in the inversion. An east west cross section (EW_N-375) on figure 13 shows the low resistivity cap as it reaches surface at Þeistareykir farm.

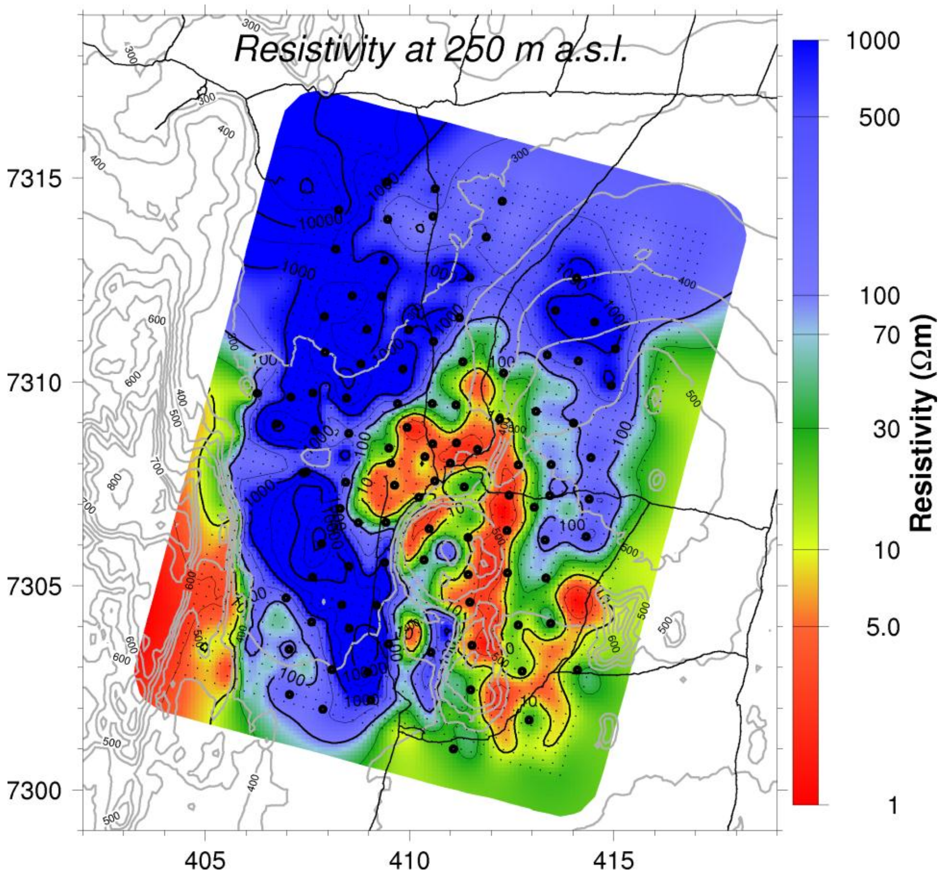

Figure 12. *Resistivity at 250 m a.s.l.*

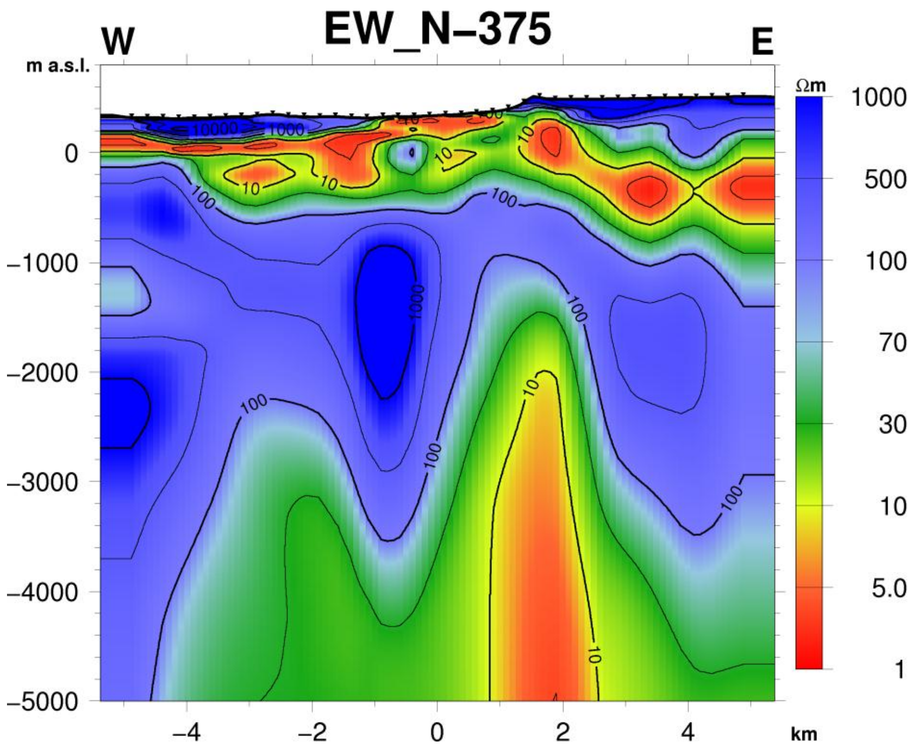

Figure 13. *A resistivity cross section through Þeistareykir and Bóndhólsskarð. Location of the cross section is shown on figure 11.*

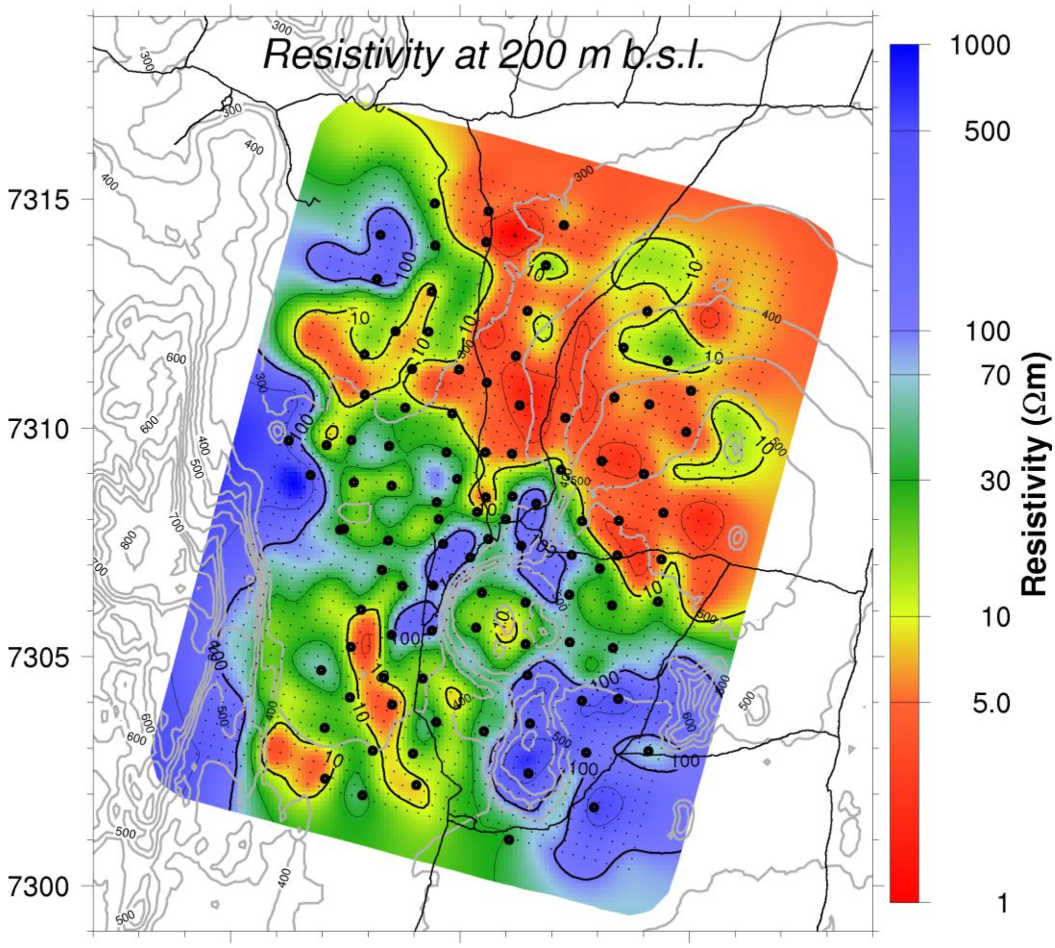

Figure 14. *Resistivity at 200 m b.s.l.*

Resistivity at 200 m b.s.l. (figure 14) reveals the high resistivity core at Þeistareykir, as it extends to the north-west and to the south-east. The low resistivity cap tilts towards north and towards south. Towards the north the low resistivity cap seems thicker and more prominent and at that depth the margin between the high resistivity core and the low resistivity cap forms a distinctive NW – SE lineament. For better clarification figures 15 to 18 show four NW-SE cross sections from surface down to 1,5 km depth. The northernmost cross section **(EW_N2375**, figure 15) shows the 400–600 m thick low resistivity cap as it tilts towards north. Cross section **EW_N625 (**figure 16) cuts through the NW – SE lineament mentioned above showing the low resistivity cap close to surface and tilting towards east. A cross section through Bæjarfjall **(EW_N-2375,** figure 17) reveals the low resistivity cap at approximately 200 m depth through the area, except under the Bæjarfjall mountain where it dips to a depth of 500 m. The southern-most cross section (**EW_N-4625**, figure 18) reveals the low resistivity cap as it tilts towards south.

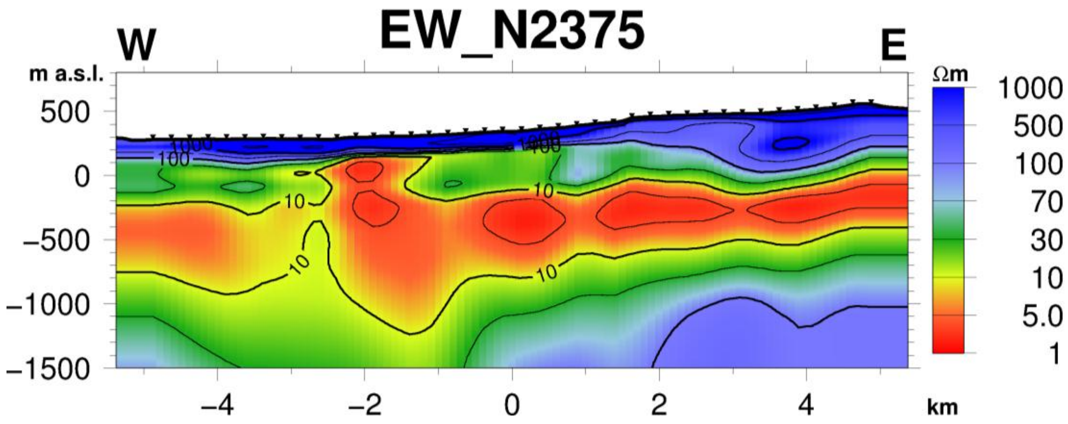

Figure 15. *A resistivity cross section through the low resistivity cap north of Ketilfjall and under Stórahversmór. Location of the cross section is shown on figure 11.*

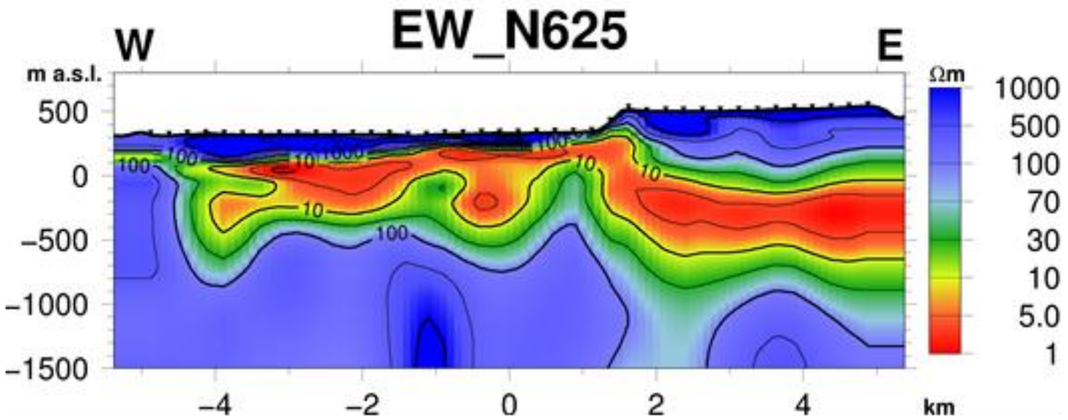

Figure 16. *A resistivity cross section through the low resistivity cap north of the Þeistareykir farm and Ketilfjall. Location of the cross section is shown on figure 11.*

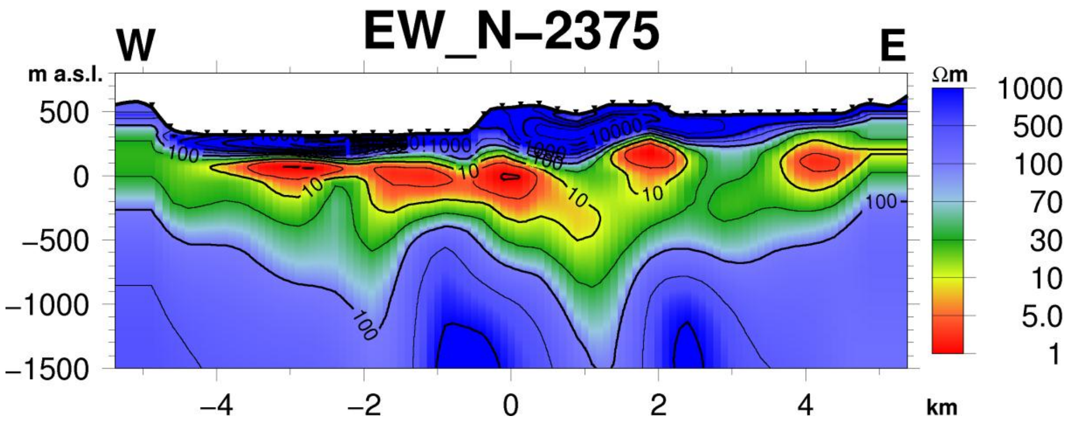

Figure 17. *A resistivity cross section through the low resistivity cap under Bæjarfjall. Location of the cross section is shown on figure 11.*

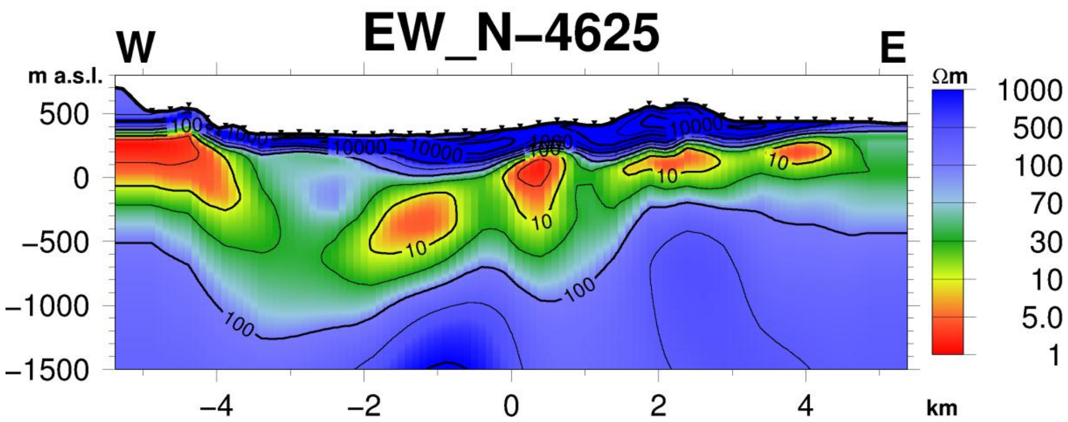

Figure 18. *A resistivity cross section through the low resistivity under Kvíhólafjöll. Location of the cross section is shown on figure 11.*

6.2 Low resistivity bodies and the Húsavík Fracture Zone

An interesting resistivity feature is encountered in the north-western part of the survey area, not usual in the resistivity structure of a high temperature field. Low resistivity bodies, extending vertically down from the low resistivity cap down to 10 km depth. This does not appear as a uniform layer but rather as distinctive bodies or chimneys, connected to the low resistivity cap. Figures 19 and 20 show N–S resistivity cross sections through the two low resistivity bodies in question (also see Appendix 3). Further to the north of that, the low resistivity cap continues towards north at 1 km depth.

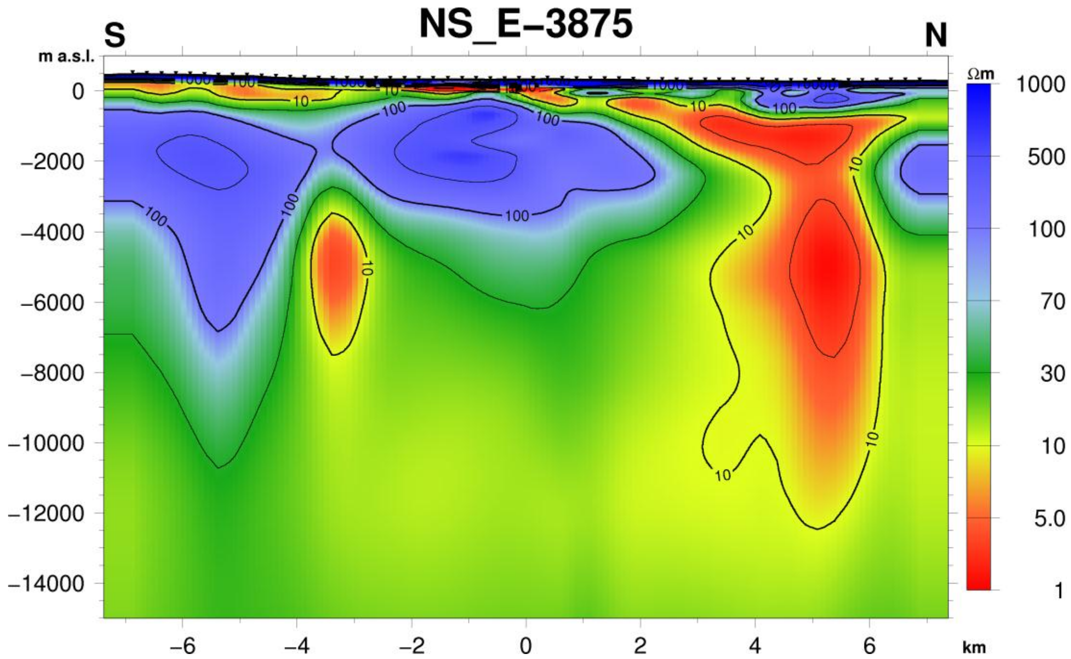

Figure 19. *A N-S resistivity cross section (3875 m west of origin). Location of the cross section is shown on figure 11.*

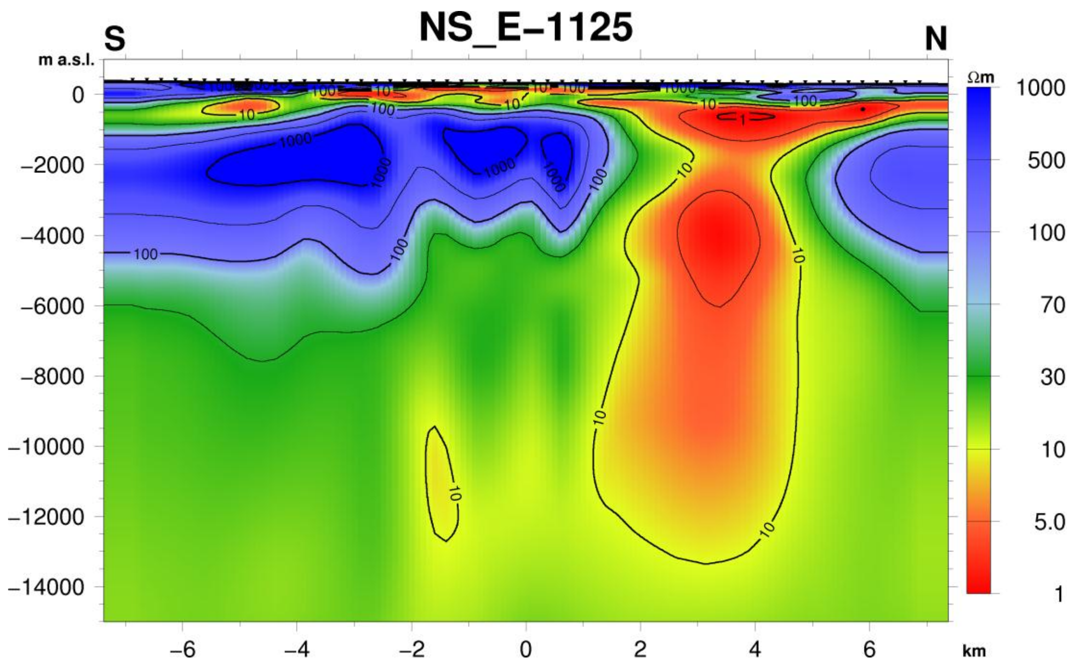

Figure 20. *A N-S resistivity cross section west of Bæjarfjall (and 1125 m west of origin). Location of the cross section is shown on figure 11.*

What could cause these low resistivity bodies is not clear. It is, however, tempting to connect this to the tectonic in this area. This is the area where the Húsavík Fracture Zone, a transform fault or fracture zone, infiltrates with the Þeistareykir fissure swarm (Kristján Sæmundsson, geology map 2012). The transform fault extends NW – SE, from the Skjálfandaflói Bay in the west, to the Þeistareykir fissure swarm in the east.

Recent studies state that intrusion occurred below Þeistareykir area around 2007–2008, inferred from GPS and InSAR techniques (Spaans et al., 2012). The model inferred indicates a volume change at 7.5–8.7 km depth under the northern part of the resistivity survey area (Spaans et al., 2012; Metzger et al., 2011).

Resistivity at 750 m b.s.l. Figure 21 shows that the high resistivity core covers all survey area except for the two low resistivity bodies allegedly connected to the Húsavík Fracture Zone mentioned earlier. A NW – SE lineament is clear and is allegedly related to the direction of the transform faults.

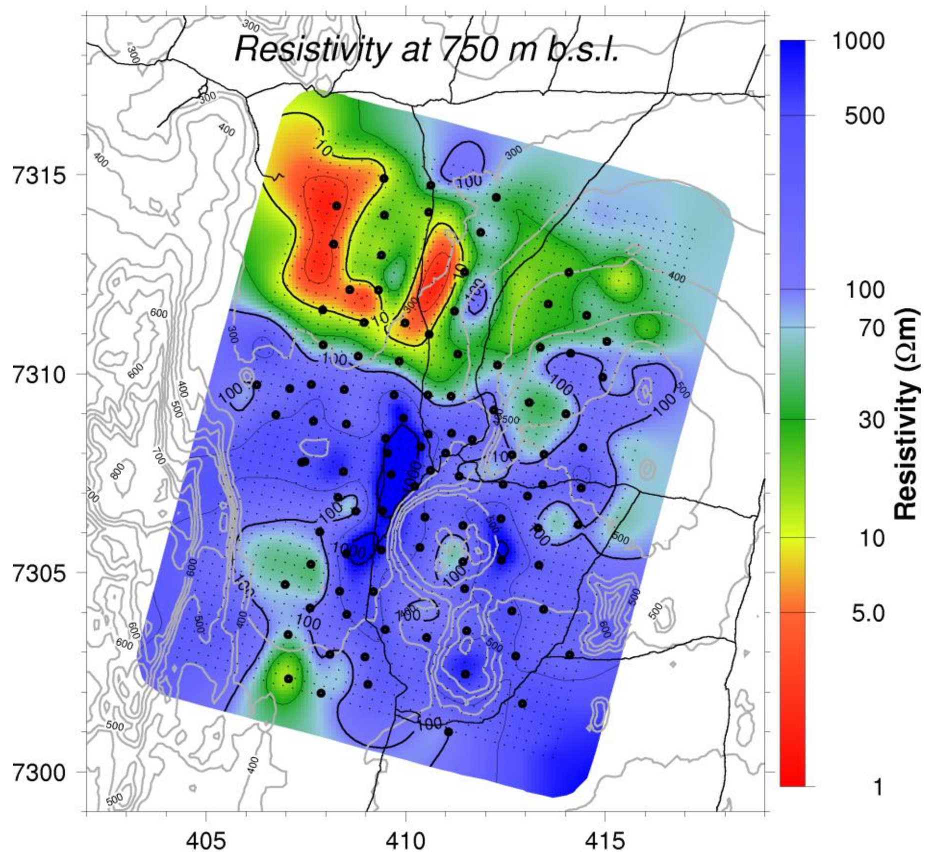

Figure 21. *Resistivity at 750 m b.s.l.*

6.3 The deep seated low resistivity layer

Resistivity at 1500 m b.s.l. Figure 22 shows the low resistivity bodies in the north-western part, but at this depth a low resistivity anomaly is visible under Ketilfjall. The anomaly under Ketilfjall has an elongated shape in the NNE-SSW strike direction and is the first sign of the deep seated low resistivity layer doming up. A hint of lower resistivity (green) is in the western part or in Stórahversmór, north of Stórihver. The low resistivity in the north eastern part is outside data coverage and must be disregarded.

Resistivity at 2000 m b.s.l. Figure 23 shows that the Ketilfjall anomaly reaches towards northeast and there is a faint hint that it extends under the eastern part of Bæjarfjall. There is also a hint of lower resistivity under Stórahversmór. There is high resistivity between the two anomalies and we see the NW-SE alignment with lower resistivity on the north eastern part.

This character will continue to greater depths, until **3500 m b.s.l.** (Figure 24) where the Ketilfjall anomaly is very prominent, reaching from Þeistareykir in the south west towards Þeistareykjabunga in the north east. The low resistivity bodies in the northern part, allegedly connected to the Húsavík Fracture Zone, are still found at this depth.

R**esistivity at 5000 m b.s.l.** Figure 25 shows that at this depth, the Ketilfjall anomaly expands to the NW and connects to one of the low resistivity bodies there. An anomaly is seen emerging under the south east of Bæjarfjall. Anomalies outside data coverage have to be disregarded.

Resistivity at 8000 m b.s.l. Figure 26 shows that the Ketilfjall anomaly and the low resistivity bodies in the NW (Húsavík Fracture Zone) are connected at this depth. A low resistivity under Stórahversmór is emerging and the anomaly under the south east part of Bæjarfjall is also becoming larger.

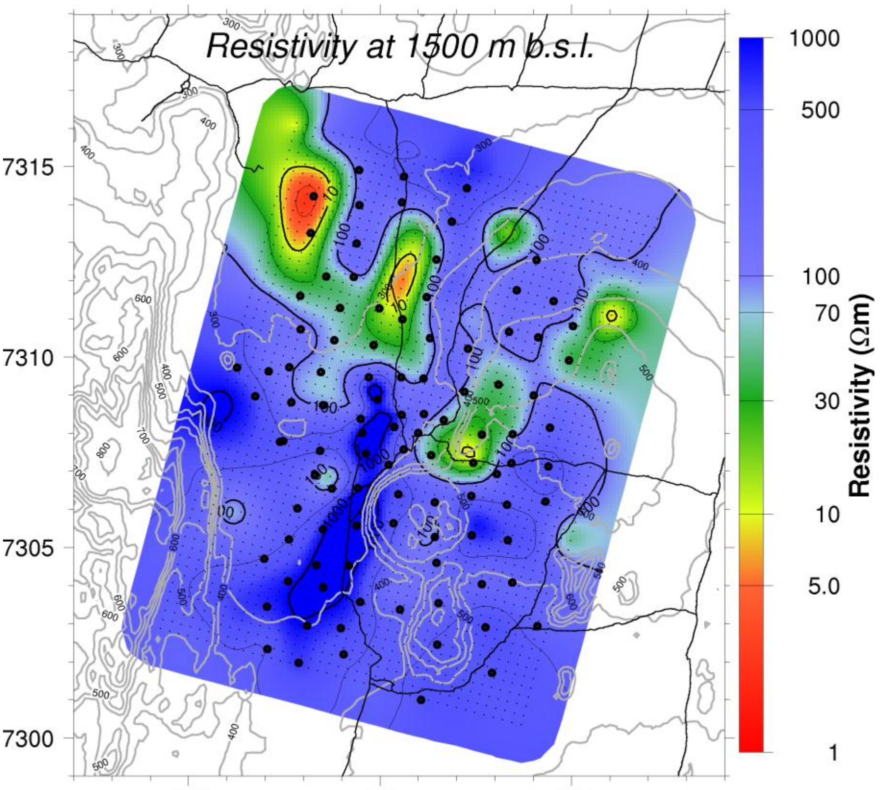

Figure 22. *Resistivity at 1500 m b.s.l.*

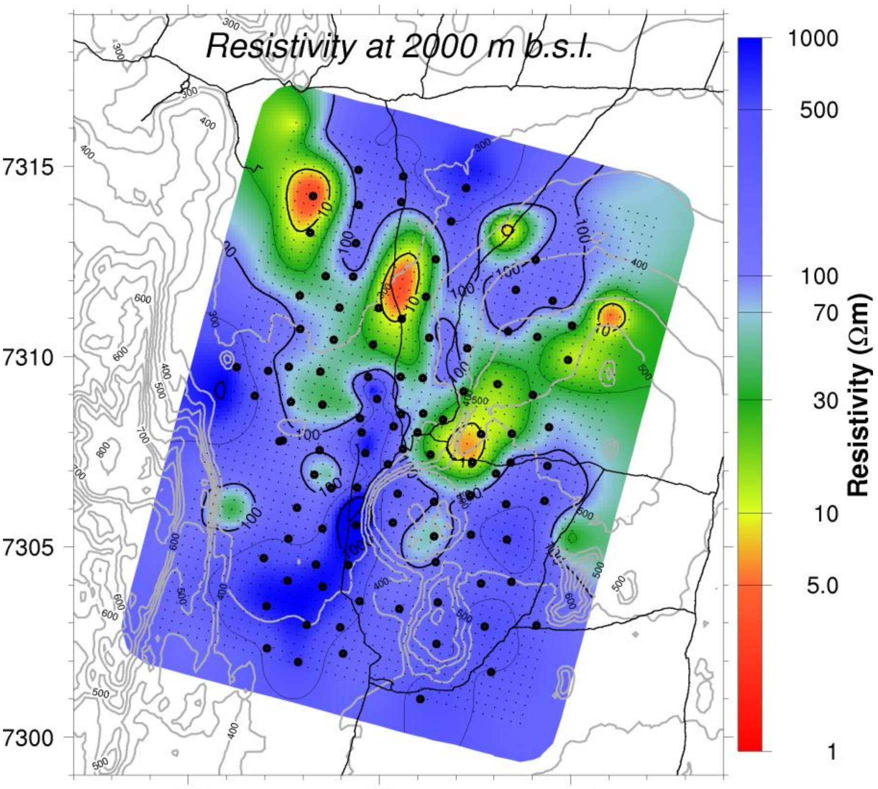

Figure 23. *Resistivity at 2000 m b.s.l.*

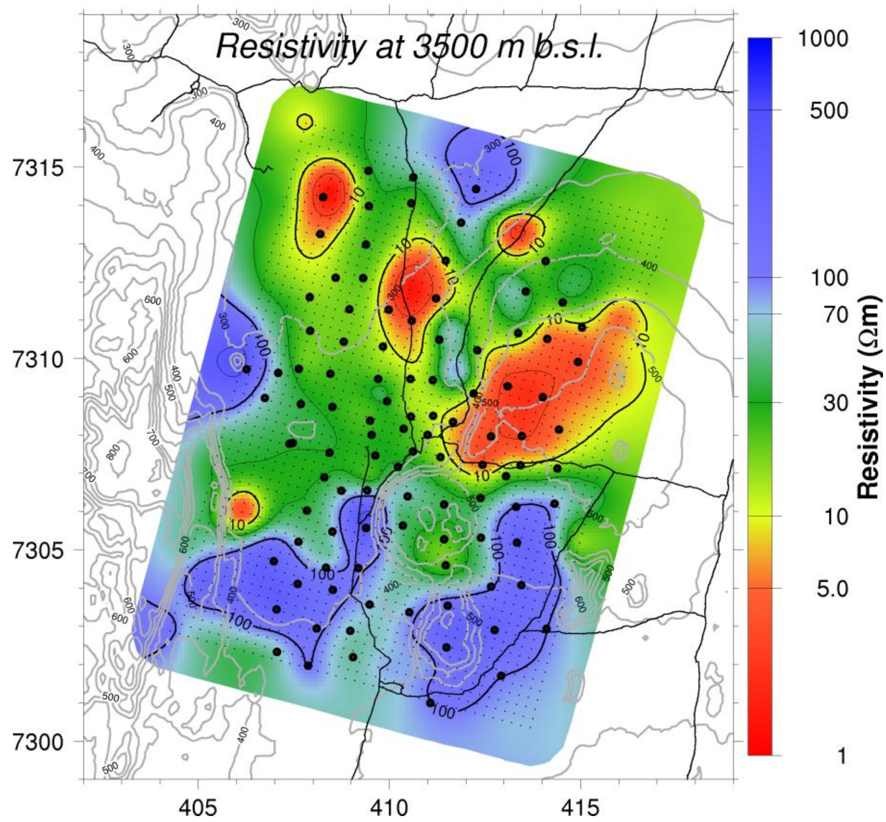

Figure 24. *Resistivity at 3500 m b.s.l.*

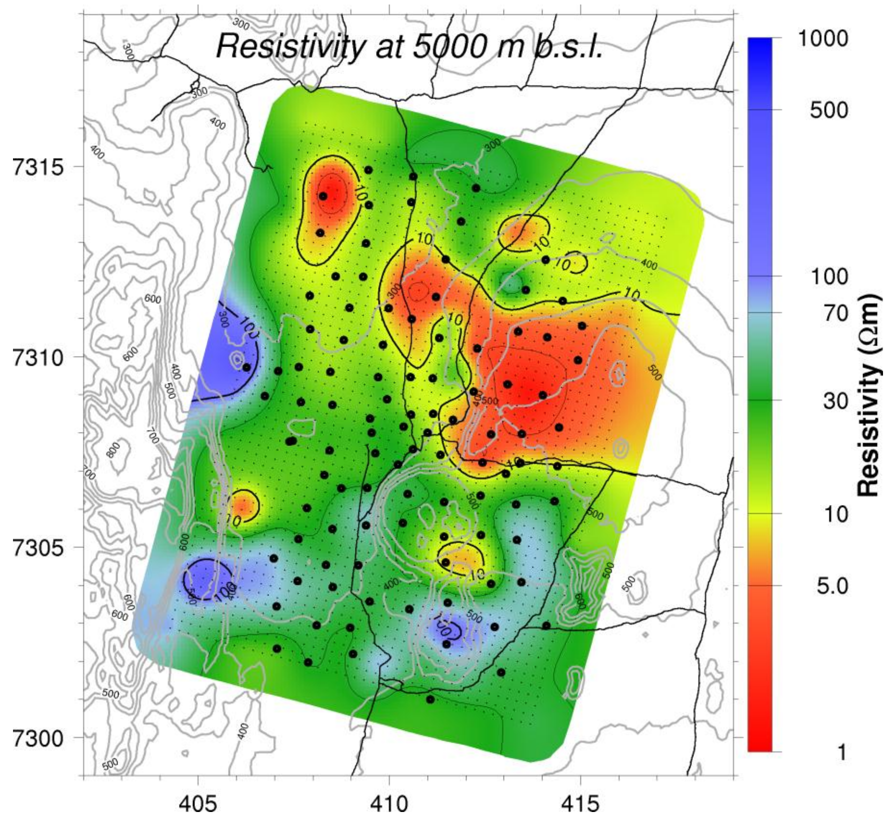

Figure 25. *Resistivity at 5000 m b.s.l.*

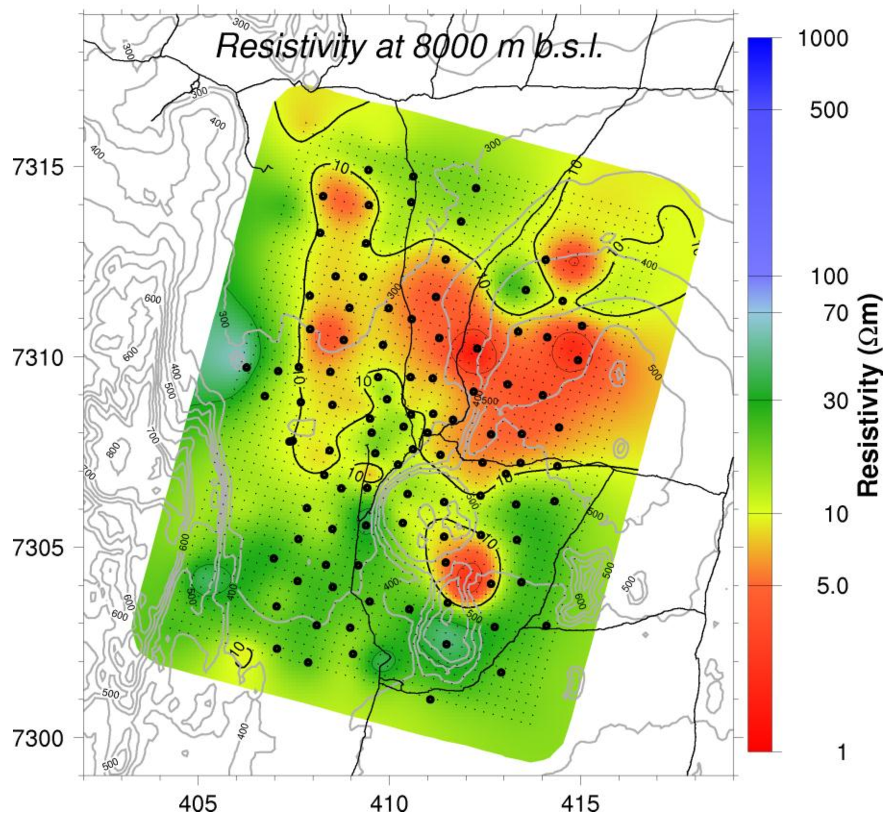

Figure 26. *Resistivity at 8000 m b.s.l.*

To investigate further the anomalies under Ketilfjall and Stórahversmór we show the resistivity cross section **EW_N-125** (Figure 27). The Ketilfjall anomaly is here very prominent and reaches from 12 km b.s.l. up to 2.5 km depth. The anomaly under Stórahversmór is at much greater depths reaching highest at 8 km depth b.s.l.

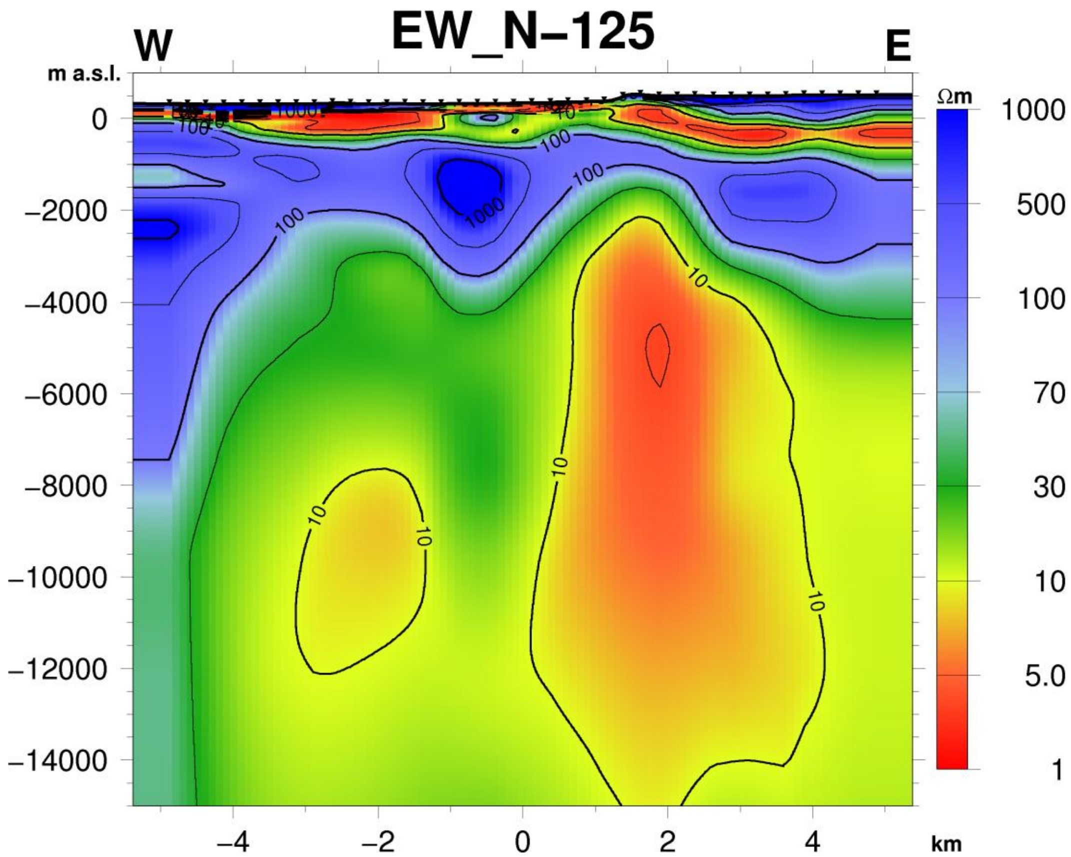

Figure 27. *A W-E resistivity cross section through the Ketilfjall (right) and Stórahversmór (left) anomalies. Location of the cross section is shown on figure 11.*

The anomaly under the southeast part of Bæjarfjall is clearly seen on the WE resistivity cross section **EW_N-2875** (Figure 28) that shows clearly that the anomaly is reaching as shallow as 5–6 km depth b.s.l. The small anomaly appearing in the western part is outside data coverage and must be disregarded.

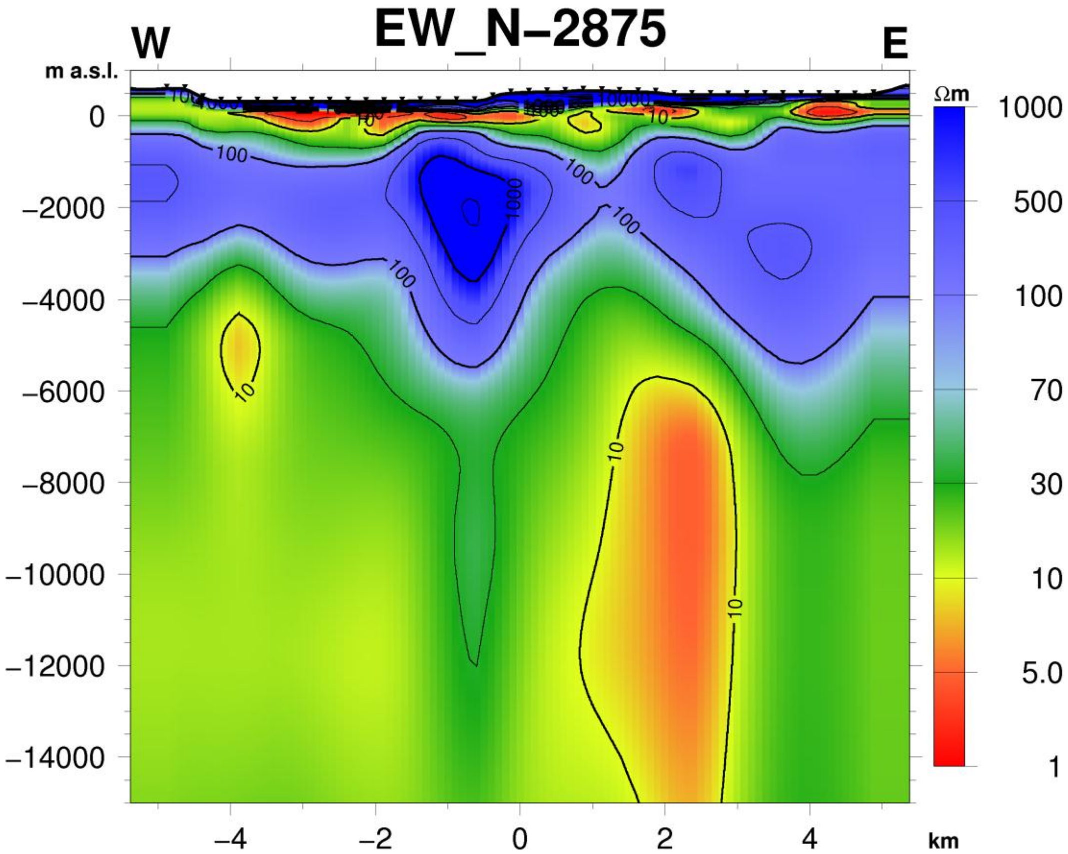

Figure 28. *A resistivity cross section through the anomaly east of Bæjarfjall. Location of the cross section is shown on figure 11.*

The resistivity cross section **EW_N3375** (Figure 29) shows the Ketilfjall anomaly connecting to the two low resistivity bodies (Húsavík Fracture Zone) in the north west. It cuts through the middle of the easternmost body and the southern part of the westernmost body. Cross sections further to the north (see appendix), show all three resistivity anomalies become disconnected.

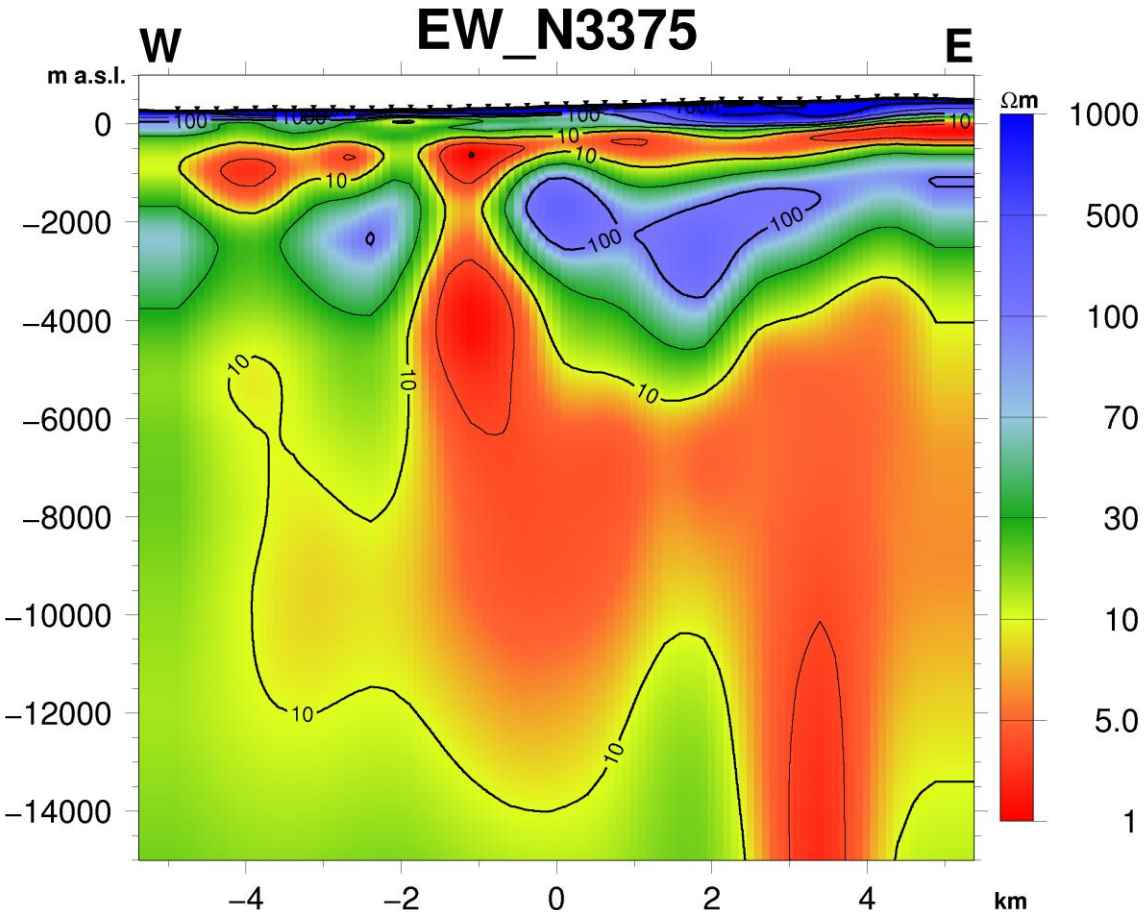

Figure 29. *A resistivity cross section through the Ketilfjall anomaly and the low resistivity bodies immediately south of the Húsavík Fracture Zone. Location of the cross section is shown on figure 11.*

Conclusion on the structure of the deep seated low resistivity layer.

The deep seated low resistivity layer appears as distinctive low resistivity bodies rather than a layer as suggested by the 1D results. That is to be expected because when inverting 3D data using 1D inversion, three dimensional features are forced into layers, i.e. some sort of average of the resistivity is calculated for different depths below the sounding sites. The most prominent low resistivity body is the body referred to as the Ketilfjall anomaly. It reaches highest to a depth of 2.5 km under the southern part of Ketilfjall and Þeistareykir. With depth it extends gradually towards northeast in the direction of Þeistareykjabunga. Two other distinctive anomalies are seen at greater depth, one under the southeast part of Bæjarfjall reaching highest up to 5–6 km depth and another under Stórahversmór, reaching as high as up to 8 km depth. The area/volume between the two anomalies, Ketilfjall and the smaller one under Stórahversmór, holds high resistivity. If the anomalies are considered to be indicative of up flow into the geothermal system the high resistivity between may indicate lower temperatures in this area.

Constraints on the deep seated low resistivity anomalies are seen in the 3D inversion run with homogeneous input model (20 Ωm). There the low resistivity under Ketilfjall is confirmed as well as the low resistivity under Stórihversmór. The low resistivity bodies connected to the Húsavík Fracture Zone are also constrained. The low resistivity under Bæjarfjall is, however, not confirmed.

The 3D model is presented in more details as resistivity maps in Appendix 1 and in resistivity cross sections in Appendices 2 through 4.

A 3D visualizing software is available at ISOR. The software has been used to display various exploration results and models of Þeistareykir. Anette Mortensen at ÍSOR has incorporated into PETREL the 3D resistivity model based on the 1D input model. A video presentation of the model in PETREL is submitted with this report on a DVD disk and is a part of the report.

7 Constraints on the 3D model

To see the constraints on the 3D model the inversion was run with a homogeneous input model with resistivity of 20 Ωm. By doing so it is possible to check where the model requires lower or/and higher resistivity in order to fit the data.

A comparison between the

- 3D model based on the 1D inversion (RMS fit = 1.45)
- 1D model
- 3D model based on a homogeneous model with initial resistivity of 100 Ωm (RMS fit = 2.20)
- 3D model based on a homogeneous model with initial resistivity of 20 Ωm (RMS fit = 1.73)

will be presented on the following pages for clarification. We look at the models at various depths from 200 m a.s.l. to 8 km b.s.l. (Figures 30–36). The 3D inversion was run with 250 m spacing in the inner part of the model grid as explained earlier. This was done for the inversion based on the 1D model and the inversion based on the homogeneous half space of 100 Ωm. It turned out that the inversion with the 100 Ωm input resistivity did not have a good resolution at depth. Hence, an inversion was run with the input resistivity of 20 Ωm for comparison, but this time with coarser grid of 500 m spacing in the inner part of the model.

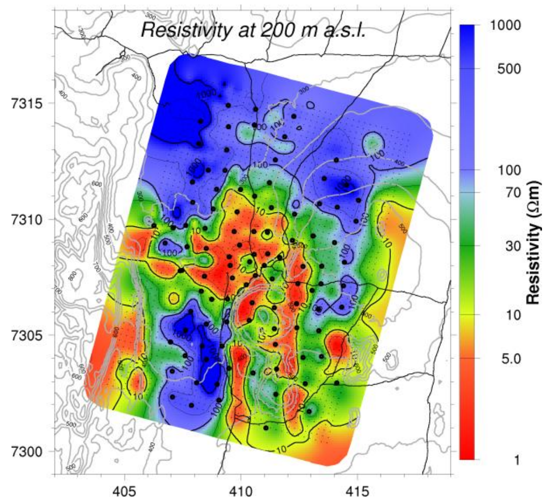

3D model with 1D input model/250g.

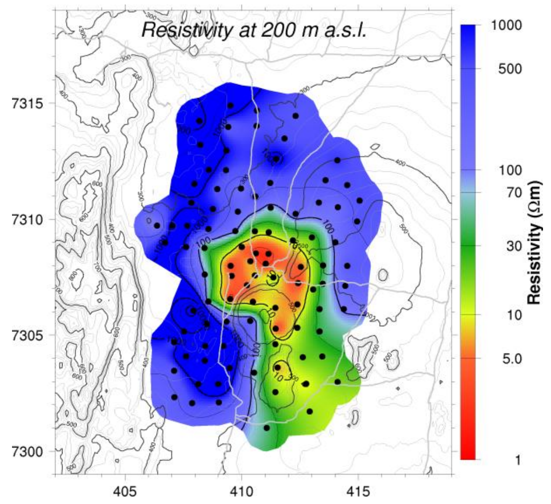

1D model.

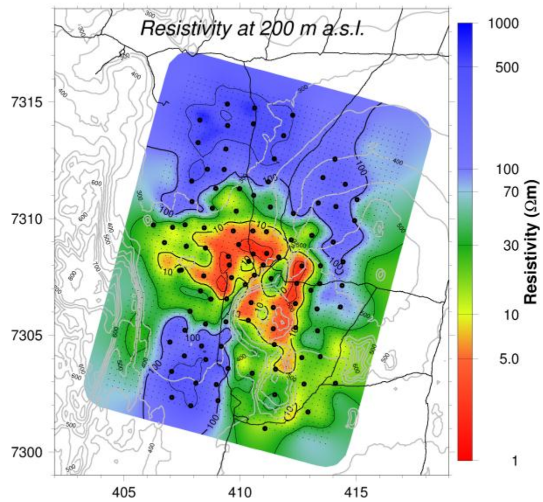

3D with homog. (100 Ωm/250grid).

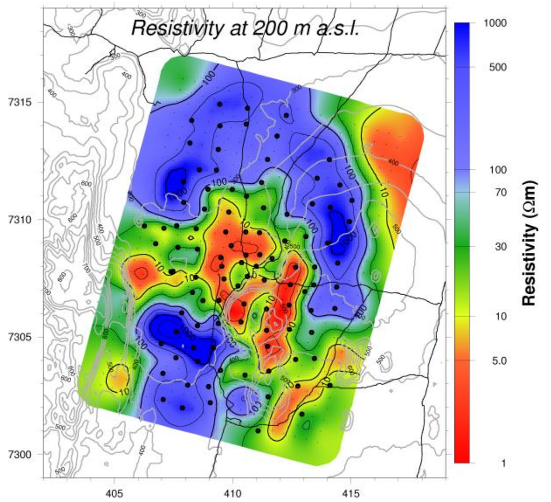

3D with homog. (20 Ωm/500grid).

Figure 30. *Comparison of models at 200 m a.s.l.*

Figure 30 shows resistivity at 200 m a.s.l. and displays the top of the low resistivity cap at approximately 200–300 m depth under surface. First it is relevant to point out that there are some artefacts outside data coverage in all 3D models. The 1D results define well the survey area and we shall disregard anomalies outside data coverage.

The same character is seen in all four maps, the only clear difference is the smoothed appearance of the 1D model. This is what is expected as the 1D model only gives 1D result for each sounding and does not resolve the volume between the soundings. All models give a clear picture of the low resistivity cap but more constraints and more details are seen in the 3D models.

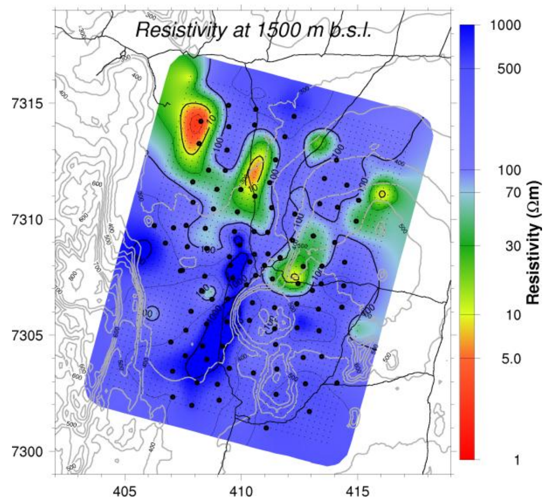

3D model with 1D input model/250g.

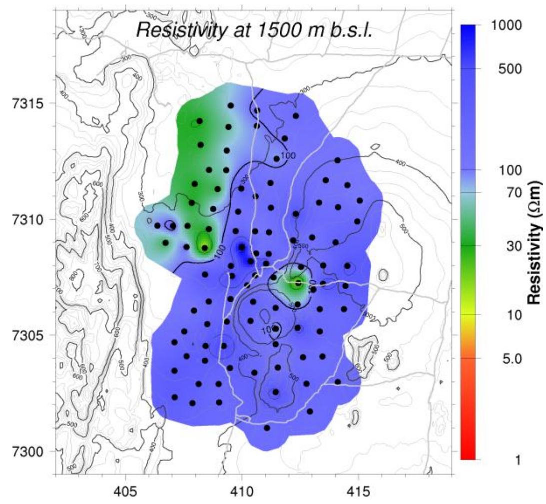

1D model.

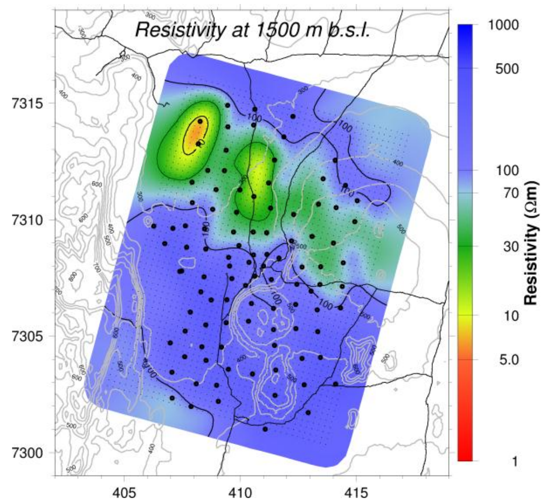

3D with homog. (100 Ωm/250grid).

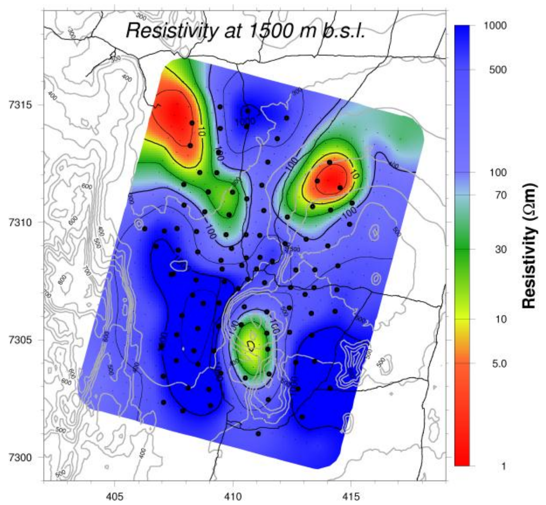

3D with homog. (20 Ωm/500grid).

Figure 31. *Comparison of models at 1500 m b.s.l.*

Figure 31 shows resistivity at 1500 m b.s.l.. The 1D model senses low resistivity in the northwestern part of the area but the 3D models resolve more clearly the low resistivity bodies, even the 3D model with the 500 m grid. Low resistivity is starting to show in Bóndhólsskarð in the 1D model as well as in the 3D model based on 1D. The 3D model /20Ωm/500grid) senses low resistivity under south eastern part of Bæjarfjall, a feature the other models see at greater depth (see later).

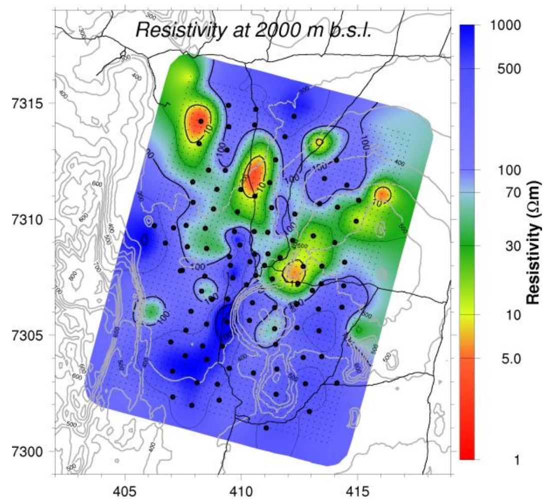

3D model with 1D input model/250g.

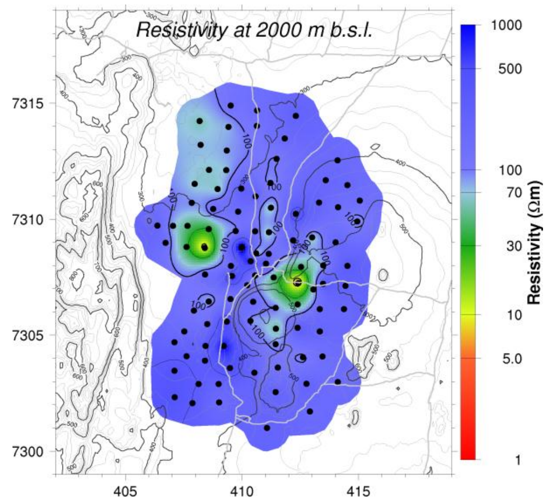

1D model.

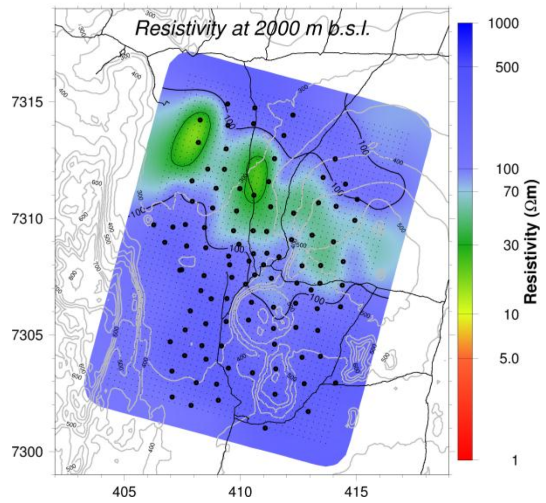

3D with homog. (100 Ωm/250grid).

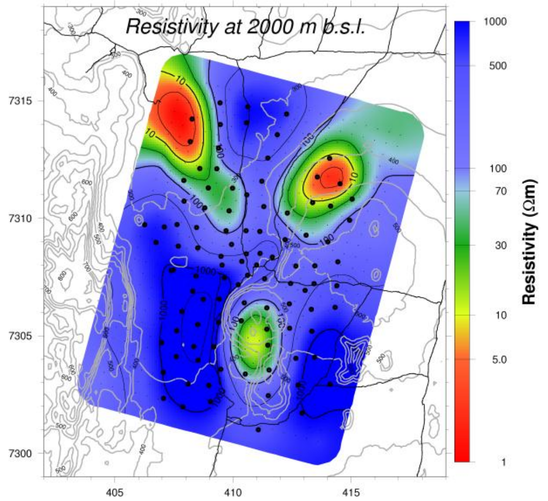

3D with homog. (20 Ωm/500grid).

Figure 32. *Comparison of models at 2000 m b.s.l.*

Figure 32 shows resistivity at 2000 m b.s.l. The 3D model based on the 1D shows the Ketilfjall anomaly starting to reach towards north east as well as under Bæjarfjall. This is confirmed by the 3D (20/500grid) but more vaguely in the 3D (100/250grid). All 3D models resolve the low resistivity bodies in the north-western part of the survey area. The low resistivity in the western part of the survey area, Stórihversmór in the 3D model based on 1D, is not supported by the other 3D models at this depth.

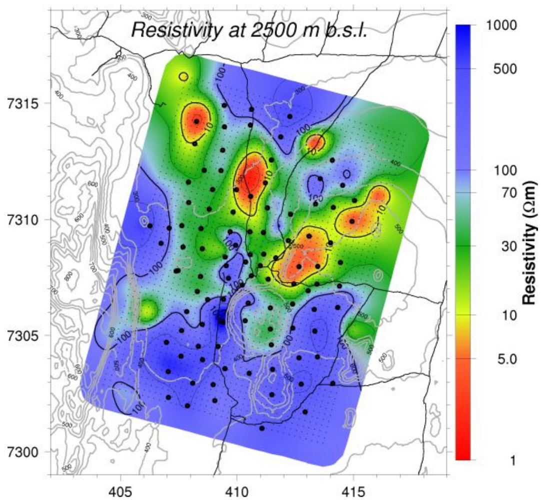

3D model with 1D input model/250g.

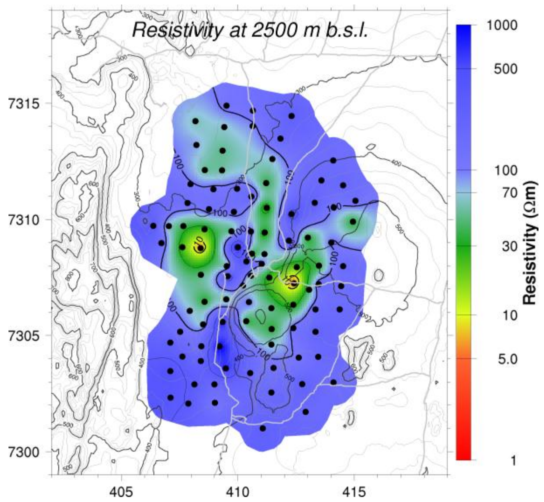

1D model.

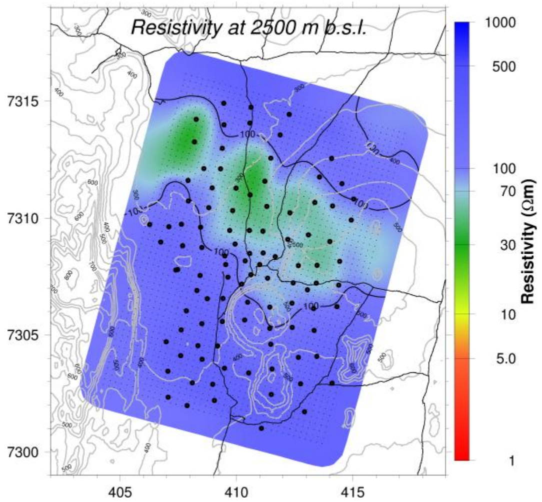

3D with homog. (100 Ωm/250grid).

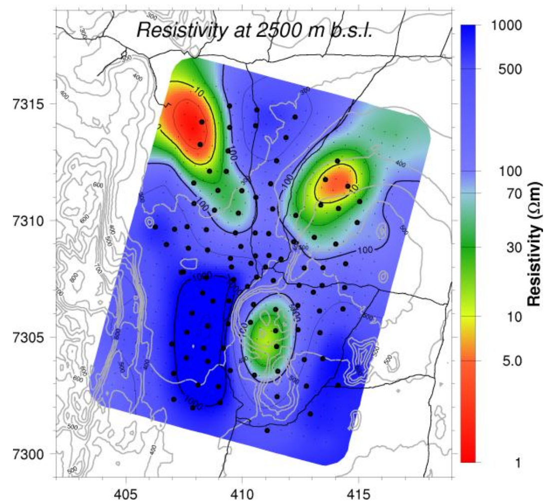

3D with homog. (20 Ωm/500grid).

Figure 33. *Comparison of models at 2500 m b.s.l.*

Figure 33 shows resistivity at 2500 m b.s.l. This is a similar picture as the one at 2000 m b.s.l. but here the 1D model resolves the low resistivity bodies better. The Ketilfjall anomaly has become more clearly elongated towards north east in the 3D model based on the 1D and this is confirmed by the 3D (20/500grid).

From this depth and down to greater depths the 3D (100/250grid) does not resolve low resistivity. Low resistivity bodies are seen vaguely as well as the Ketilfjall anomaly reaching towards south under Bæjarfjall. The explanation may be that the input resistivity of 100 Ωm is too high, or in other words too far off from the actual resistivity, so that the inversion is not able to resolve the resistivity at depths below 2500 m b.s.l

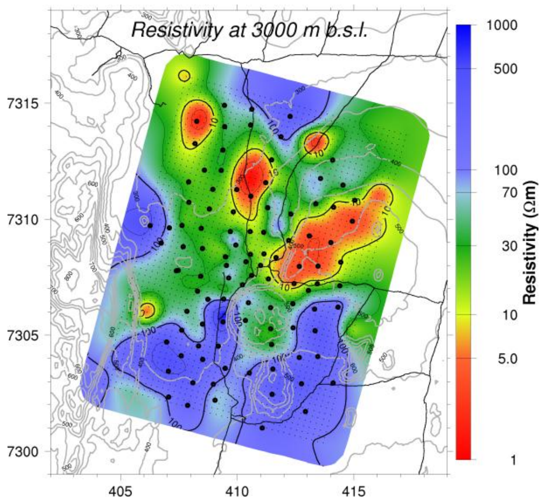

3D model with 1D input model/250g.

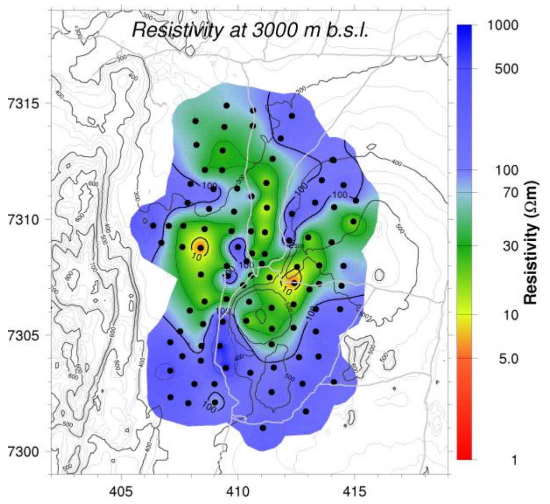

1D model.

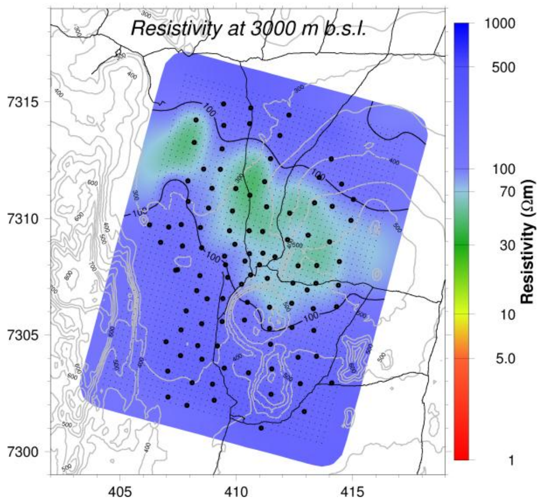

3D with homog. (100 Ωm/250grid).

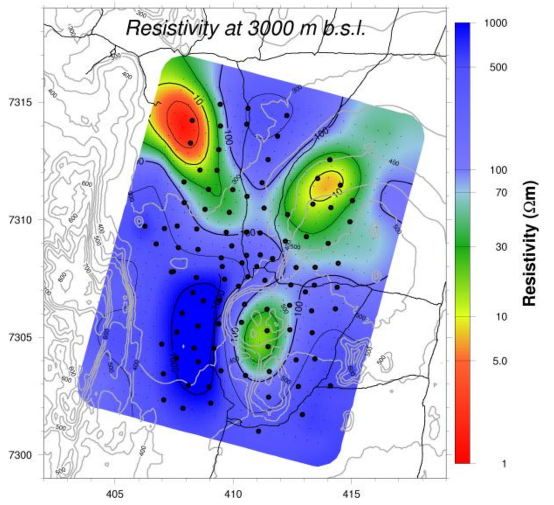

3D with homog. (20 Ωm/500grid).

Figure 34. *Comparison of models at 3000 m b.s.l.*

Figure 34 shows resistivity at 3000 m b.s.l. Here the 3D model based on 1D shows a clear and more distinctive picture of the resistivity than the smoothed version of the 1D. This is as expected and confirmed by the 3D (20/500grid).

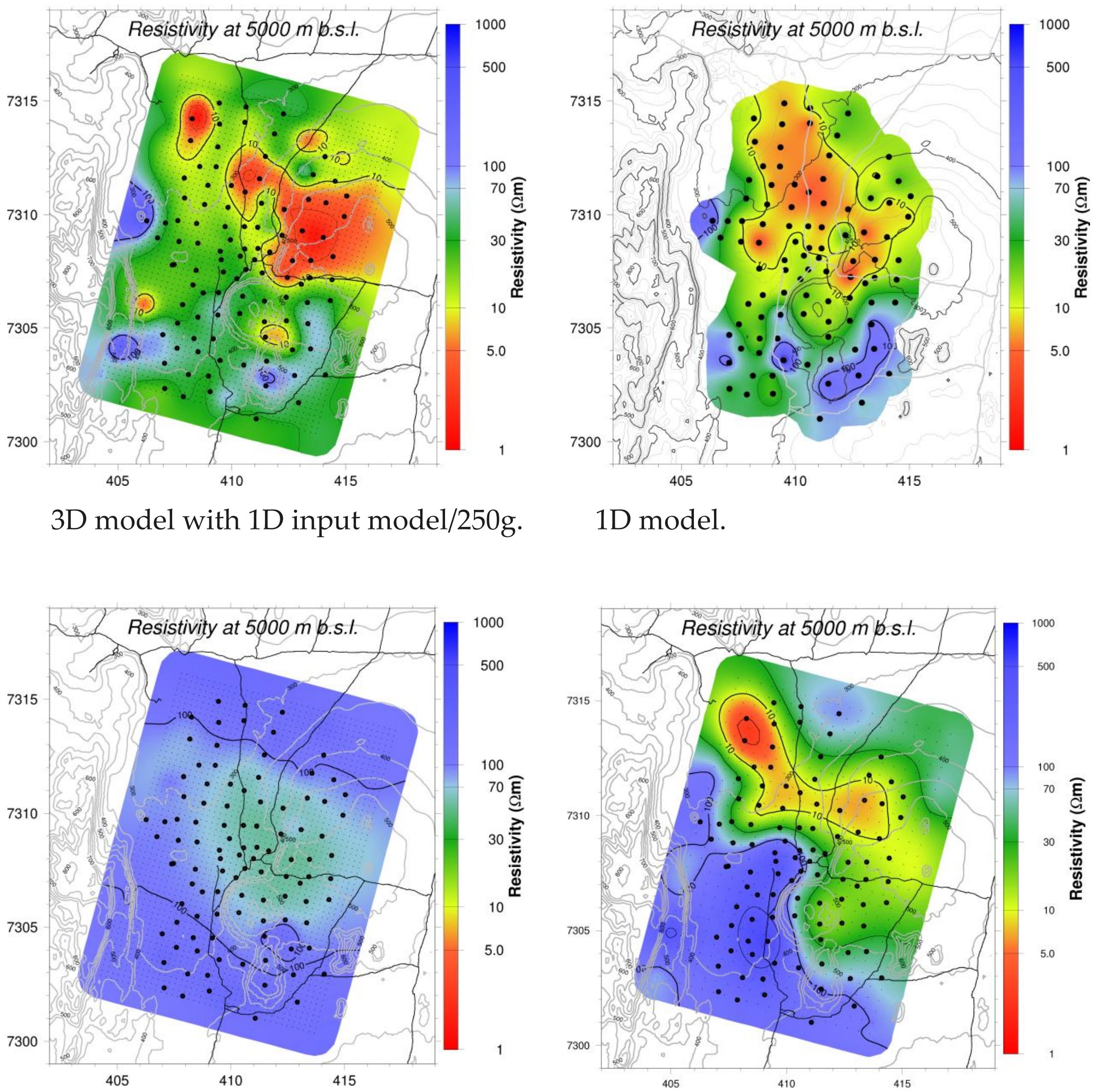

3D model with 1D input model/250g.

1D model.

3D with homog. (100 Ωm/250grid).

3D with homog. (20 Ωm/500grid).

Figure 35. *Comparison of models at 5000 m b.s.l.*

Figure 35 shows resistivity at 5000 m b.s.l. Here the anomalies in the north connect as discussed before in the 1D and 3D based on 1D as well as the 3D (20/500). The 3D (100/250) does not resolve the resistivity properly at this depth as noted earlier.

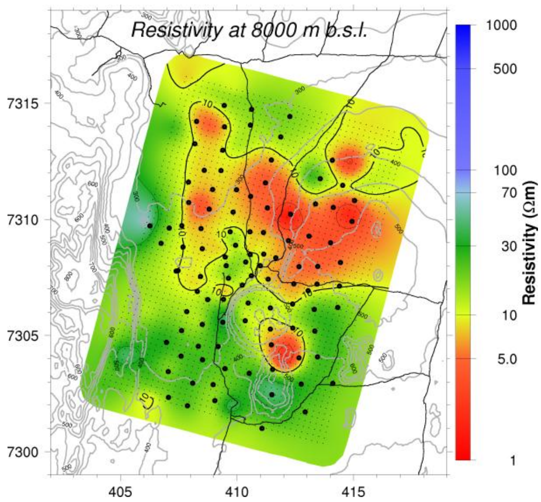

3D model with 1D input model/250g.

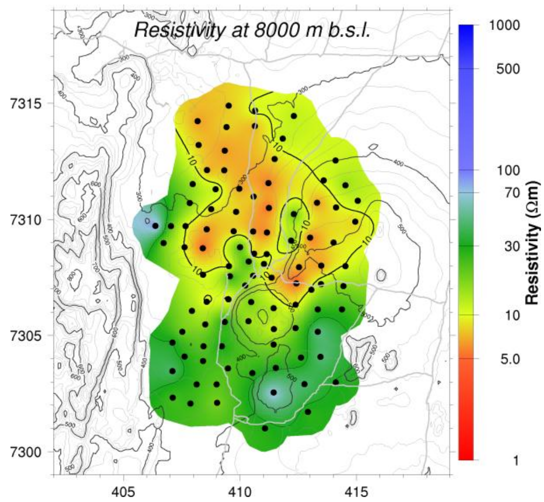

1D model.

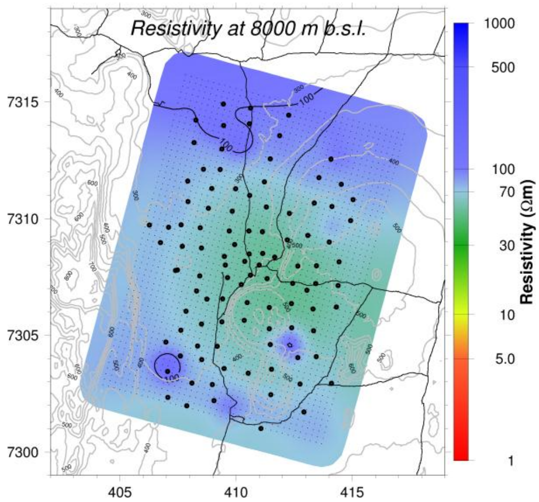

3D with homog. (100 Ωm/250grid).

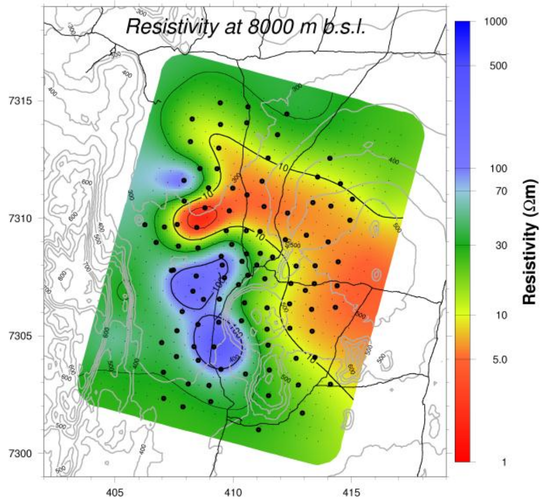

3D with homog. (20 Ωm/500grid).

Figure 36. *Comparison of models at 8000 m b.s.l.*

Figure 36 shows resistivity at 8000 m b.s.l. Here the main features are the connected low resistivity anomalies, the Ketilfjall anomaly and the two low resistivity bodies in the northwestern part of the survey area. Here a low resistivity is seen under Bæjarfjall in the 3D model based on 1D but not in the 1D model. At this depth a deep seated low resistivity is seen under Stórahversmór in the western part of the area, confirmed by all models except 3D (100/250grid).

8 The 3D model and data from existing boreholes

Resistivity well logs are available from the wells in Þeistareykir. For a detailed comparison of the resistivity log data to other borehole data, such as geology, the resistivity logs need to undergo corrections. These are elevation and depth corrections and corrections that take into account the effect of the resistivity and temperature of the well fluid and the width of the well. Resistivity logs from the Þeistareykir wells have not been corrected yet. In a comparison to, in this respect, the coarse grid of the 3D model, the uncorrected? resistivity logs can show the main character of the resistivity in the well. If however, the resistivity logs are needed. For a more detailed studies the resistivity well logs need, however, to be corrected for the effects mentioned above.

The available resistivity well logs have been presented along with the 3D resistivity model in *PETREL visualization software*. Other data now incorporated into Petrel are: Data on petrology from the cuttings, data on alteration minerals/zones from X-ray diffraction, temperature distribution from temperature logs as well as inferred data from the inspection of the wells, such as location of feed zones, fractures and faults.

It is recommended that a further and more detailed comparison of all data available for the Þeistareykir field be done utilizing Petrel. Visualizing the data 3D gives opportunity to compare one data set to another from various angels and adding data gradually ("layer by layer") to the picture in an attempt to understand the inner structure and physical conditions within a geothermal system.

Examples of sections through the resistivity model from PETREL (also see the DVD submitted with this report) with the wells and temperature data area displayed in figures 37 and 38.

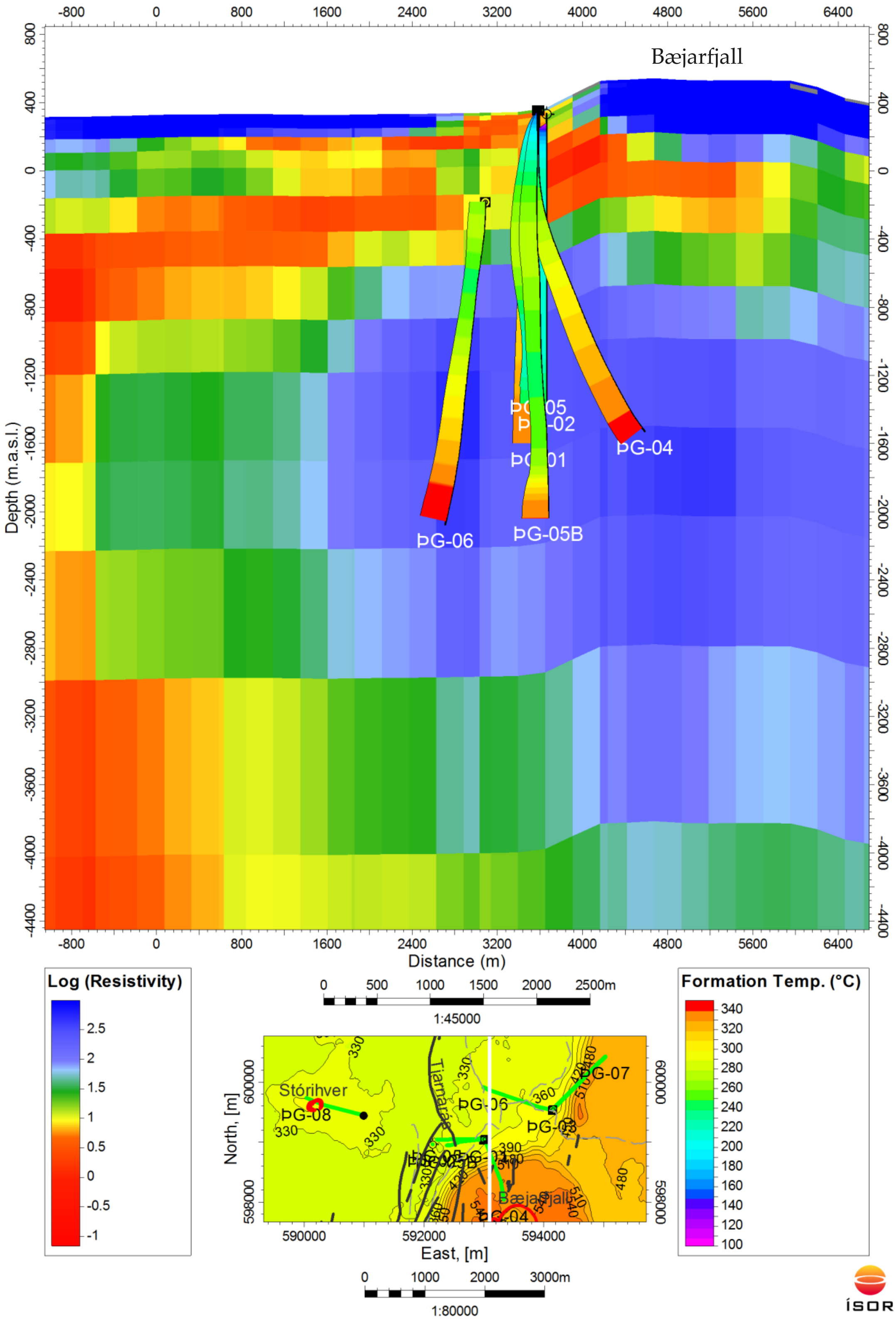

Figure 37. *A NS cross section through the 3D resistivity model with well trajectories and temperature data from adjacent wells.*

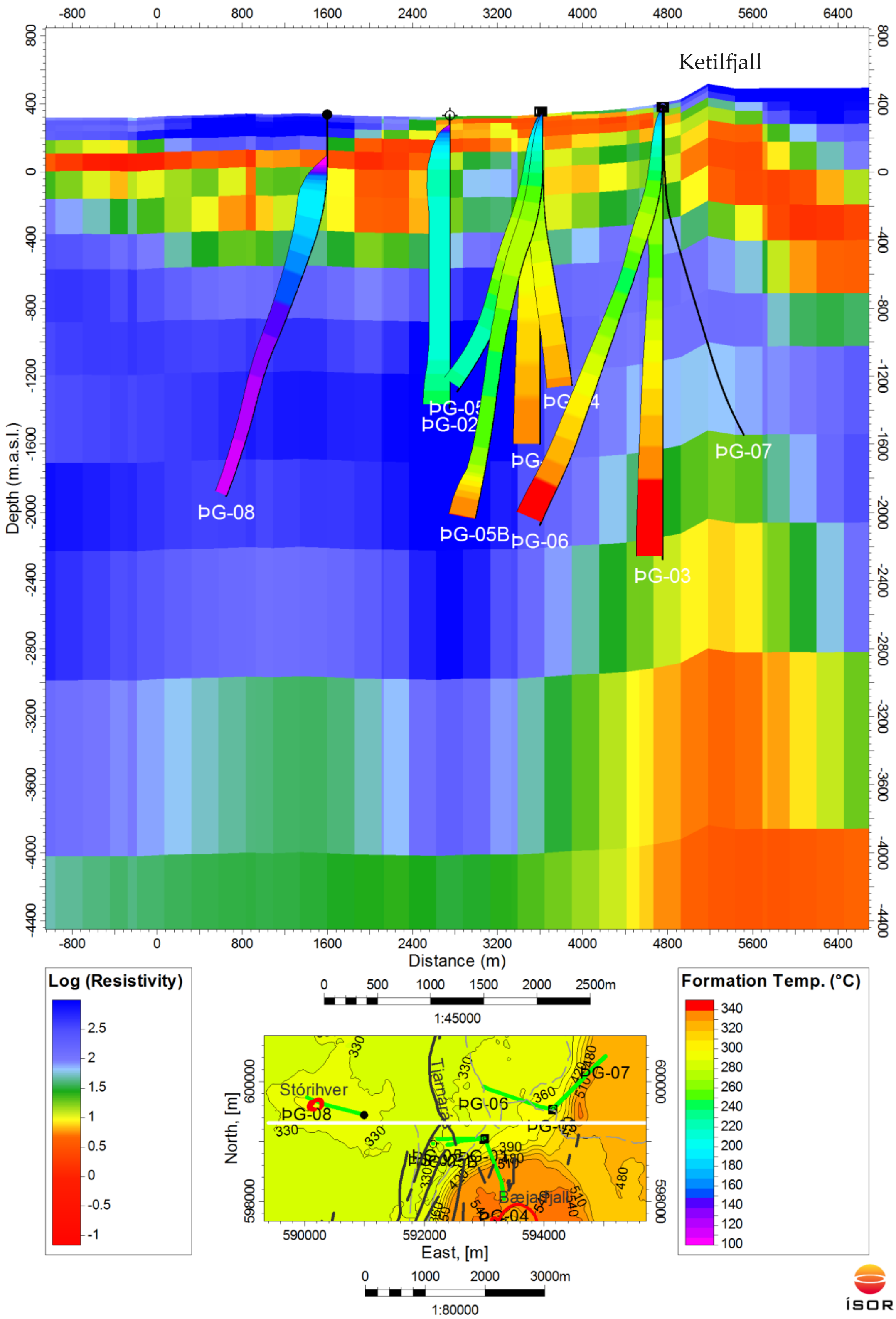

Figure 38. *An EW cross section through the 3D resistivity model with well trajectories and temperature data from adjacent wells.*

9 Conclusions

The TEM/MT survey at Þeistareykir reveals a conventional resistivity structure of a high temperature field i.e. a low resistivity cap with an underlying high resistivity core and a low resistivity bodies at depth indicating the heat source.

- A **low resistivity cap**, that reflects the zeolite/smectite zone, covers the whole survey area. It reaches surface at Þeistareykir farm and dips down to 400–800 m (the upper limit) depth in all directions. The low resistivity cap takes an interesting and unexplained dive under Bæjarfjall. In the 3D model the low resistivity cap does not appear as a uniform layer but rather as connected low resistivity bodies. How this landscape within the low resistivity cap compares to the data from wells is best done in the visualization software PETREL on a DVD submitted with this report.

- A **high resistivity core** reflecting the chlorite/epidote zone underlies the low resistivity cap. The margin between the two comprises the 230–240°C temperature boundary provided that there is a thermal equilibrium within the geothermal system. The high resistivity core reaches highest under Þeistareykir to approximately 200 m b.s.l.

- Deep low resistivity bodies that may indicate the heat source and upflow zones of geothermal fluid into the system are the Ketilfjall anomaly and the Bæjarfjall anomalies and the Stórahversmór anomaly.
  Ketilfjall anomaly reaches highest under Bóndhólsskarð/Þeistareykir and the southern part of Ketilfjall, or up to 2 km b.s.l. With depth it extends gradually further north and northeast in direction of Þeistareykjabunga. The Ketilfjall anomaly is by far the most prominent low resistivity body that allegedly indicates the main heat source of the geothermal system.
  Bæjarfjall anomaly reaches highest under the south eastern part of Bæjarfjall up to 6 km depth b.s.l.
  Stórihversmór anomaly reaches highest under Stórihversmór, north of Stórihver to about 8 km b.s.l.

- Two distinctive low resistivity bodies are present under the north western part of the survey area. They are connected to the low resistivity cap and reach down to 10 km b.s.l. It is not known if they indicate heat source or something else. It is, however, tempting to connect them to the Húsavík Fracture Zone as they are to the immediate south of, or within, the area where the fracture zone infiltrates with the Þeistareykir fissure swarm (Figure 19 and 20).

- Recent studies state that intrusion occurred below Þeistareykir area around 2007–2008, inferred from GPS and InSAR techniques. The model inferred indicates a volume change at 7.5–8.7 km depth under the northern part of the resistivity survey area. According to these studies the intrusions are to the south of the above mentioned low resistivity bodies. We do not know how well constrained the models are but it is tempting to connect the two phenomena i.e. the intrusions inferred from GPS and InSAR techniques and the two low resistivity bodies.

- As mentioned earlier a DVD disc presenting the 3D resistivity model in the visualizing software PETREL along with various other data from wells will be submitted with this report. It will not do the visualization in the PETREL software any justice to even try to describe in words how the data compare to each other. One picture says more than hundred words.

  It is highly relevant and recommended to do a comparison of all available data at Þeistareykir in a 3D visualization.

10 References

Árnason, K. (2008). *The Magnetotelluric static shift problem*. Iceland GeoSurvey, short report, ÍSOR-08088, 16 pp.

Árnason, K., Eysteinsson, H. and Hersir, G. P. (2010). Joint 1D inversion of TEM and MT data and 3D inversion of MT data in the Hengill area, SW Iceland. *Geothermics 39*, 13–34.

Árnason, K., Karlsdóttir, R., Eysteinsson, H., Flóvenz, Ó. G., and Gudlaugsson, S. Th., (2000). The resistivity structure of high-temperature geothermal systems in Iceland. *Proceedings of the World Geothermal Congress 2000, Kyushu-Tohoku, Japan*, 923–928.

Constable, C. S., Parker, R. L. and Constable, C. G. (1987). Occam's inversion: a practical algorithm for generating smooth models from electromagnetic sounding data. *Geophysics 52*, 289–300.

Egbert, G. D. and Booker, J. R. (1986). Robust estimation of geomagnetic transfer functions. *Geophys. J. R. Astr. Soc. 87*, 173–194.

Flóvenz, Ó. G., Spangenberg, E., Kulenkamff, J., Árnason, K., Karlsdóttir, R. and Huenges, E. (2005). The role of electrical interface conduction in geothermal exploration. Oral presentation at IGA, *World Geothermal Congress, in Turkey 2005*. Published in conference proceedings.

Gíslason, G., Johnsen, G. V., Ármannsson, H., Torfason, H. and Árnason, K. (1984). *Þeistareykir. Surface exploration of the high temperature field.* National Energy Authority, report, OS-84089, 134 pp. (In Icelandic).

Grönvold, K. and Karlsdóttir, R. (1975). *Surface exploration of the geothermal field. A preliminary report.* National Energy Authority, report, OS-JHD-7501. 37 pp. (In Icelandic).

Karlsdóttir, R., Eysteinsson, H., Magnússon, I. Þ., Árnason, K. and Kaldal, I. (2006). *Tem measurements at Theistareykir and Gjástykki 2004–2006* (in Icelandic). Iceland GeoSurvey, ÍSOR-2006/028, 87 pp.

Metzger, S., Jónsson, S. and Geirsson, H. (2011). Locking depth and slip-rate of the Húsavík Flatey fault, north Iceland, derived from continuous GPS data 2006–2010. *Geophysical Journal International, 187*, 564.

Mortensen, A. K., Guðmundsson, Á., Steingrímsson, B., Sigmundsson, F., Axelsson, G., Ármannsson, H., Björnsson, H., Ágústsson, K., Sæmundsson, K., Ólafsson, M., Karlsdóttir, R., Halldórsdóttir, S. and Hauksson, T. (2009). *Krafla Geothermal System. Conceptual Model.* Report ÍSOR-2009/057, LV-2009/111. In Icelandic. 206 pp.

Phoenix Geophysics (2005). *Data Processing User Guide.* Phoenix Geophysics. 201 pp.

Phoenix Geophysics (2009). *V5 System 2000 MTU/MTU-A User Guide*. Phoenix Geophysics. 178 pp.

SEG (1991). *MT/EMAP data interchange standard*. Society of Exploration Geophysicists, 112 pp.

Siripunvaraporn, W., Egbert, G., Lenbury, Y. and Uyeshima, M. (2005). Three-dimensional magnetotelluric inversion: data-space method. *Phys. Earth Planet. Int. 150,* 3–14.

Siripunvaraporn, W. and Egbert, G. (2009). WSINV3DMT: Vertical magnetic field transfer function inversion and parallel implementation. *Phys. Earth Planet. Int. 173,* 317–329.

Spaans, K., Sigmundsson, F. and Hreinsdóttir, S. (2012). *Crustal deformation in the Krafla, Gjástykki and Þeistareykir areas inferred from GPS and InSAR techniques*. *Status report.* Institute of Earth Sciences. University of Iceland. 23 pp.

Sternberg, B. K., Washburne, J. C. and Pellerin, L. (1988). Correction for the static shift in magnetotellurics using transient electromagnetic soundings. *Geophysics, vol. 53,* 1459–1468.

Vilhjálmsson, A. M., Flóvenz, Ó. G., Karlsdóttir, R., Árnason, K., Eysteinsson, H. and Sæmundsson, K. (2008). Geophysical evidence for magmatic Transportin the Lower Crust in Iceland. *Poster at AGU conference 2008*. Paper number MR43A-1803.

Violay, M., Gibert, B., Azais, P., Lods, G. and Pezard, P. (2010). *A new cell for electrical conductivity measurement on saturated samples at upper crust conditions*. Submitted to Transport in porus media.

Weidelt, P. (1972). The inverse problem of geomagnetic induction. *J. Geophys., 38*, 257–289.

Appendix 1

Resistivity maps

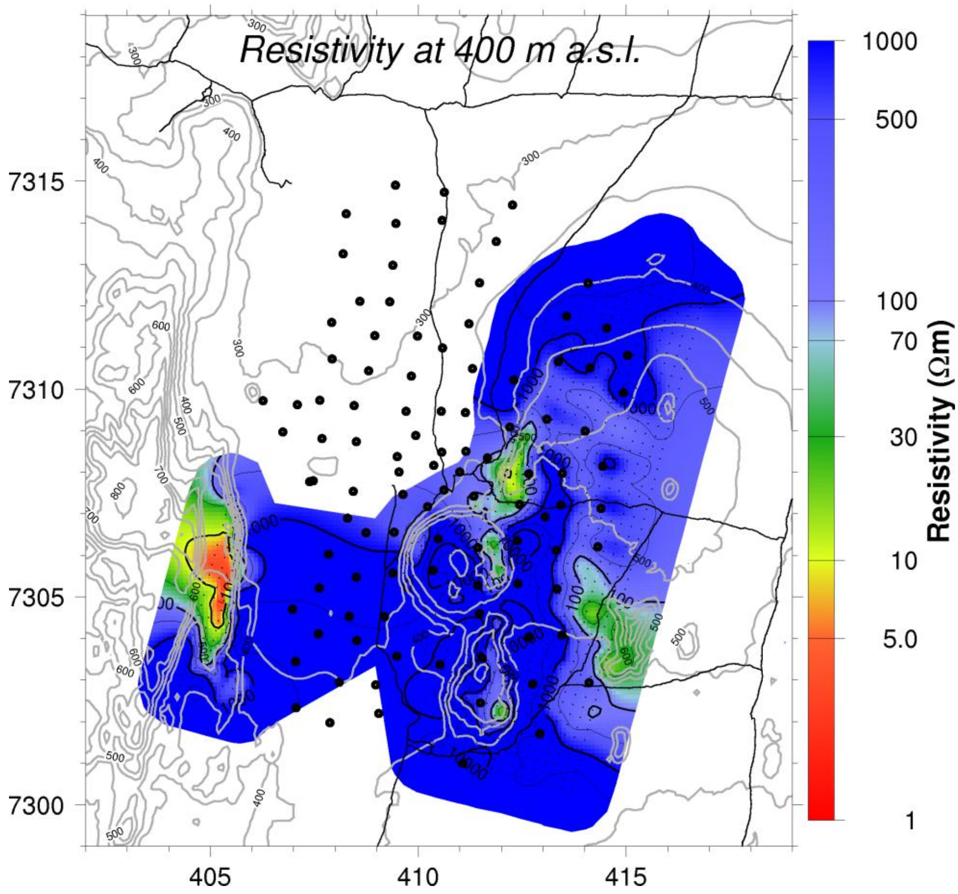
Resistivity at 400 m a.s.l.
Resistivity (Ωm)
1000
500
100
70
30
10
5.0
1
7315
7310
7305
7300
405
410
415

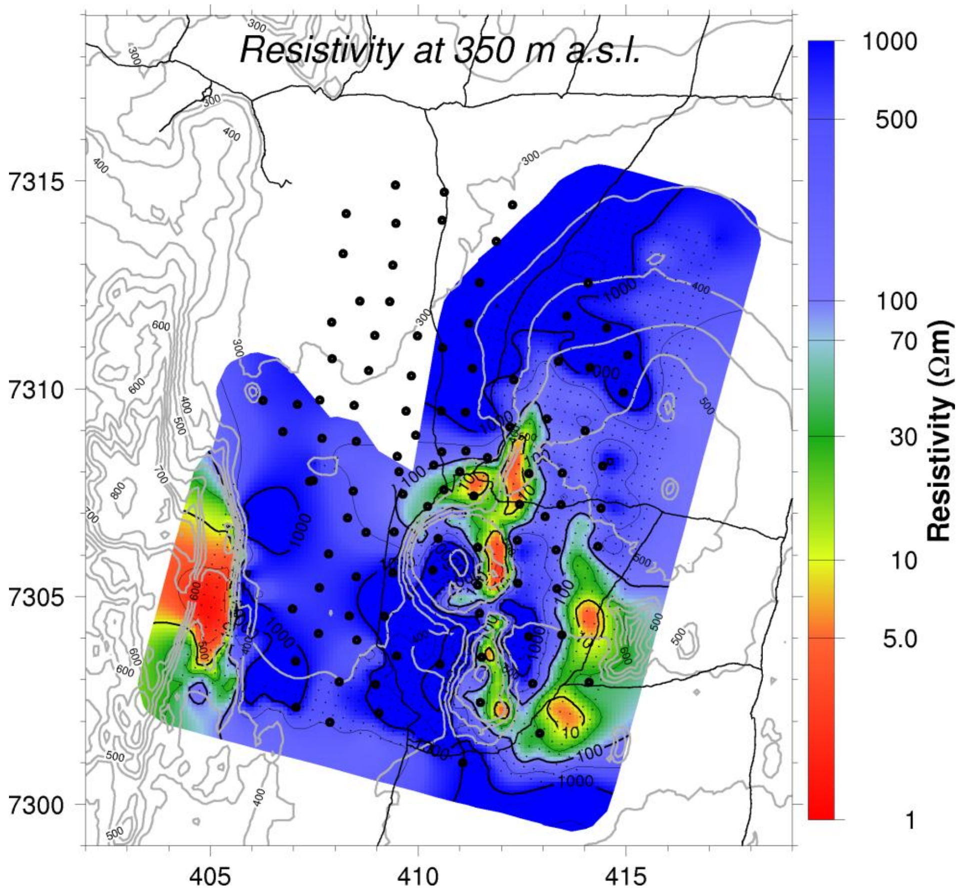
Resistivity at 350 m a.s.l.
Resistivity (Ωm)
1000
500
100
70
30
10
5.0
1
7315
7310
7305
7300
405
410
415

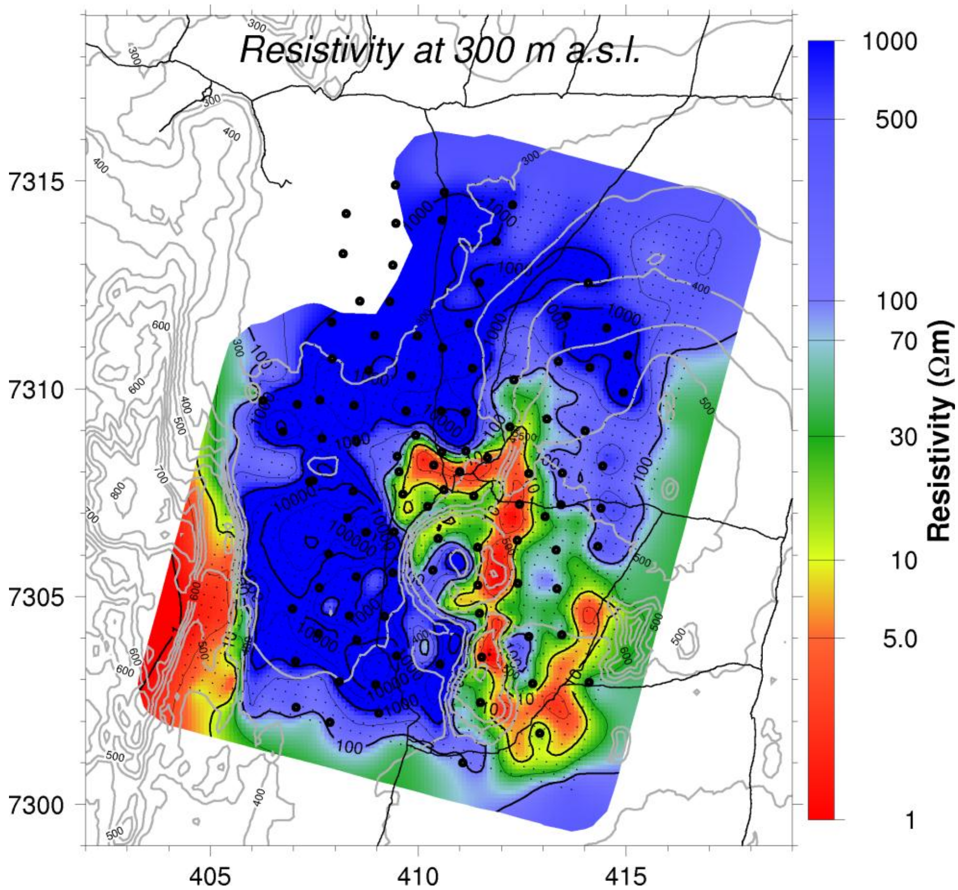
Resistivity at 300 m a.s.l.
Resistivity (Ωm)
1000
500
100
70
30
10
5.0
1
7315
7310
7305
7300
405
410
415

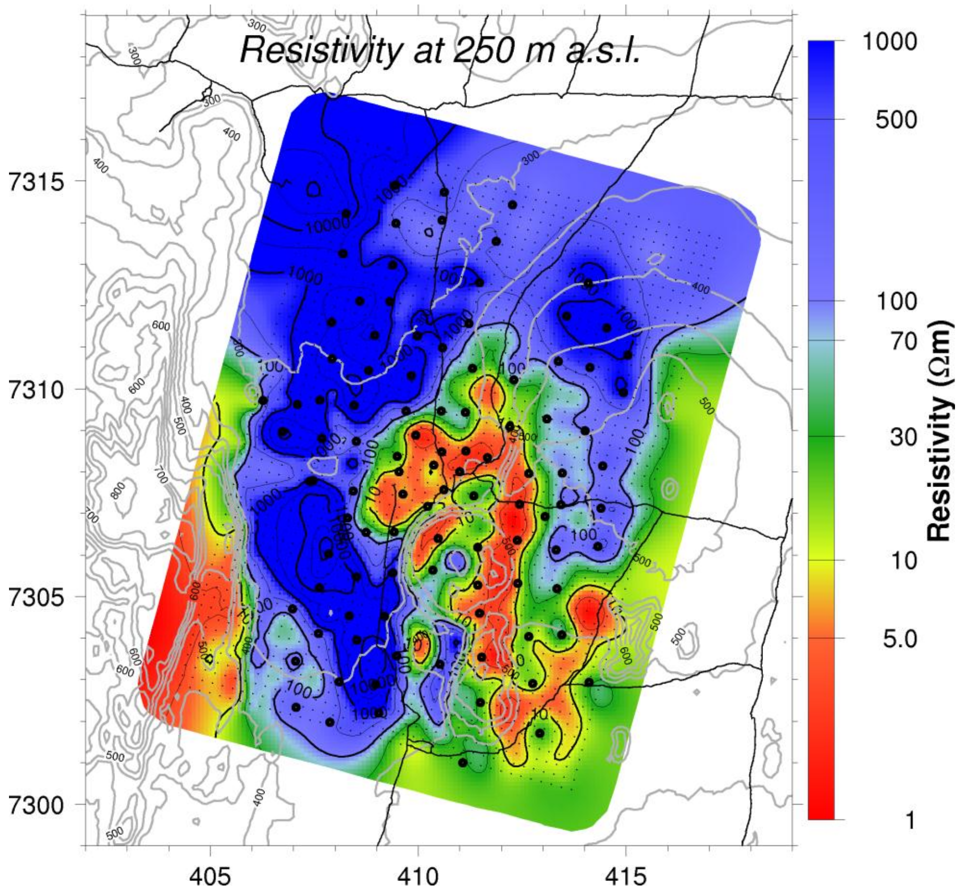
Resistivity at 250 m a.s.l.
Resistivity (Ωm)
1000
500
100
70
30
10
5.0
1
7315
7310
7305
7300
405
410
415

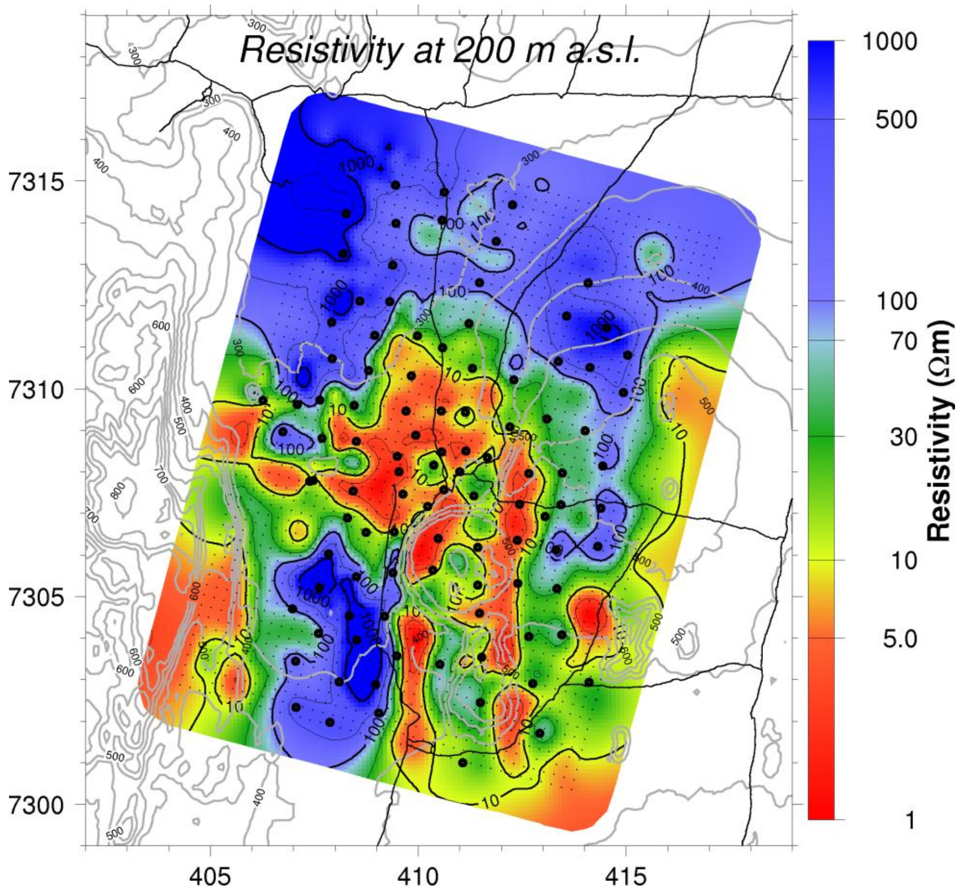
Resistivity at 200 m a.s.l.
7315
7310
7305
7300
405
410
415
1000
500
100
70
30
10
5.0
1
Resistivity (Ωm)

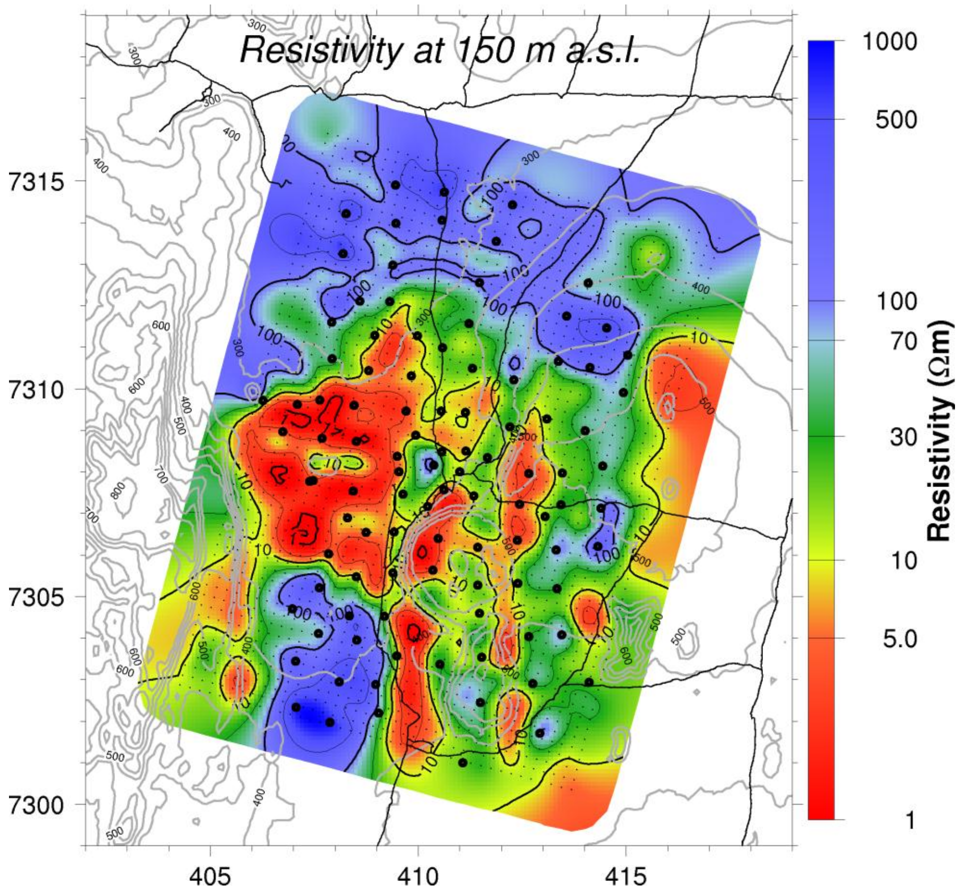
Resistivity at 150 m a.s.l.
7315
7310
7305
7300
405
410
415
1000
500
100
70
30
10
5.0
1
Resistivity (Ωm)

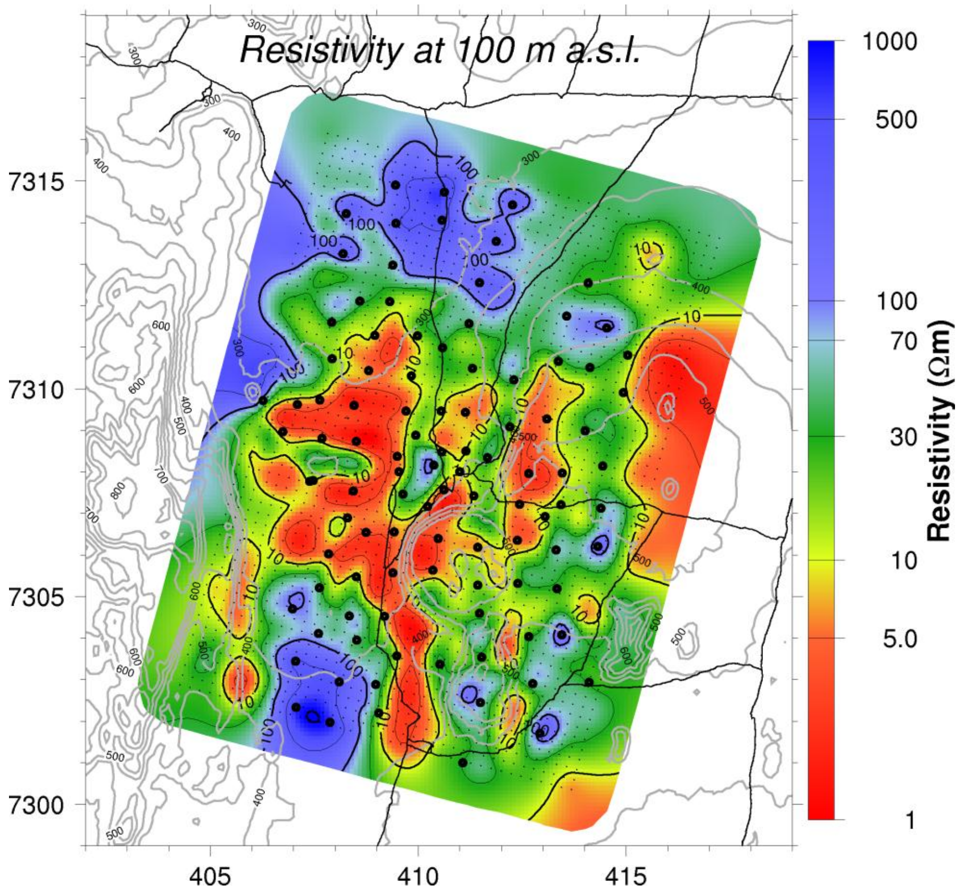
Resistivity at 100 m a.s.l.
Resistivity (Ωm)
1000
500
100
70
30
10
5.0
1
7315
7310
7305
7300
405
410
415

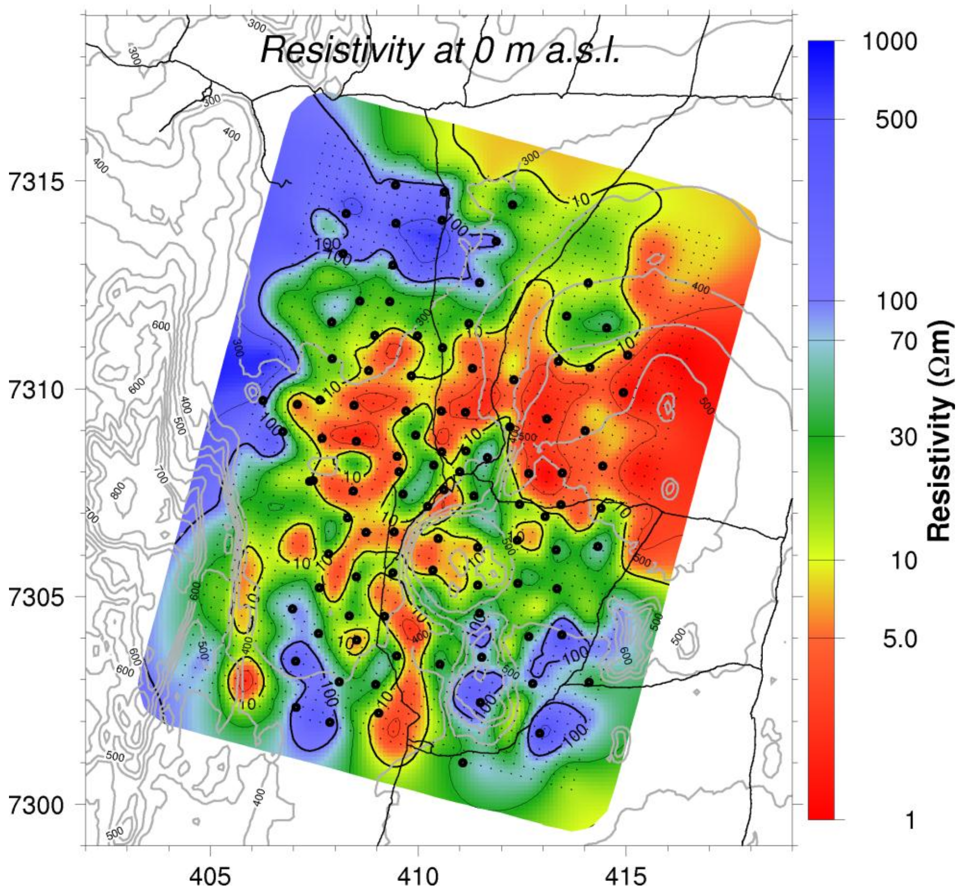
Resistivity at 0 m a.s.l.
Resistivity (Ωm)
1000
500
100
70
30
10
5.0
1
7315
7310
7305
7300
405
410
415

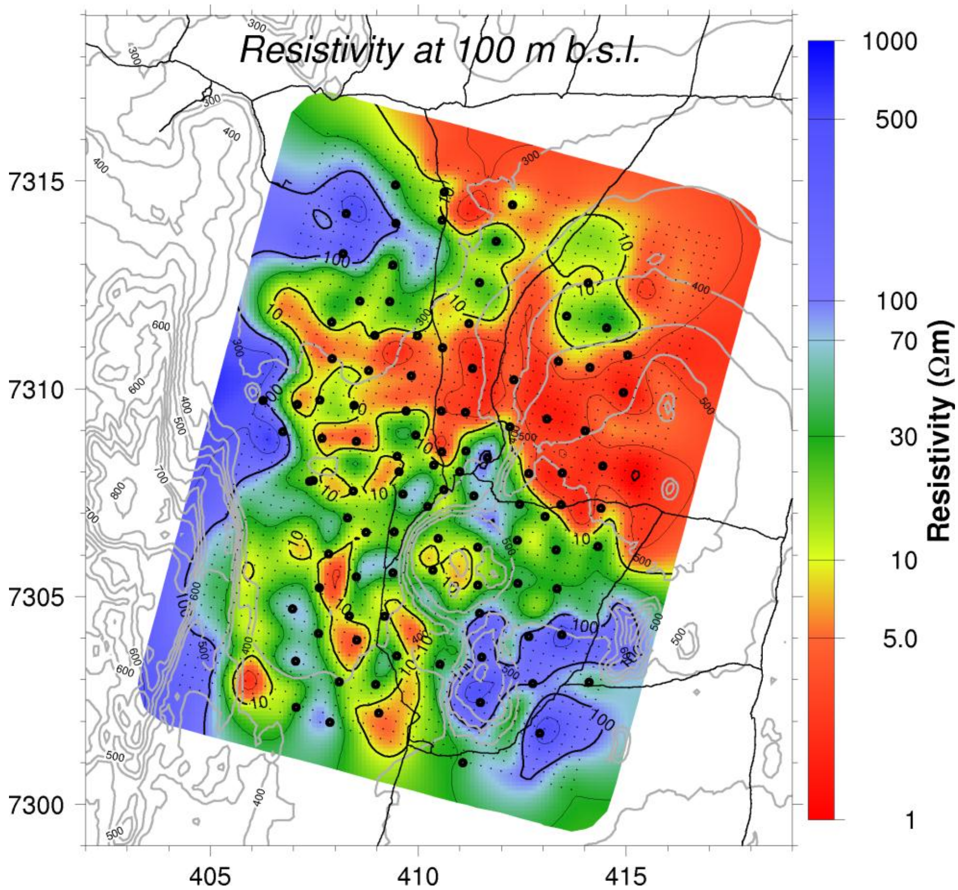
Resistivity at 100 m b.s.l.
Resistivity (Ωm)
1000
500
100
70
30
10
5.0
1
7315
7310
7305
7300
405
410
415

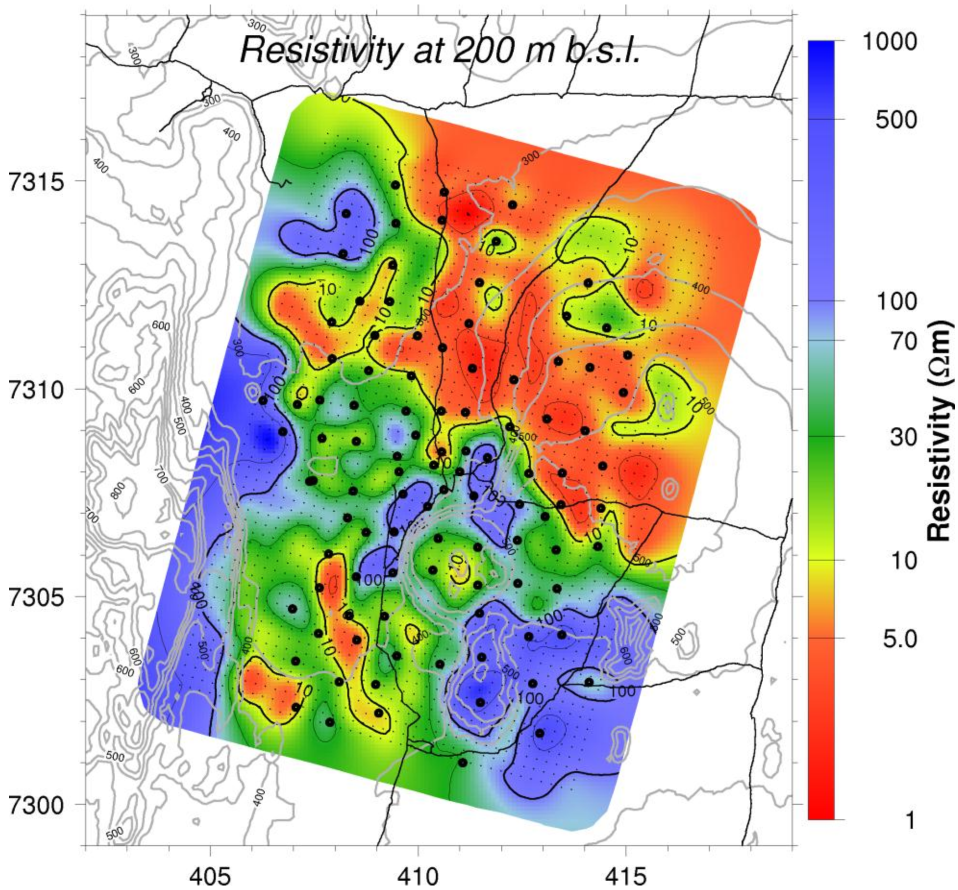
Resistivity at 200 m b.s.l.
Resistivity (Ωm)
1000
500
100
70
30
10
5.0
1
7315
7310
7305
7300
405
410
415

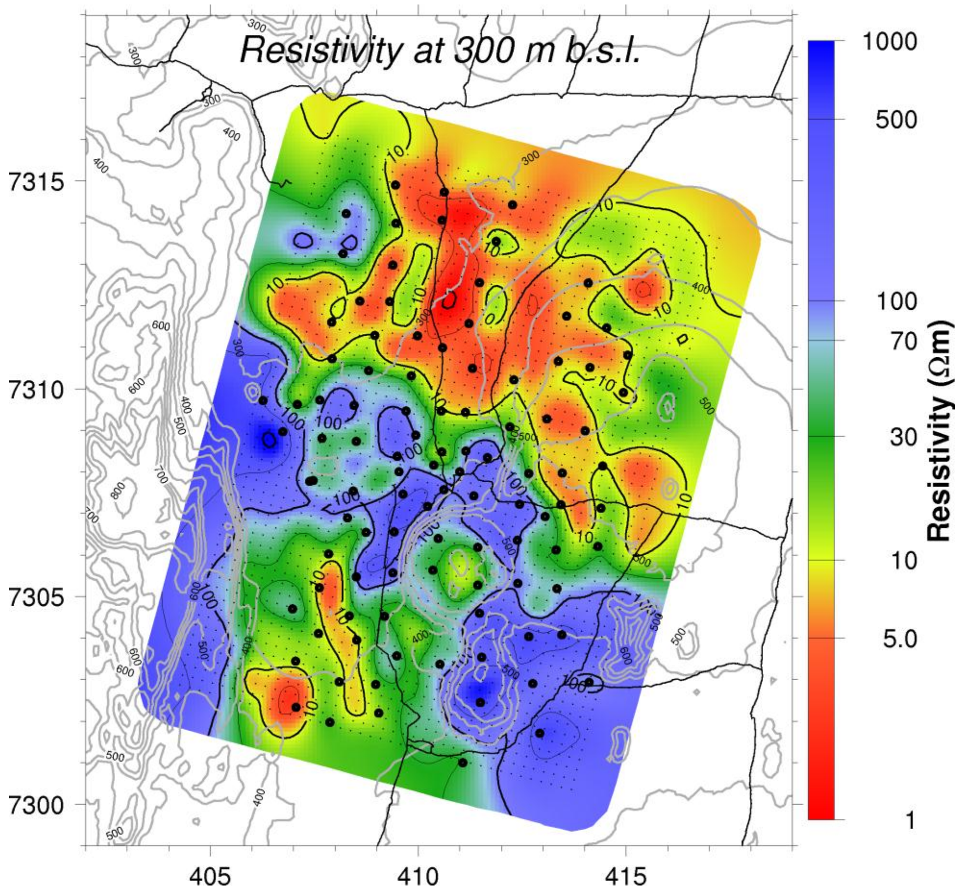
Resistivity at 300 m b.s.l.
Resistivity (Ωm)
1000
500
100
70
30
10
5.0
1
7315
7310
7305
7300
405
410
415

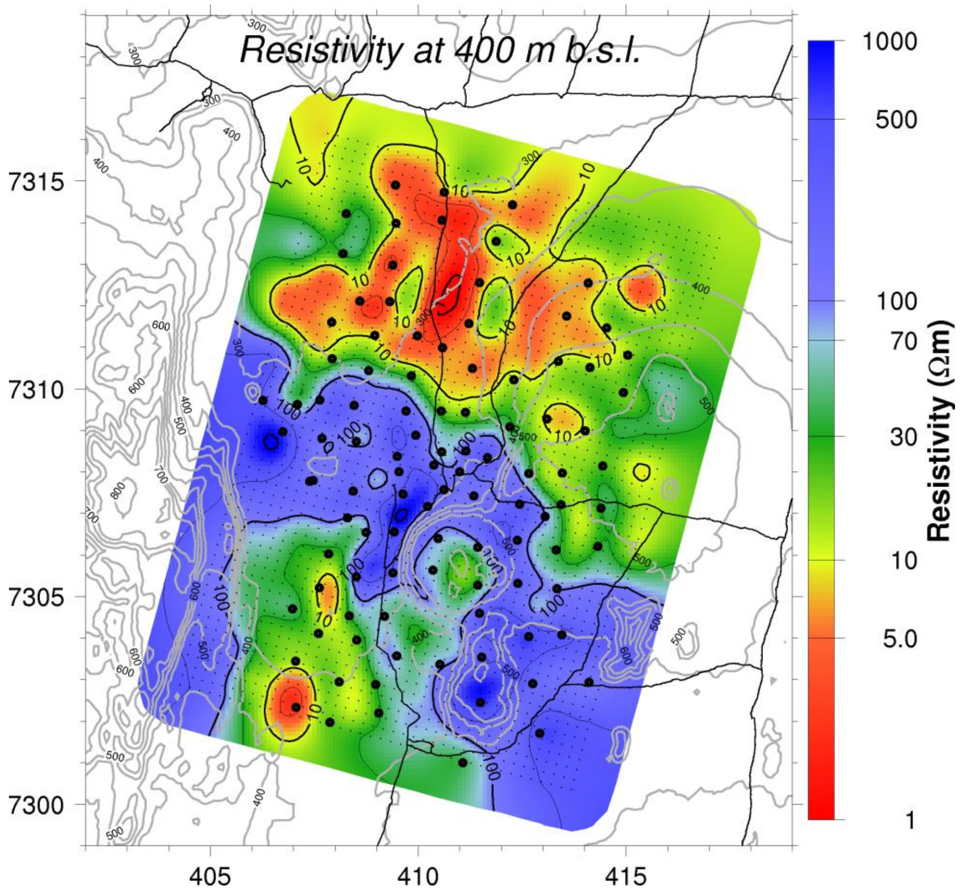
Resistivity at 400 m b.s.l.
Resistivity (Ωm)
1000
500
100
70
30
10
5.0
1
7315
7310
7305
7300
405
410
415

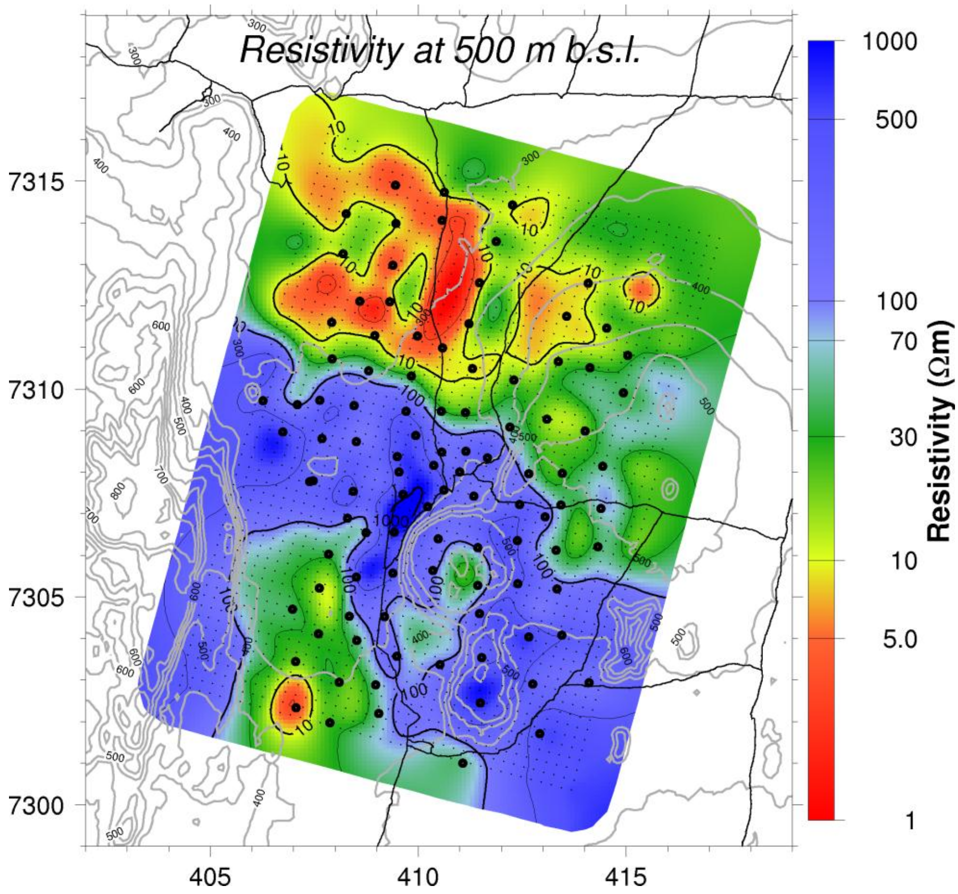
Resistivity at 500 m b.s.l.
Resistivity (Ωm)

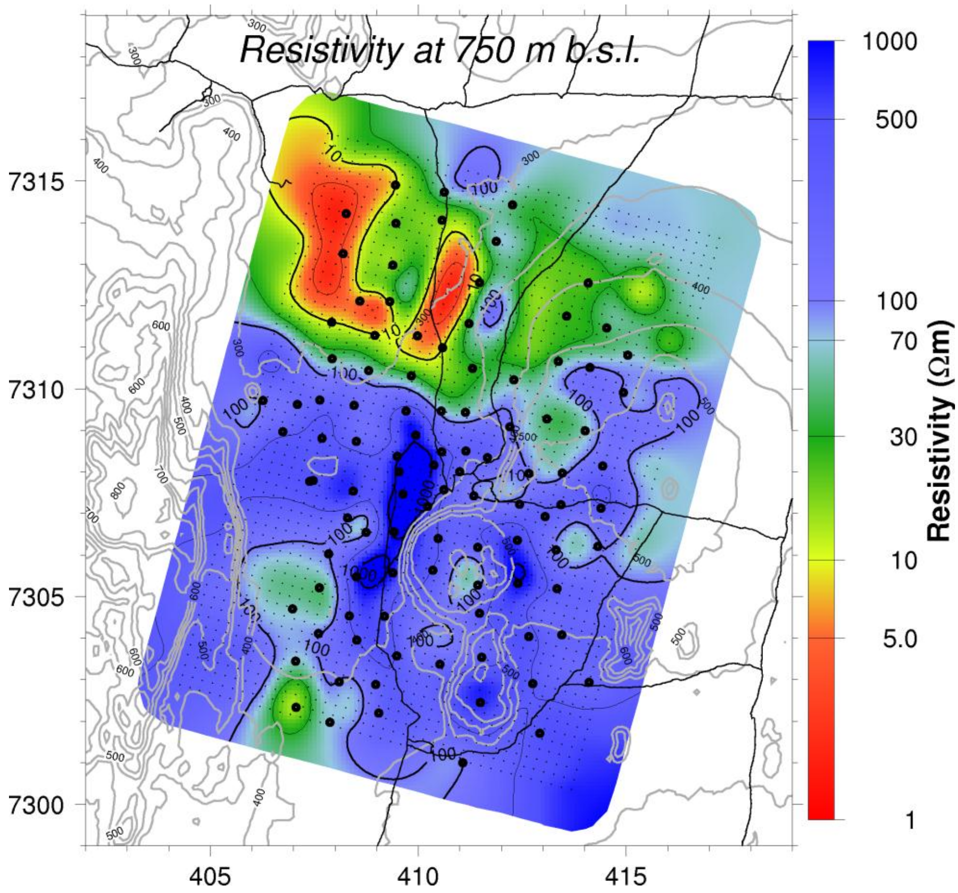
Resistivity at 750 m b.s.l.
Resistivity (Ωm)

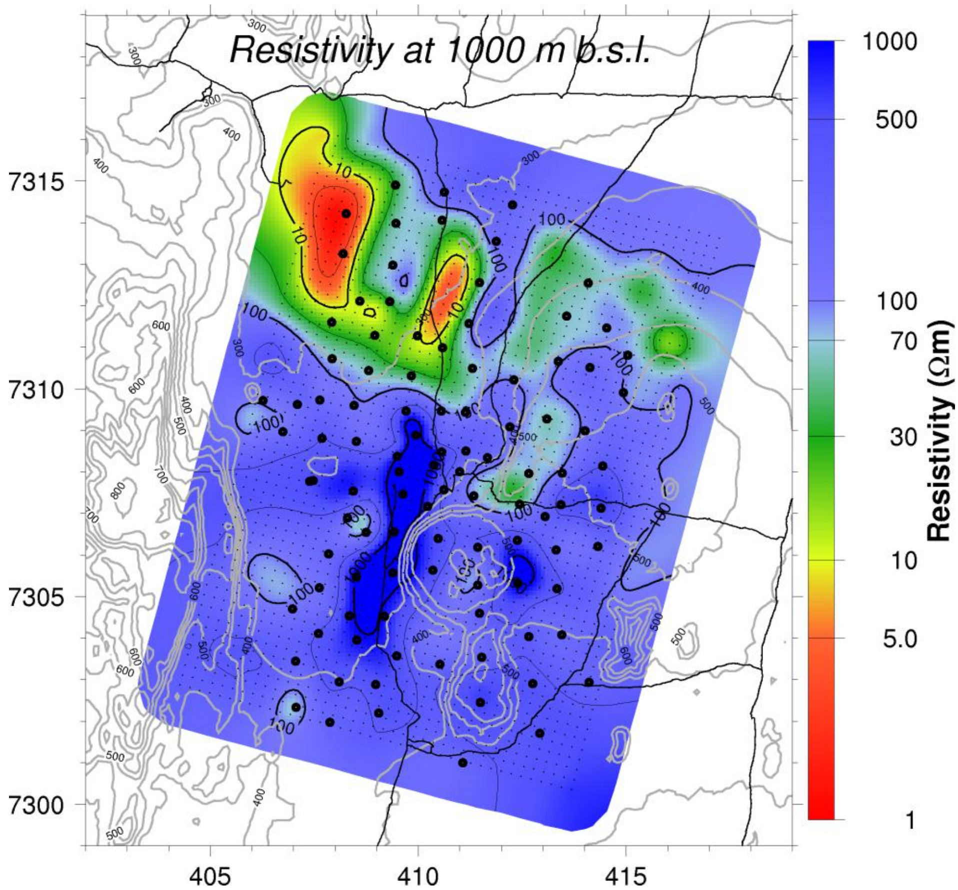
Resistivity at 1000 m b.s.l.
Resistivity (Ωm)
1000
500
100
70
30
10
5.0
1
7315
7310
7305
7300
405
410
415

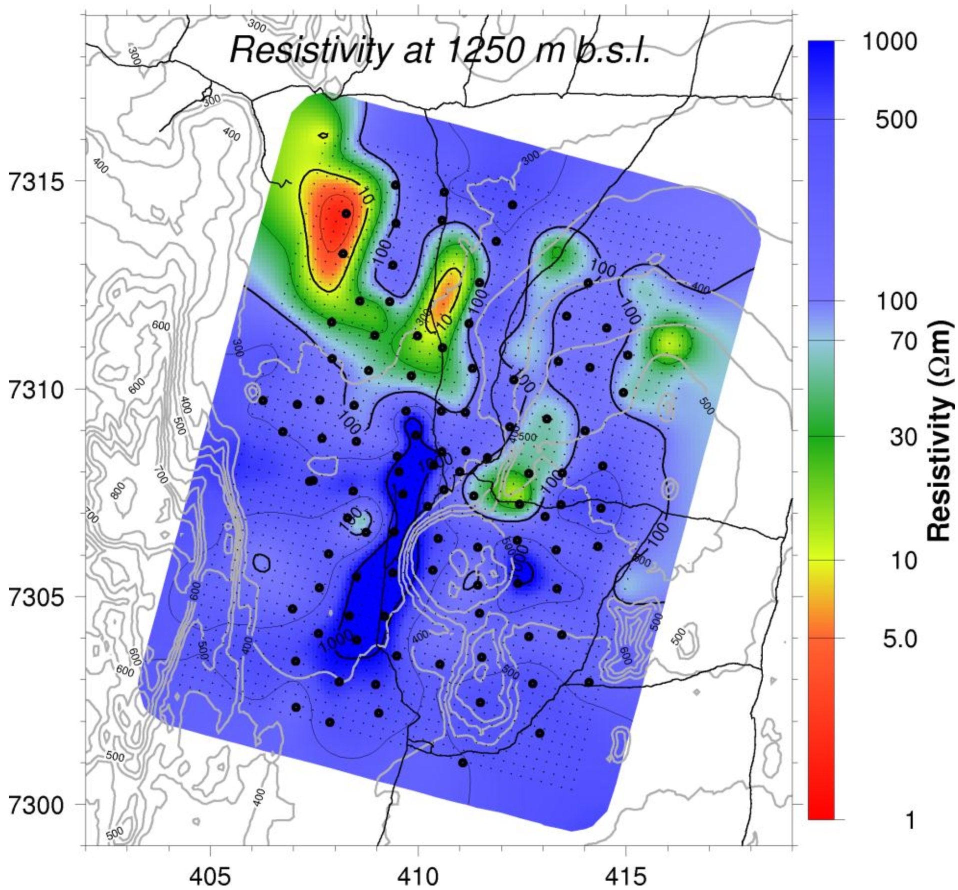
Resistivity at 1250 m b.s.l.
Resistivity (Ωm)
1000
500
100
70
30
10
5.0
1
7315
7310
7305
7300
405
410
415

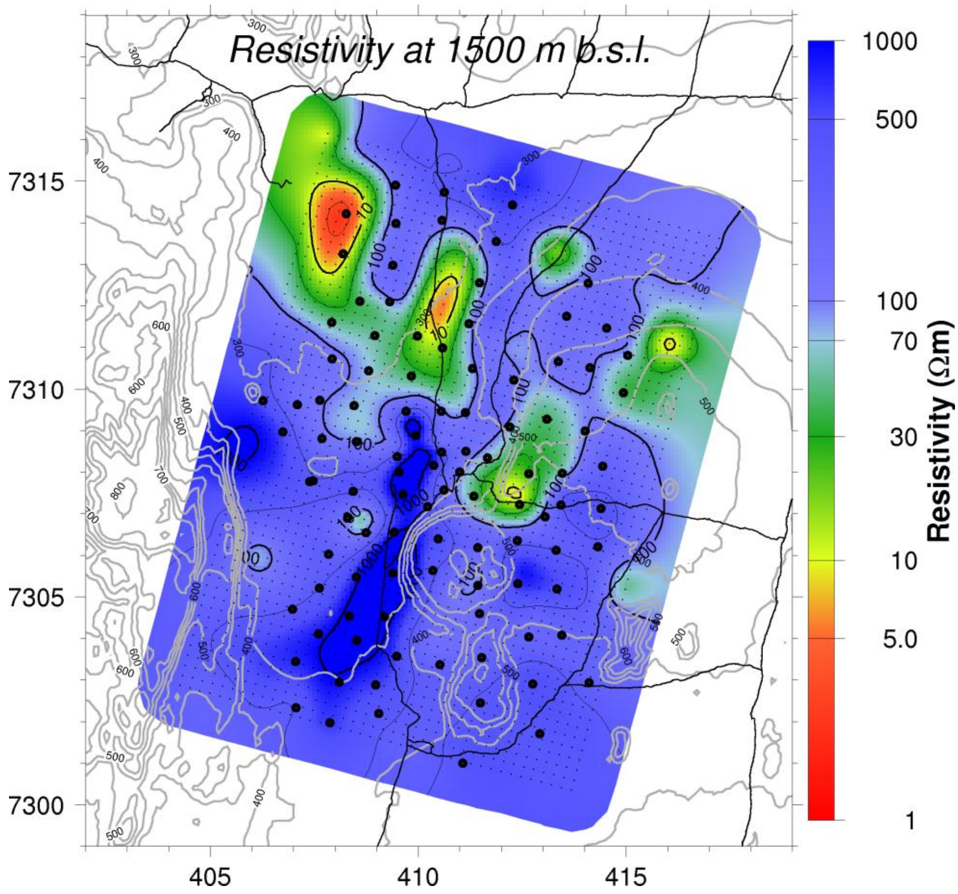
Resistivity at 1500 m b.s.l.
7315
7310
7305
7300
405
410
415
1000
500
100
70
30
10
5.0
1
Resistivity (Ωm)

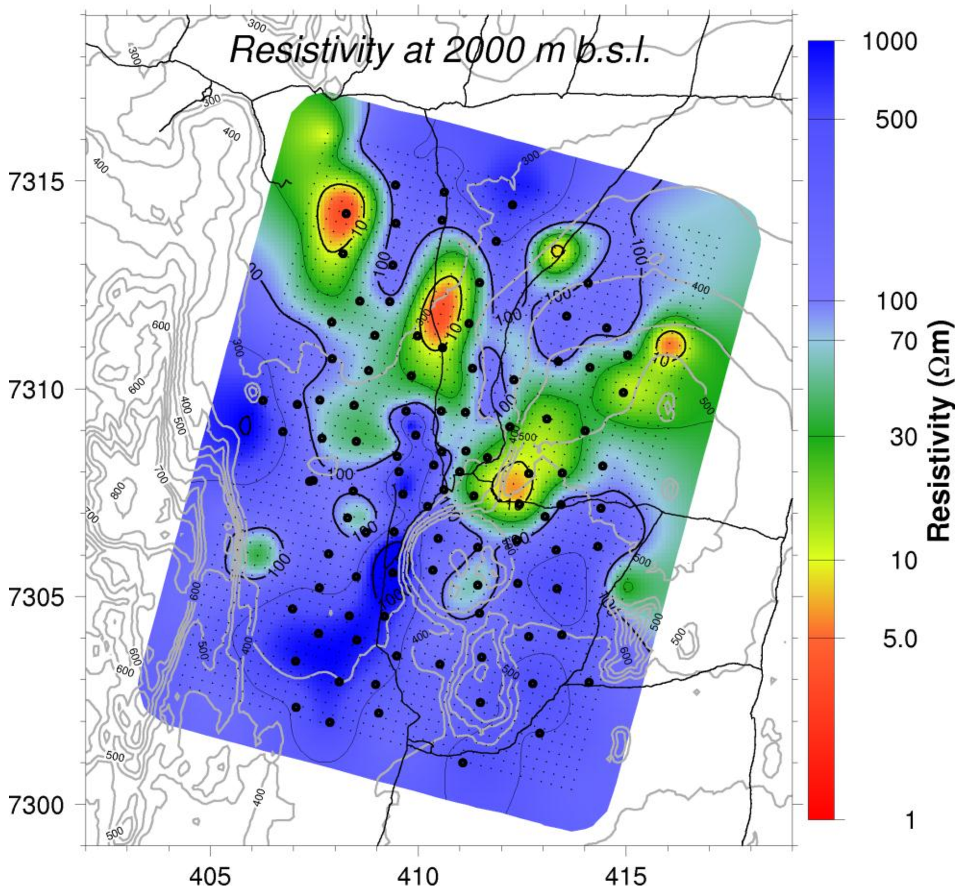
Resistivity at 2000 m b.s.l.
7315
7310
7305
7300
405
410
415
1000
500
100
70
30
10
5.0
1
Resistivity (Ωm)

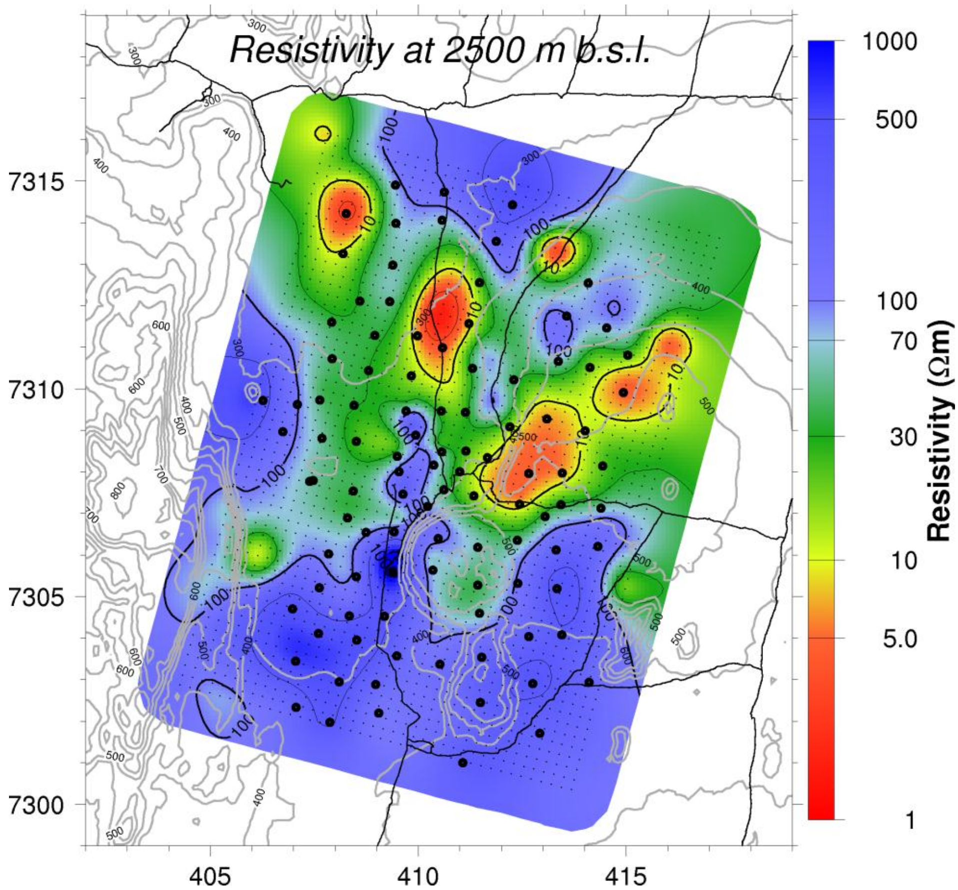
Resistivity at 2500 m b.s.l.
Resistivity (Ωm)
1000
500
100
70
30
10
5.0
1
7315
7310
7305
7300
405
410
415

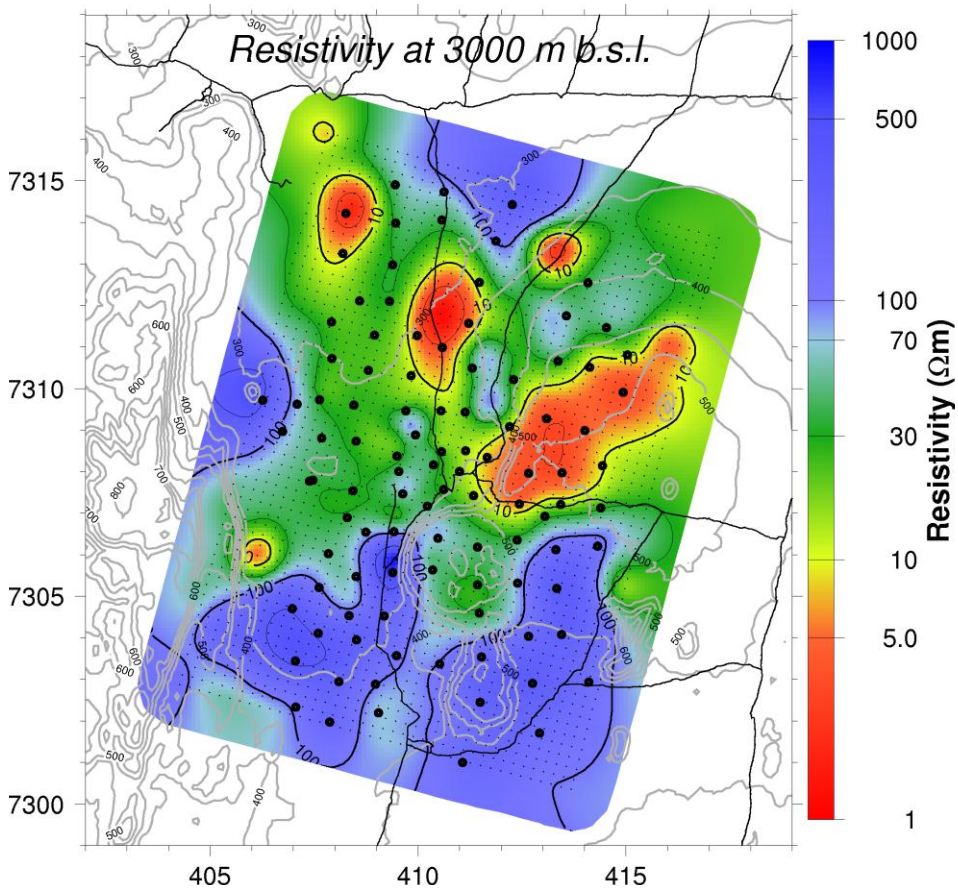
Resistivity at 3000 m b.s.l.
Resistivity (Ωm)
1000
500
100
70
30
10
5.0
1
7315
7310
7305
7300
405
410
415

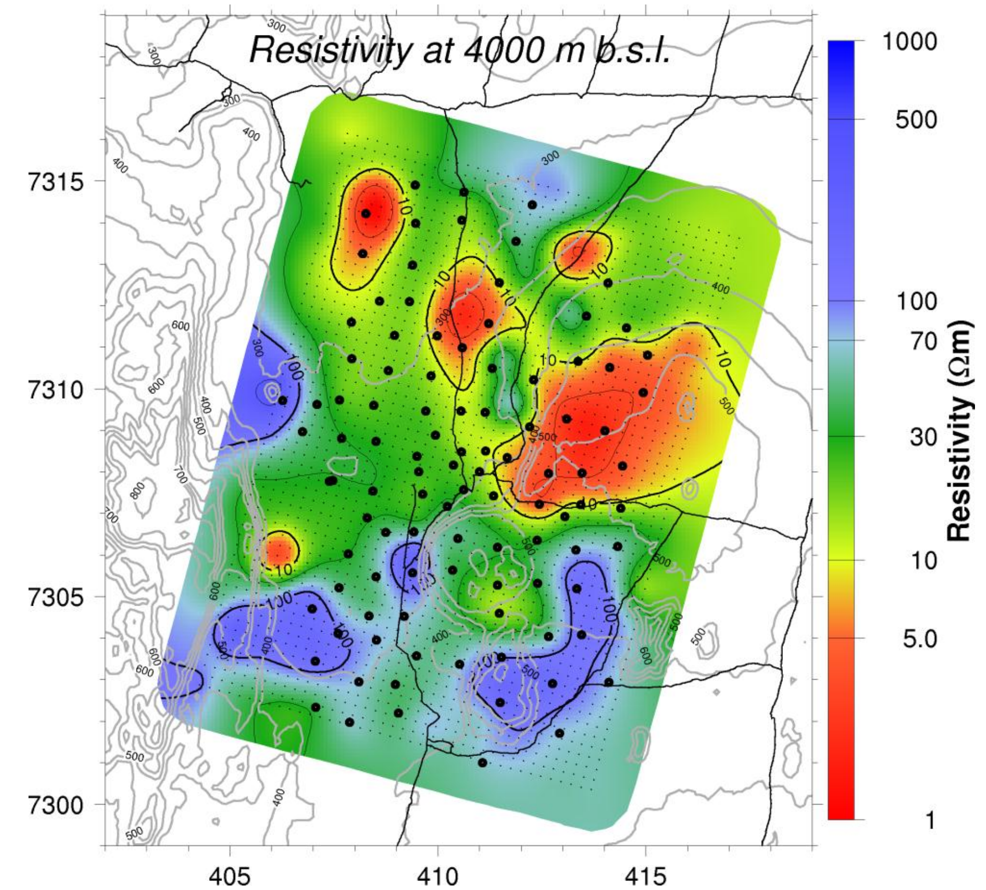

Resistivity at 4000 m b.s.l.
Resistivity (Ωm)
1000
500
100
70
30
10
5.0
1
7315
7310
7305
7300
405
410
415

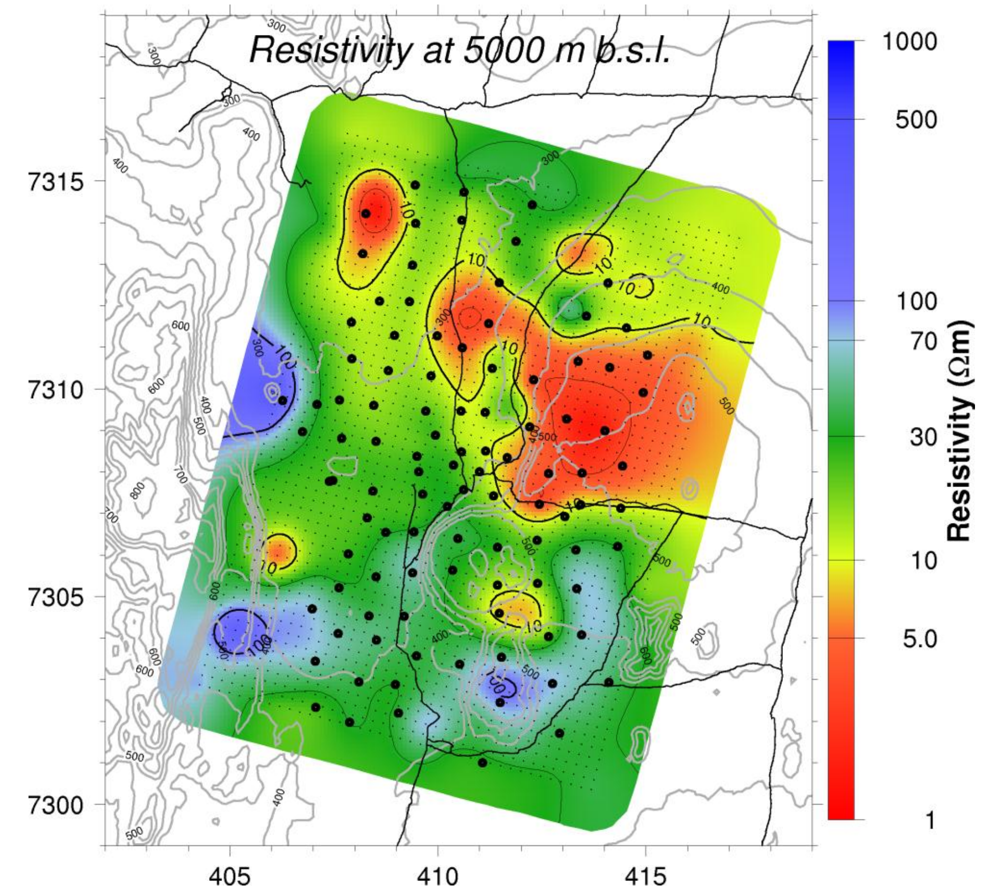

Resistivity at 5000 m b.s.l.
Resistivity (Ωm)
1000
500
100
70
30
10
5.0
1
7315
7310
7305
7300
405
410
415

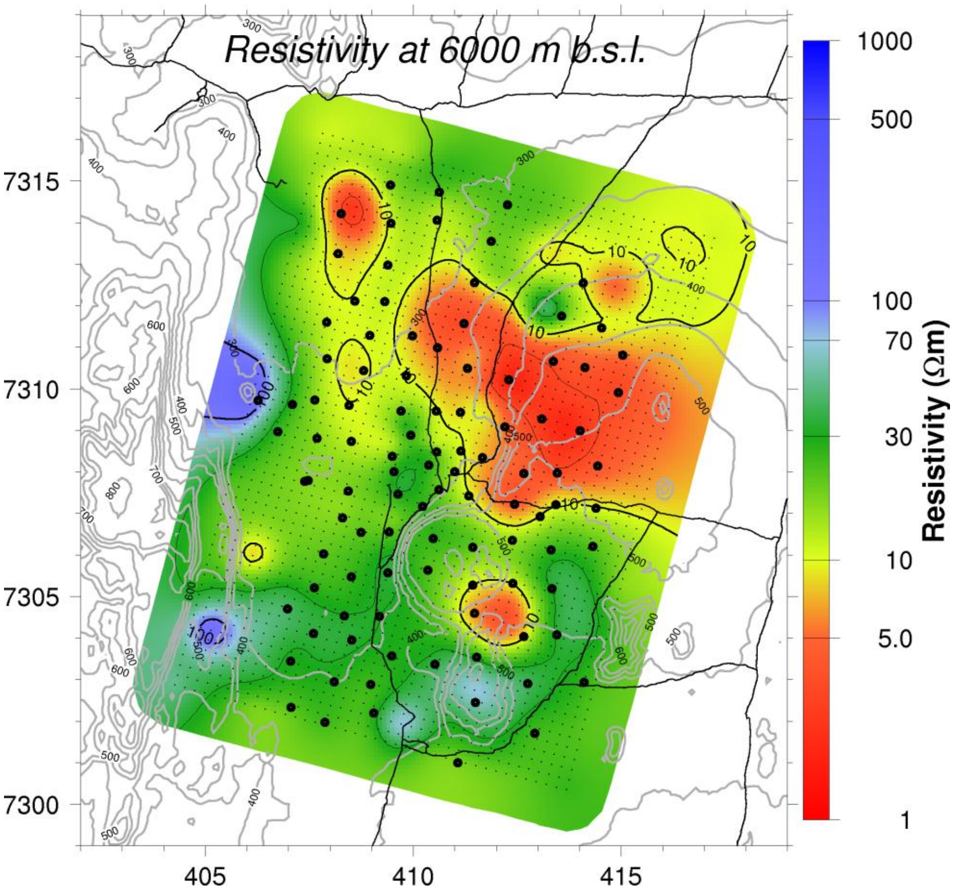
Resistivity at 6000 m b.s.l.
7315
7310
7305
7300
405
410
415
1000
500
100
70
30
10
5.0
1
Resistivity (Ωm)

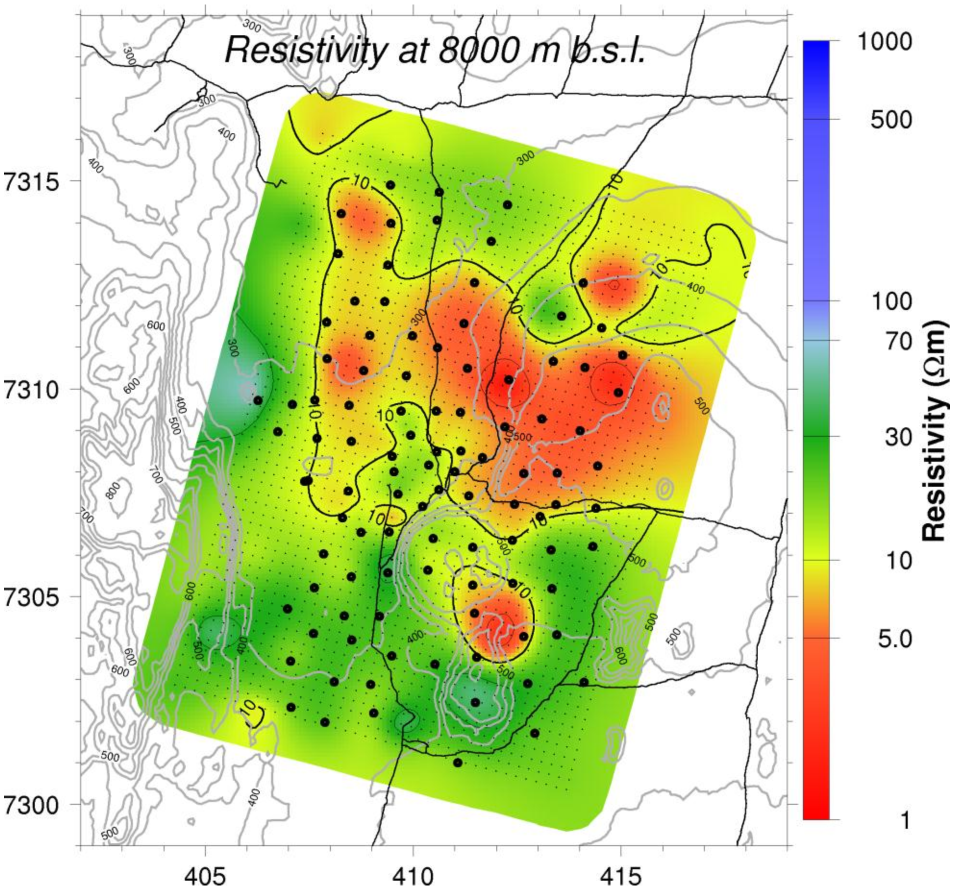
Resistivity at 8000 m b.s.l.
7315
7310
7305
7300
405
410
415
1000
500
100
70
30
10
5.0
1
Resistivity (Ωm)

Appendix 2

North – South
Resistivity cross sections

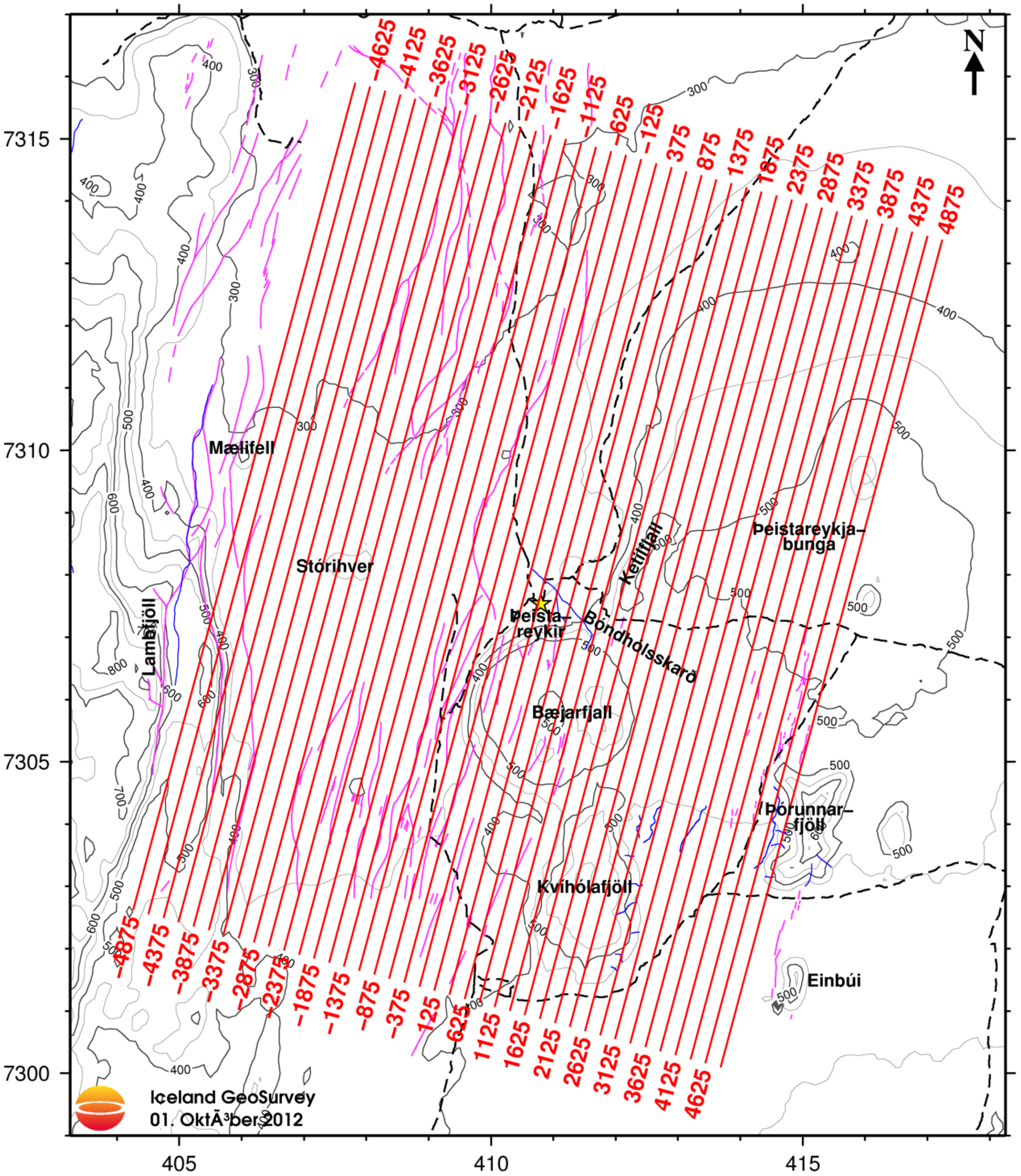

N
7315
7310
7305
7300
405
410
415
-4625
-4125
-3625
-3125
-2625
-2125
-1625
-1125
-625
-125
375
875
1375
1875
2375
2875
3375
3875
4375
4875
-4875
-4375
-3875
-3375
-2875
-2375
-1875
-1375
-875
-375
125
625
1125
1625
2125
2625
3125
3625
4125
4625
Mælifell
Stórihver
Lambafjöll
Þeista-
reykir
Bóndhólsskarð
Ketilfjall
Þeistareykja-
bunga
Bæjarfjall
Þórunnar-
fjöll
Kvíhólafjöll
Einbúi
Iceland GeoSurvey
01. OktÃ³ber 2012

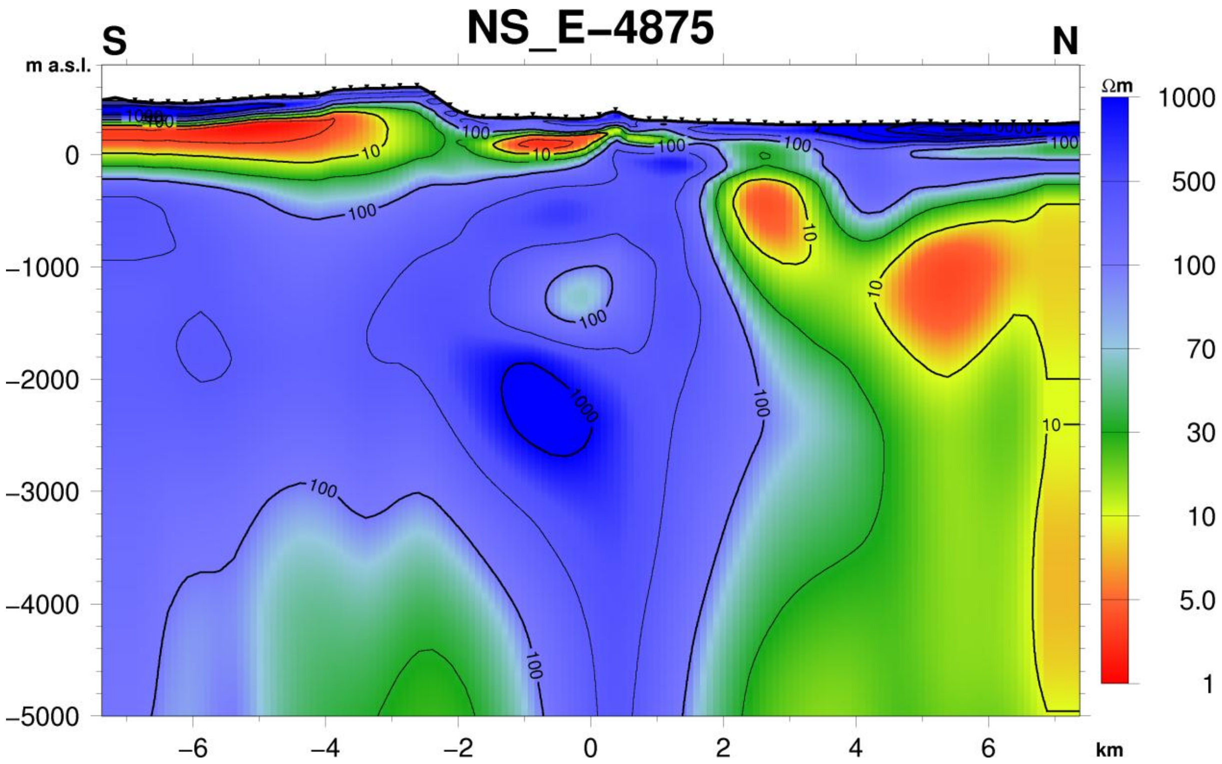
NS_E–4875
S
N
m a.s.l.
Ωm
1000
500
100
70
30
10
5.0
1
0
−1000
−2000
−3000
−4000
−5000
−6
−4
−2
0
2
4
6
km

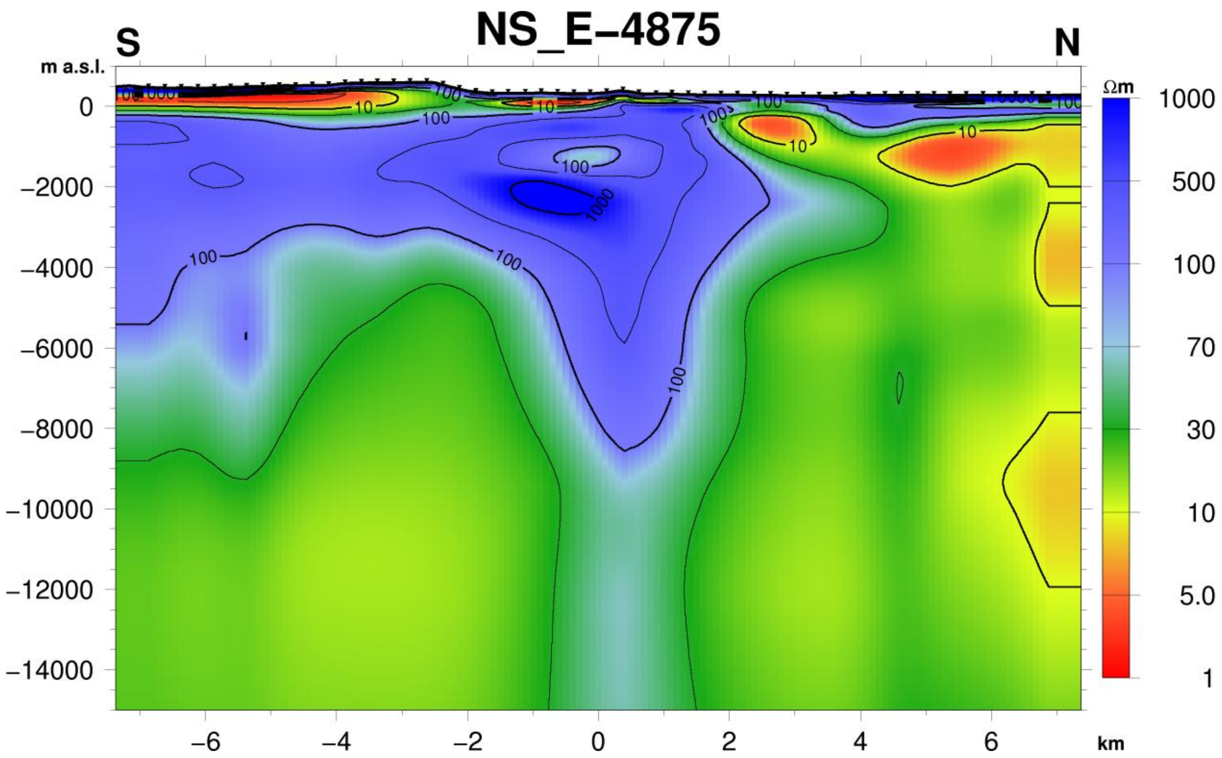
NS_E–4875
S
N
m a.s.l.
Ωm
1000
500
100
70
30
10
5.0
1
0
−2000
−4000
−6000
−8000
−10000
−12000
−14000
−6
−4
−2
0
2
4
6
km

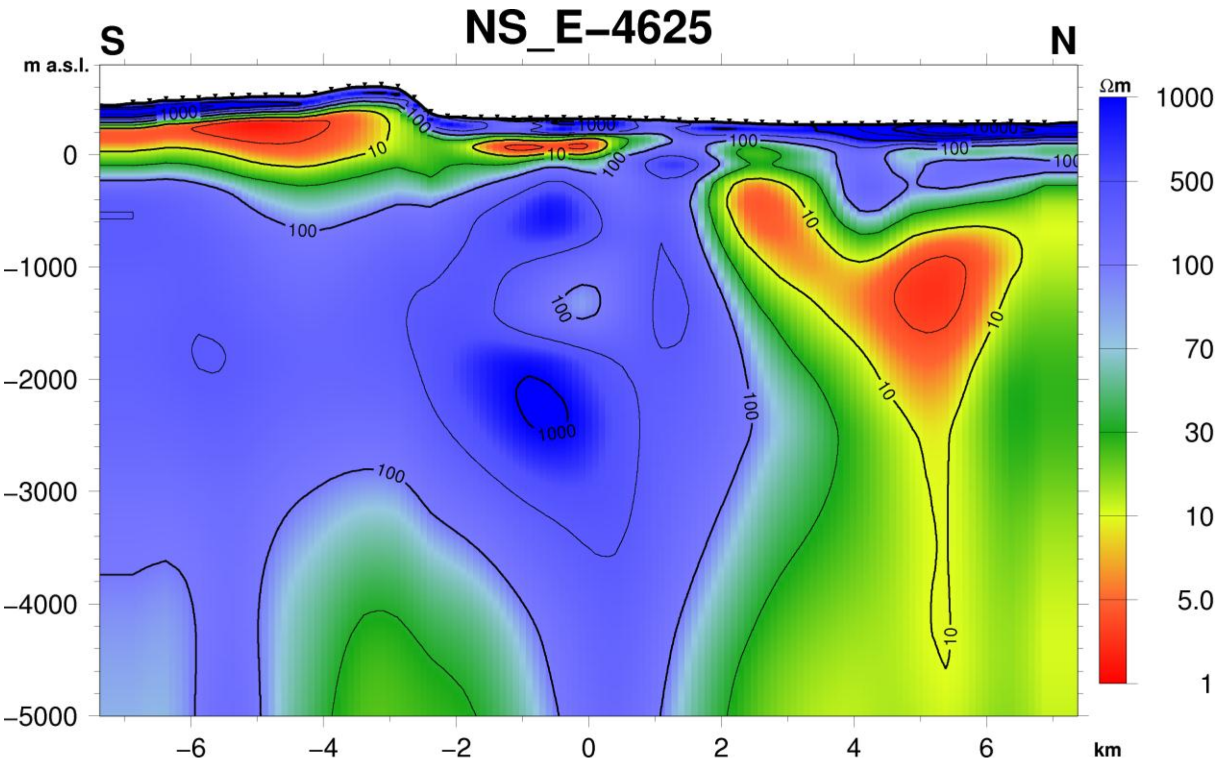
NS_E–4625
S
N
m a.s.l.
0
−1000
−2000
−3000
−4000
−5000
−6
−4
−2
0
2
4
6
km
Ωm
1000
500
100
70
30
10
5.0
1

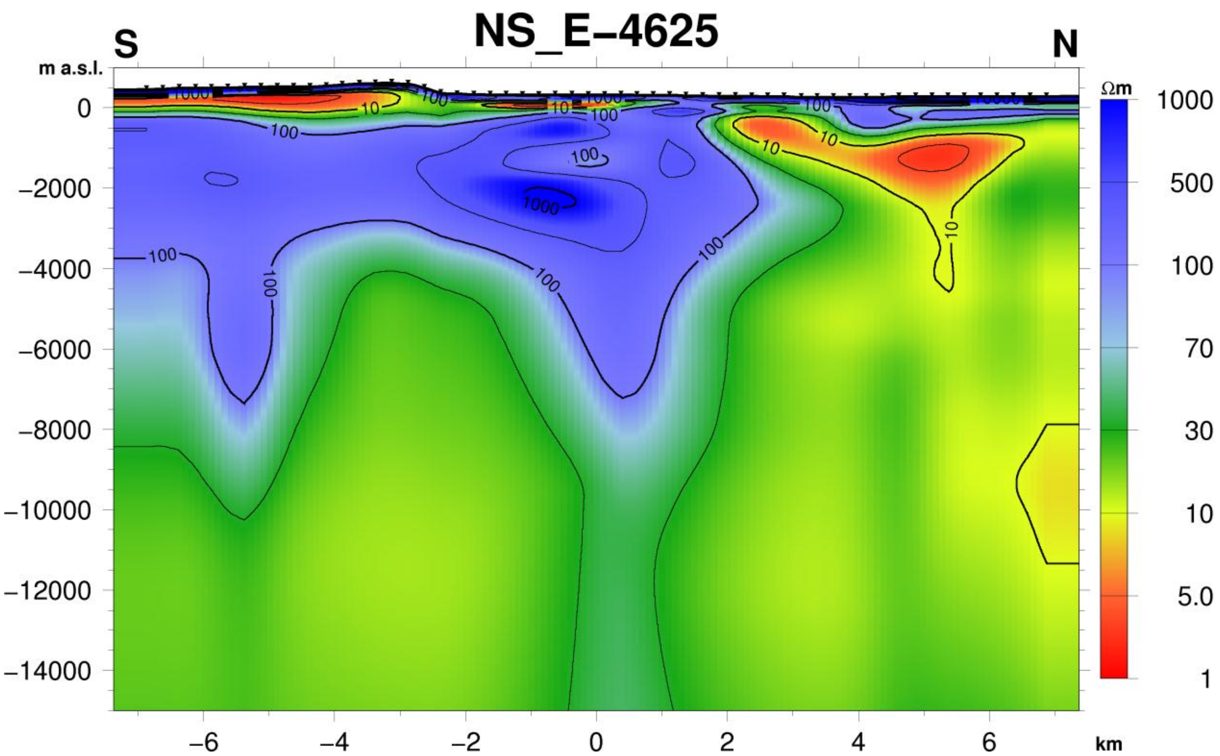
NS_E–4625
S
N
m a.s.l.
0
−2000
−4000
−6000
−8000
−10000
−12000
−14000
−6
−4
−2
0
2
4
6
km
Ωm
1000
500
100
70
30
10
5.0
1

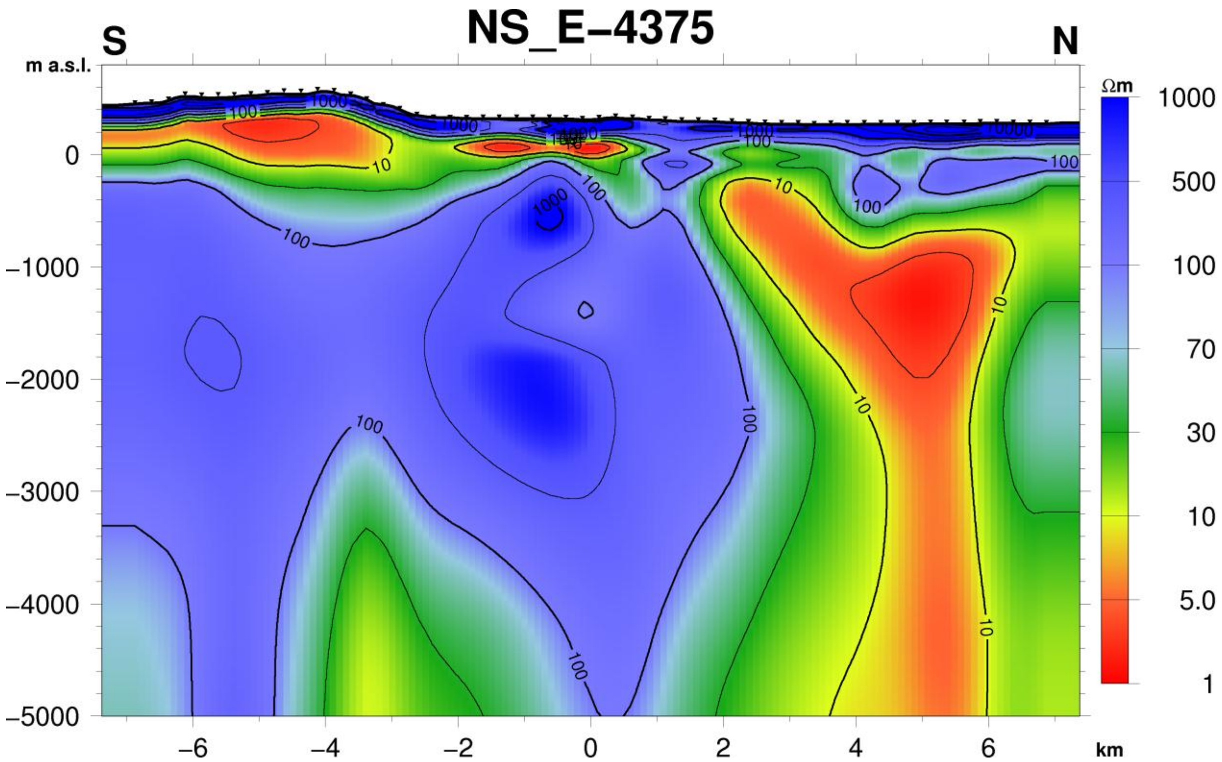

NS_E–4375
S
N
m a.s.l.
Ωm
1000
500
100
70
30
10
5.0
1
0
−1000
−2000
−3000
−4000
−5000
−6
−4
−2
0
2
4
6
km

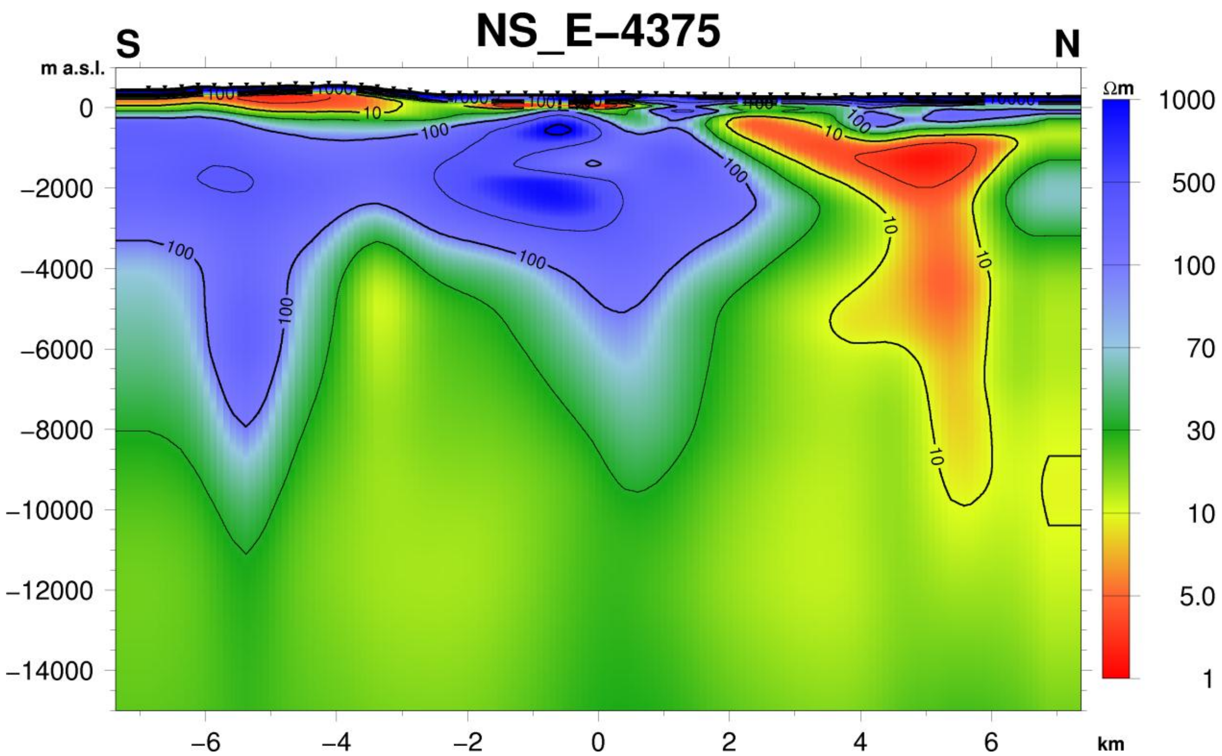

NS_E–4375
S
N
m a.s.l.
Ωm
1000
500
100
70
30
10
5.0
1
0
−2000
−4000
−6000
−8000
−10000
−12000
−14000
−6
−4
−2
0
2
4
6
km

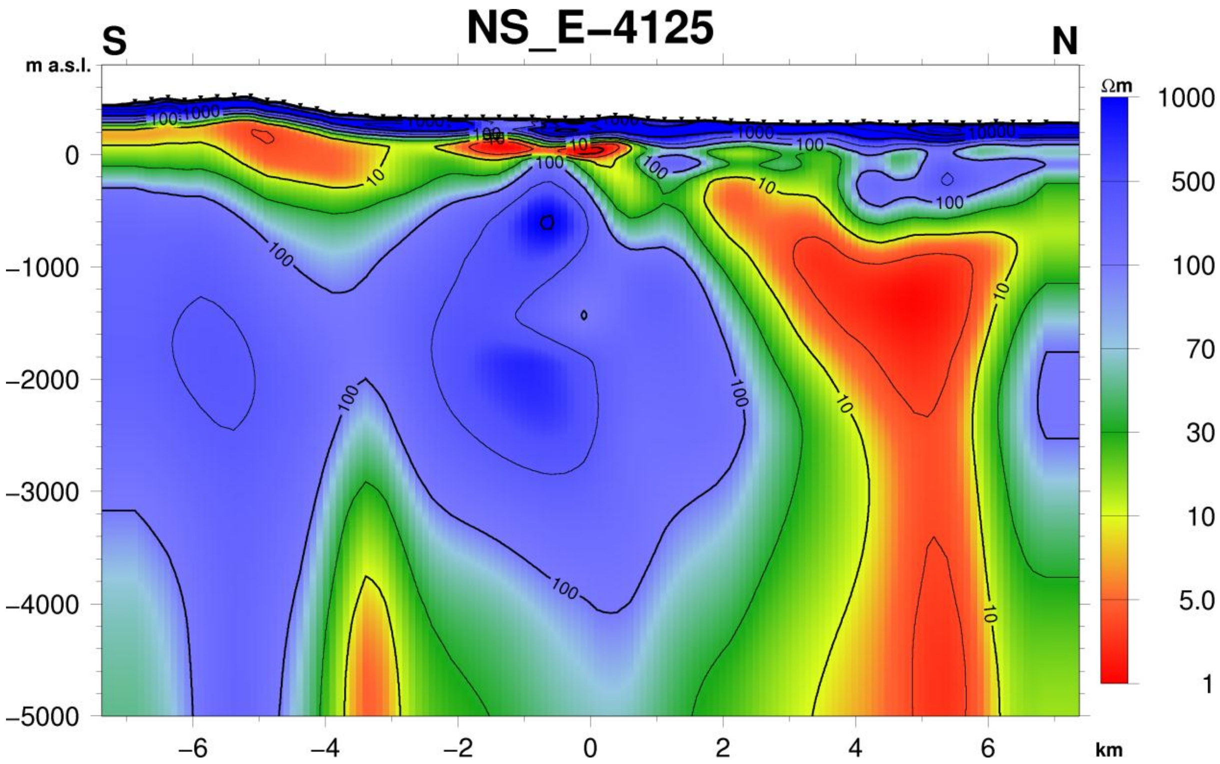
NS_E–4125
S
N
m a.s.l.
0
–1000
–2000
–3000
–4000
–5000
–6
–4
–2
0
2
4
6
km
Ωm
1000
500
100
70
30
10
5.0
1

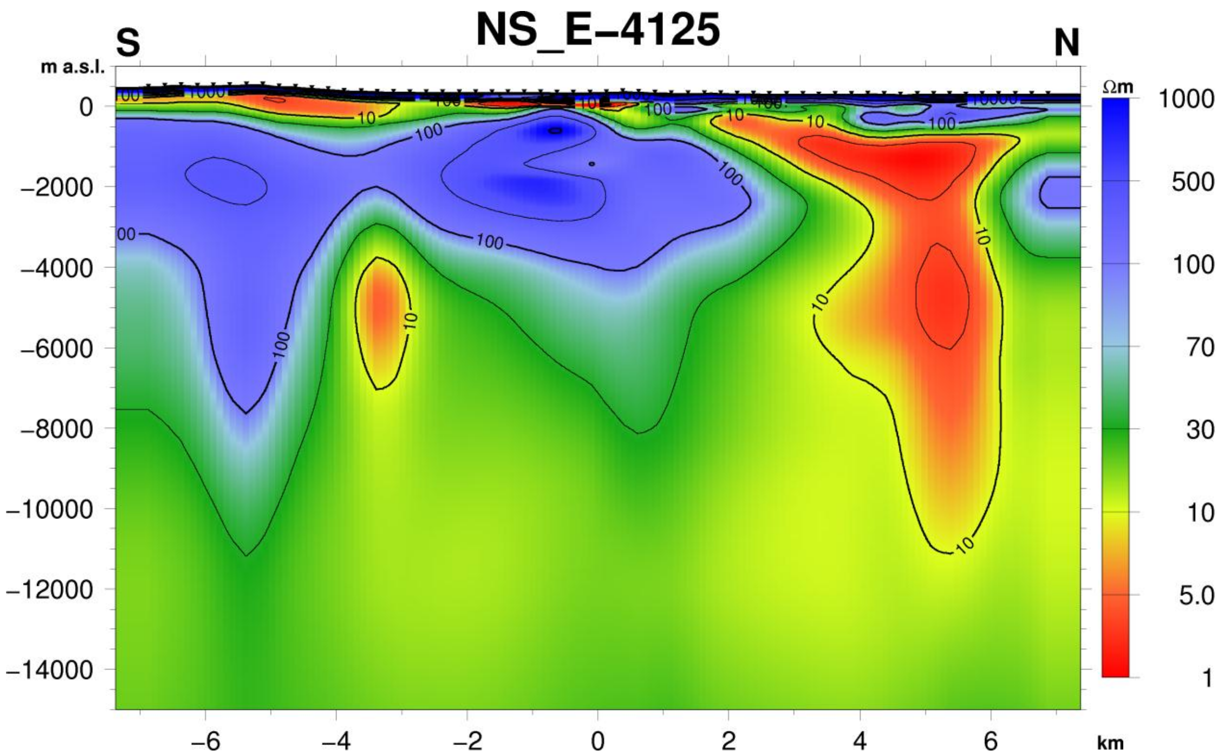
NS_E–4125
S
N
m a.s.l.
0
–2000
–4000
–6000
–8000
–10000
–12000
–14000
–6
–4
–2
0
2
4
6
km
Ωm
1000
500
100
70
30
10
5.0
1

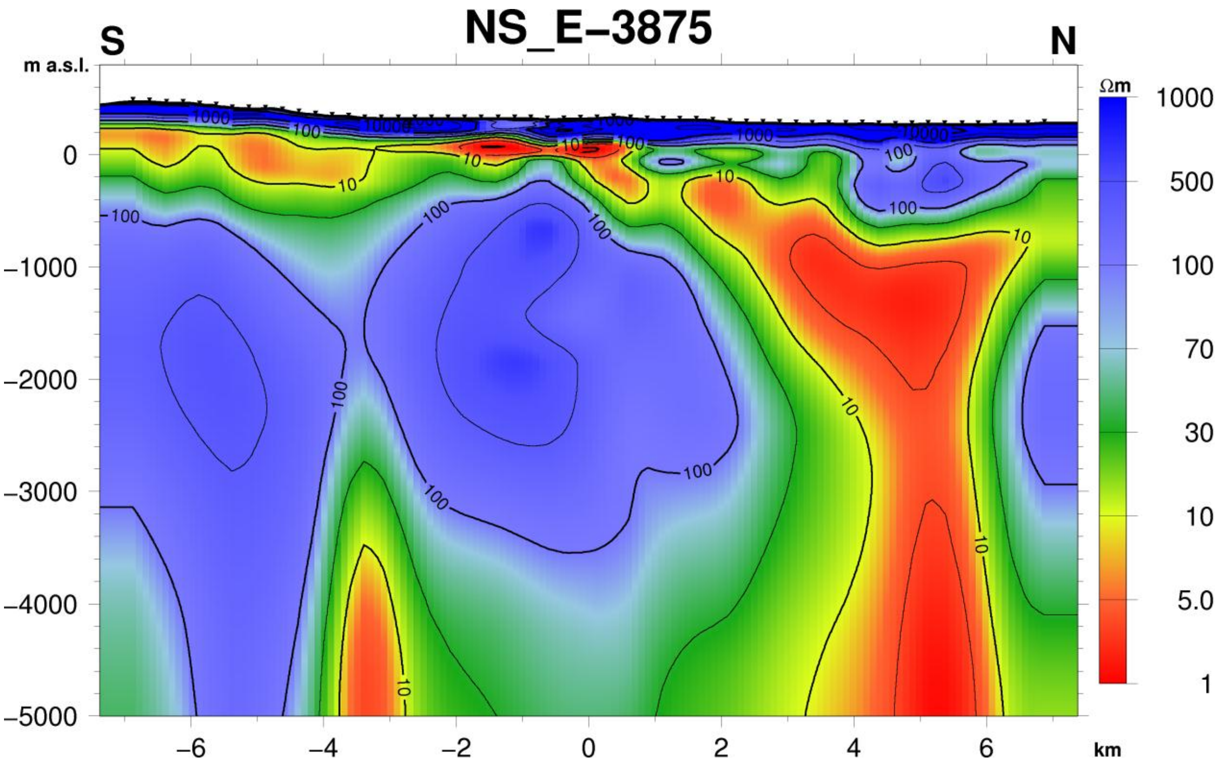
NS_E–3875
S
N
m a.s.l.
Ωm
1000
500
100
70
30
10
5.0
1
0
−1000
−2000
−3000
−4000
−5000
−6
−4
−2
0
2
4
6
km

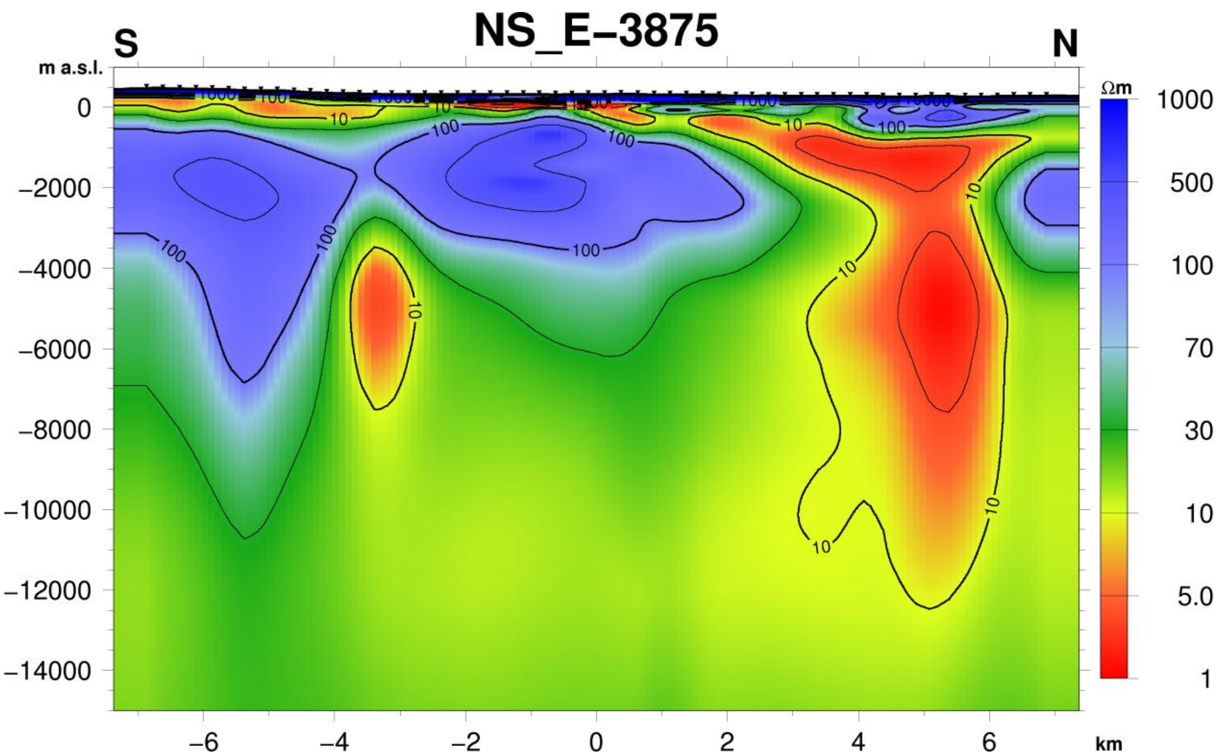
NS_E–3875
S
N
m a.s.l.
Ωm
1000
500
100
70
30
10
5.0
1
0
−2000
−4000
−6000
−8000
−10000
−12000
−14000
−6
−4
−2
0
2
4
6
km

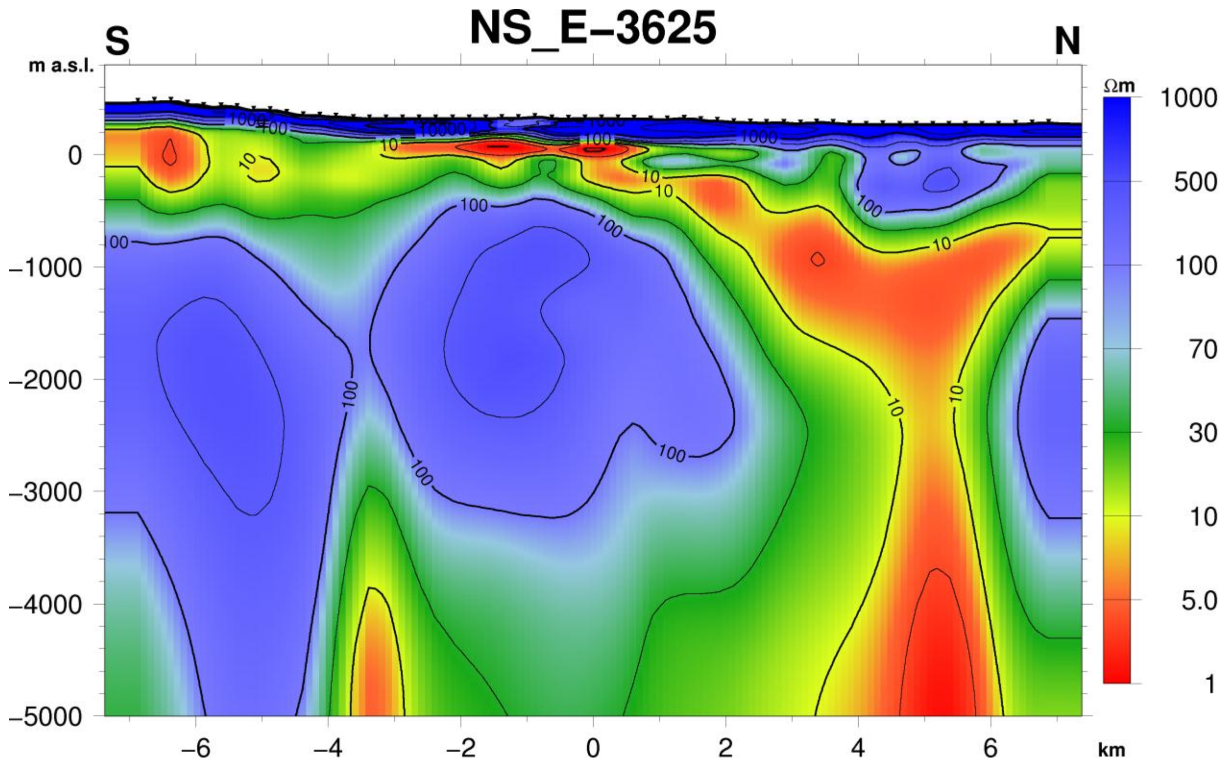
NS_E–3625
S
N
m a.s.l.
Ωm
km

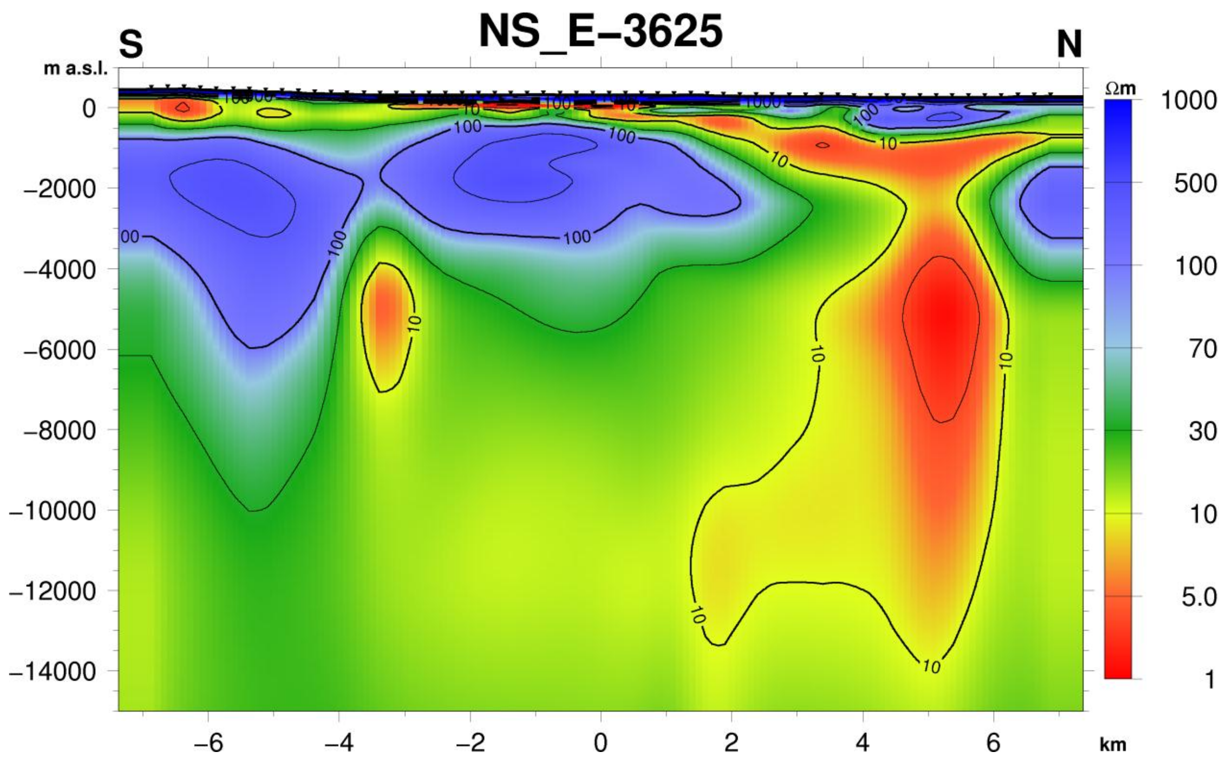
NS_E–3625
S
N
m a.s.l.
Ωm
km

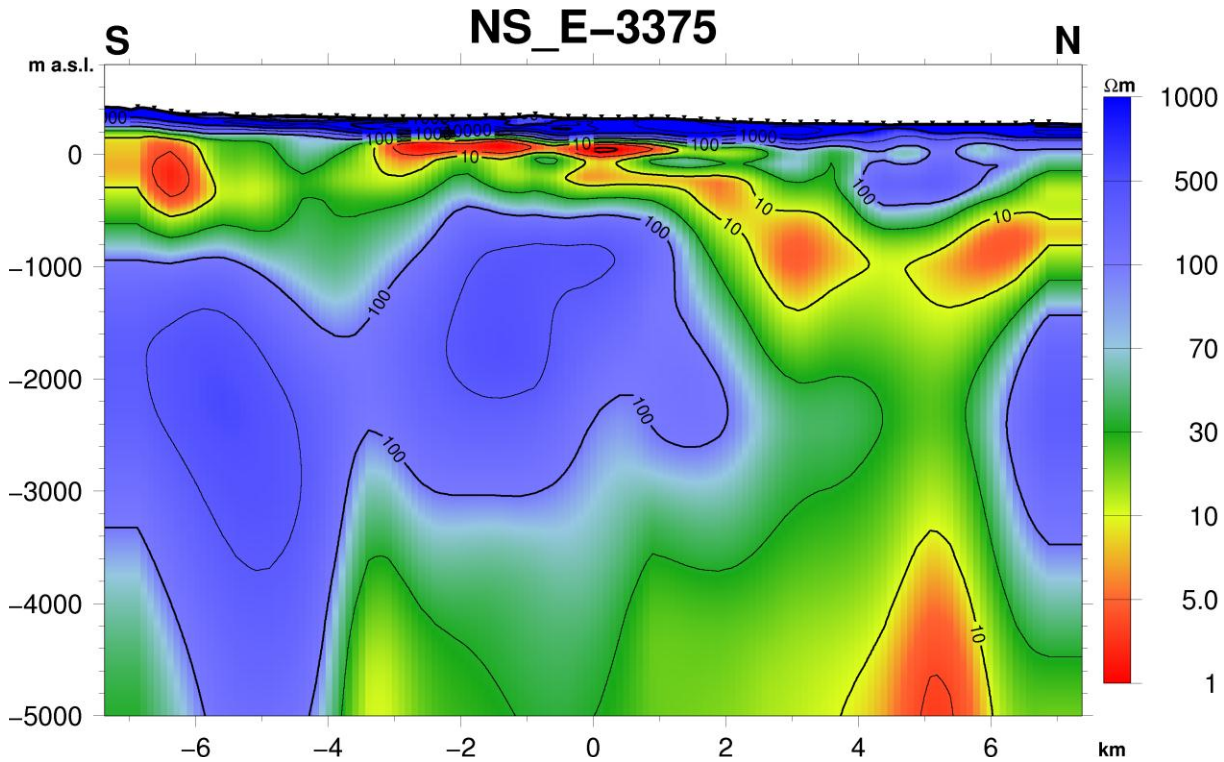
NS_E–3375
S
N
m a.s.l.
Ωm
1000
500
100
70
30
10
5.0
1
0
−1000
−2000
−3000
−4000
−5000
−6
−4
−2
0
2
4
6
km

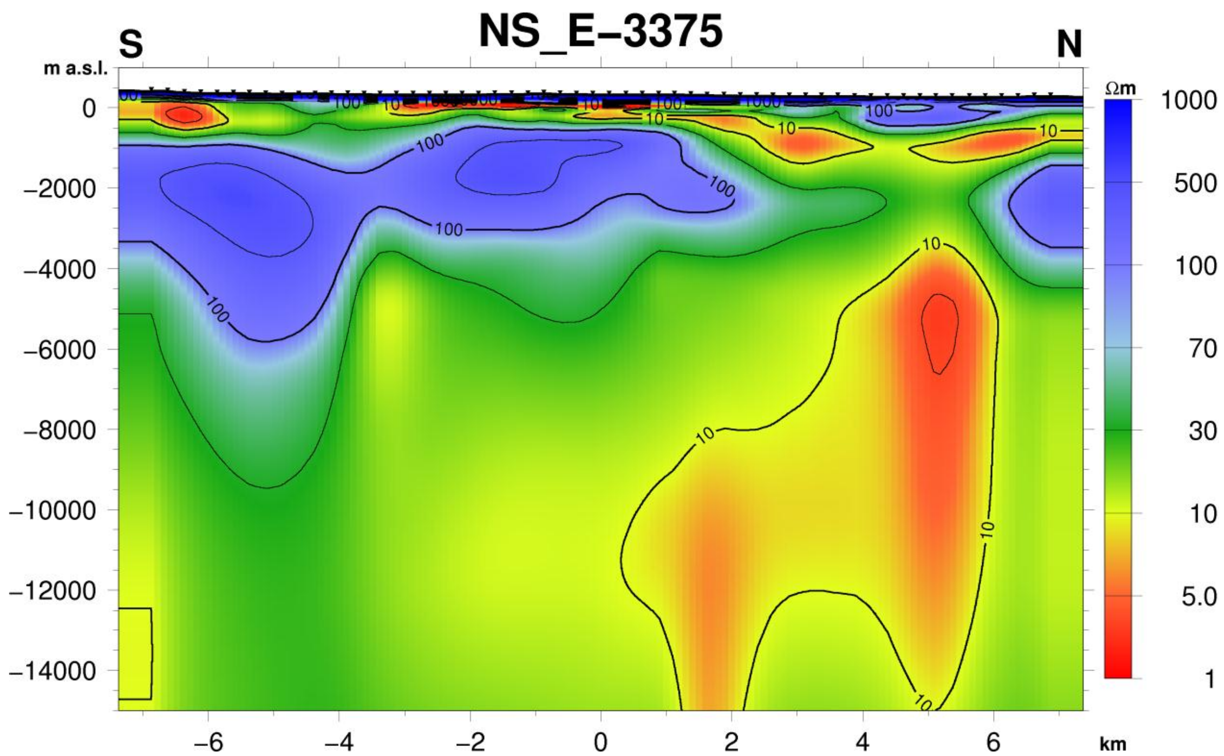
NS_E–3375
S
N
m a.s.l.
Ωm
1000
500
100
70
30
10
5.0
1
0
−2000
−4000
−6000
−8000
−10000
−12000
−14000
−6
−4
−2
0
2
4
6
km

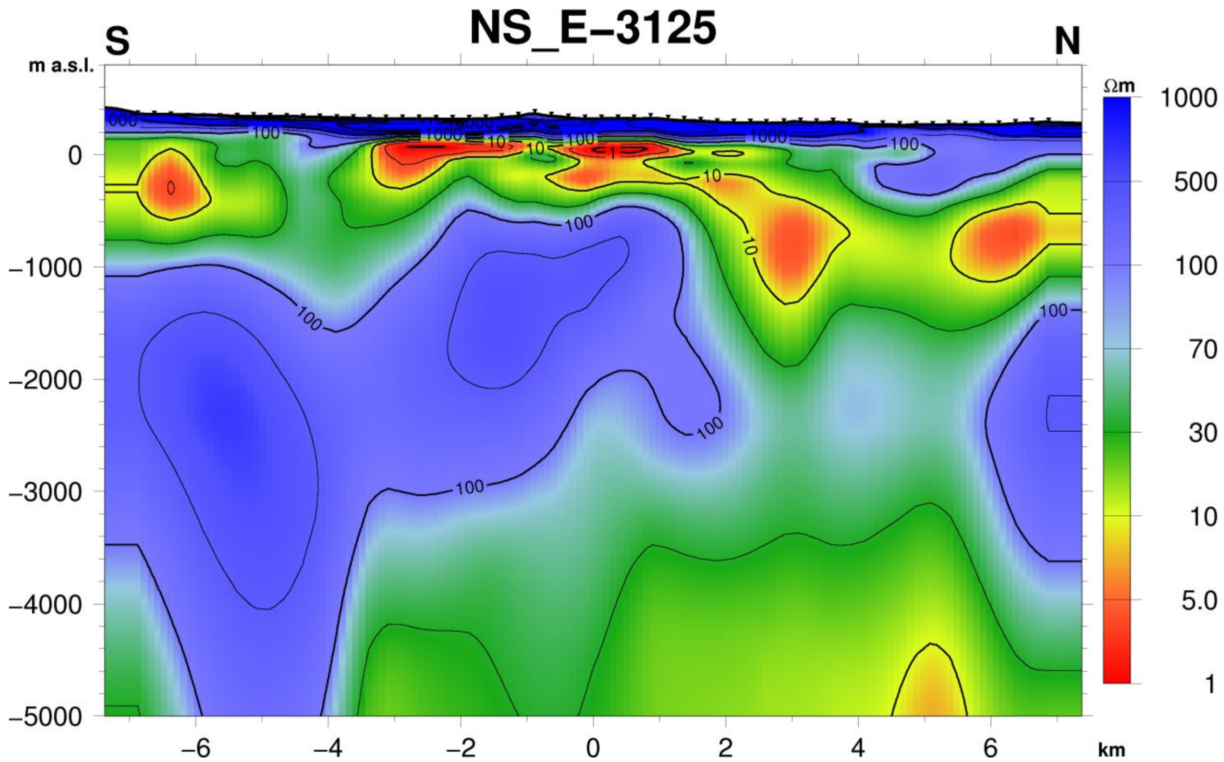
NS_E–3125
S
N
m a.s.l.
Ωm
1000
500
100
70
30
10
5.0
1
0
−1000
−2000
−3000
−4000
−5000
−6
−4
−2
0
2
4
6
km

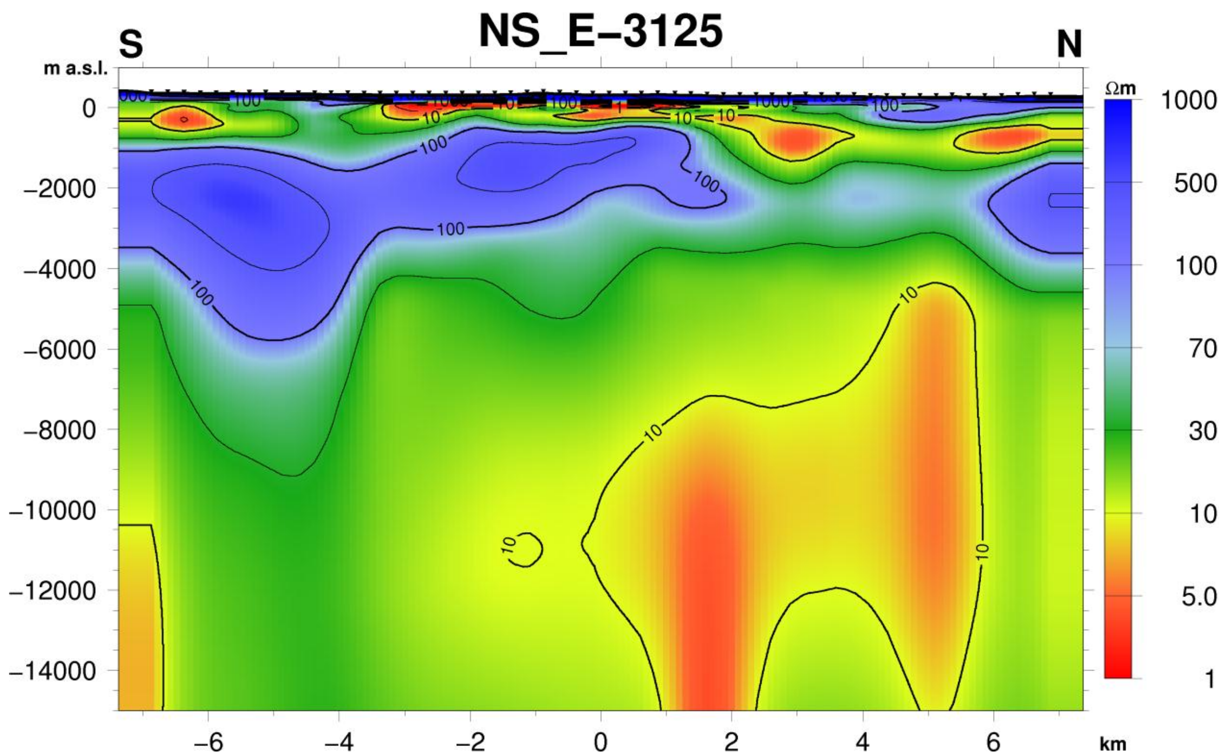
NS_E–3125
S
N
m a.s.l.
Ωm
1000
500
100
70
30
10
5.0
1
0
−2000
−4000
−6000
−8000
−10000
−12000
−14000
−6
−4
−2
0
2
4
6
km

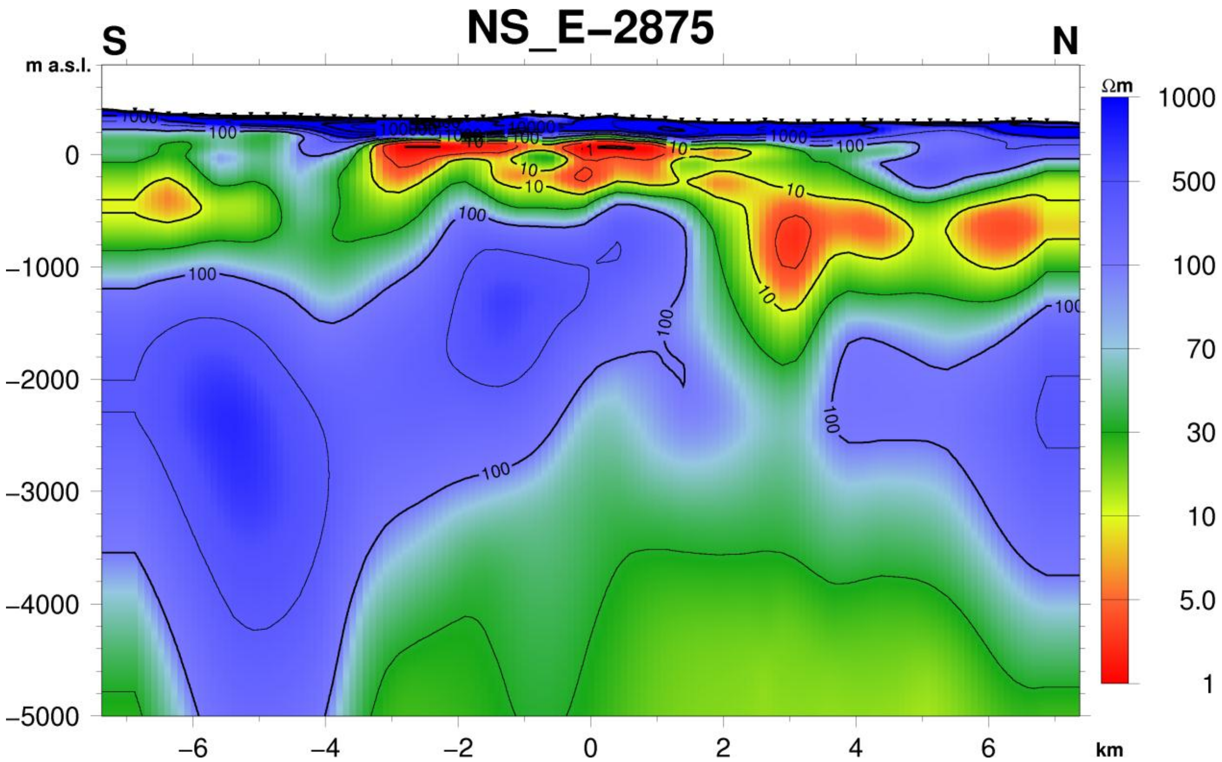

NS_E–2875
S
N
m a.s.l.
0
−1000
−2000
−3000
−4000
−5000
−6
−4
−2
0
2
4
6
km
Ωm
1000
500
100
70
30
10
5.0
1

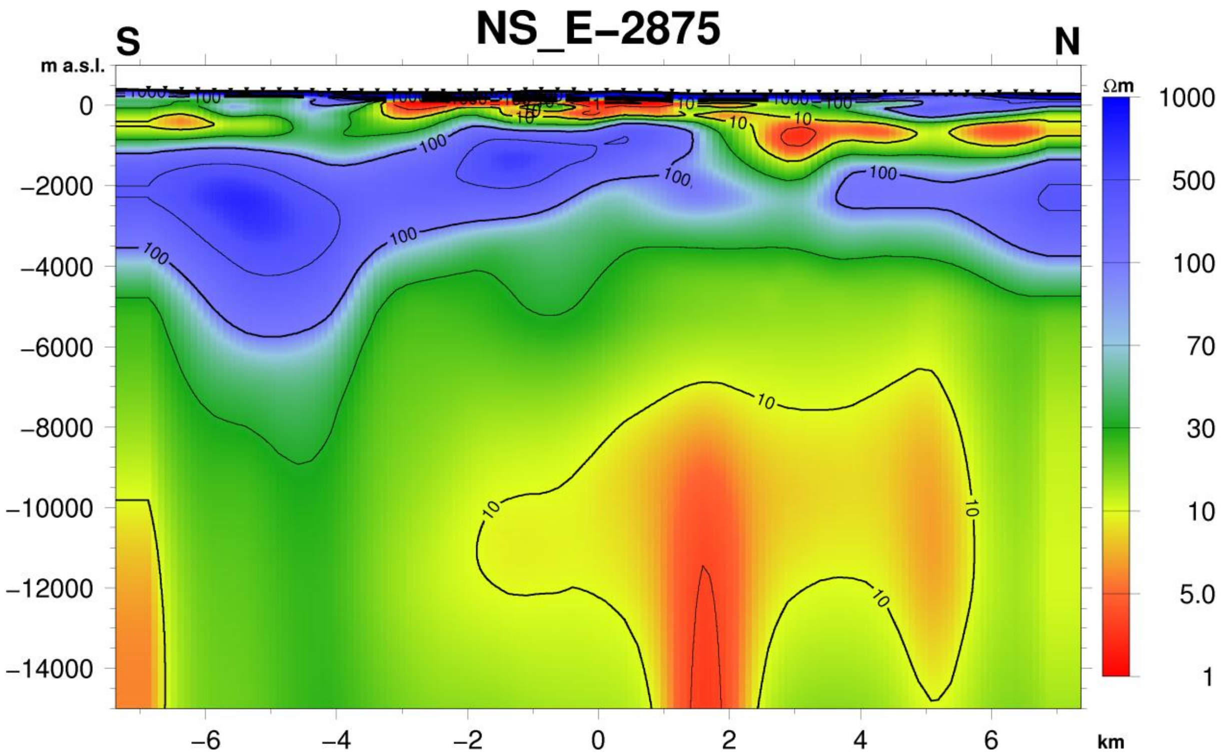

NS_E–2875
S
N
m a.s.l.
0
−2000
−4000
−6000
−8000
−10000
−12000
−14000
−6
−4
−2
0
2
4
6
km
Ωm
1000
500
100
70
30
10
5.0
1

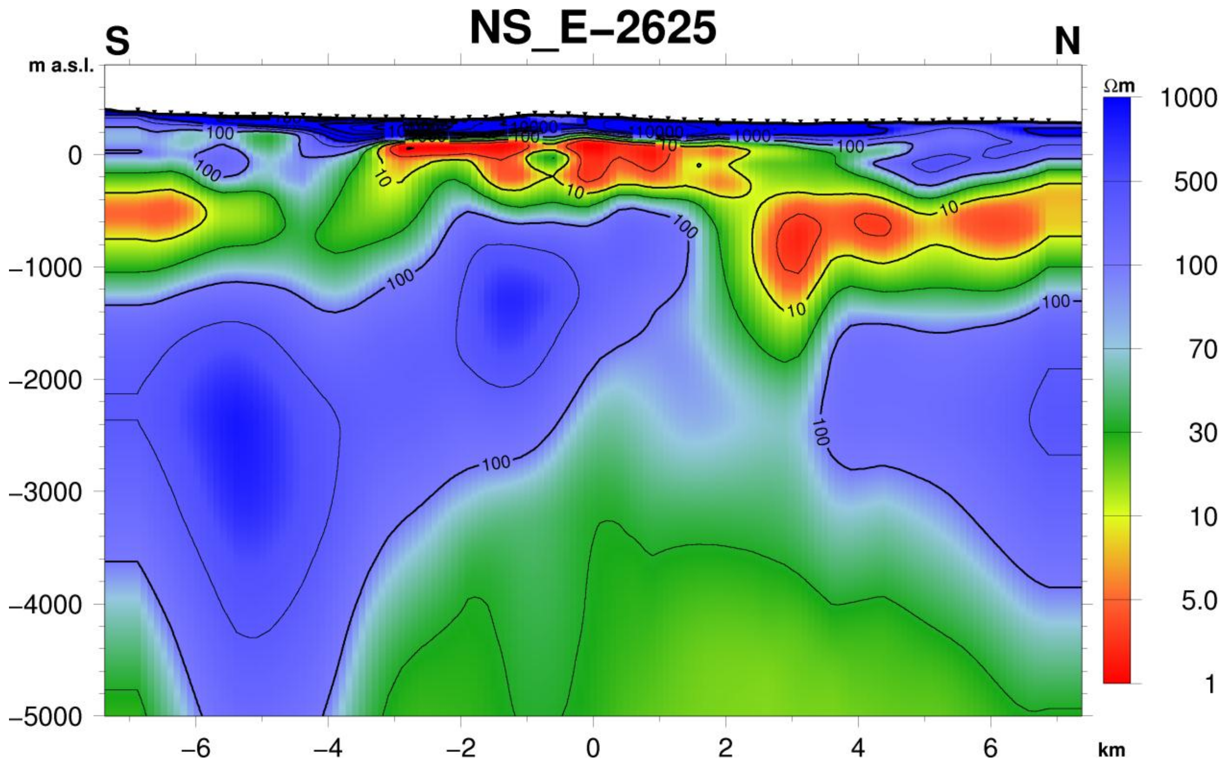
NS_E–2625
S
N
m a.s.l.
0
−1000
−2000
−3000
−4000
−5000
−6
−4
−2
0
2
4
6
km
Ωm
1000
500
100
70
30
10
5.0
1

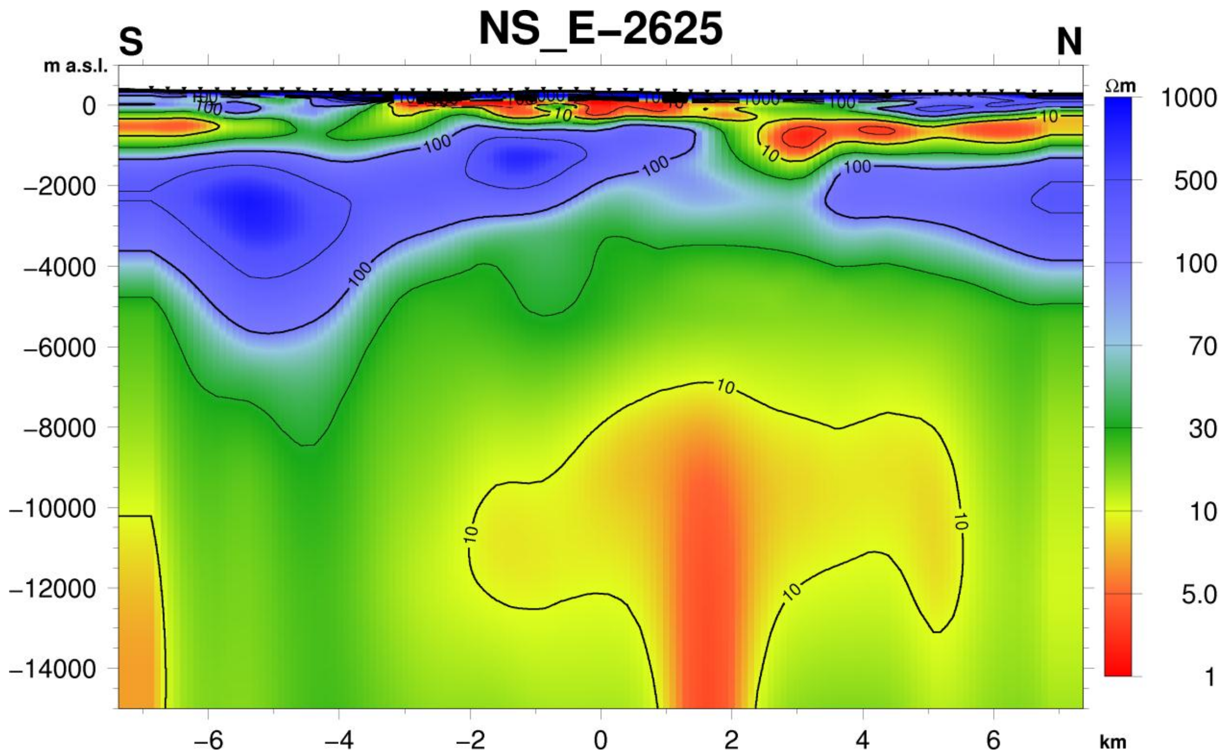
NS_E–2625
S
N
m a.s.l.
0
−2000
−4000
−6000
−8000
−10000
−12000
−14000
−6
−4
−2
0
2
4
6
km
Ωm
1000
500
100
70
30
10
5.0
1

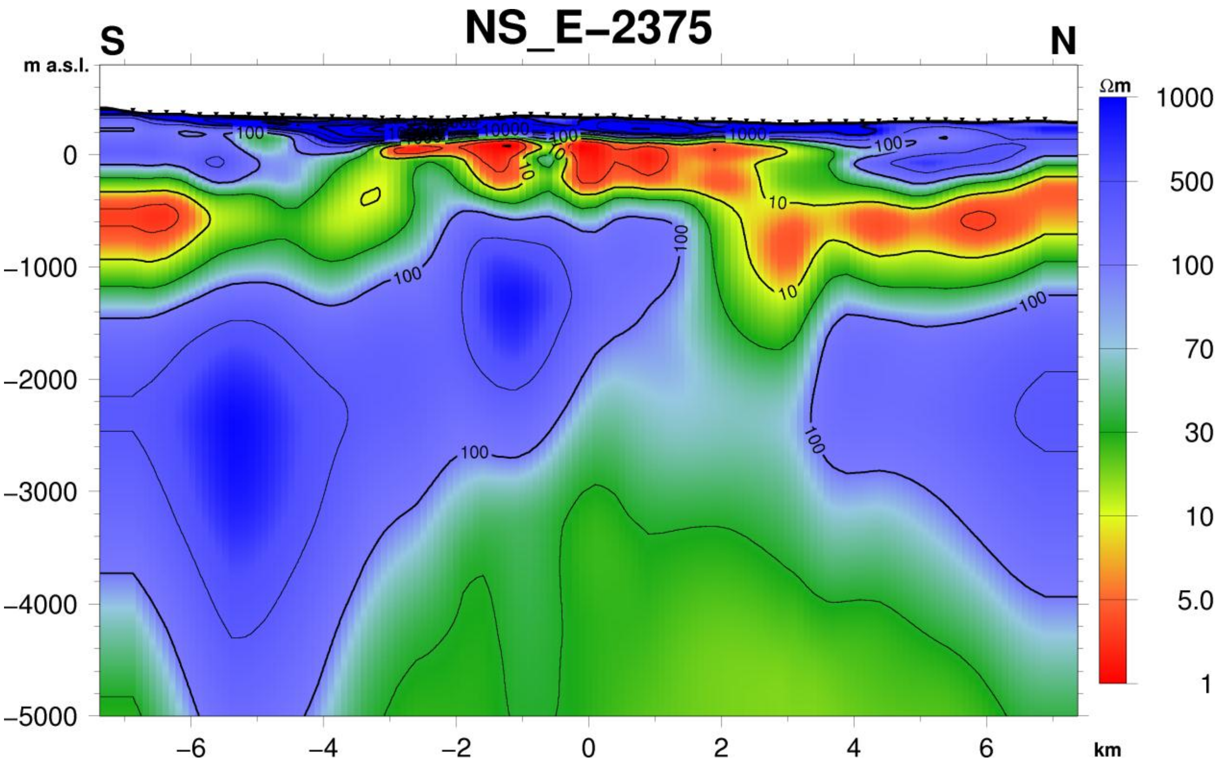
NS_E–2375
S
N
m a.s.l.
Ωm
1000
500
100
70
30
10
5.0
1
0
−1000
−2000
−3000
−4000
−5000
−6
−4
−2
0
2
4
6
km

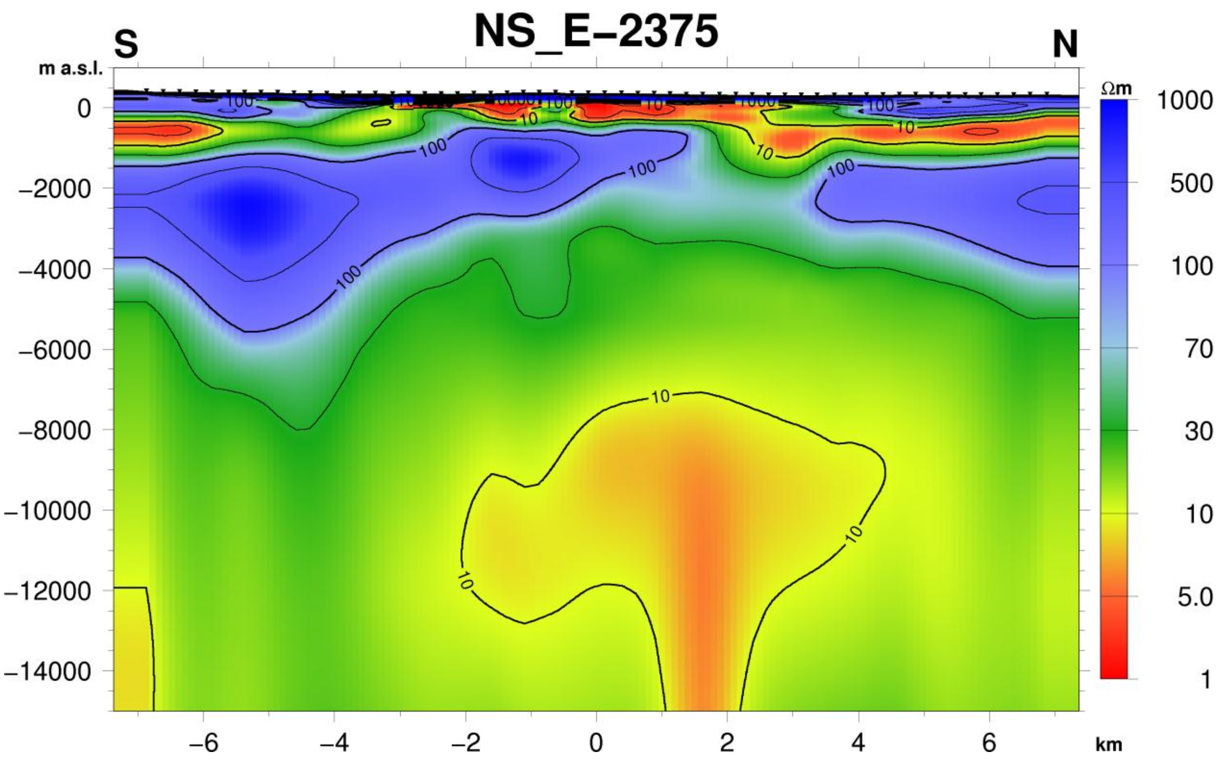
NS_E–2375
S
N
m a.s.l.
Ωm
1000
500
100
70
30
10
5.0
1
0
−2000
−4000
−6000
−8000
−10000
−12000
−14000
−6
−4
−2
0
2
4
6
km

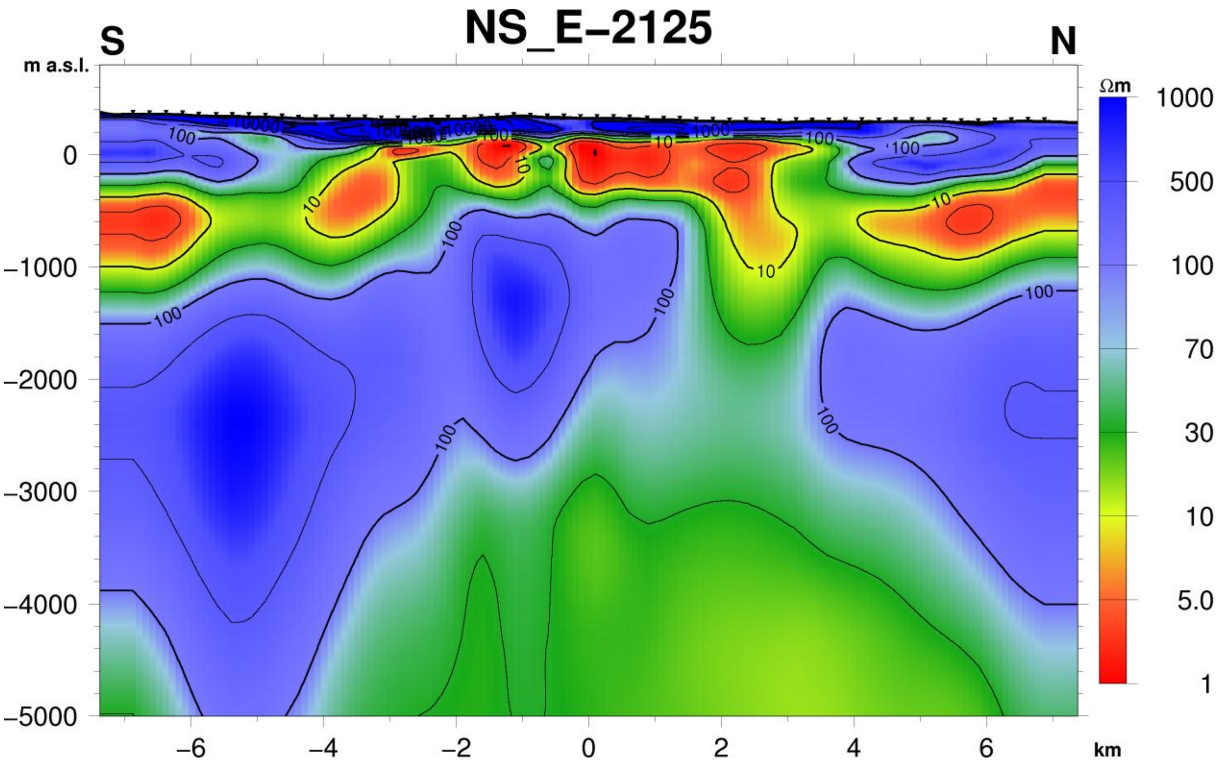
NS_E–2125
S
N
m a.s.l.
Ωm
0
–1000
–2000
–3000
–4000
–5000
–6
–4
–2
0
2
4
6
km
1000
500
100
70
30
10
5.0
1

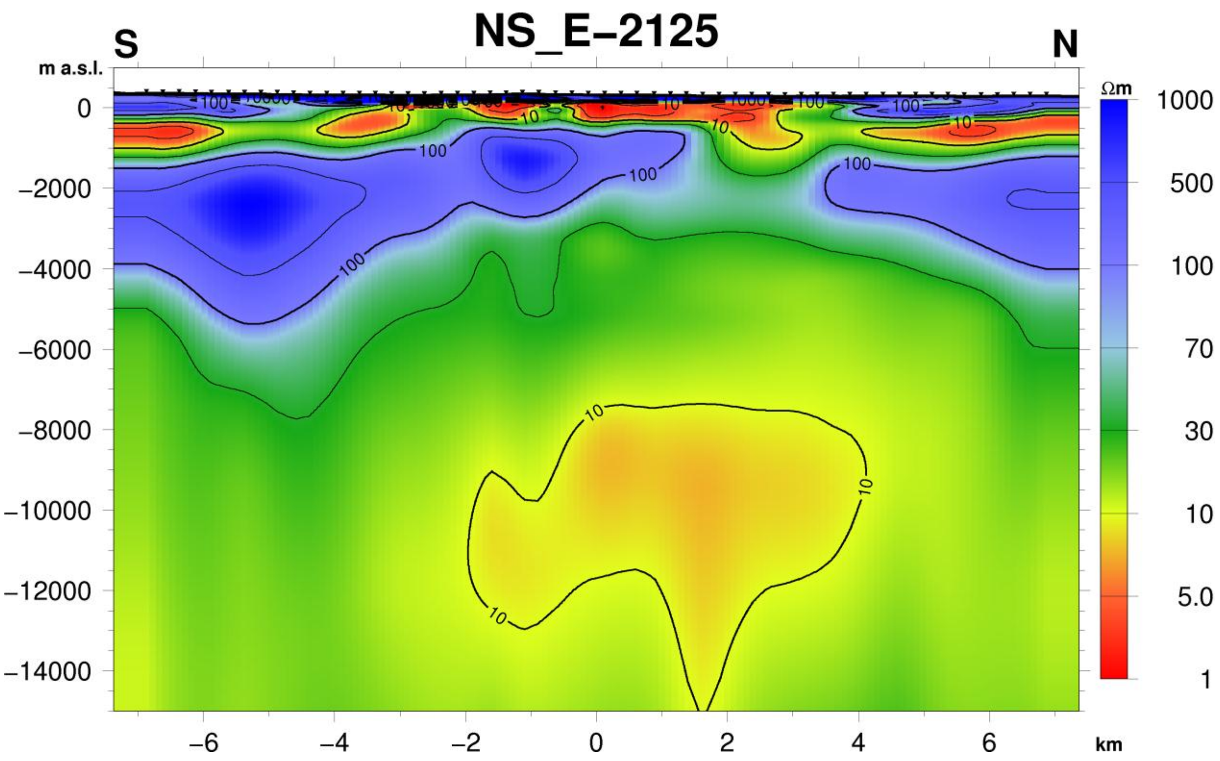
NS_E–2125
S
N
m a.s.l.
Ωm
0
–2000
–4000
–6000
–8000
–10000
–12000
–14000
–6
–4
–2
0
2
4
6
km
1000
500
100
70
30
10
5.0
1

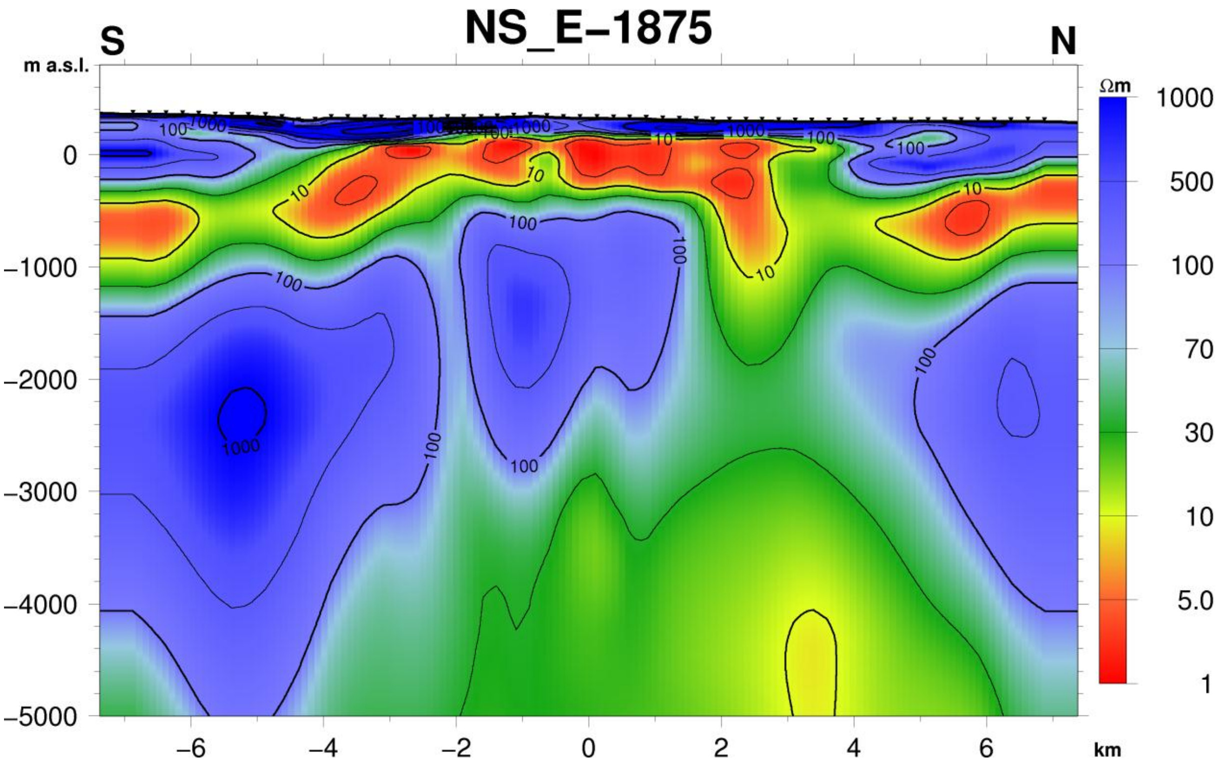
NS_E−1875
S
N
m a.s.l.
0
−1000
−2000
−3000
−4000
−5000
−6
−4
−2
0
2
4
6
km
Ωm
1000
500
100
70
30
10
5.0
1

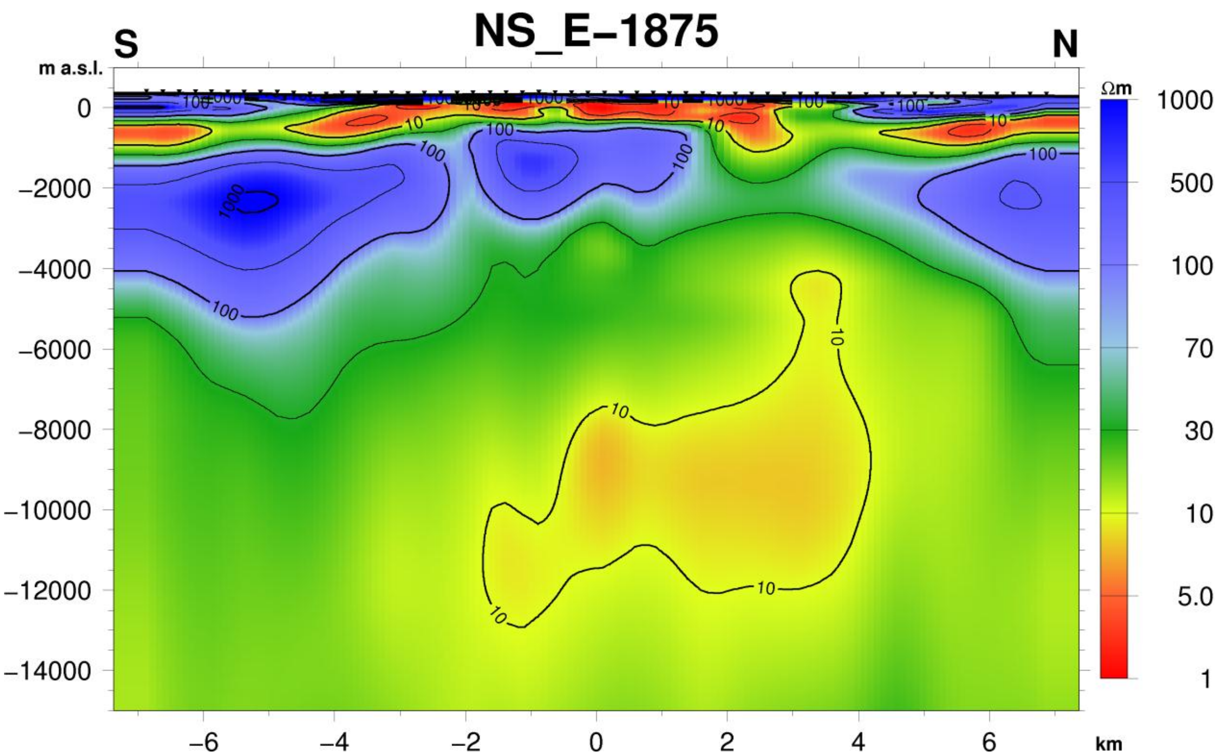
NS_E−1875
S
N
m a.s.l.
0
−2000
−4000
−6000
−8000
−10000
−12000
−14000
−6
−4
−2
0
2
4
6
km
Ωm
1000
500
100
70
30
10
5.0
1

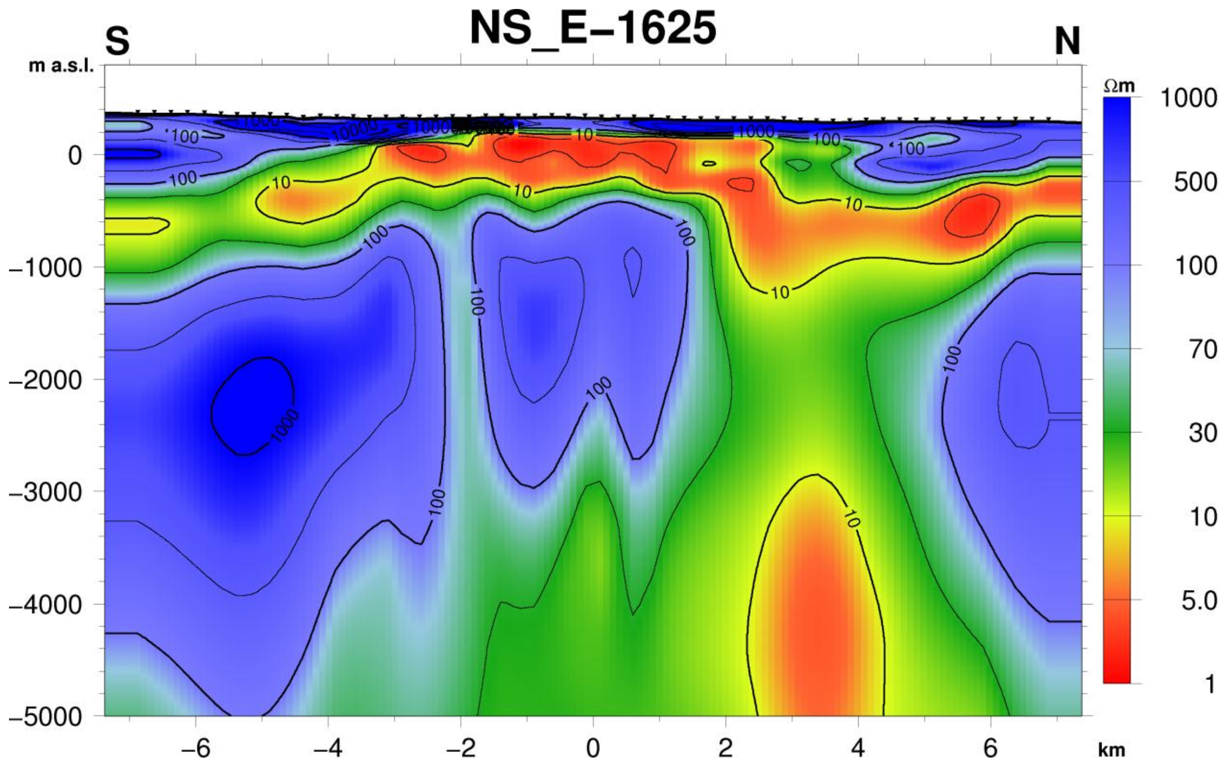
NS_E−1625
S
N
m a.s.l.
0
−1000
−2000
−3000
−4000
−5000
−6
−4
−2
0
2
4
6
km
Ωm
1000
500
100
70
30
10
5.0
1

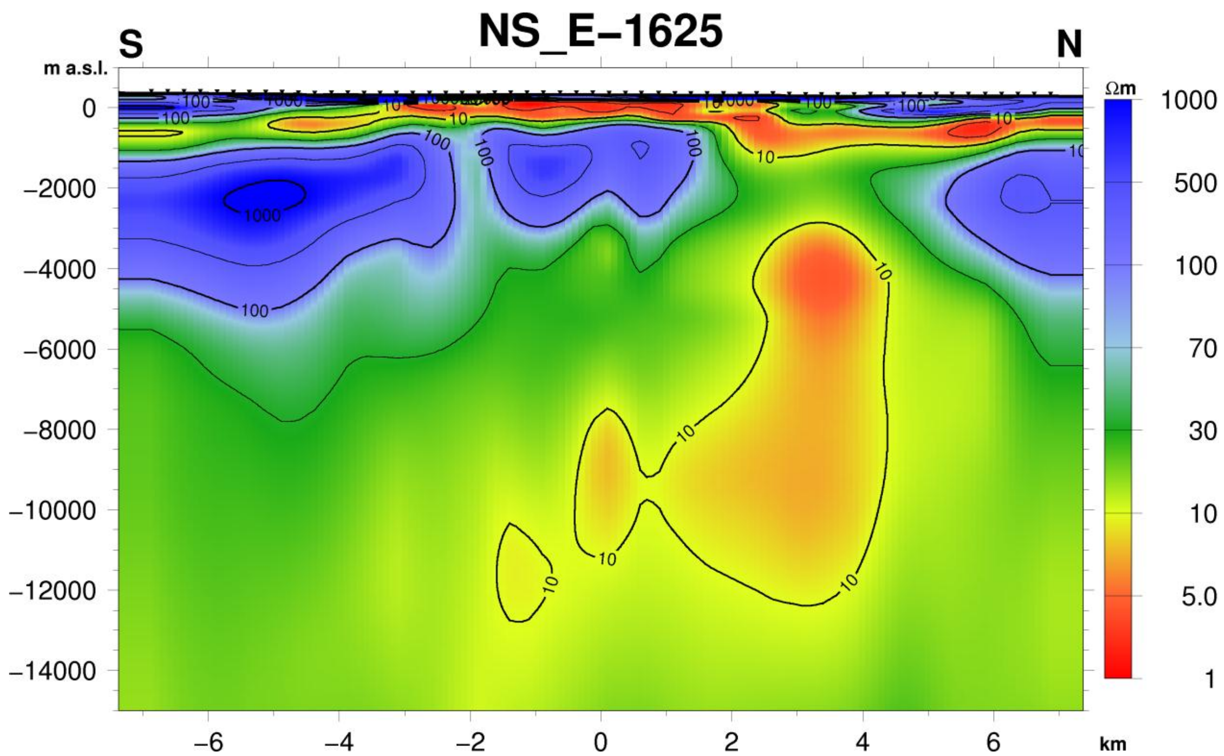
NS_E−1625
S
N
m a.s.l.
0
−2000
−4000
−6000
−8000
−10000
−12000
−14000
−6
−4
−2
0
2
4
6
km
Ωm
1000
500
100
70
30
10
5.0
1

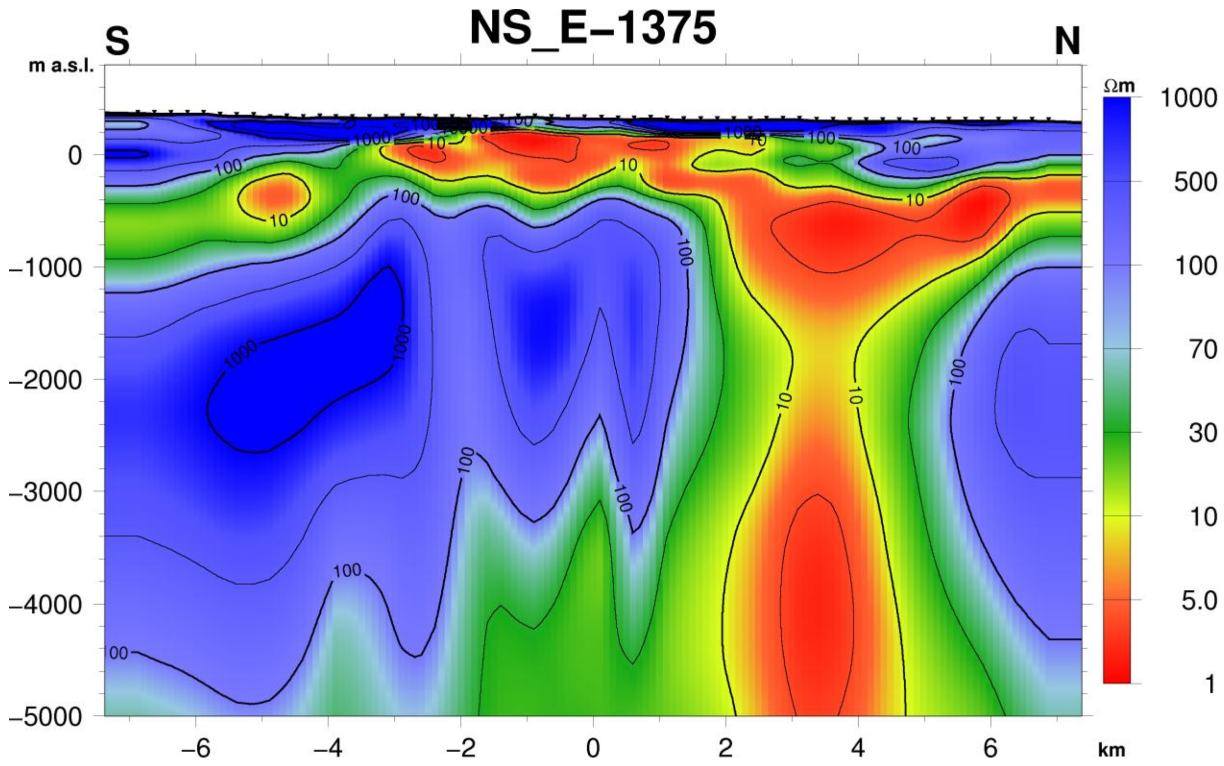
NS_E−1375
S
N
m a.s.l.
Ωm
km

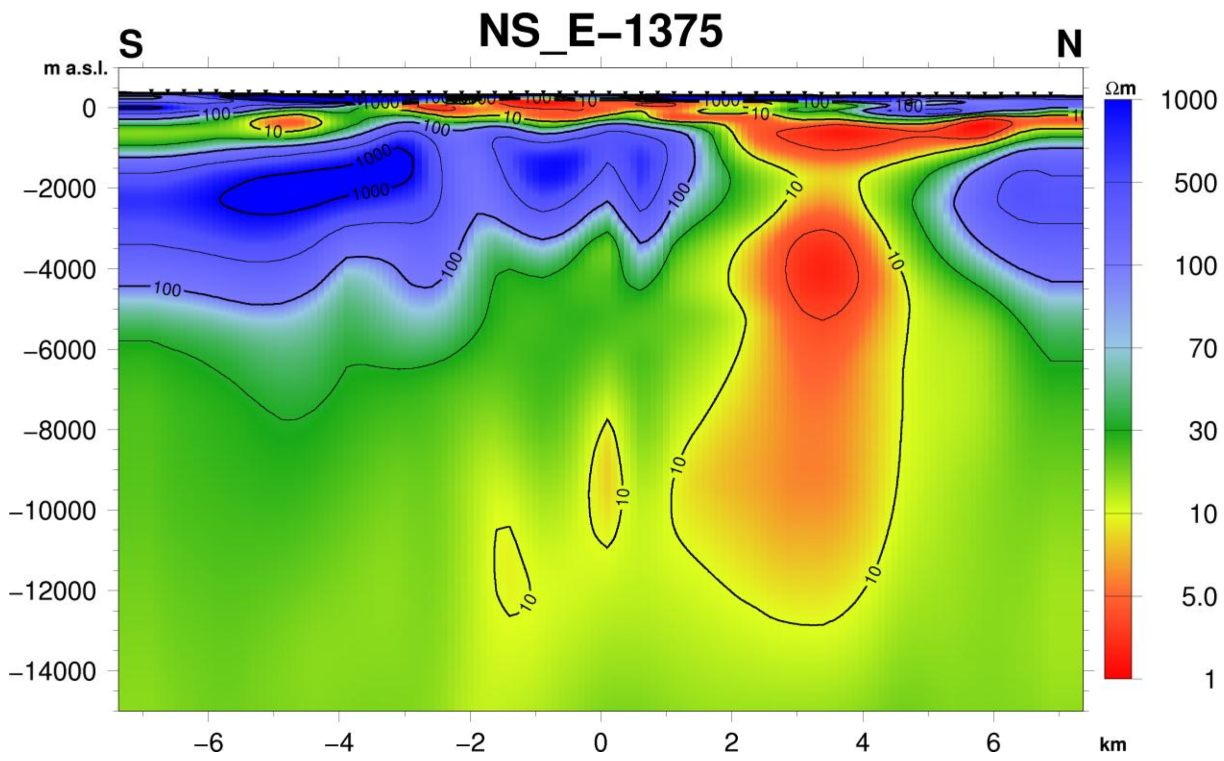
NS_E−1375
S
N
m a.s.l.
Ωm
km

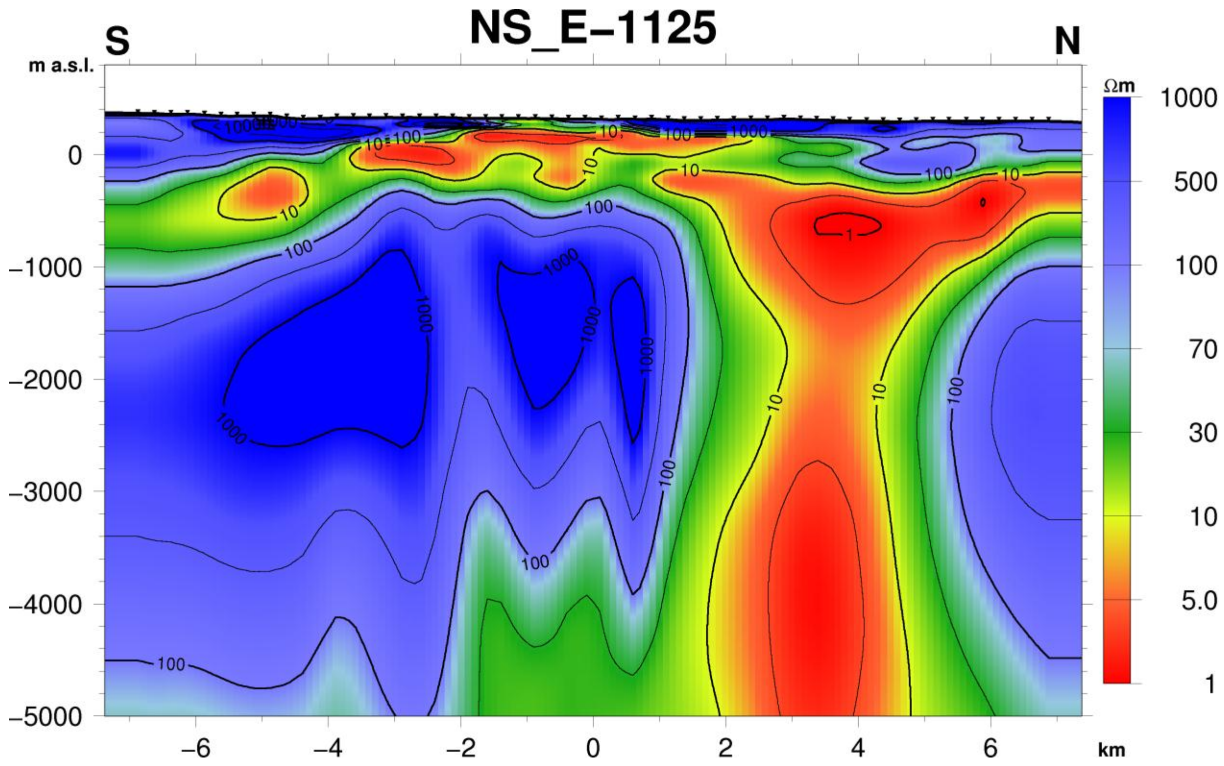
NS_E-1125
S
N
m a.s.l.
0
−1000
−2000
−3000
−4000
−5000
−6
−4
−2
0
2
4
6
km
Ωm
1000
500
100
70
30
10
5.0
1

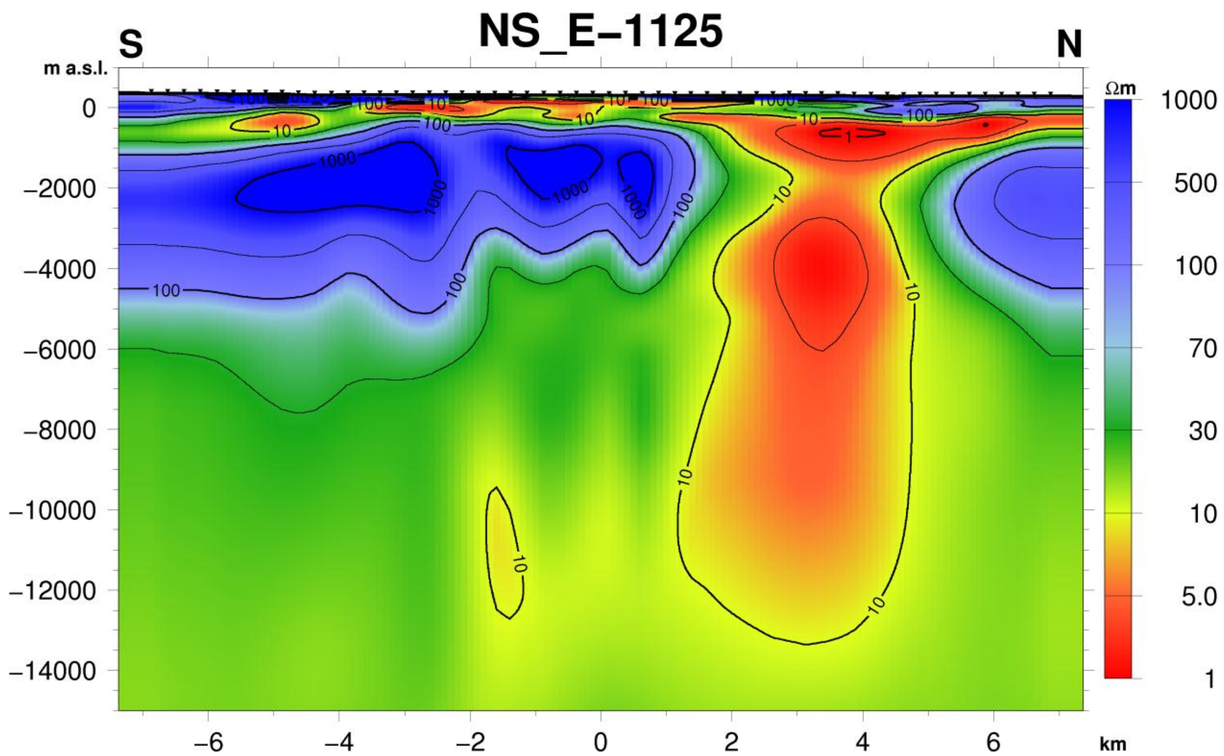
NS_E-1125
S
N
m a.s.l.
0
−2000
−4000
−6000
−8000
−10000
−12000
−14000
−6
−4
−2
0
2
4
6
km
Ωm
1000
500
100
70
30
10
5.0
1

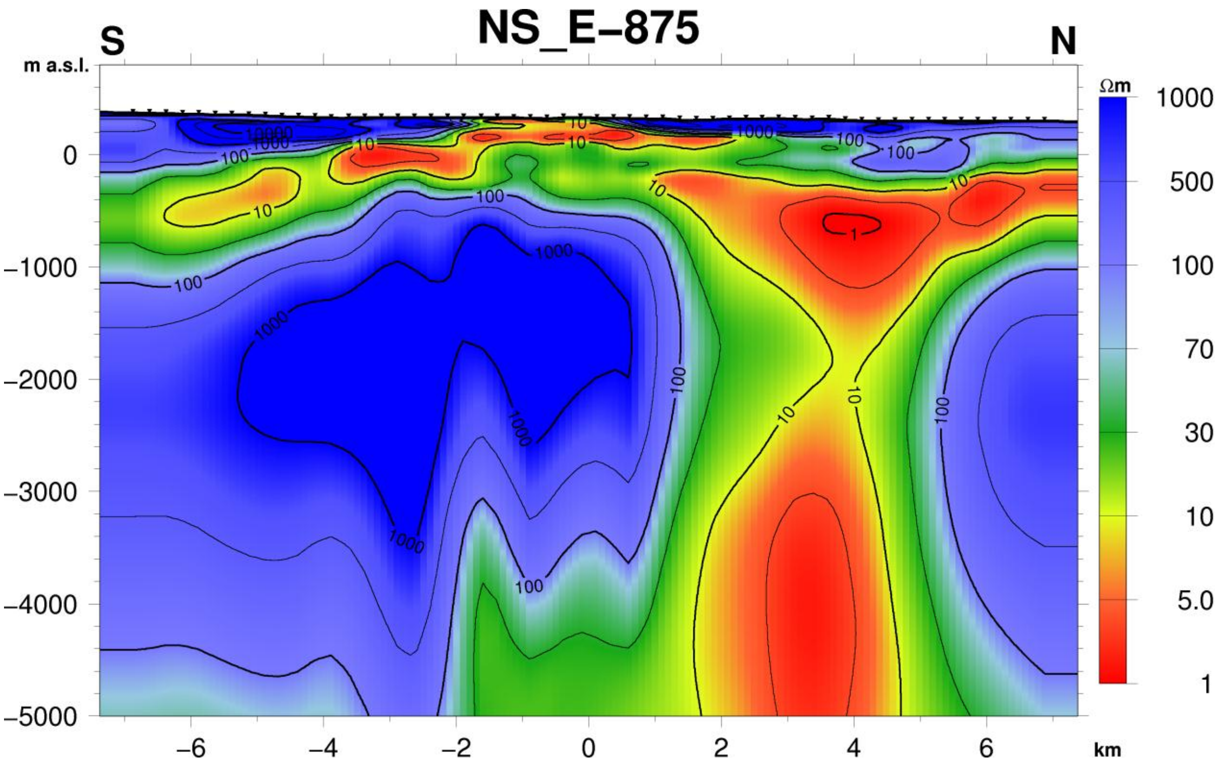
NS_E–875
S
N
m a.s.l.
Ωm
1000
500
100
70
30
10
5.0
1
0
−1000
−2000
−3000
−4000
−5000
−6
−4
−2
0
2
4
6
km

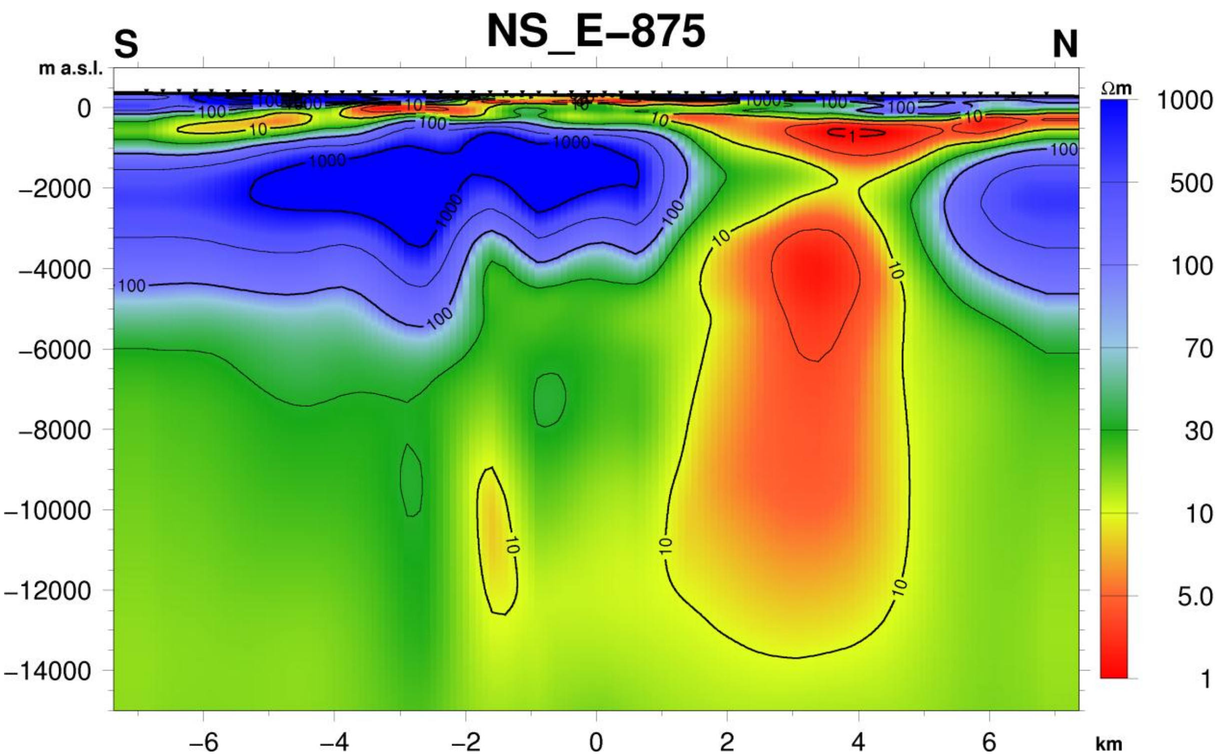
NS_E–875
S
N
m a.s.l.
Ωm
1000
500
100
70
30
10
5.0
1
0
−2000
−4000
−6000
−8000
−10000
−12000
−14000
−6
−4
−2
0
2
4
6
km

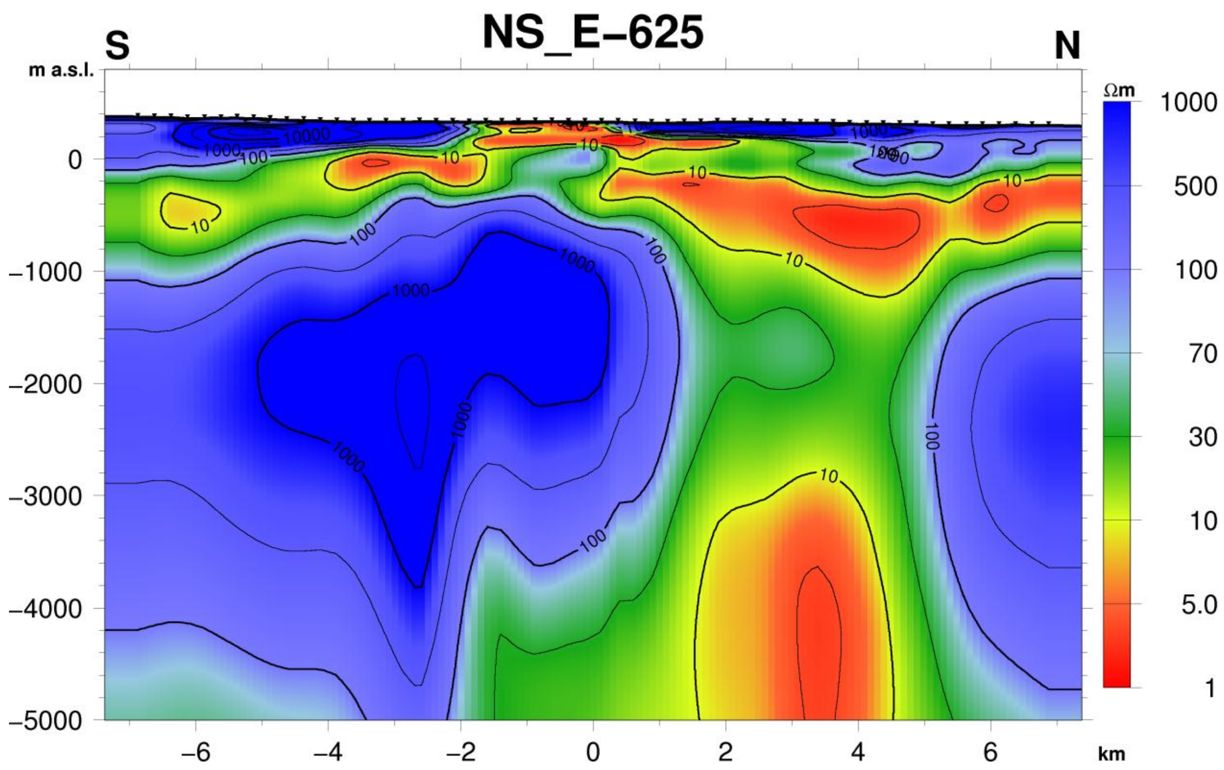
NS_E–625
S
N
m a.s.l.
Ωm
1000
500
100
70
30
10
5.0
1
0
−1000
−2000
−3000
−4000
−5000
−6
−4
−2
0
2
4
6
km

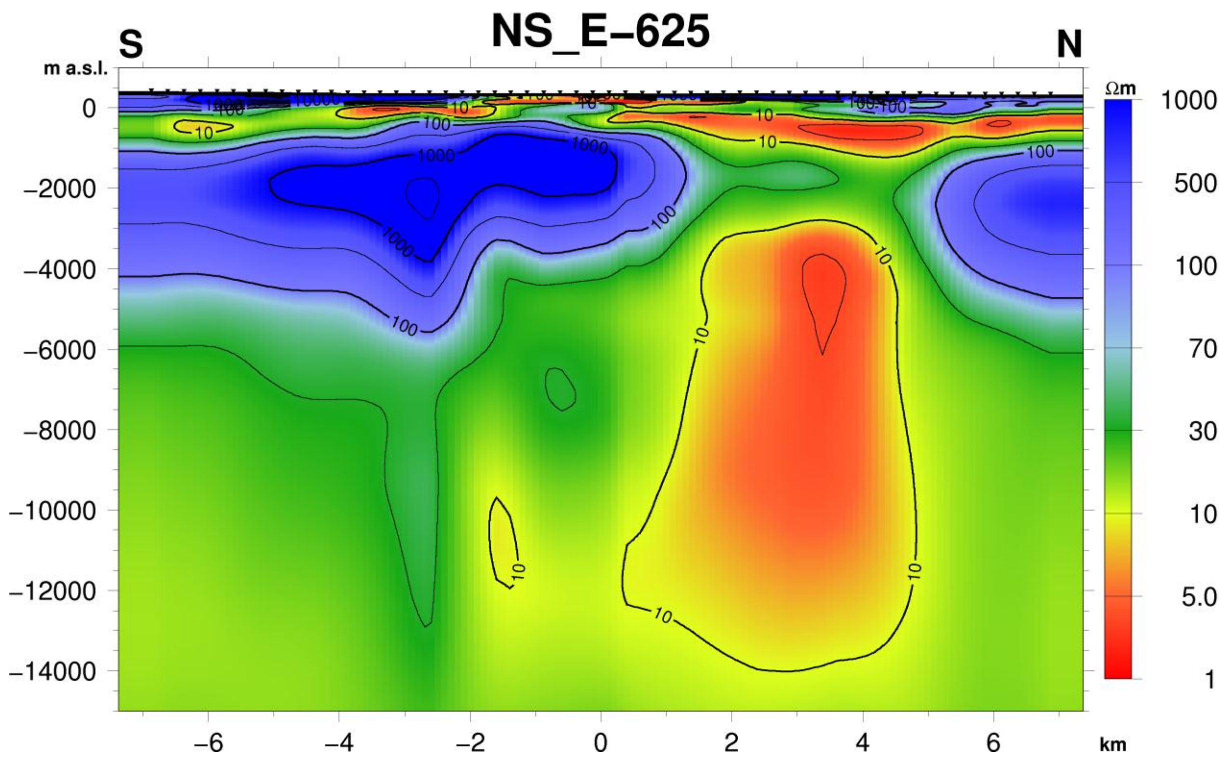
NS_E–625
S
N
m a.s.l.
Ωm
1000
500
100
70
30
10
5.0
1
0
−2000
−4000
−6000
−8000
−10000
−12000
−14000
−6
−4
−2
0
2
4
6
km

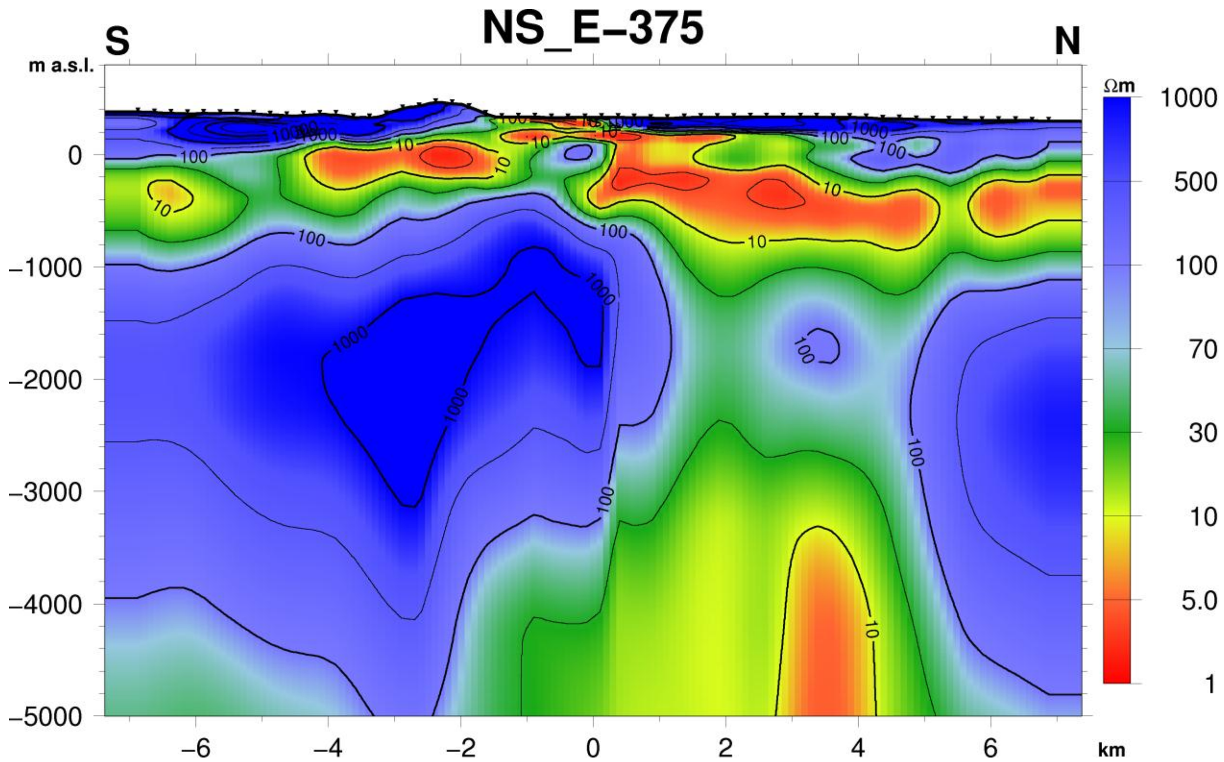
NS_E–375
S
N
m a.s.l.
Ωm
1000
500
100
70
30
10
5.0
1
0
–1000
–2000
–3000
–4000
–5000
–6
–4
–2
0
2
4
6
km

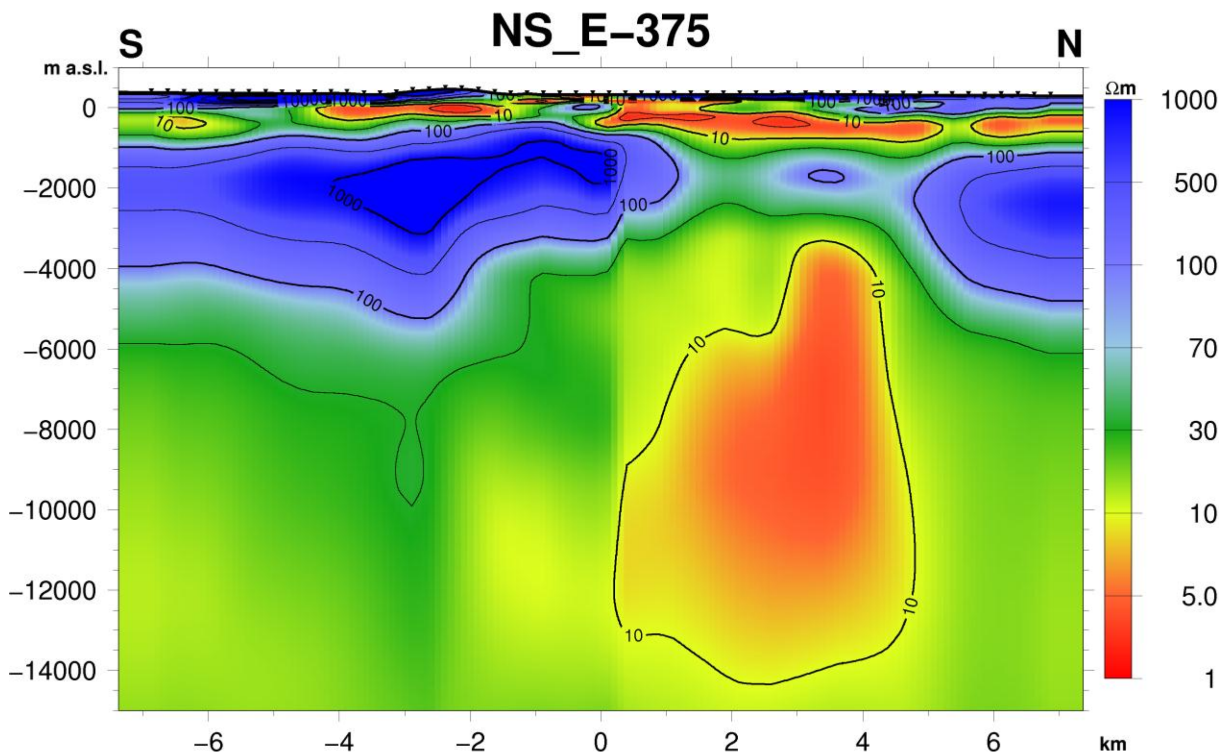
NS_E–375
S
N
m a.s.l.
Ωm
1000
500
100
70
30
10
5.0
1
0
–2000
–4000
–6000
–8000
–10000
–12000
–14000
–6
–4
–2
0
2
4
6
km

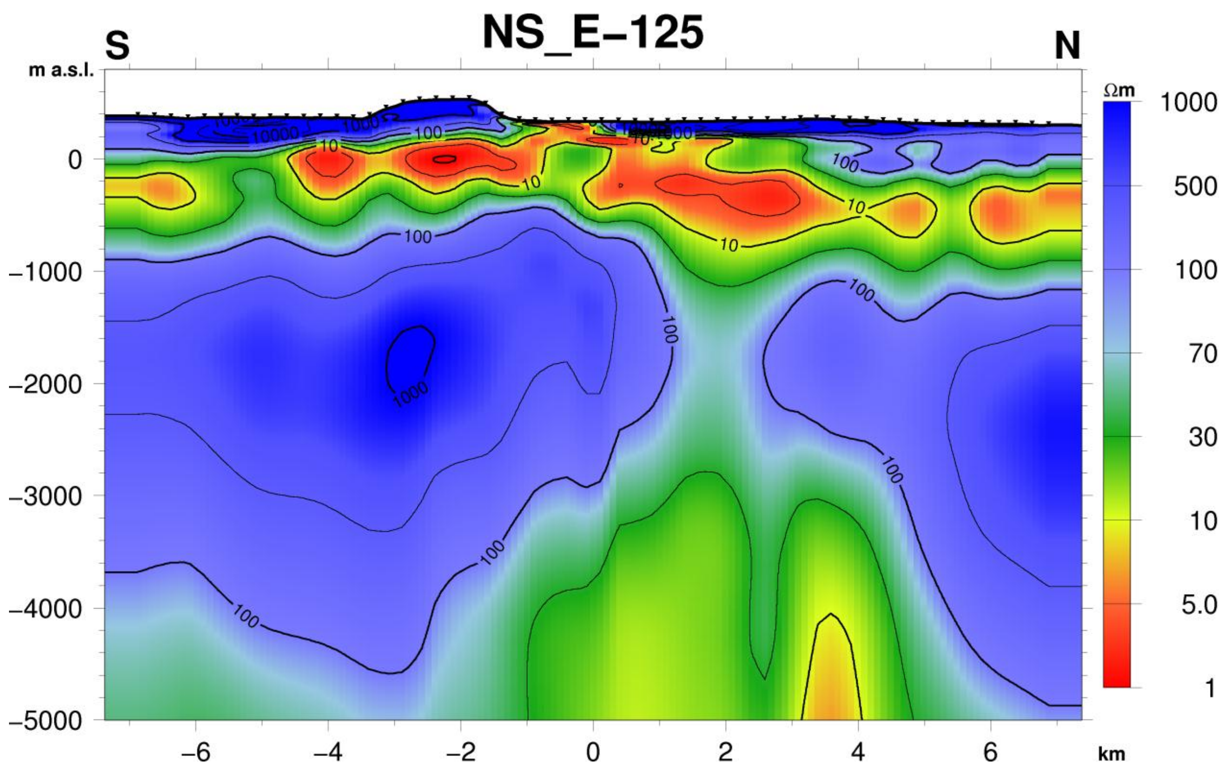

NS_E–125
S
N
m a.s.l.
0
–1000
–2000
–3000
–4000
–5000
–6
–4
–2
0
2
4
6
km
Ωm
1000
500
100
70
30
10
5.0
1

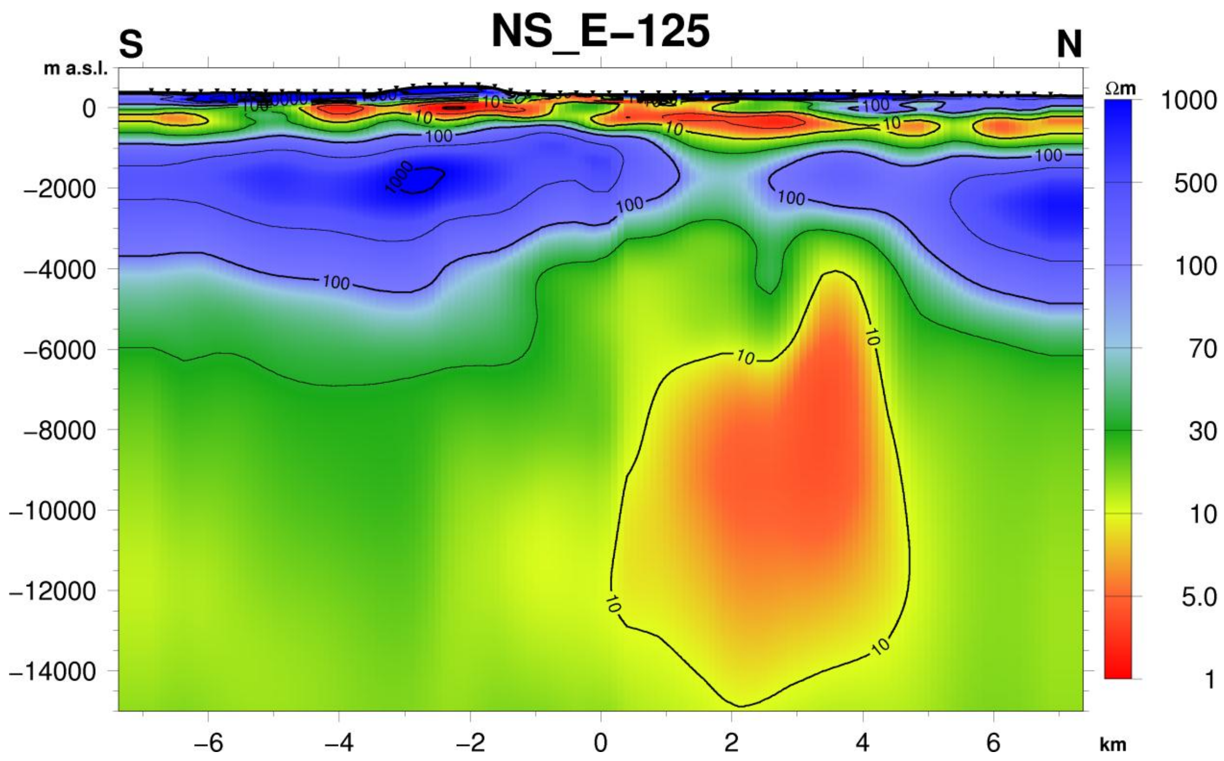

NS_E–125
S
N
m a.s.l.
0
–2000
–4000
–6000
–8000
–10000
–12000
–14000
–6
–4
–2
0
2
4
6
km
Ωm
1000
500
100
70
30
10
5.0
1

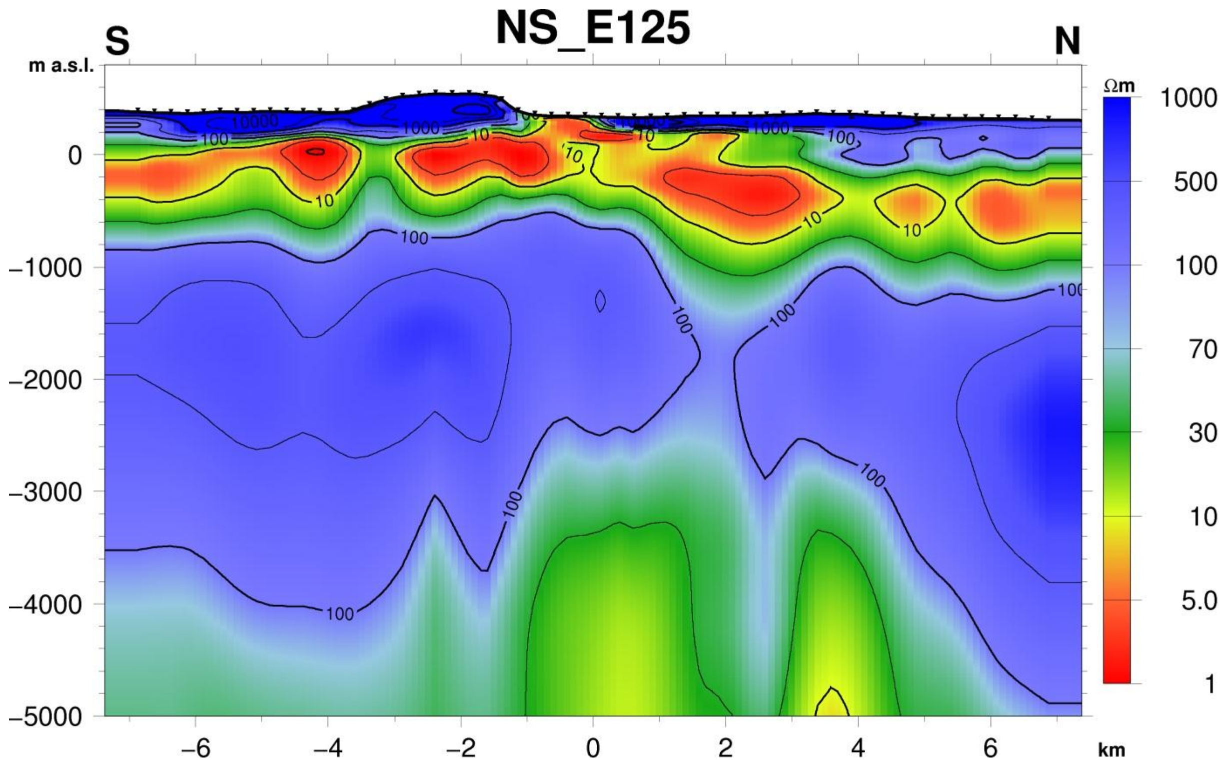
NS_E125
S
N
m a.s.l.
km
Ωm
1000
500
100
70
30
10
5.0
1

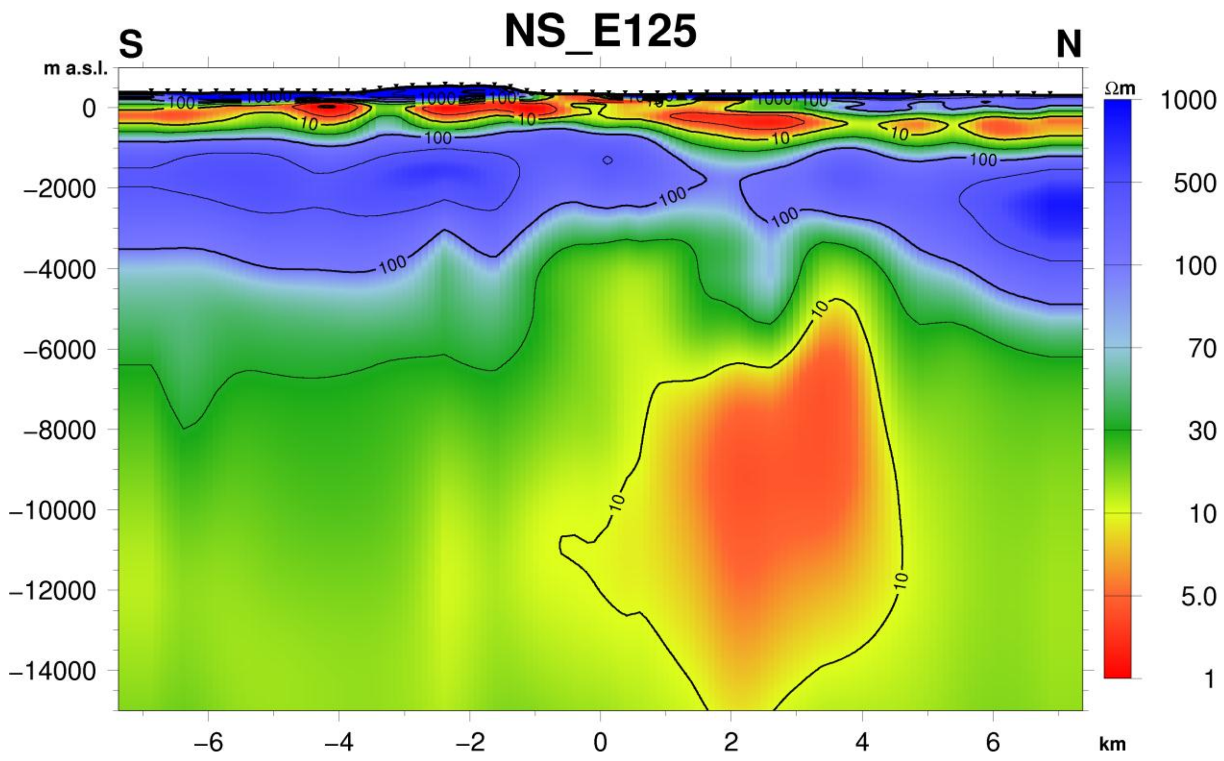
NS_E125
S
N
m a.s.l.
km
Ωm
1000
500
100
70
30
10
5.0
1

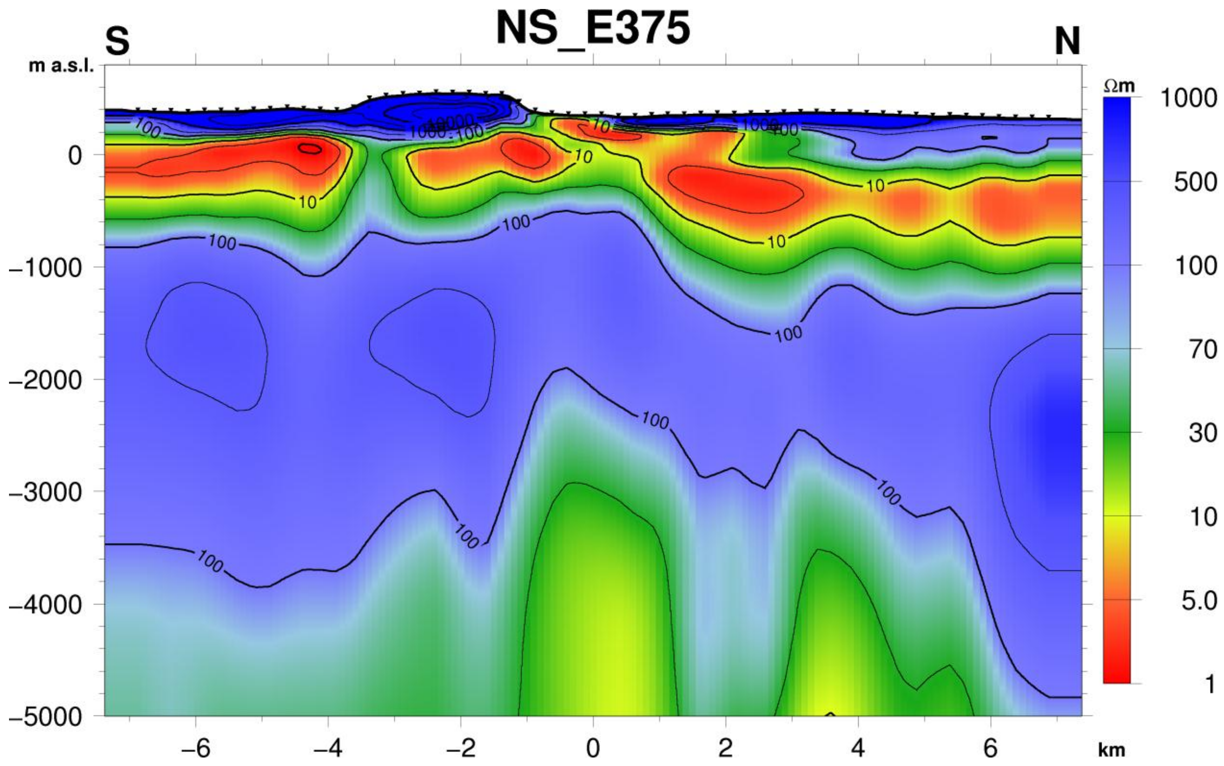
NS_E375
S
N
m a.s.l.
Ωm
1000
500
100
70
30
10
5.0
1
0
−1000
−2000
−3000
−4000
−5000
−6
−4
−2
0
2
4
6
km

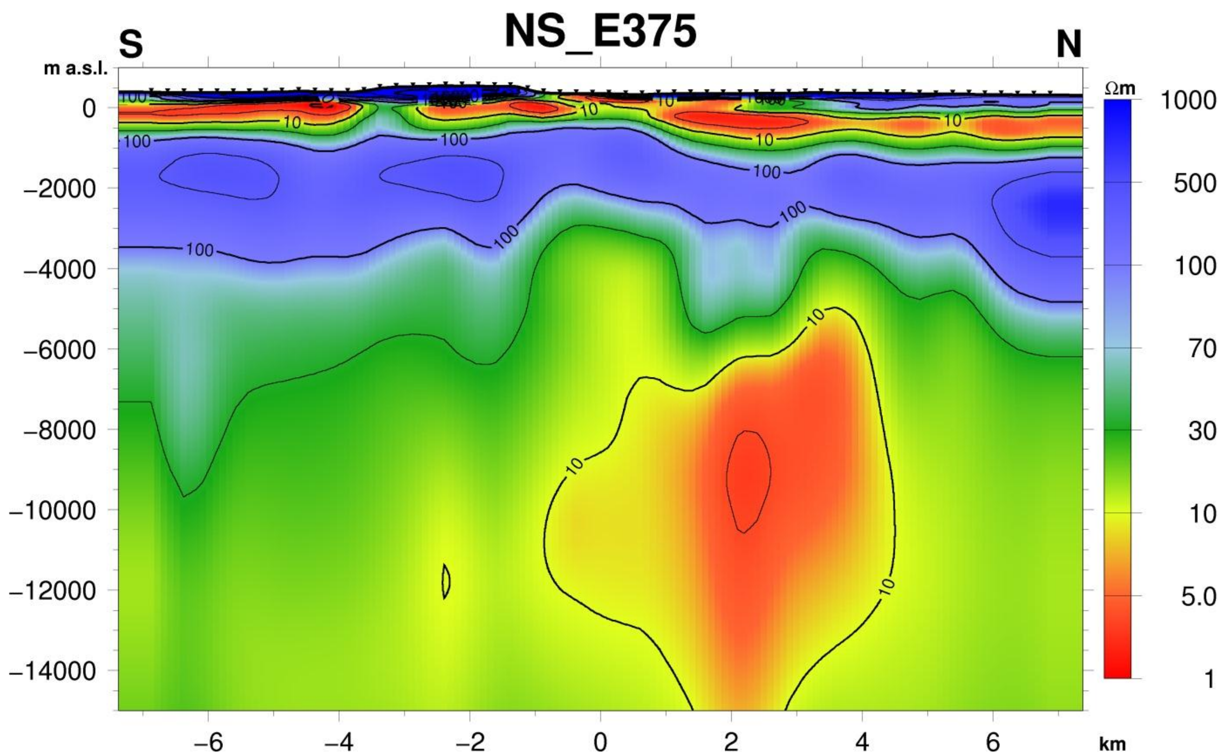
NS_E375
S
N
m a.s.l.
Ωm
1000
500
100
70
30
10
5.0
1
0
−2000
−4000
−6000
−8000
−10000
−12000
−14000
−6
−4
−2
0
2
4
6
km

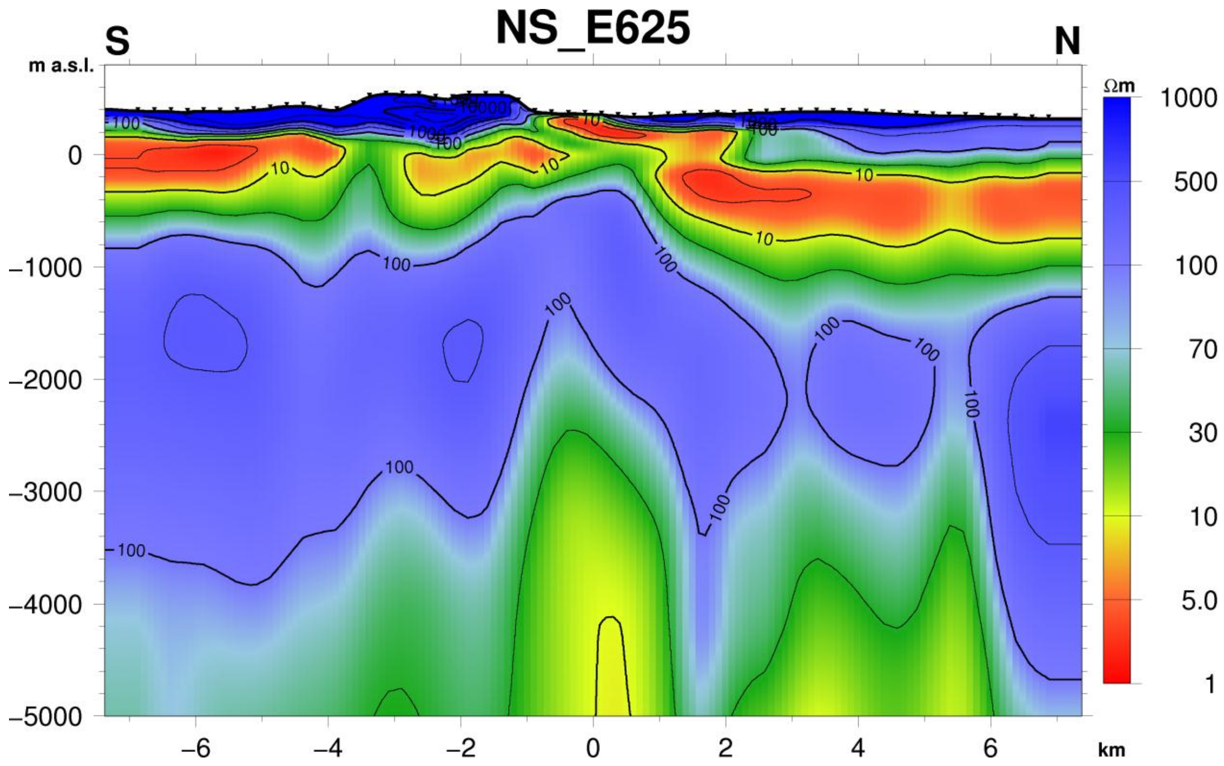
NS_E625
S
N
m a.s.l.
Ωm
1000
500
100
70
30
10
5.0
1
0
−1000
−2000
−3000
−4000
−5000
−6
−4
−2
0
2
4
6
km

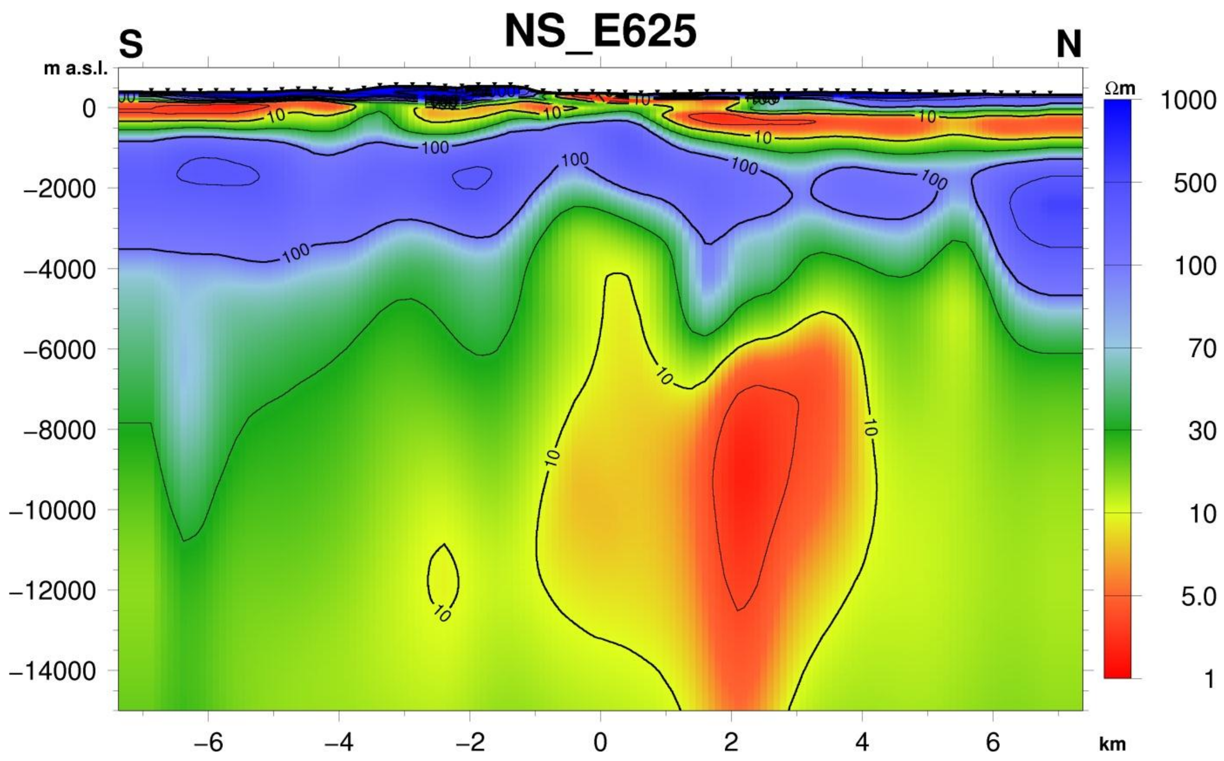
NS_E625
S
N
m a.s.l.
Ωm
1000
500
100
70
30
10
5.0
1
0
−2000
−4000
−6000
−8000
−10000
−12000
−14000
−6
−4
−2
0
2
4
6
km

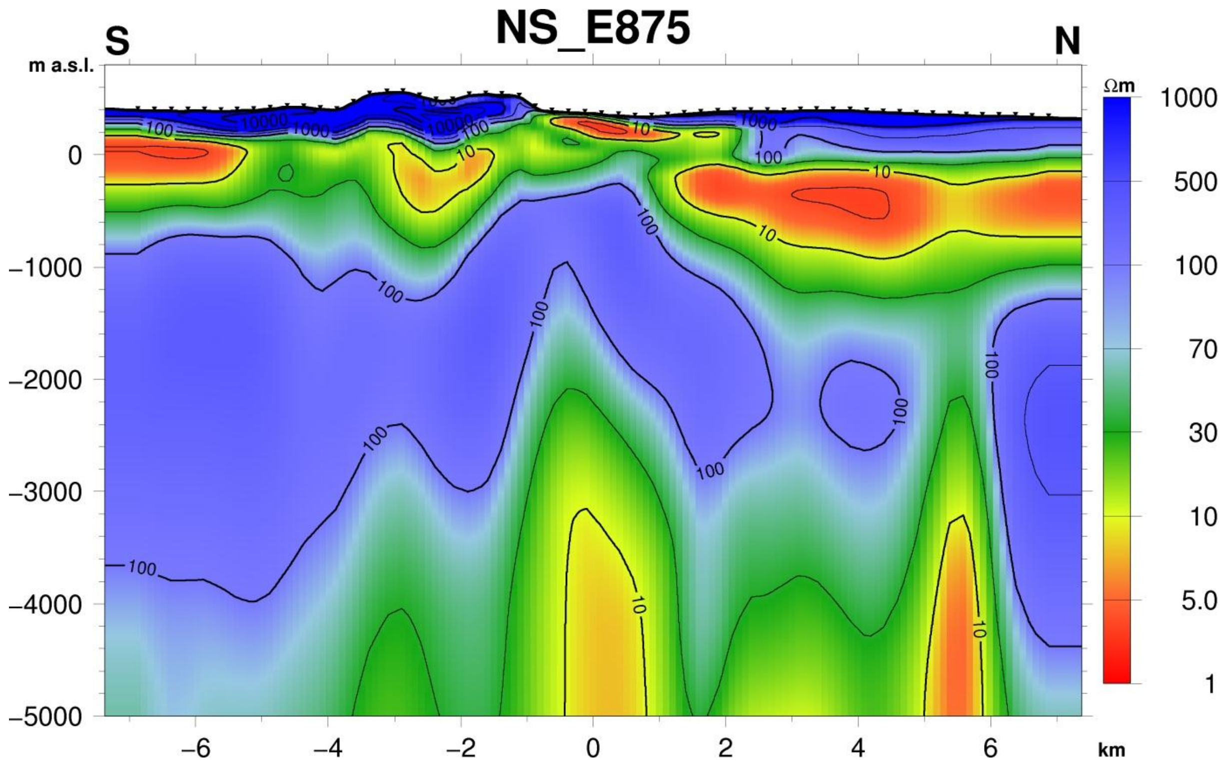
NS_E875
S
N
m a.s.l.
Ωm
km

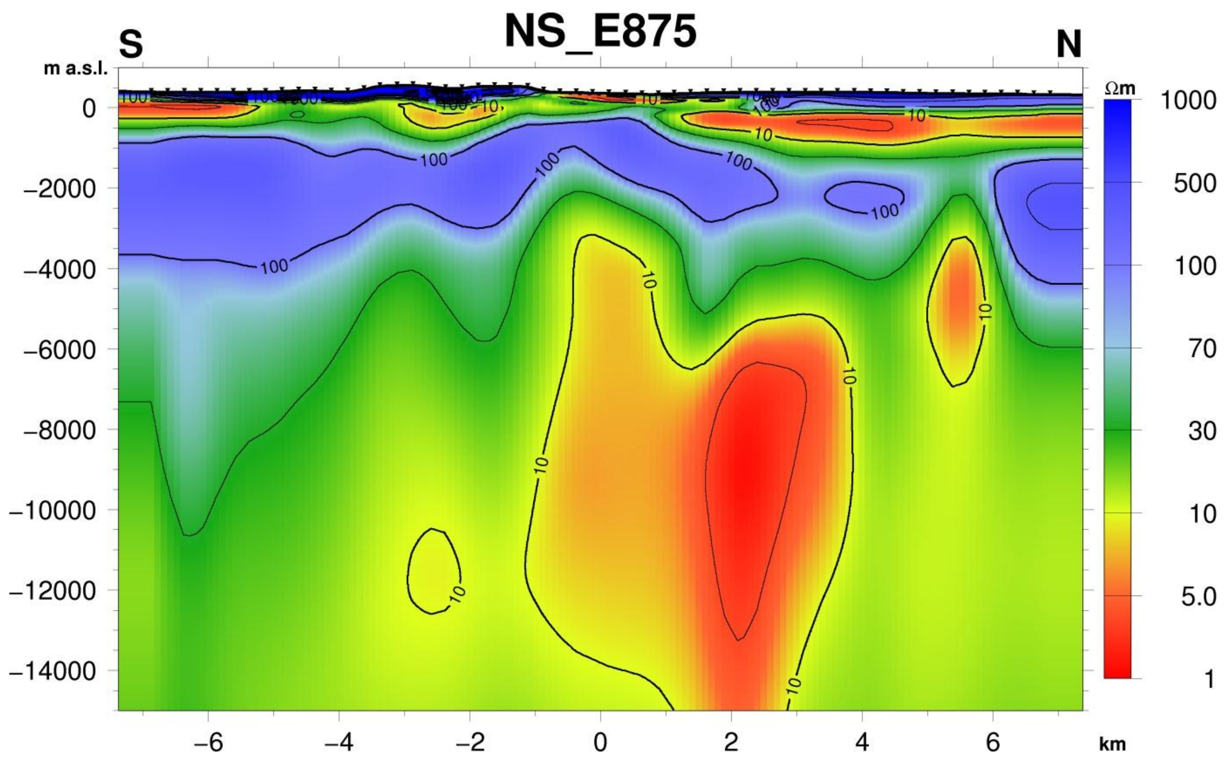
NS_E875
S
N
m a.s.l.
Ωm
km

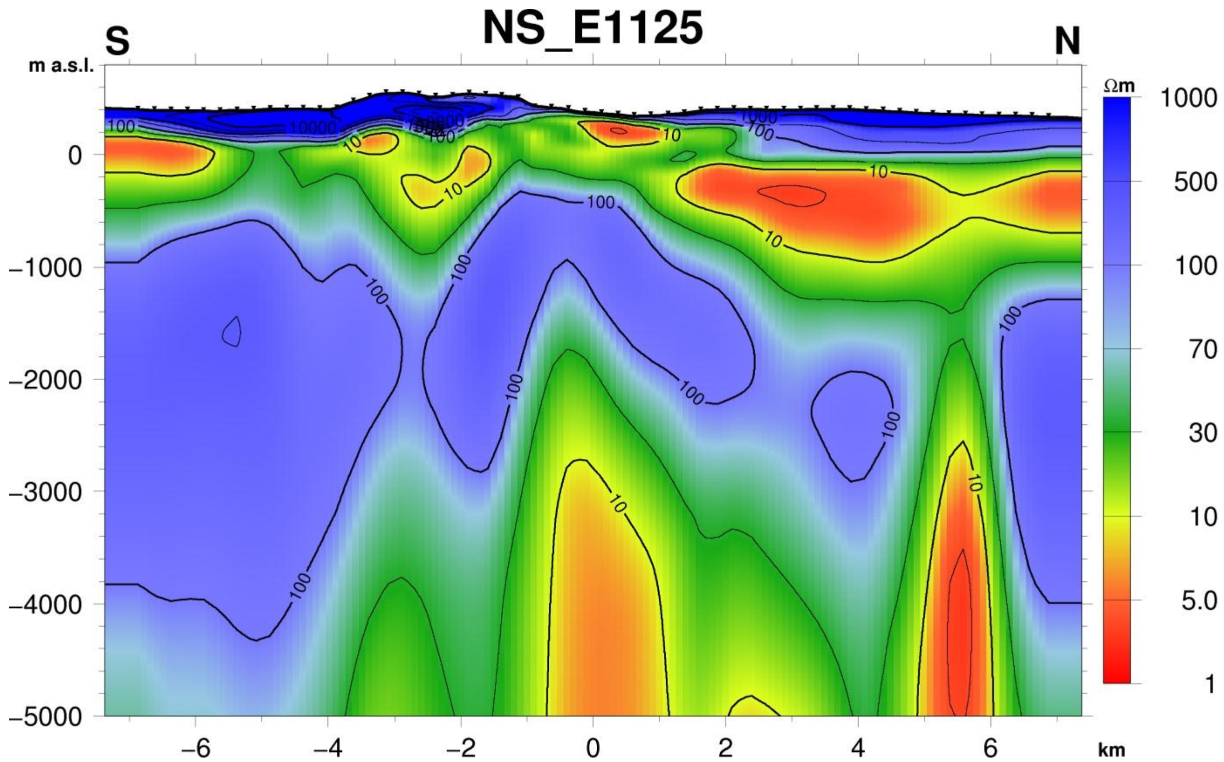
NS_E1125
S
N
m a.s.l.
0
−1000
−2000
−3000
−4000
−5000
−6
−4
−2
0
2
4
6
km
Ωm
1000
500
100
70
30
10
5.0
1

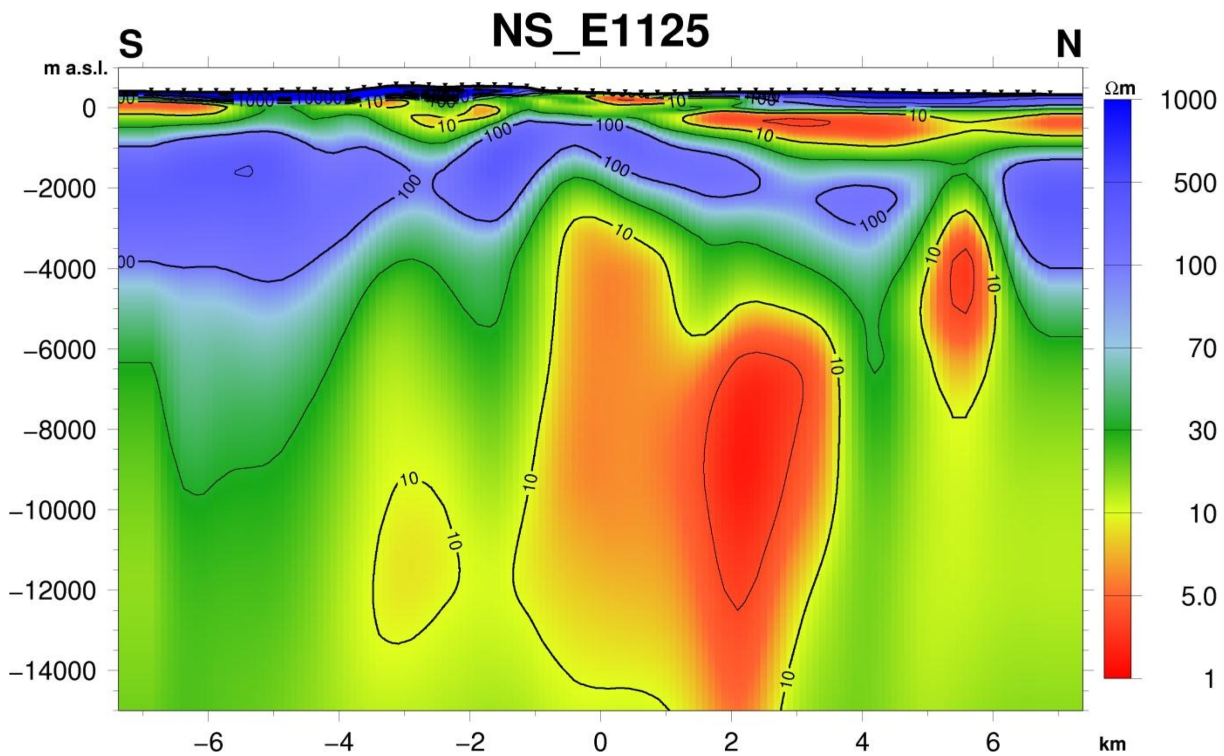
NS_E1125
S
N
m a.s.l.
0
−2000
−4000
−6000
−8000
−10000
−12000
−14000
−6
−4
−2
0
2
4
6
km
Ωm
1000
500
100
70
30
10
5.0
1

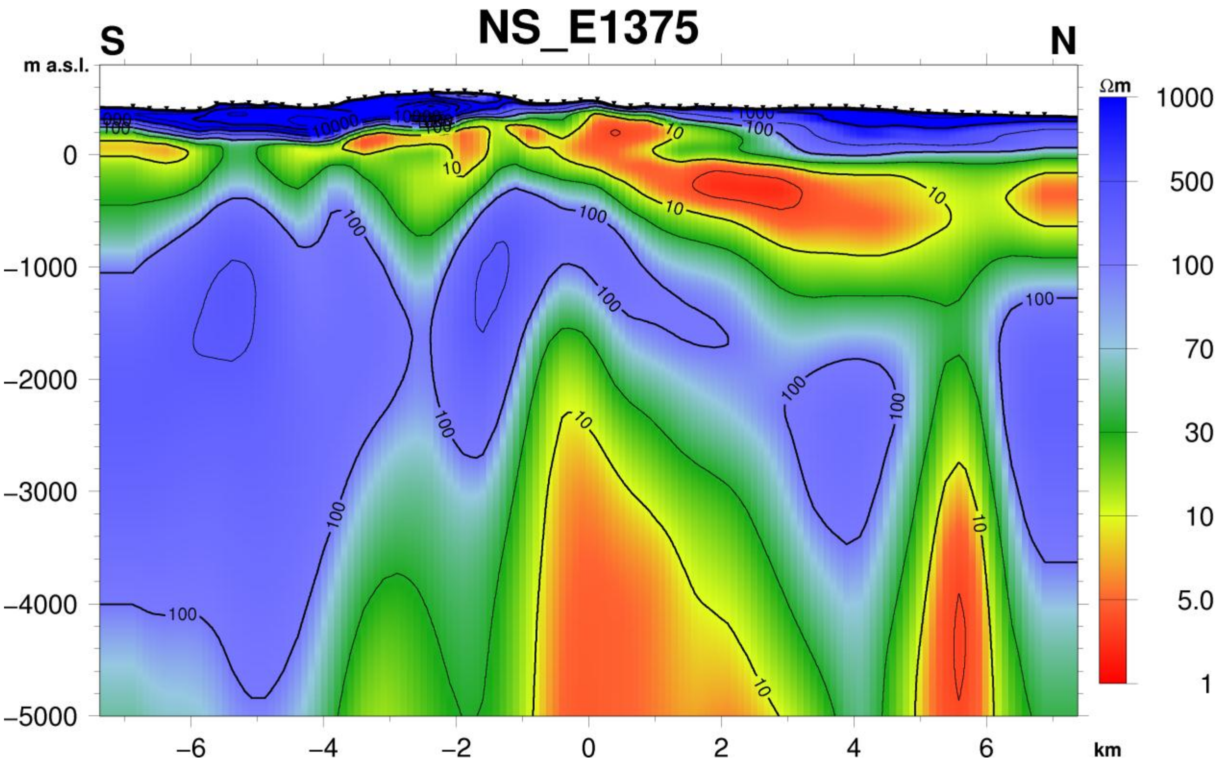

NS_E1375
S
N
m a.s.l.
Ωm
1000
500
100
70
30
10
5.0
1
0
−1000
−2000
−3000
−4000
−5000
−6
−4
−2
0
2
4
6
km

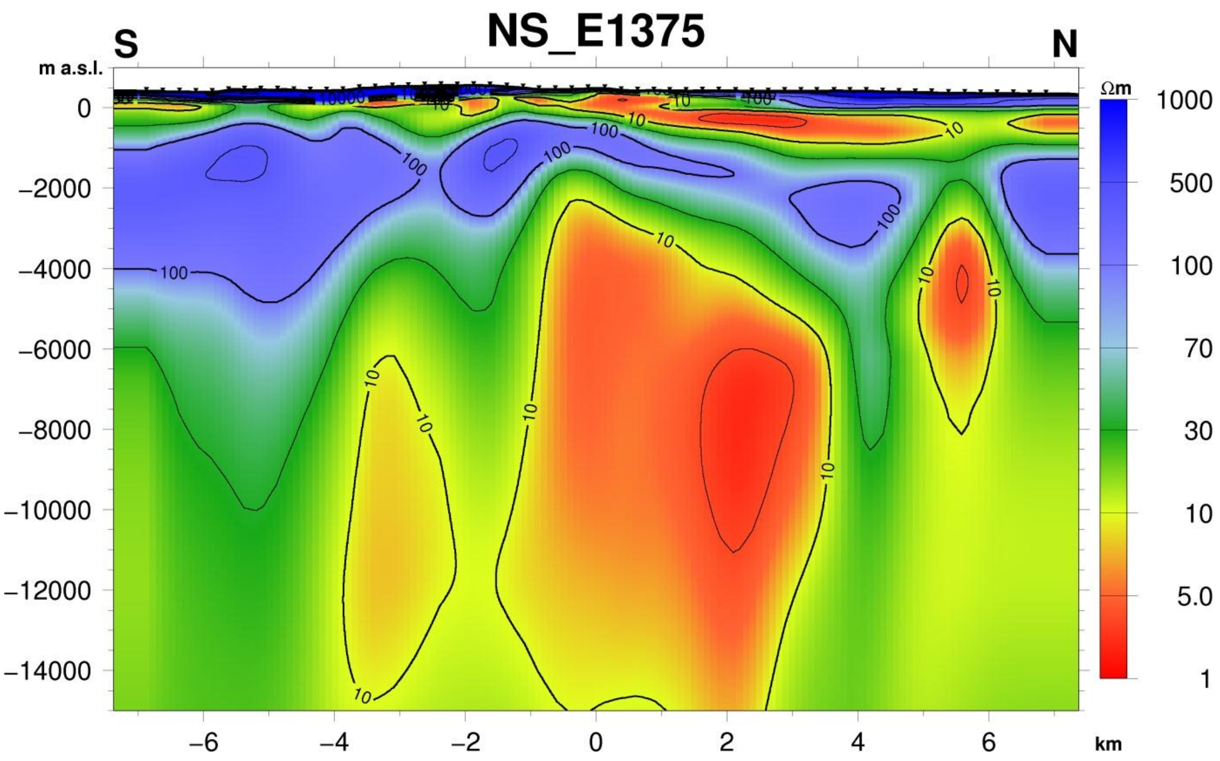

NS_E1375
S
N
m a.s.l.
Ωm
1000
500
100
70
30
10
5.0
1
0
−2000
−4000
−6000
−8000
−10000
−12000
−14000
−6
−4
−2
0
2
4
6
km

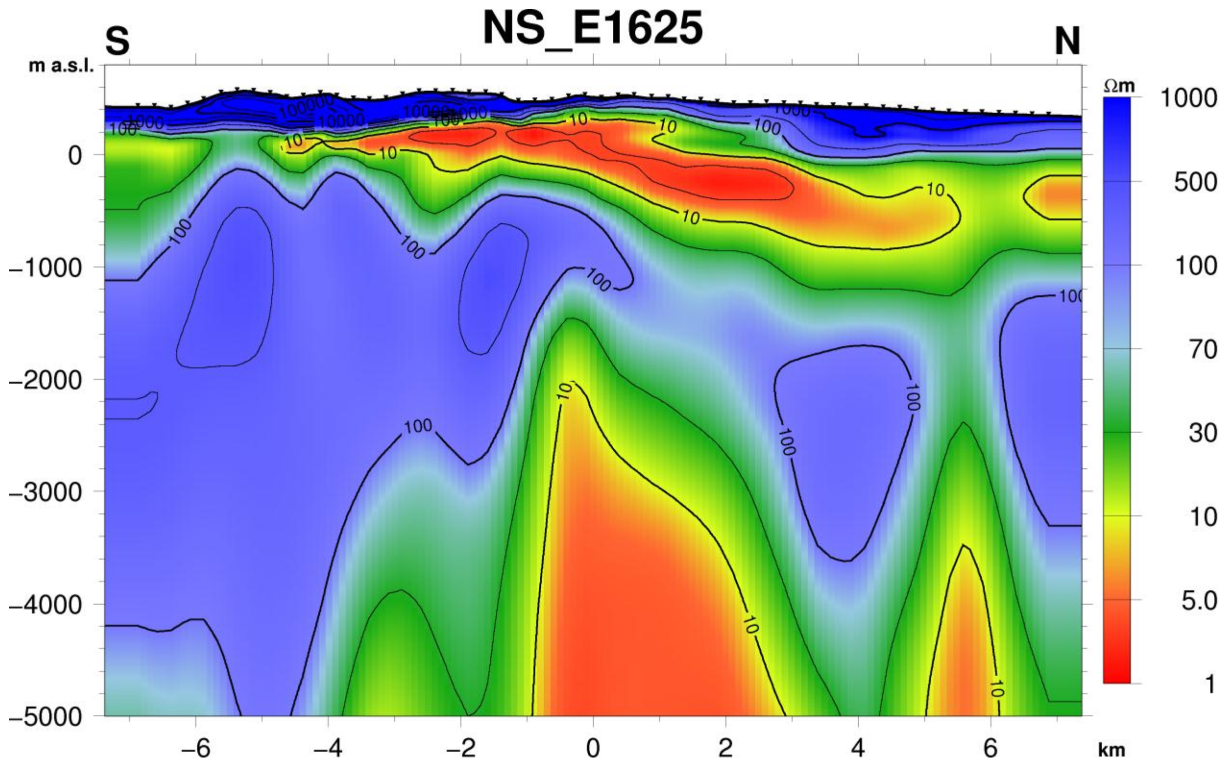

NS_E1625
S
N
m a.s.l.
0
−1000
−2000
−3000
−4000
−5000
−6
−4
−2
0
2
4
6
km
Ωm
1000
500
100
70
30
10
5.0
1

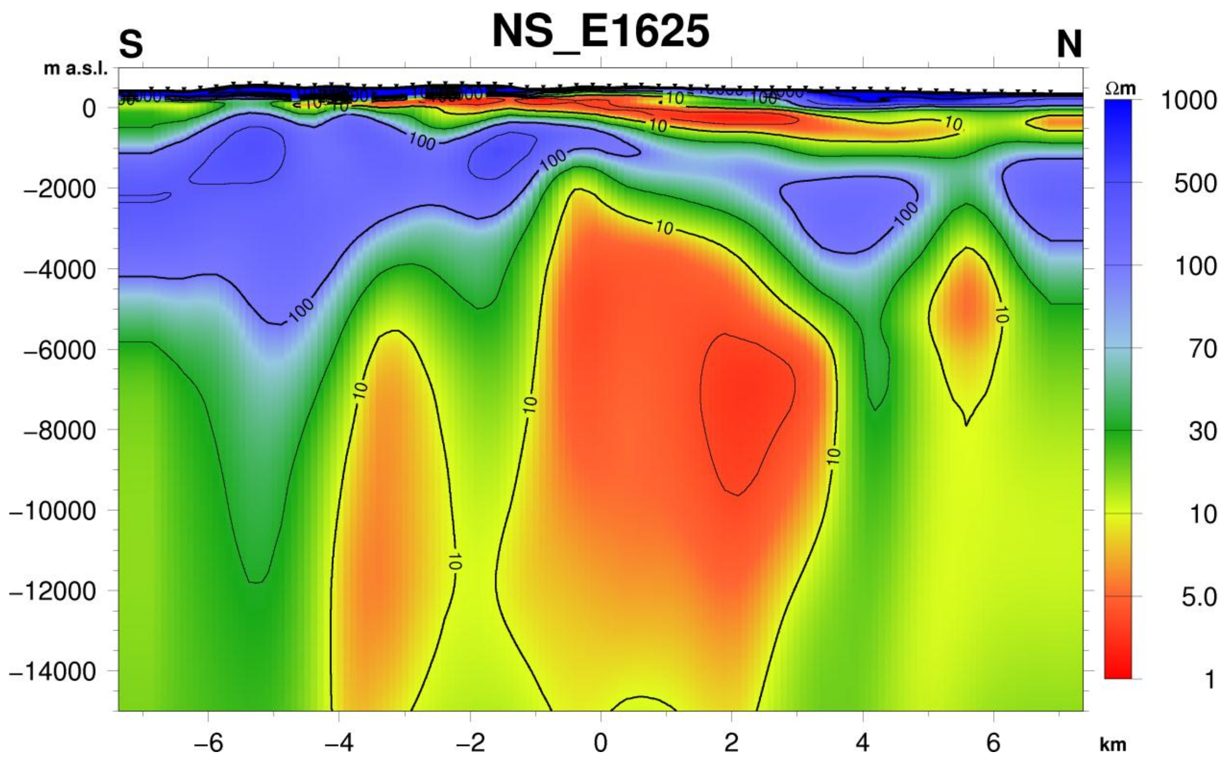

NS_E1625
S
N
m a.s.l.
0
−2000
−4000
−6000
−8000
−10000
−12000
−14000
−6
−4
−2
0
2
4
6
km
Ωm
1000
500
100
70
30
10
5.0
1

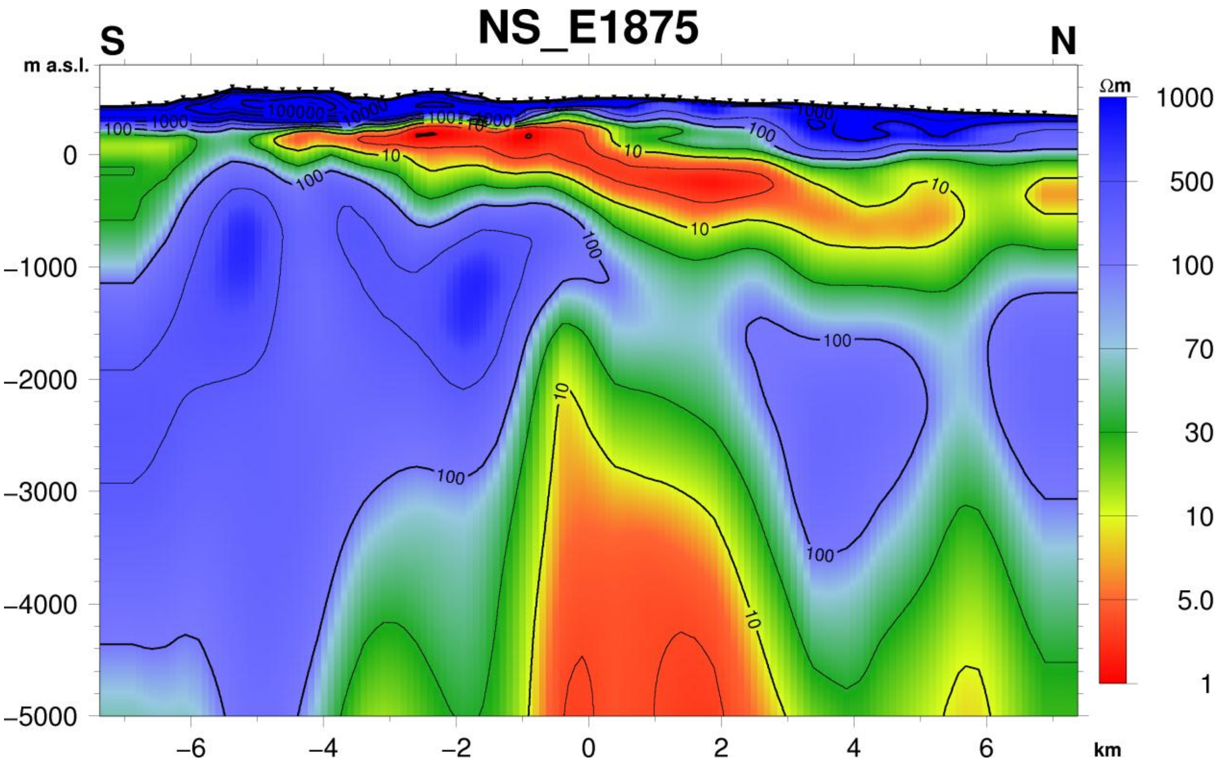
NS_E1875
S
N
m a.s.l.
0
−1000
−2000
−3000
−4000
−5000
−6
−4
−2
0
2
4
6
km
Ωm
1000
500
100
70
30
10
5.0
1

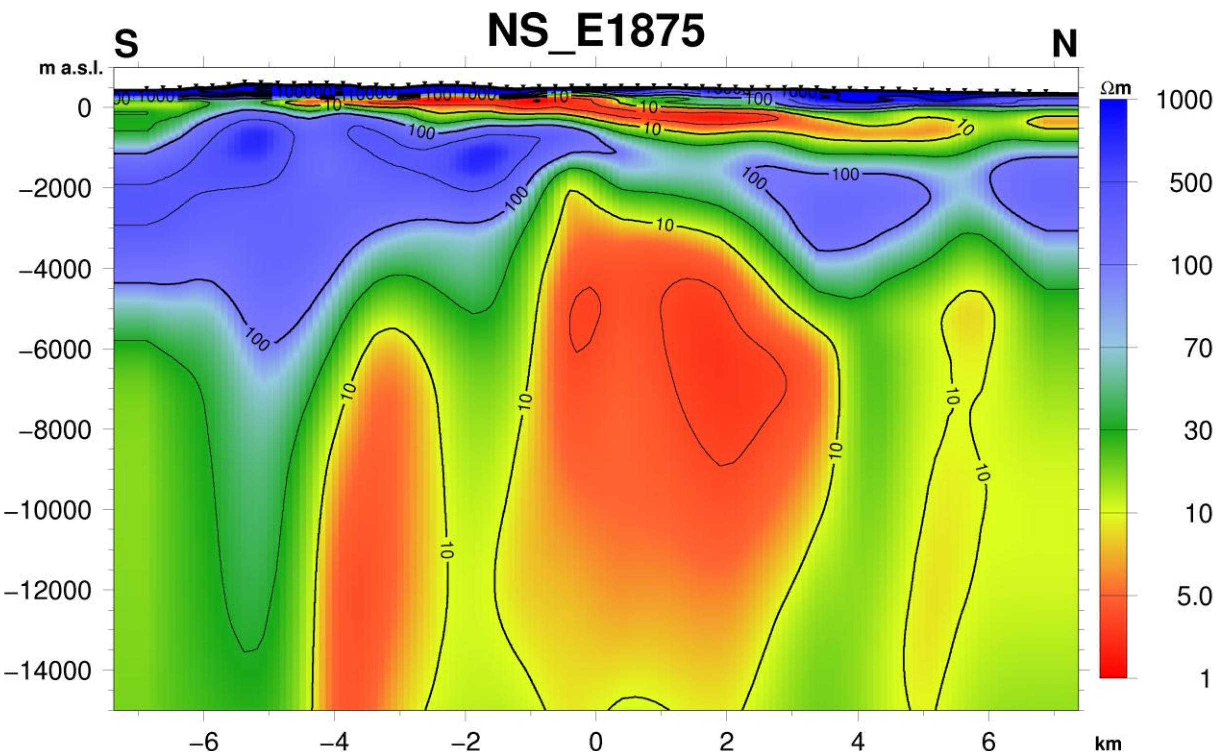
NS_E1875
S
N
m a.s.l.
0
−2000
−4000
−6000
−8000
−10000
−12000
−14000
−6
−4
−2
0
2
4
6
km
Ωm
1000
500
100
70
30
10
5.0
1

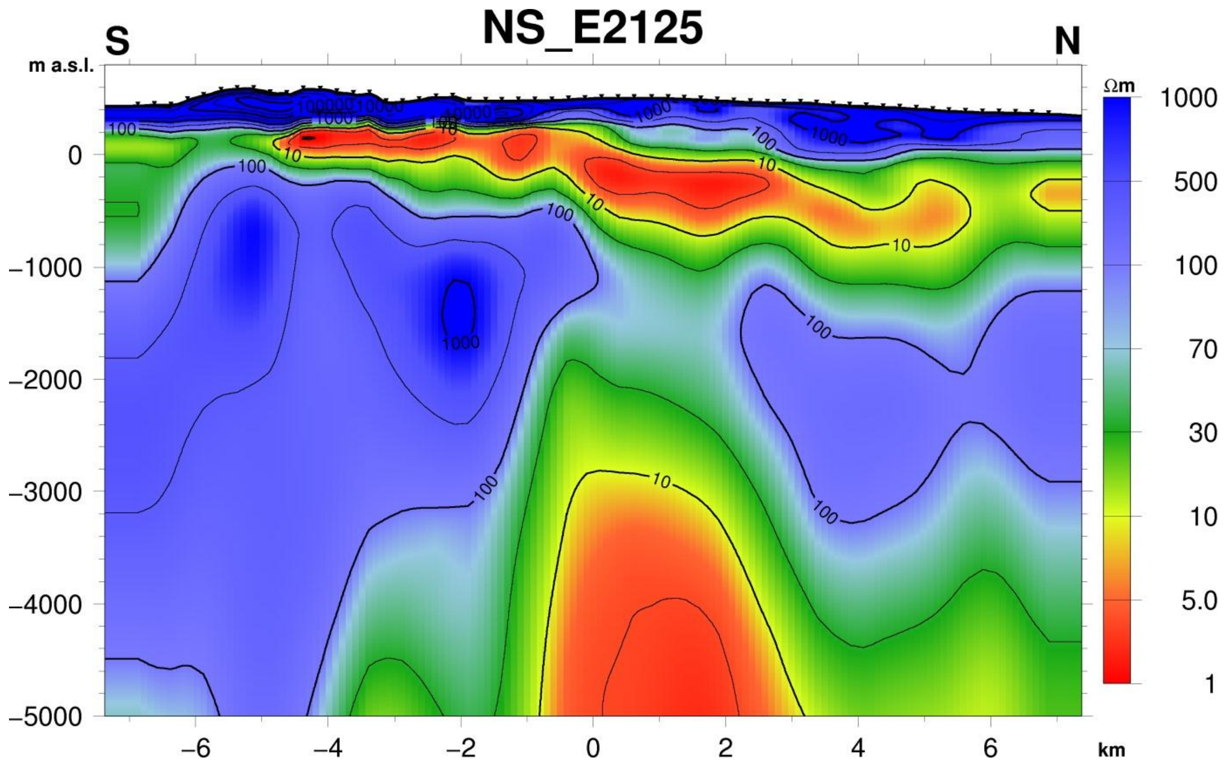

NS_E2125
S
N
m a.s.l.
0
−1000
−2000
−3000
−4000
−5000
−6
−4
−2
0
2
4
6
km
Ωm
1000
500
100
70
30
10
5.0
1

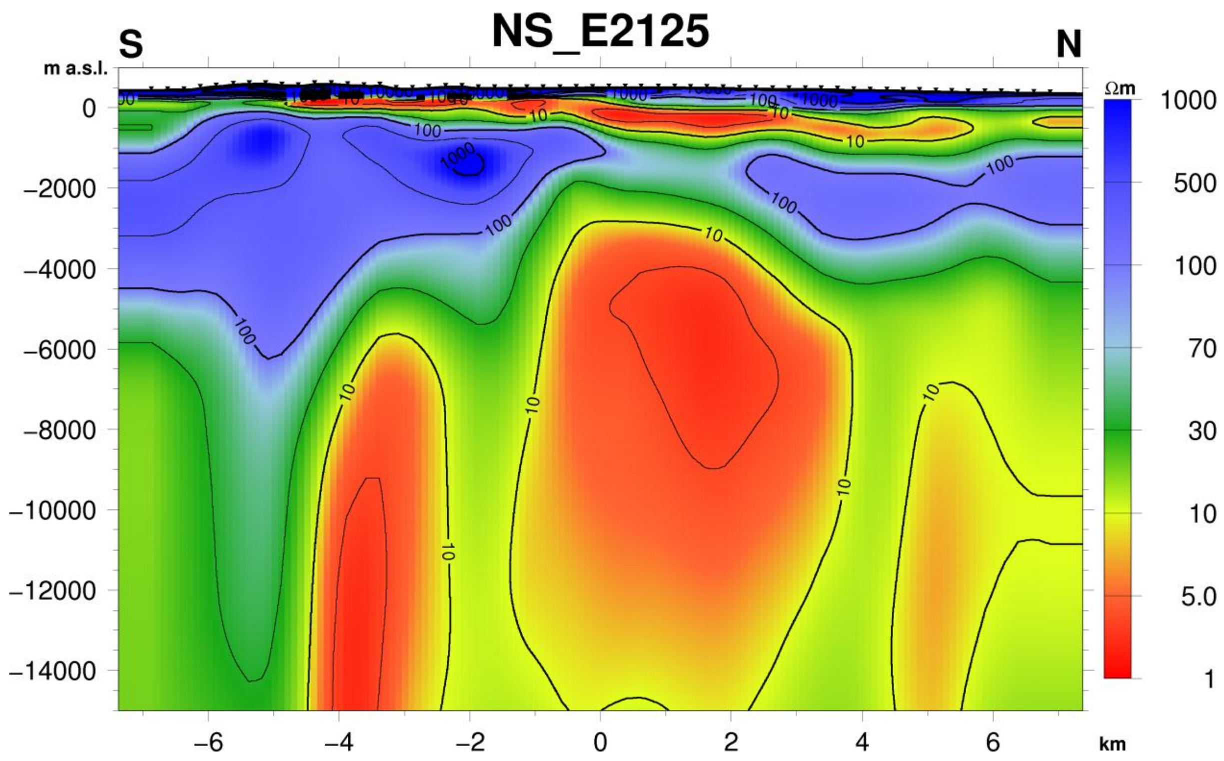

NS_E2125
S
N
m a.s.l.
0
−2000
−4000
−6000
−8000
−10000
−12000
−14000
−6
−4
−2
0
2
4
6
km
Ωm
1000
500
100
70
30
10
5.0
1

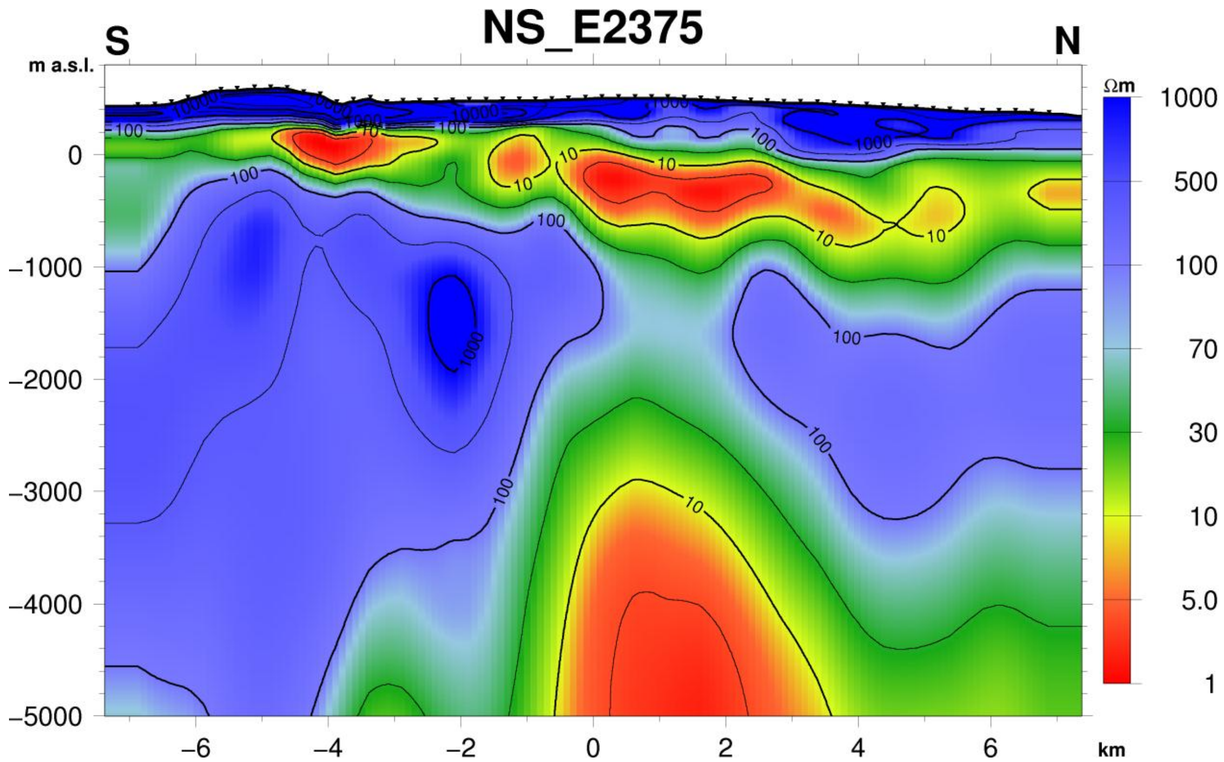

NS_E2375
S
N
m a.s.l.
Ωm
km

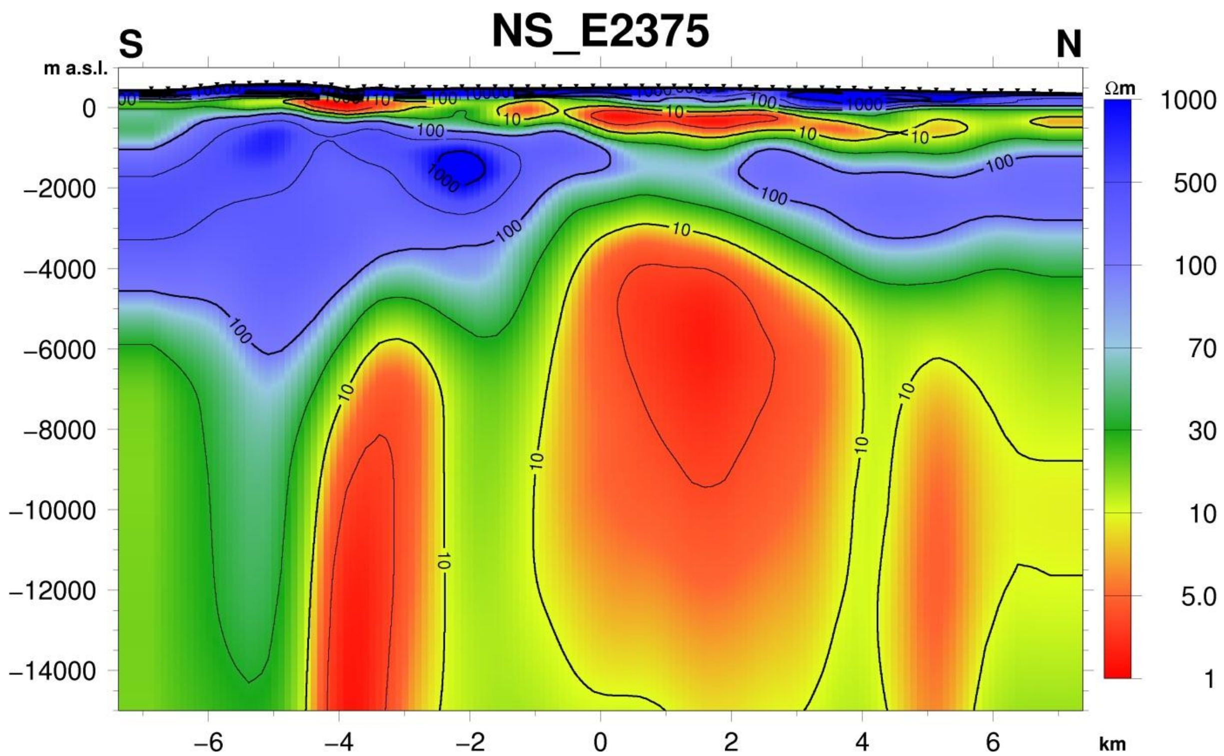

NS_E2375
S
N
m a.s.l.
Ωm
km

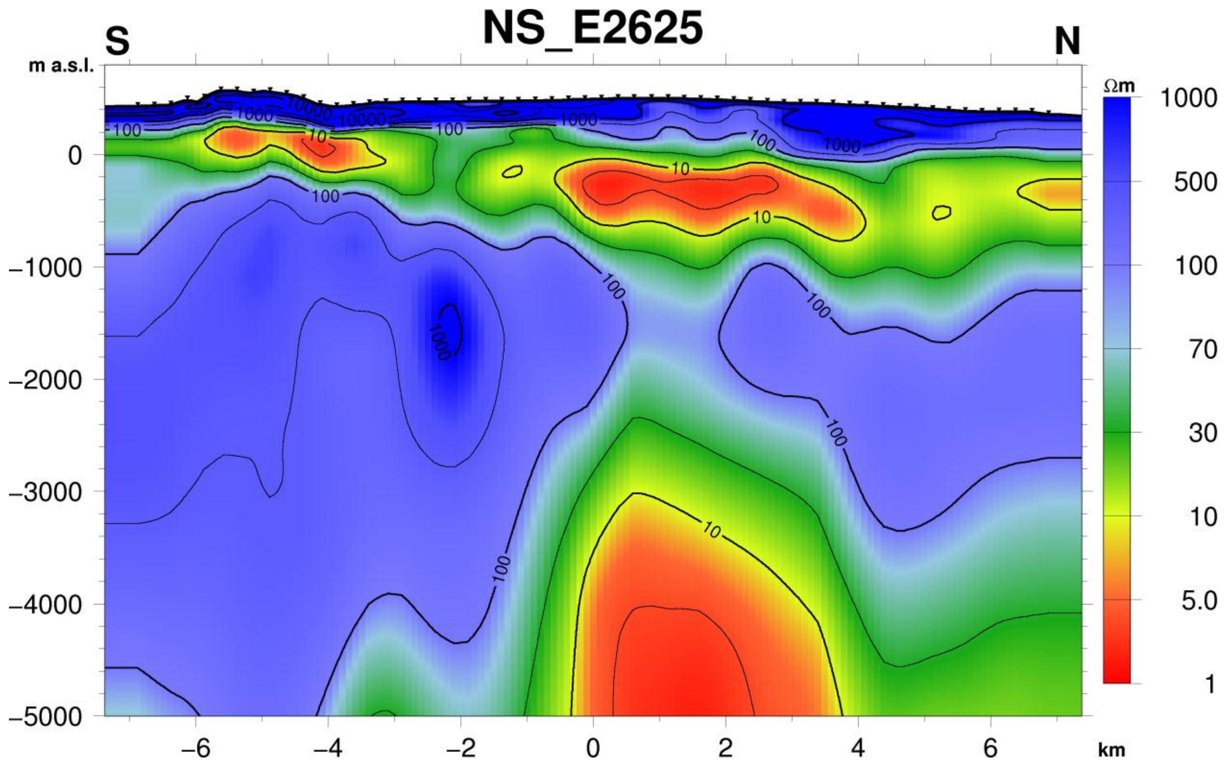
NS_E2625
S
N
m a.s.l.
Ωm
0
−1000
−2000
−3000
−4000
−5000
−6
−4
−2
0
2
4
6
km
1000
500
100
70
30
10
5.0
1

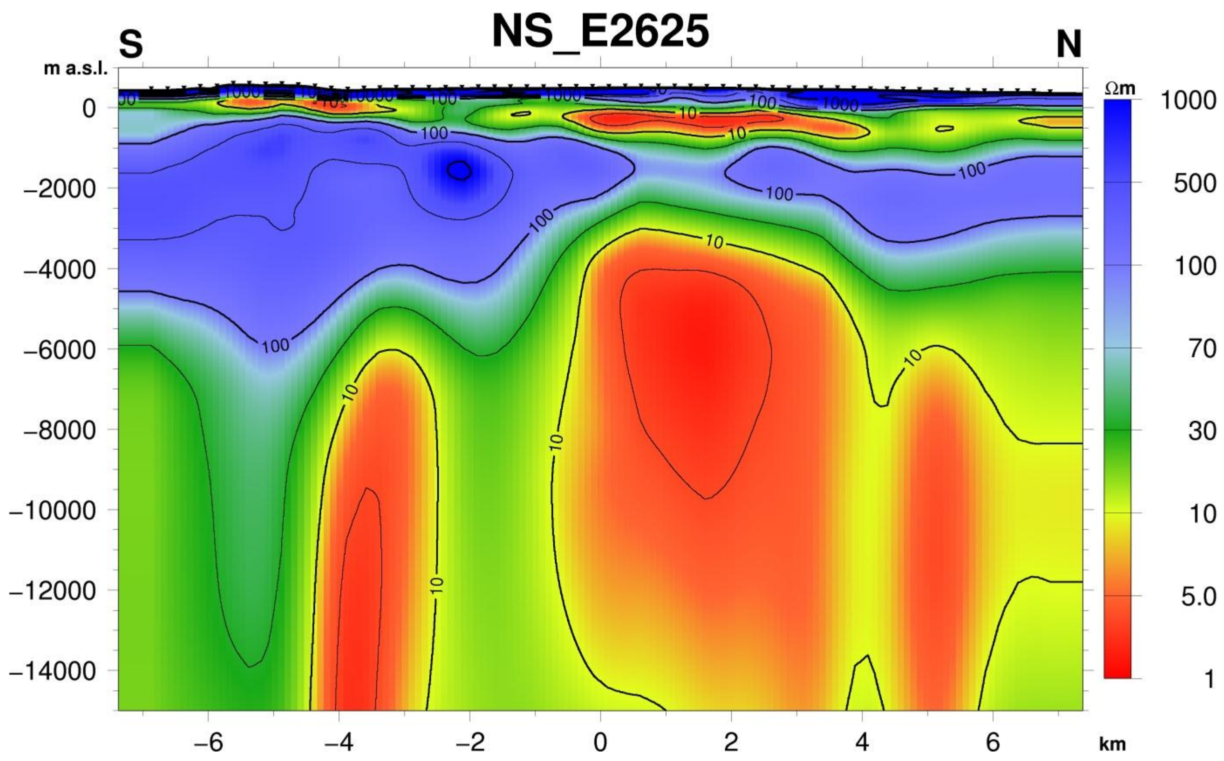
NS_E2625
S
N
m a.s.l.
Ωm
0
−2000
−4000
−6000
−8000
−10000
−12000
−14000
−6
−4
−2
0
2
4
6
km
1000
500
100
70
30
10
5.0
1

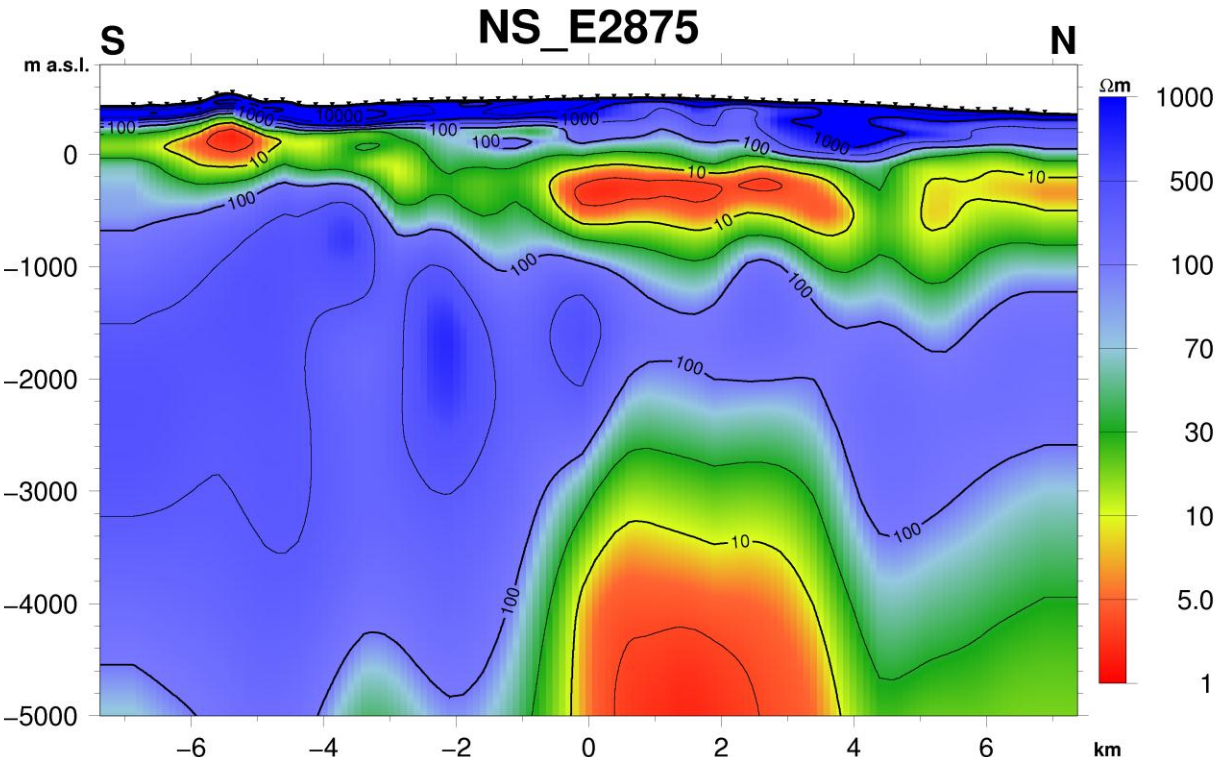
NS_E2875
S
N
m a.s.l.
0
−1000
−2000
−3000
−4000
−5000
−6
−4
−2
0
2
4
6
km
Ωm
1000
500
100
70
30
10
5.0
1
10000
1000
100
10

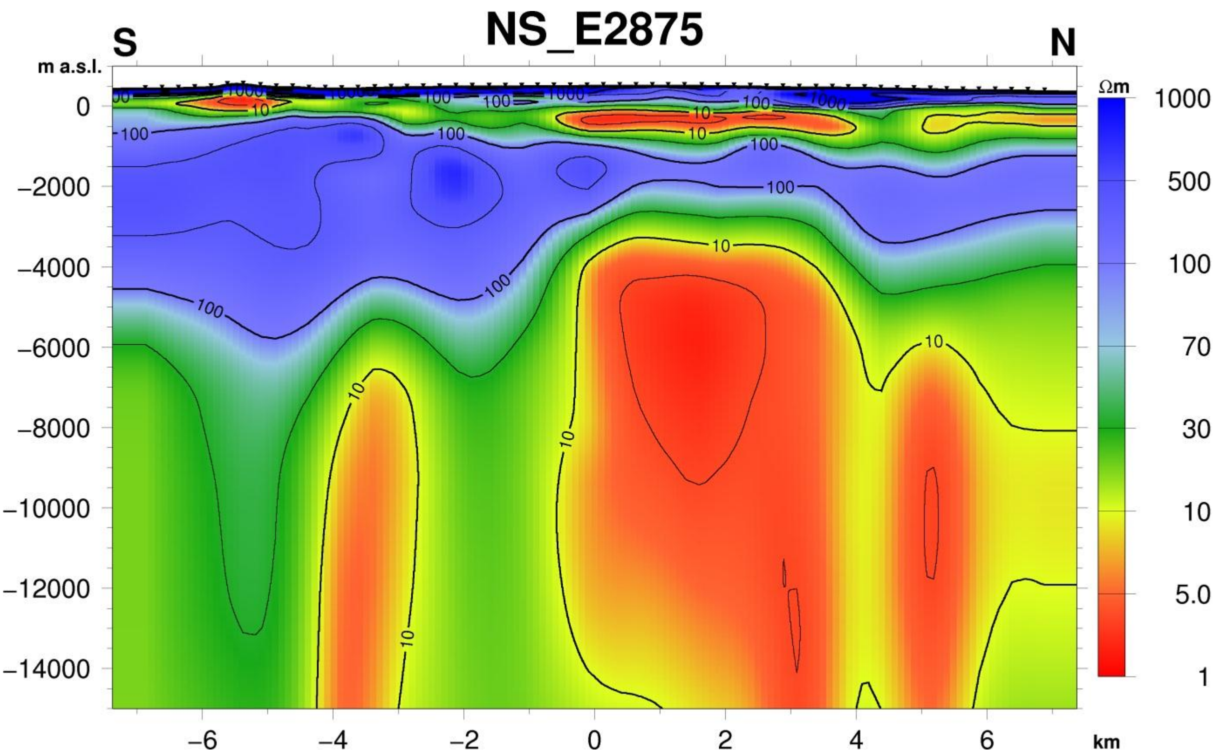
NS_E2875
S
N
m a.s.l.
0
−2000
−4000
−6000
−8000
−10000
−12000
−14000
−6
−4
−2
0
2
4
6
km
Ωm
1000
500
100
70
30
10
5.0
1
1000
100
10

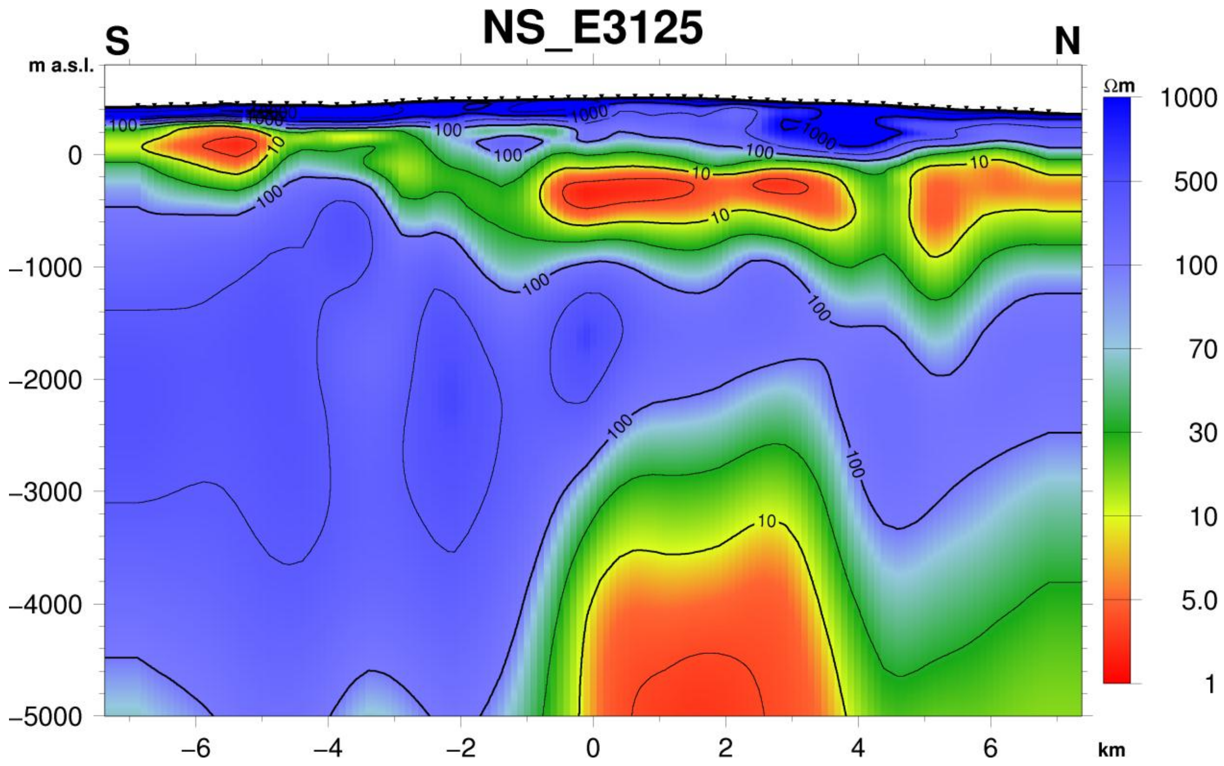
NS_E3125
S
N
m a.s.l.
Ωm
1000
500
100
70
30
10
5.0
1
0
−1000
−2000
−3000
−4000
−5000
−6
−4
−2
0
2
4
6
km

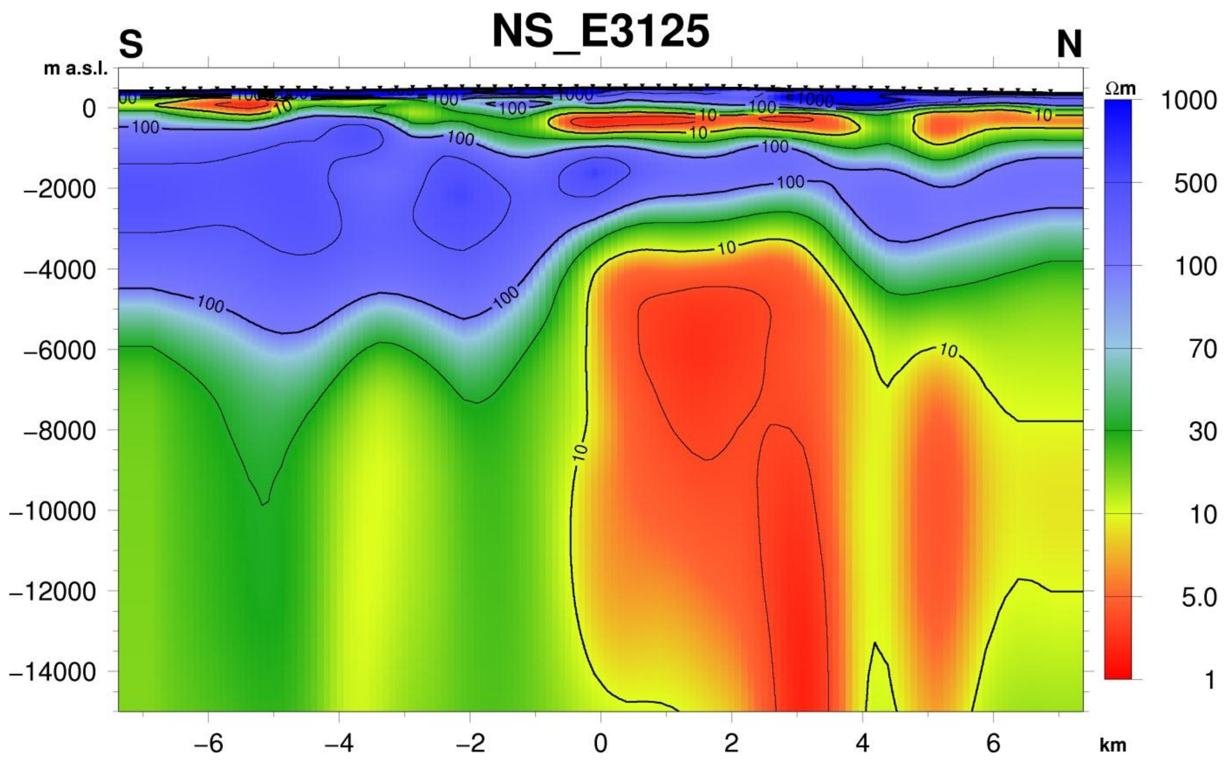
NS_E3125
S
N
m a.s.l.
Ωm
1000
500
100
70
30
10
5.0
1
0
−2000
−4000
−6000
−8000
−10000
−12000
−14000
−6
−4
−2
0
2
4
6
km

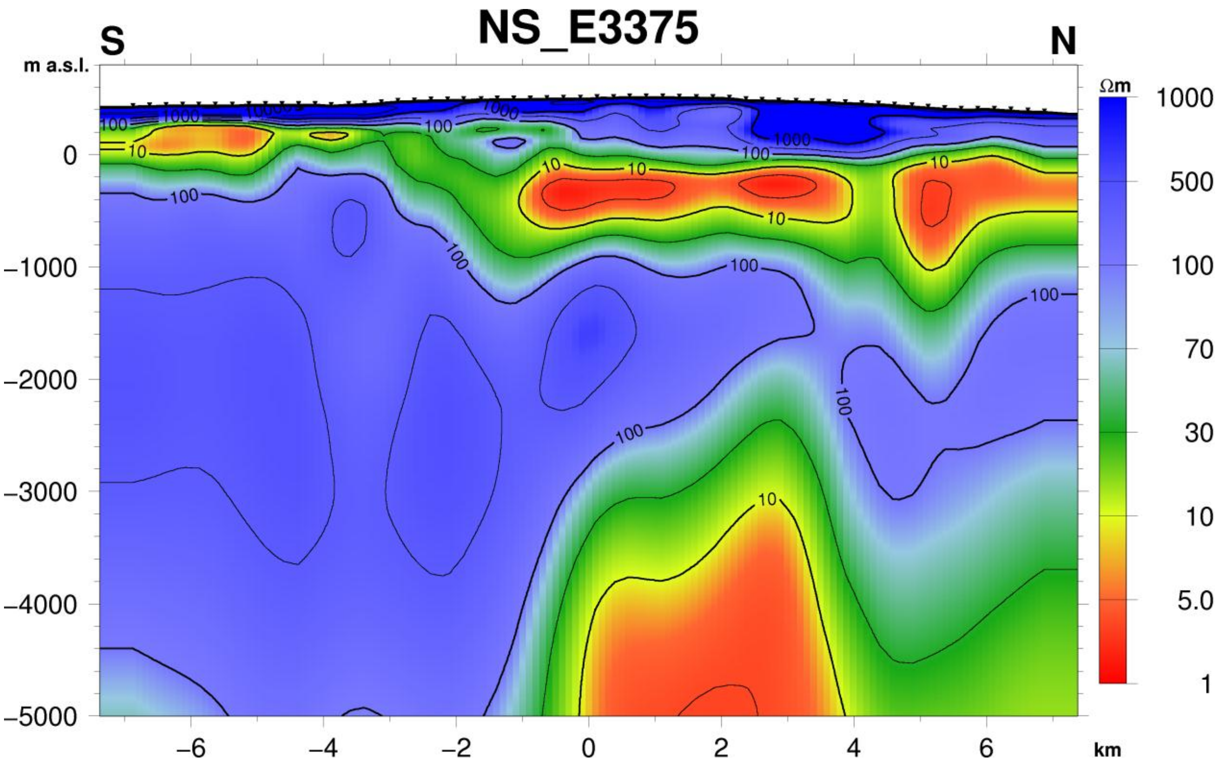

NS_E3375
S
N
m a.s.l.
0
−1000
−2000
−3000
−4000
−5000
−6
−4
−2
0
2
4
6
km
Ωm
1000
500
100
70
30
10
5.0
1

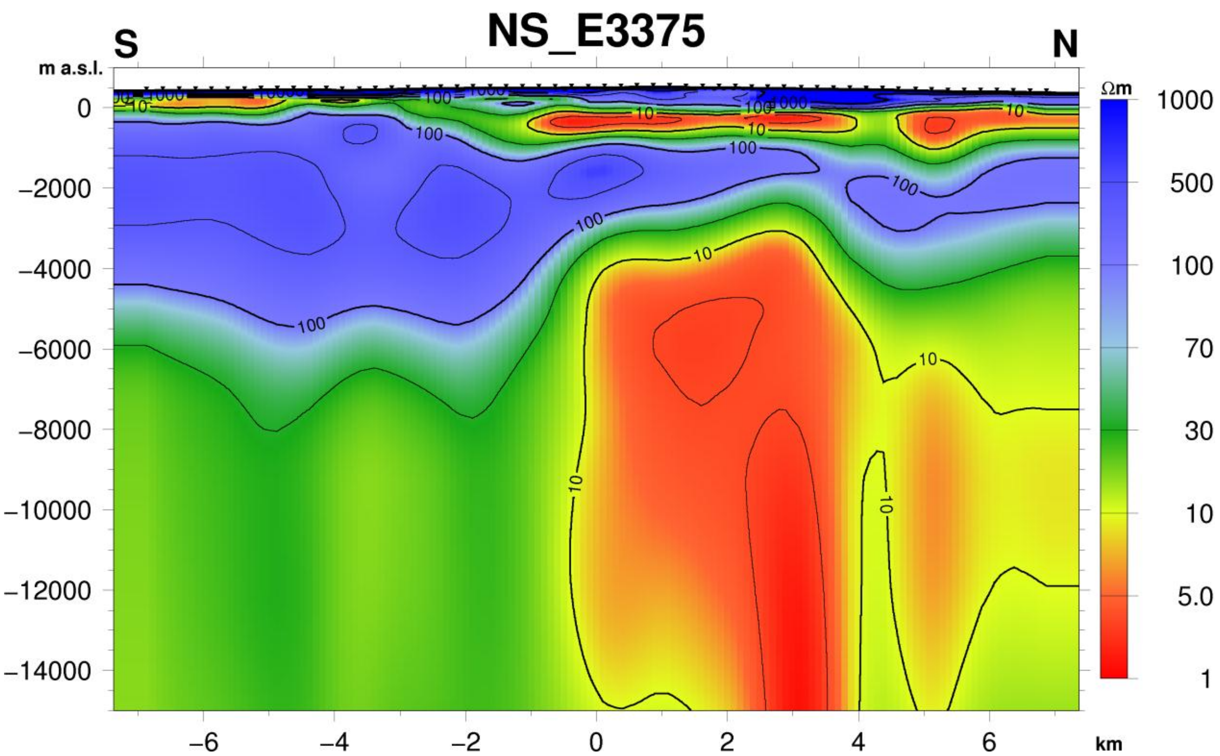

NS_E3375
S
N
m a.s.l.
0
−2000
−4000
−6000
−8000
−10000
−12000
−14000
−6
−4
−2
0
2
4
6
km
Ωm
1000
500
100
70
30
10
5.0
1

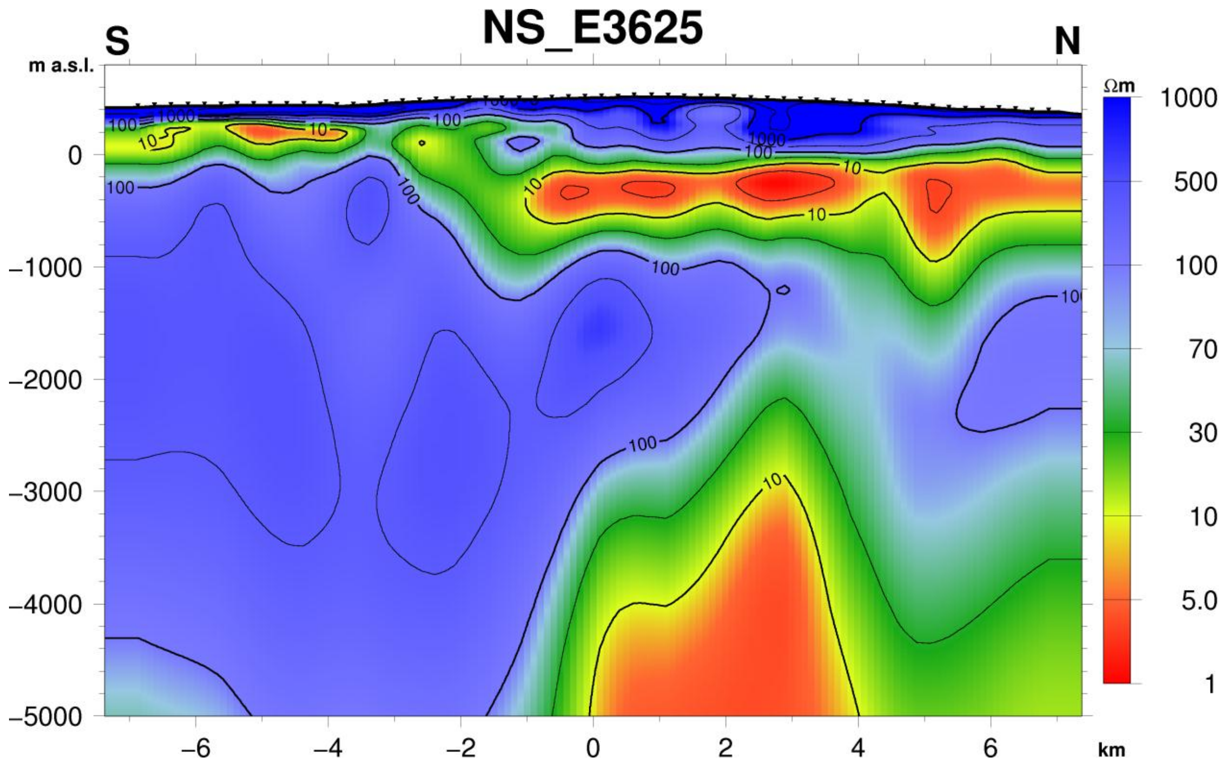
NS_E3625
S
N
m a.s.l.
Ωm
1000
500
100
70
30
10
5.0
1
0
−1000
−2000
−3000
−4000
−5000
−6
−4
−2
0
2
4
6
km

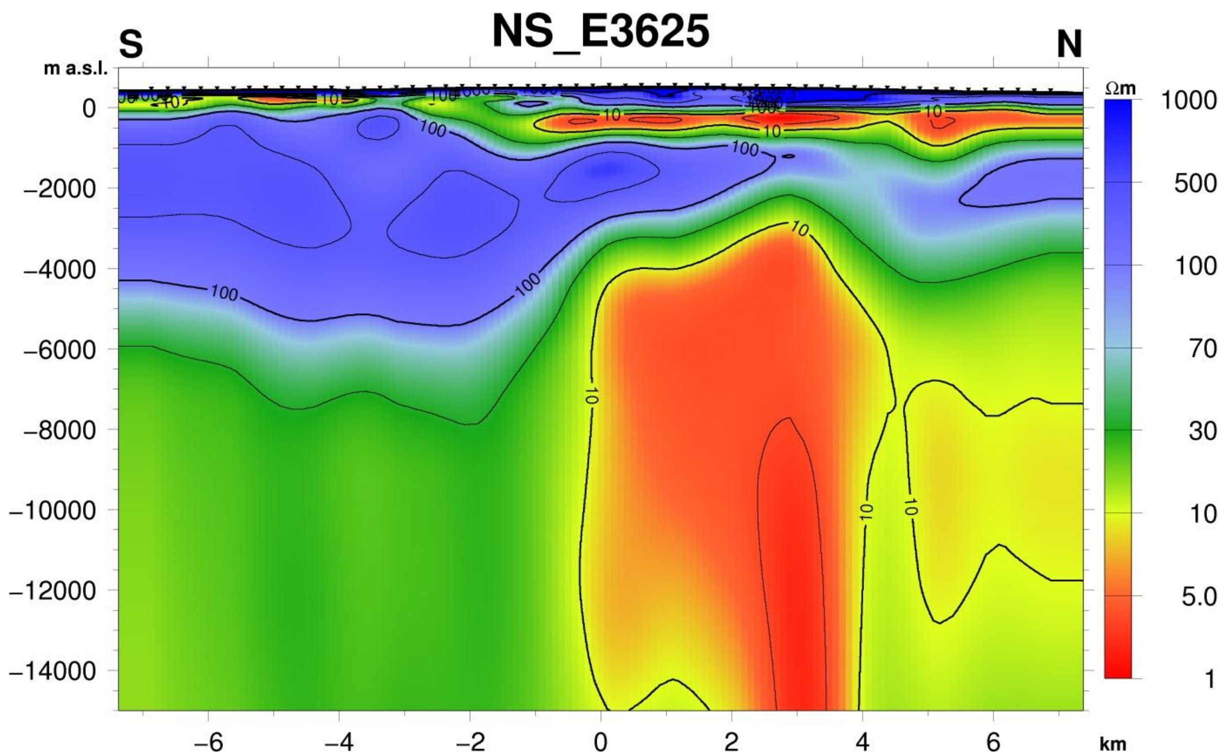
NS_E3625
S
N
m a.s.l.
Ωm
1000
500
100
70
30
10
5.0
1
0
−2000
−4000
−6000
−8000
−10000
−12000
−14000
−6
−4
−2
0
2
4
6
km

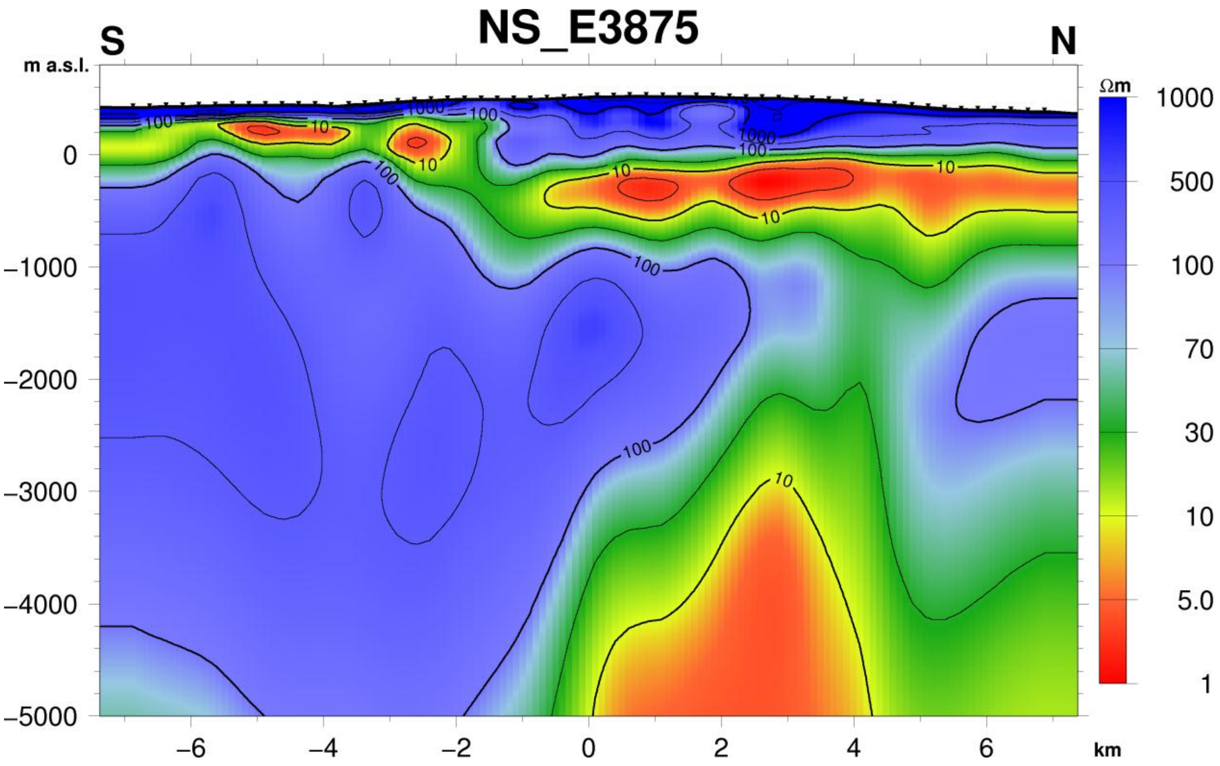
NS_E3875
S
N
m a.s.l.
0
−1000
−2000
−3000
−4000
−5000
−6
−4
−2
0
2
4
6
km
Ωm
1000
500
100
70
30
10
5.0
1

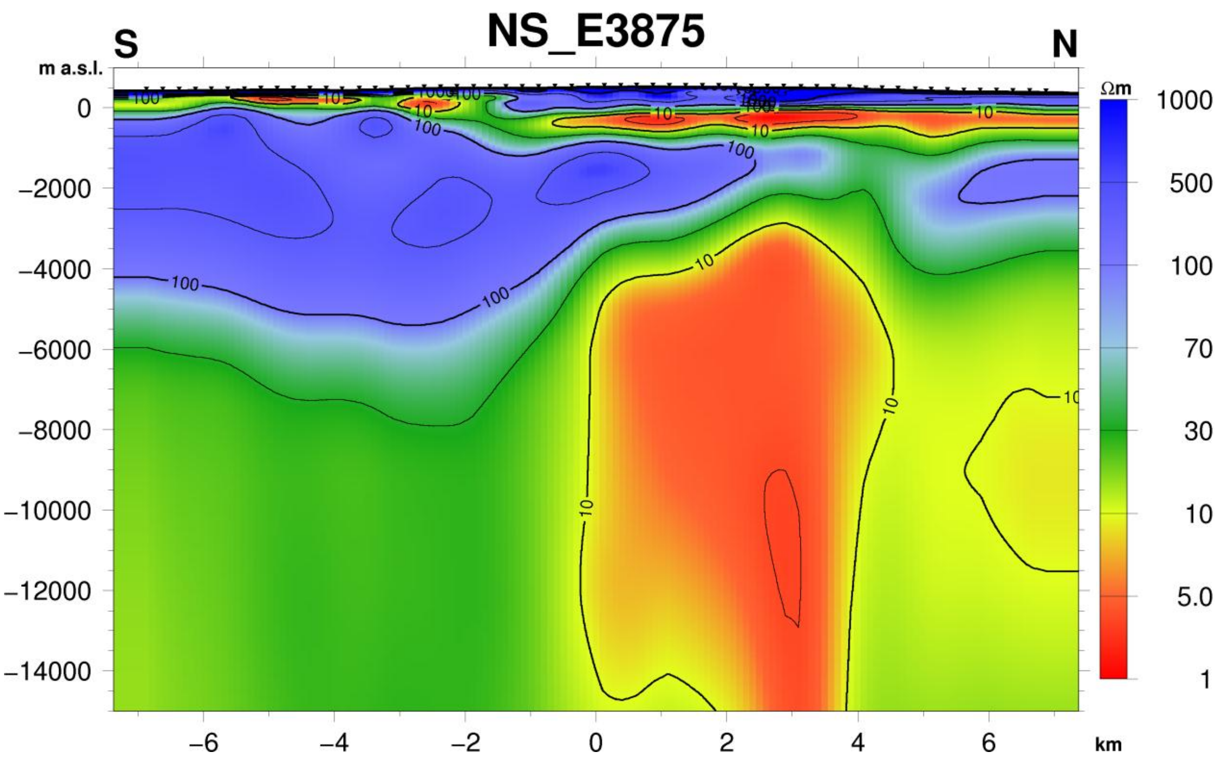
NS_E3875
S
N
m a.s.l.
0
−2000
−4000
−6000
−8000
−10000
−12000
−14000
−6
−4
−2
0
2
4
6
km
Ωm
1000
500
100
70
30
10
5.0
1

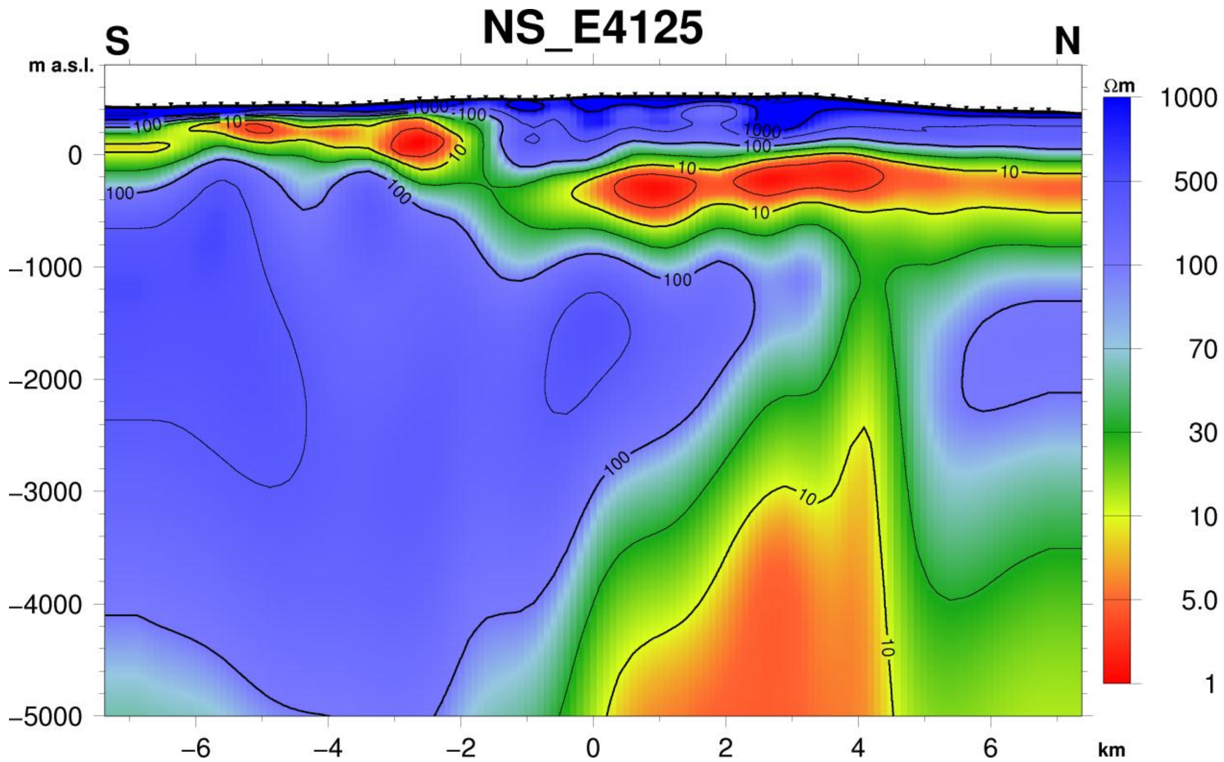
NS_E4125
S
N
m a.s.l.
0
−1000
−2000
−3000
−4000
−5000
−6
−4
−2
0
2
4
6
km
Ωm
1000
500
100
70
30
10
5.0
1

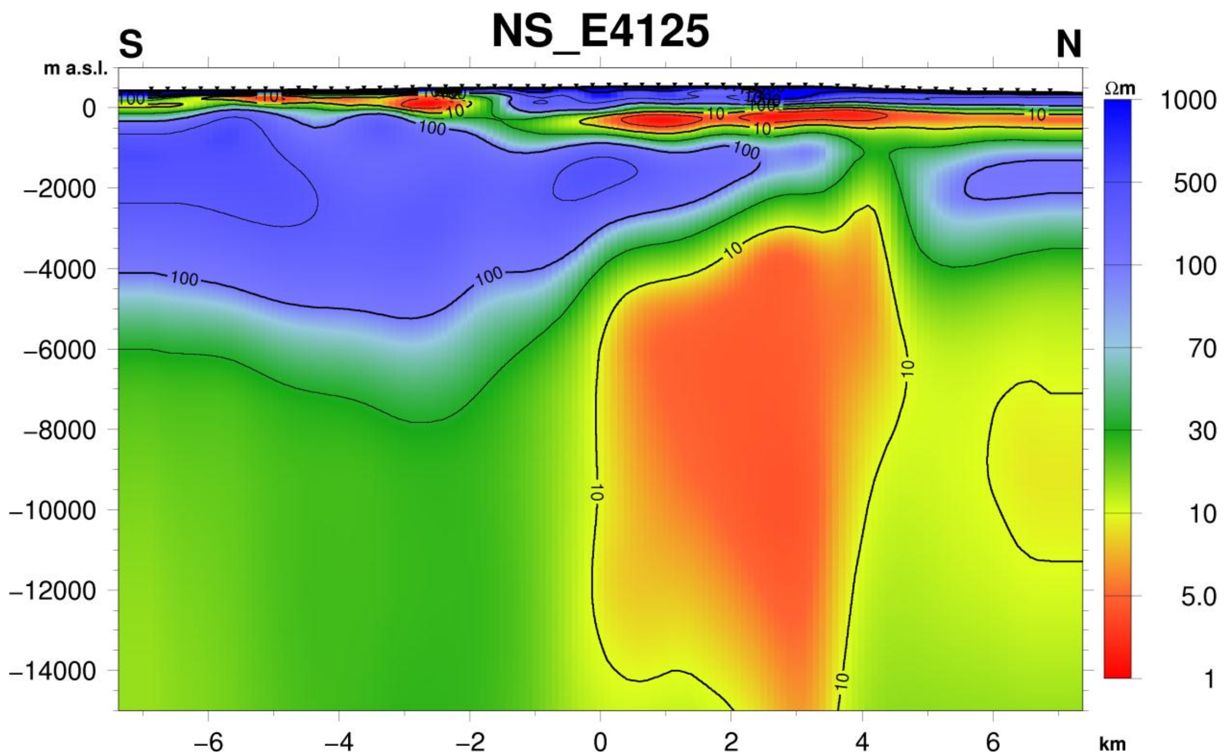
NS_E4125
S
N
m a.s.l.
0
−2000
−4000
−6000
−8000
−10000
−12000
−14000
−6
−4
−2
0
2
4
6
km
Ωm
1000
500
100
70
30
10
5.0
1

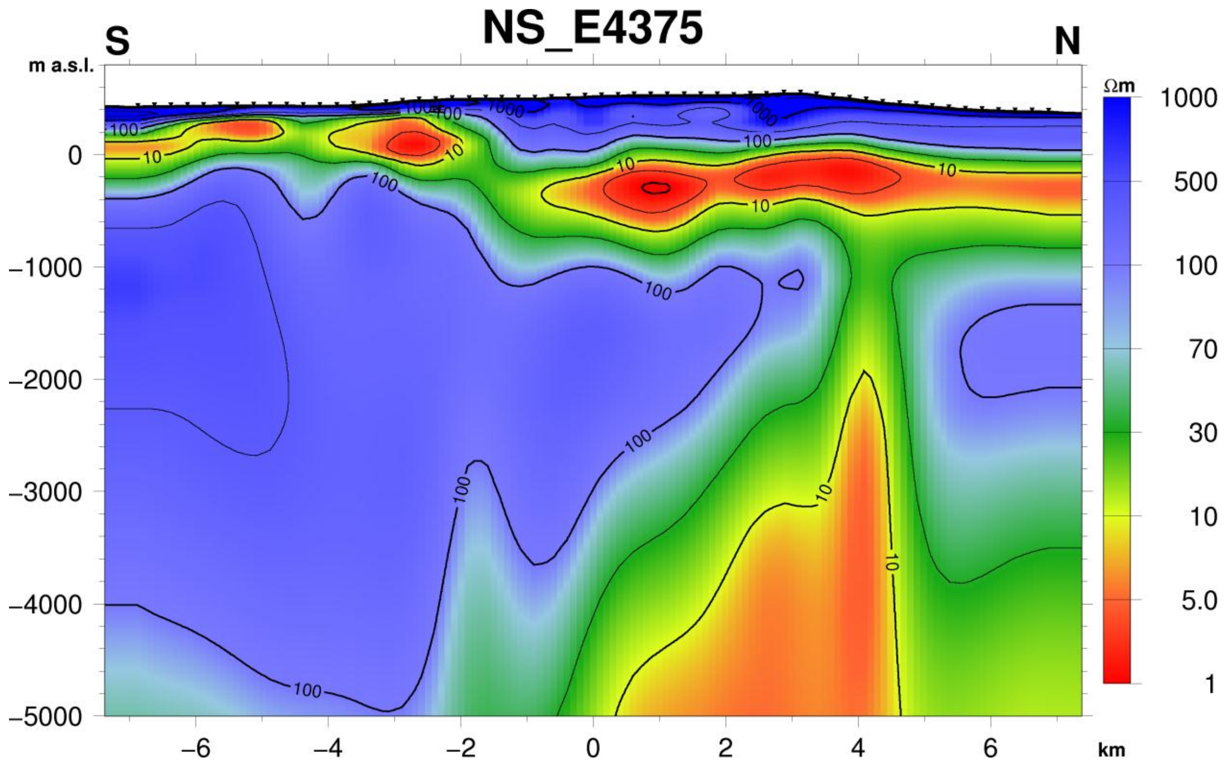
NS_E4375
S
N
m a.s.l.
Ωm
1000
500
100
70
30
10
5.0
1
0
−1000
−2000
−3000
−4000
−5000
−6
−4
−2
0
2
4
6
km

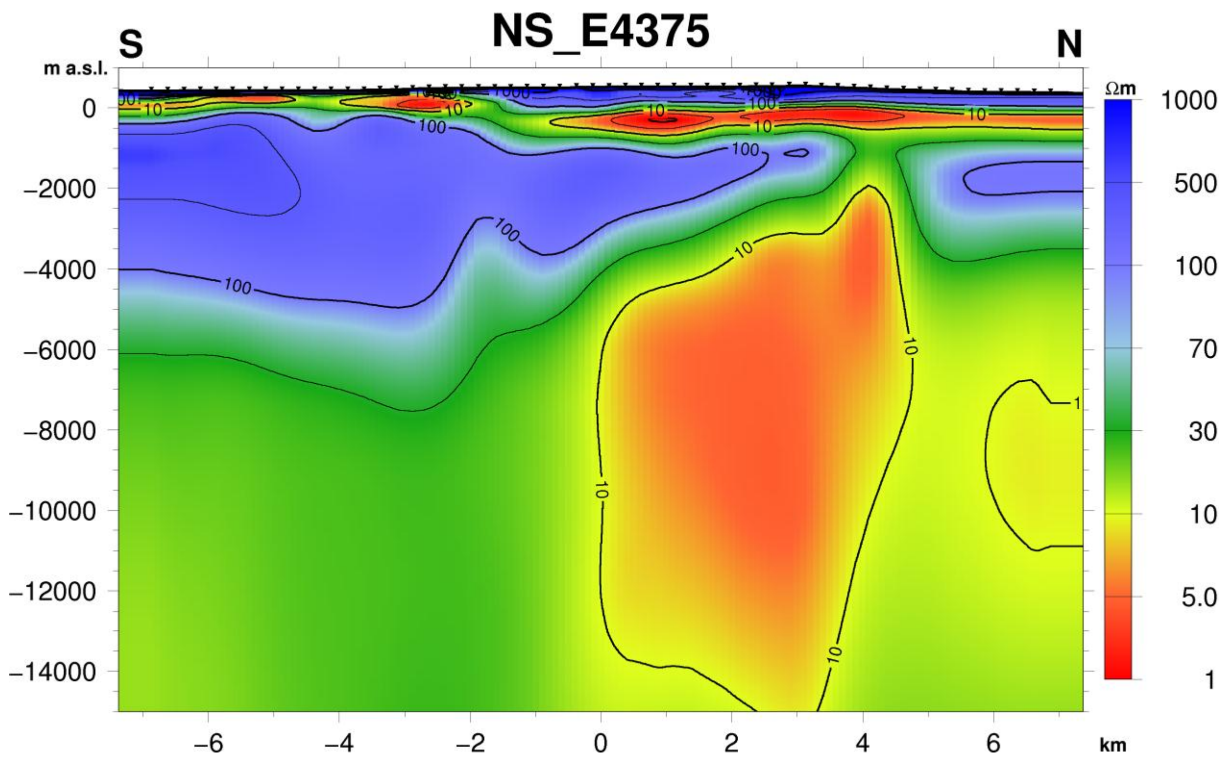
NS_E4375
S
N
m a.s.l.
Ωm
1000
500
100
70
30
10
5.0
1
0
−2000
−4000
−6000
−8000
−10000
−12000
−14000
−6
−4
−2
0
2
4
6
km

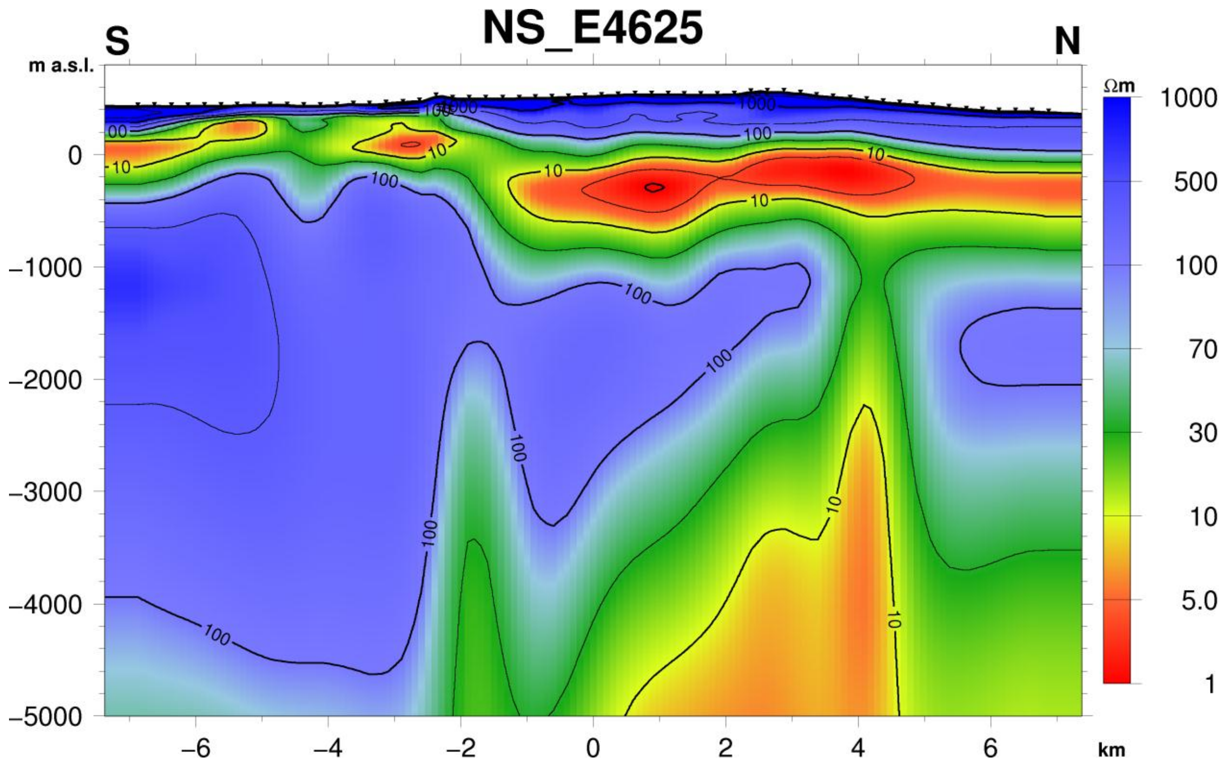
NS_E4625
S
N
m a.s.l.
Ωm
km

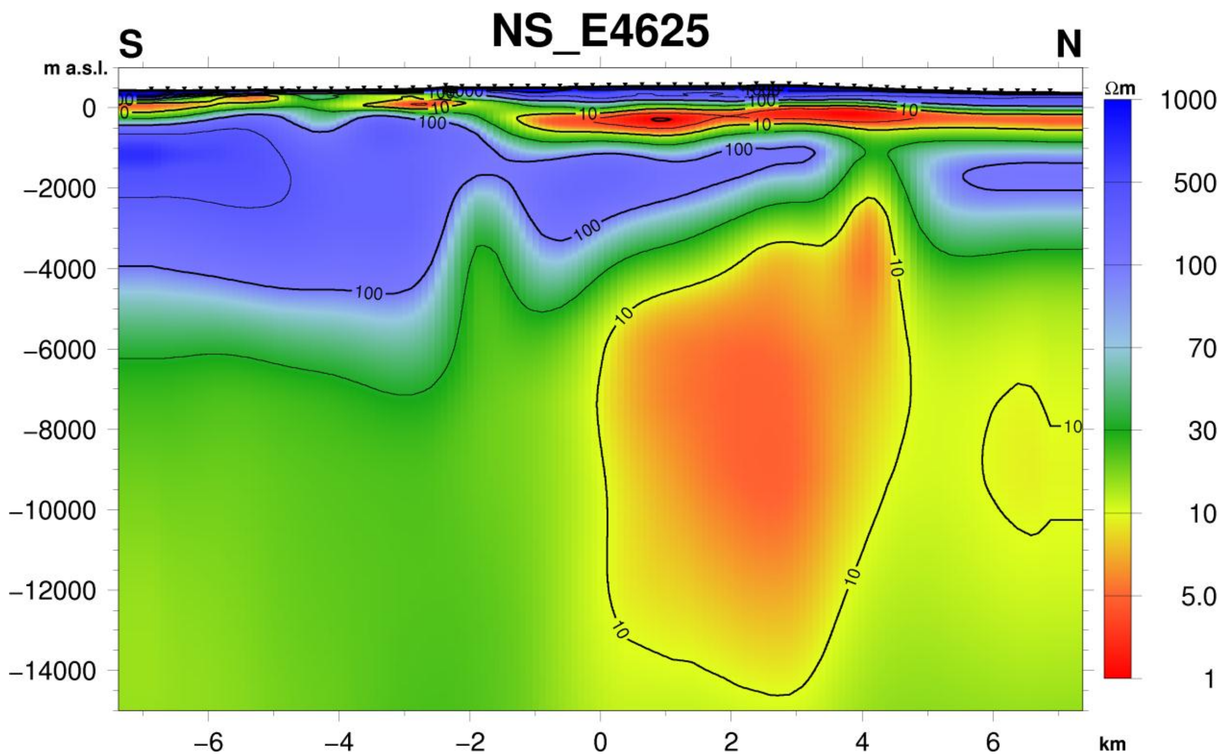
NS_E4625
S
N
m a.s.l.
Ωm
km

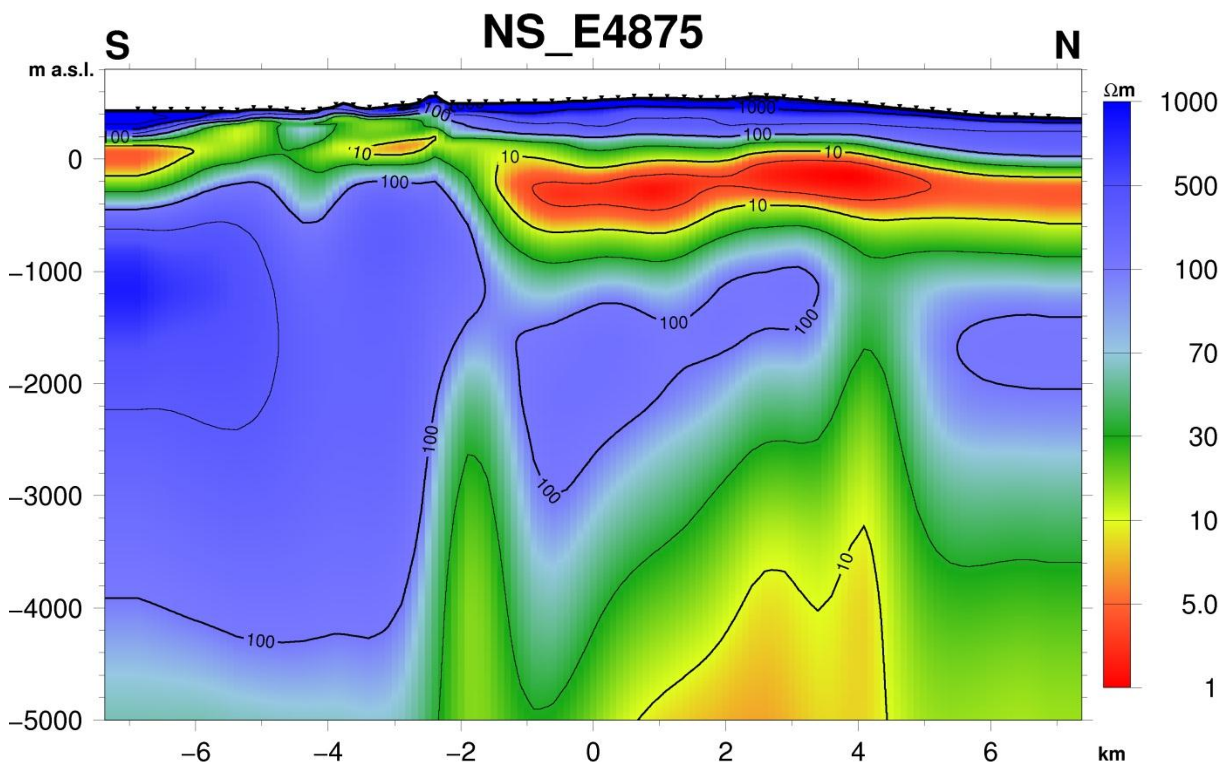

NS_E4875
S
N
m a.s.l.
0
−1000
−2000
−3000
−4000
−5000
−6
−4
−2
0
2
4
6
km
Ωm
1000
500
100
70
30
10
5.0
1

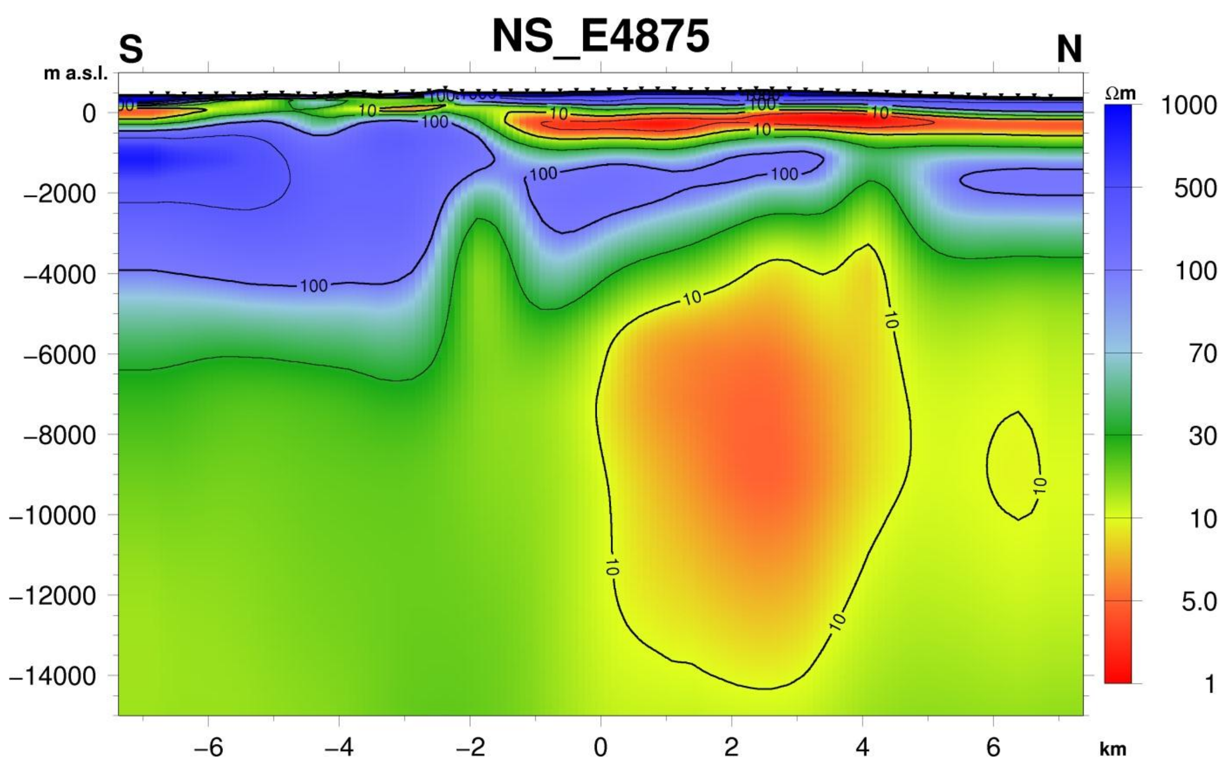

NS_E4875
S
N
m a.s.l.
0
−2000
−4000
−6000
−8000
−10000
−12000
−14000
−6
−4
−2
0
2
4
6
km
Ωm
1000
500
100
70
30
10
5.0
1

Appendix 3

East – West

Resistivity cross sections

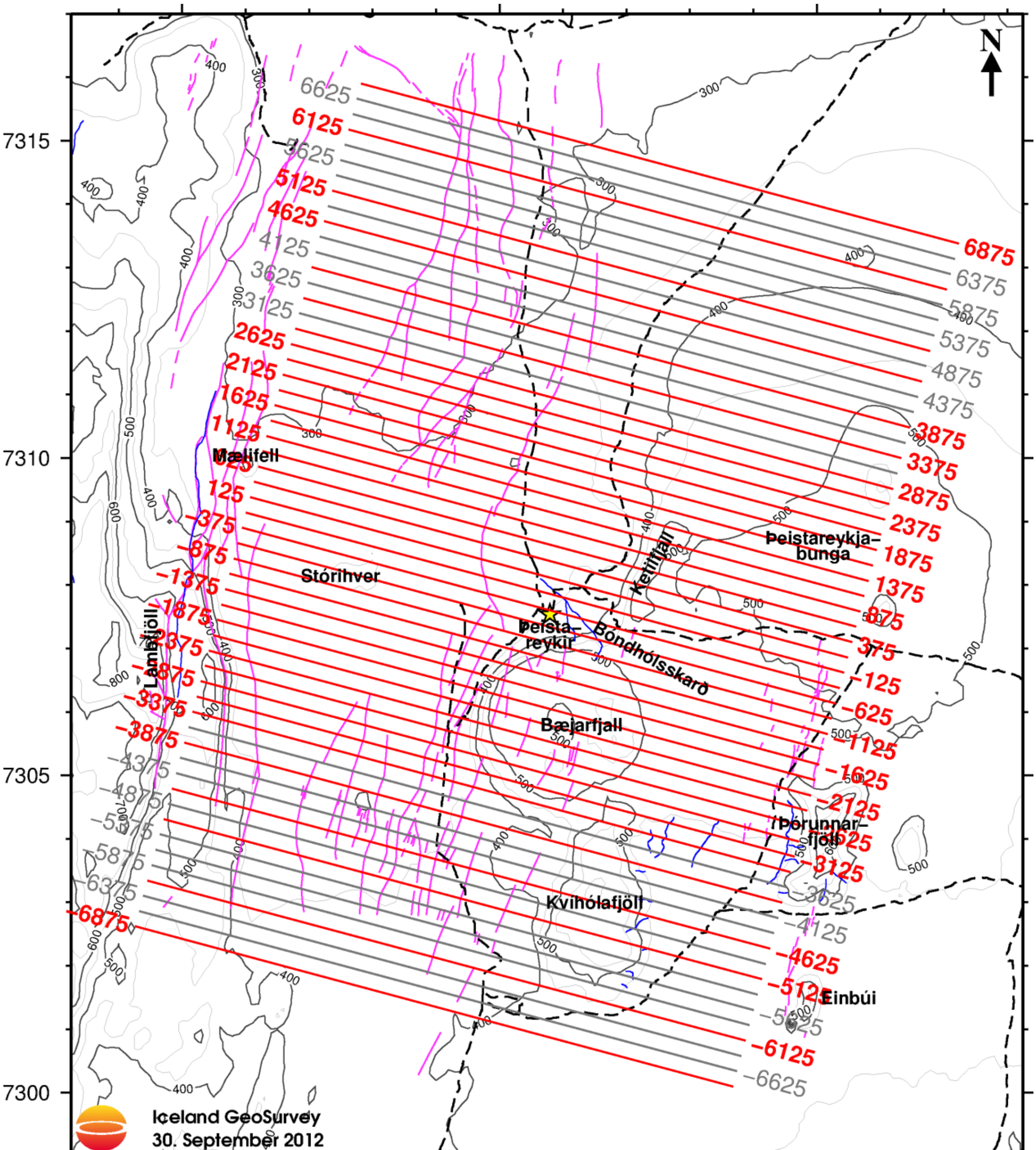

Mælifell
Stórihver
Lambafjöll
Þeistareykir
Bóndhólsskarð
Bæjarfjall
Kvíhólafjöll
Ketilfjall
Þeistareykjabunga
Þórunnarfjöll
Einbúi
Iceland GeoSurvey
30. September 2012
N

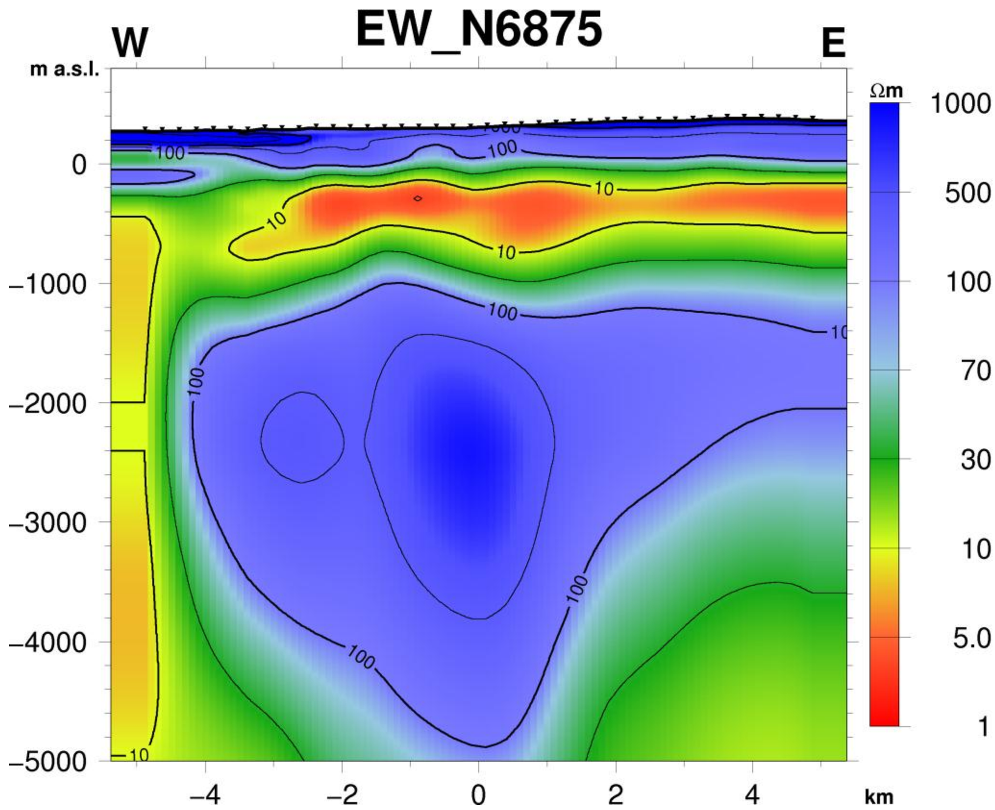
EW_N6875
W
E
m a.s.l.
Ωm
1000
500
100
70
30
10
5.0
1
0
−1000
−2000
−3000
−4000
−5000
−4
−2
0
2
4
km
100
10

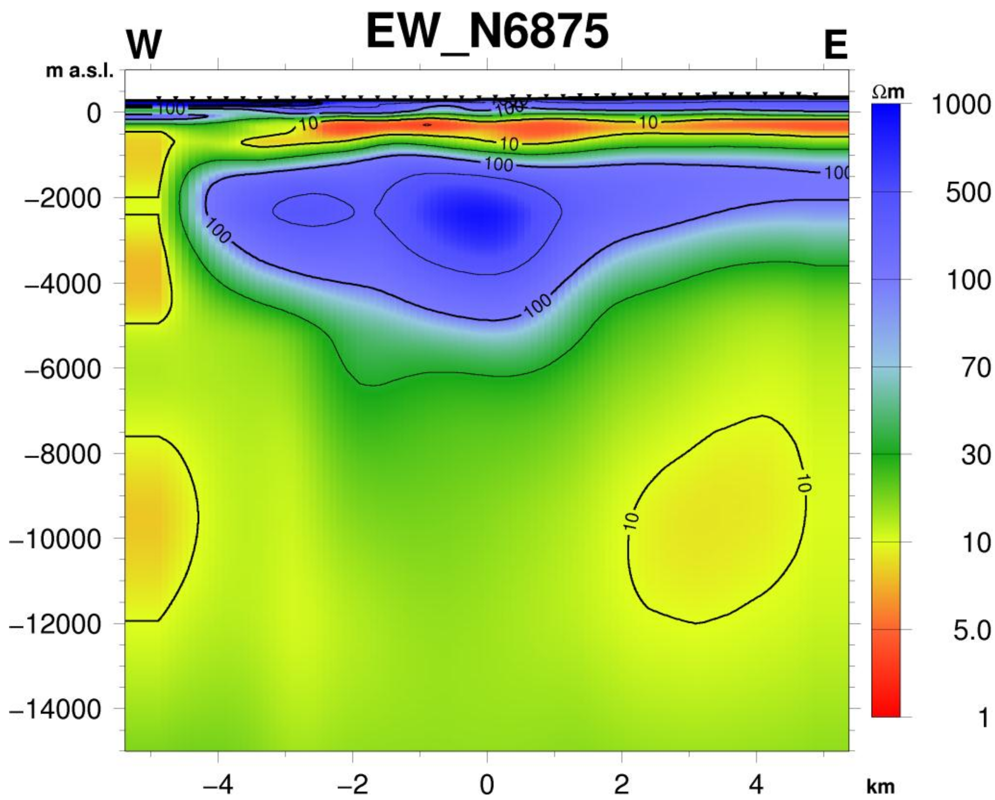
EW_N6875
W
E
m a.s.l.
Ωm
1000
500
100
70
30
10
5.0
1
0
−2000
−4000
−6000
−8000
−10000
−12000
−14000
−4
−2
0
2
4
km
100
10

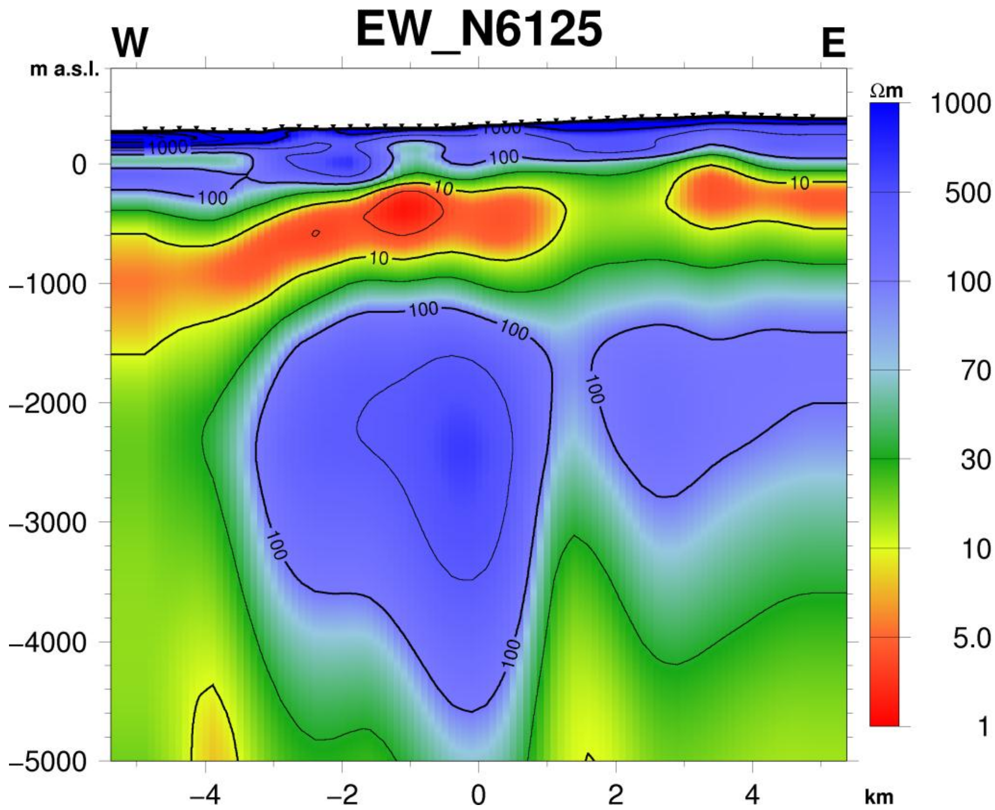
EW_N6125
W
E
m a.s.l.
Ωm
1000
500
100
70
30
10
5.0
1
0
−1000
−2000
−3000
−4000
−5000
−4
−2
0
2
4
km

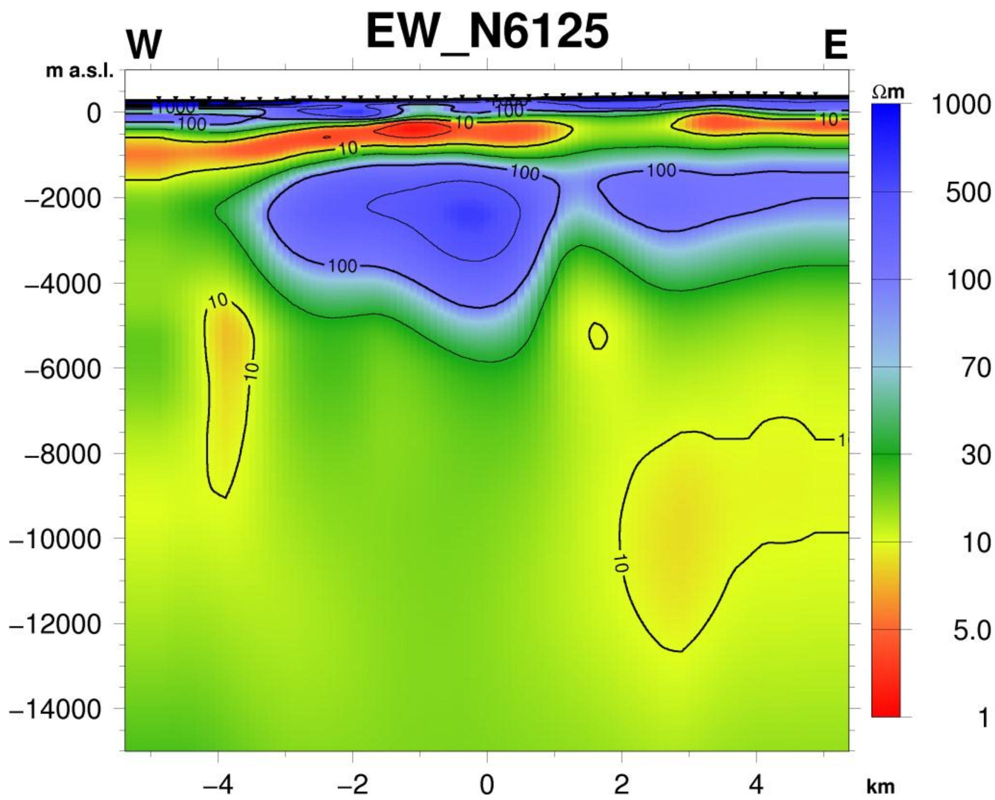
EW_N6125
W
E
m a.s.l.
Ωm
1000
500
100
70
30
10
5.0
1
0
−2000
−4000
−6000
−8000
−10000
−12000
−14000
−4
−2
0
2
4
km

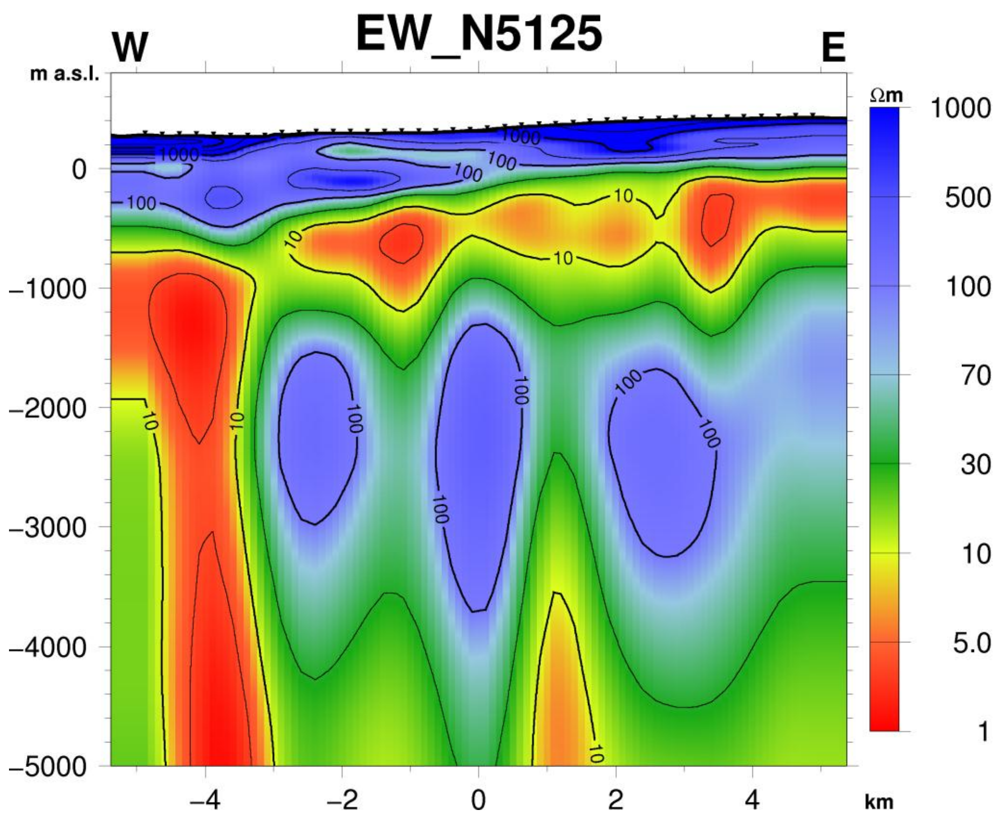
EW_N5125
W
E
m a.s.l.
Ωm
1000
500
100
70
30
10
5.0
1
0
−1000
−2000
−3000
−4000
−5000
−4
−2
0
2
4
km

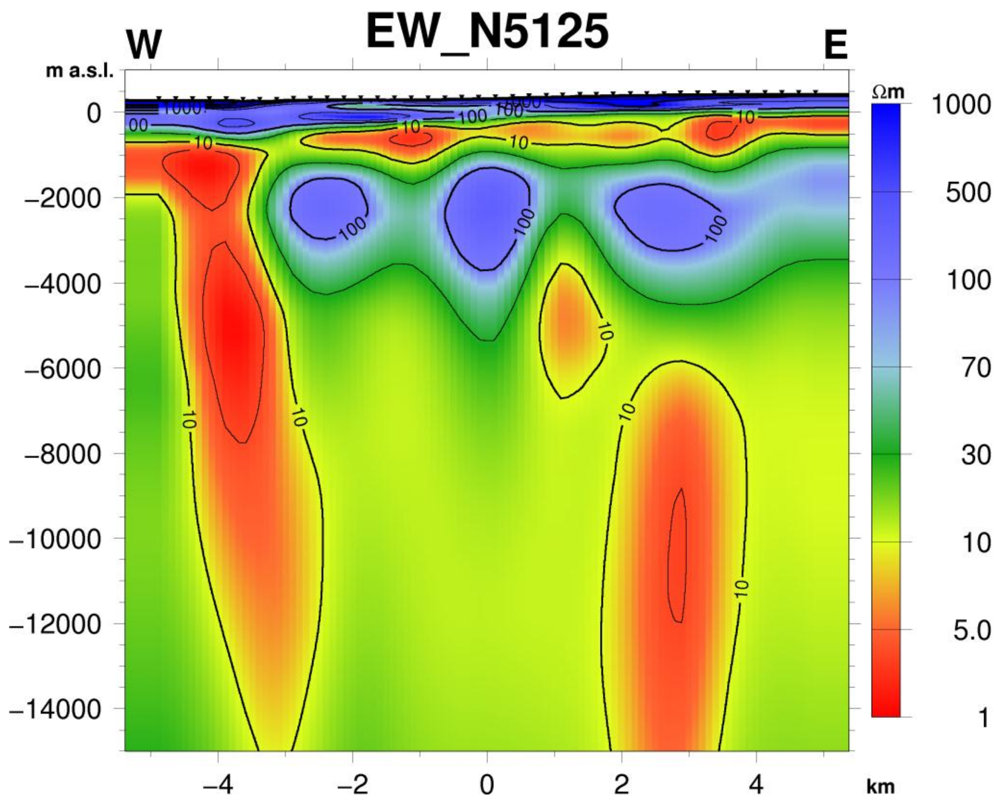
EW_N5125
W
E
m a.s.l.
Ωm
1000
500
100
70
30
10
5.0
1
0
−2000
−4000
−6000
−8000
−10000
−12000
−14000
−4
−2
0
2
4
km

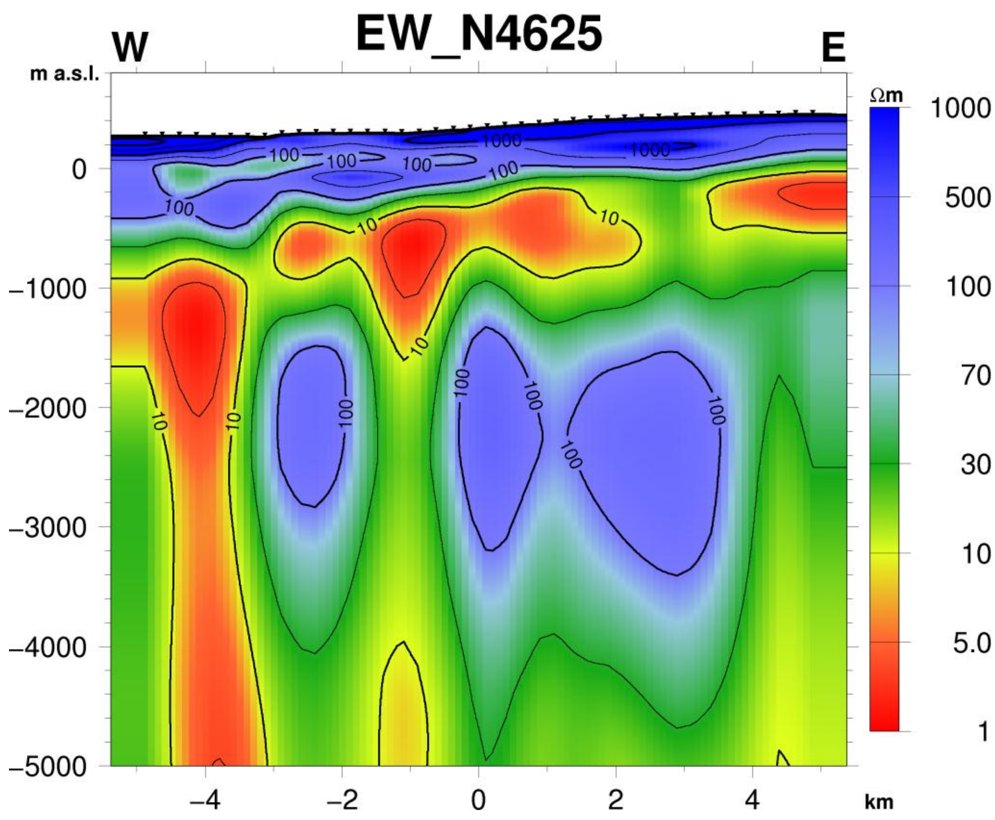
EW_N4625
W
E
m a.s.l.
Ωm
1000
500
100
70
30
10
5.0
1
0
−1000
−2000
−3000
−4000
−5000
−4
−2
0
2
4
km

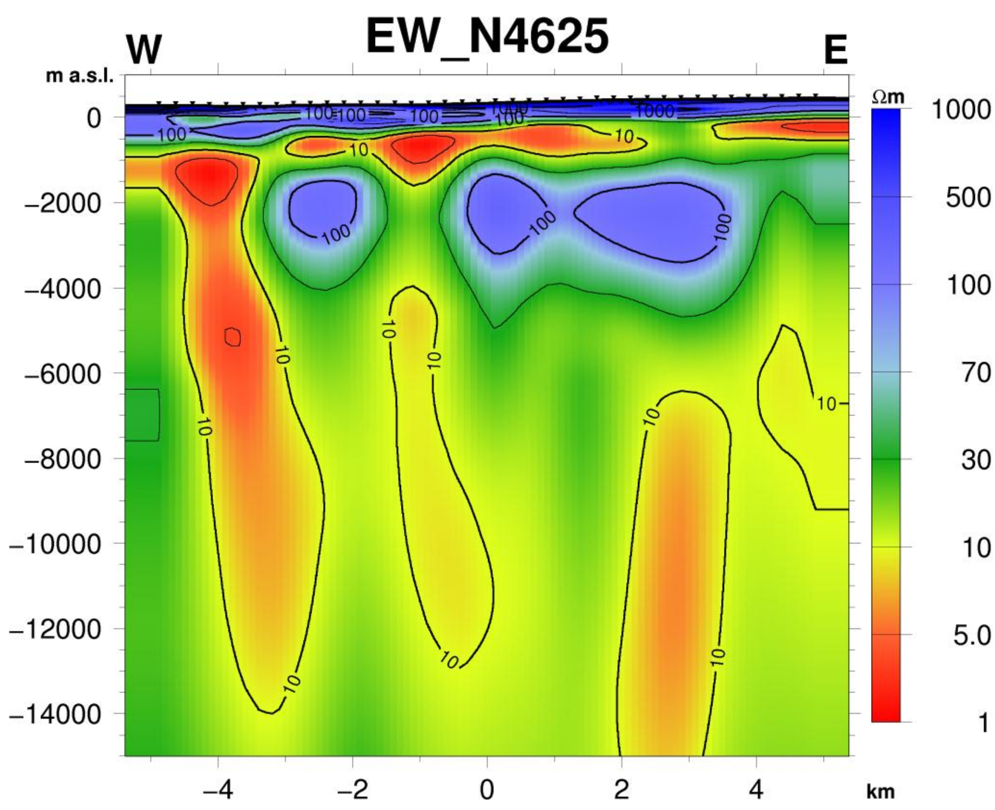
EW_N4625
W
E
m a.s.l.
Ωm
1000
500
100
70
30
10
5.0
1
0
−2000
−4000
−6000
−8000
−10000
−12000
−14000
−4
−2
0
2
4
km

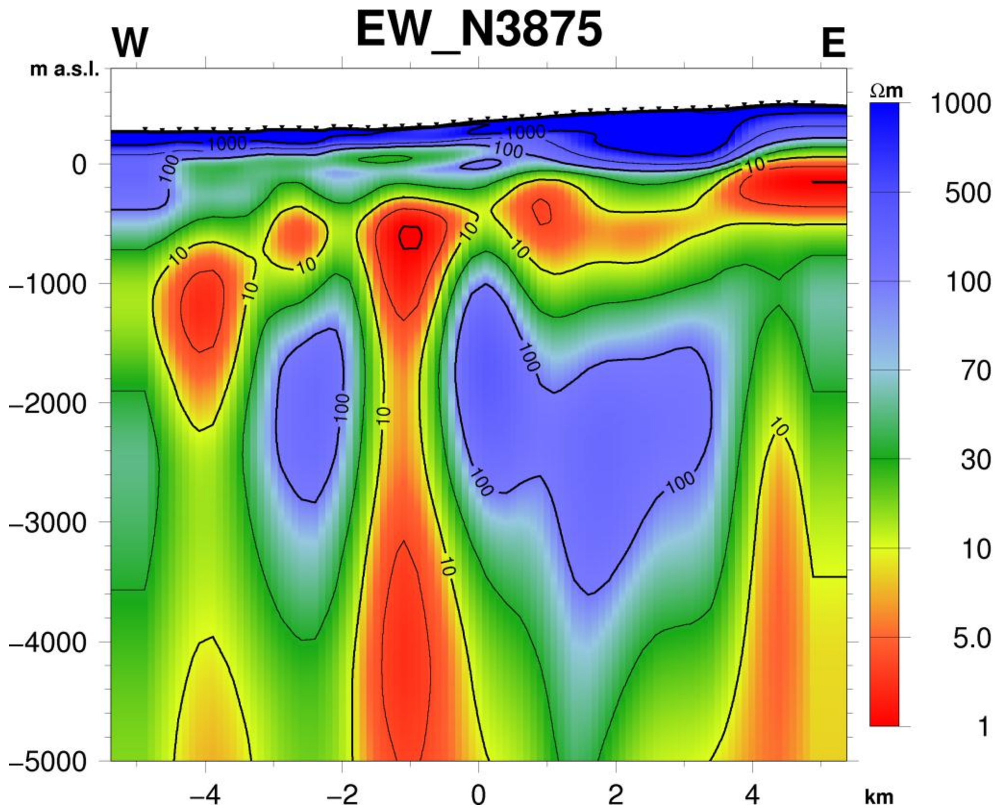
EW_N3875
W
E
m a.s.l.
0
−1000
−2000
−3000
−4000
−5000
−4
−2
0
2
4
km
Ωm
1000
500
100
70
30
10
5.0
1

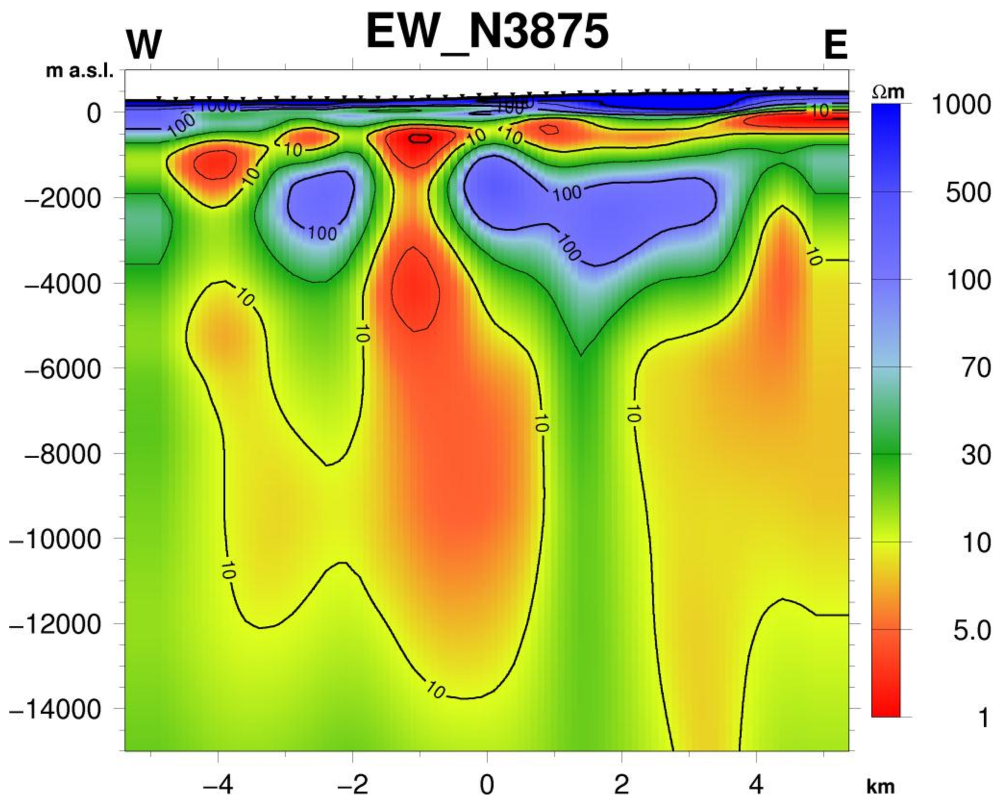
EW_N3875
W
E
m a.s.l.
0
−2000
−4000
−6000
−8000
−10000
−12000
−14000
−4
−2
0
2
4
km
Ωm
1000
500
100
70
30
10
5.0
1

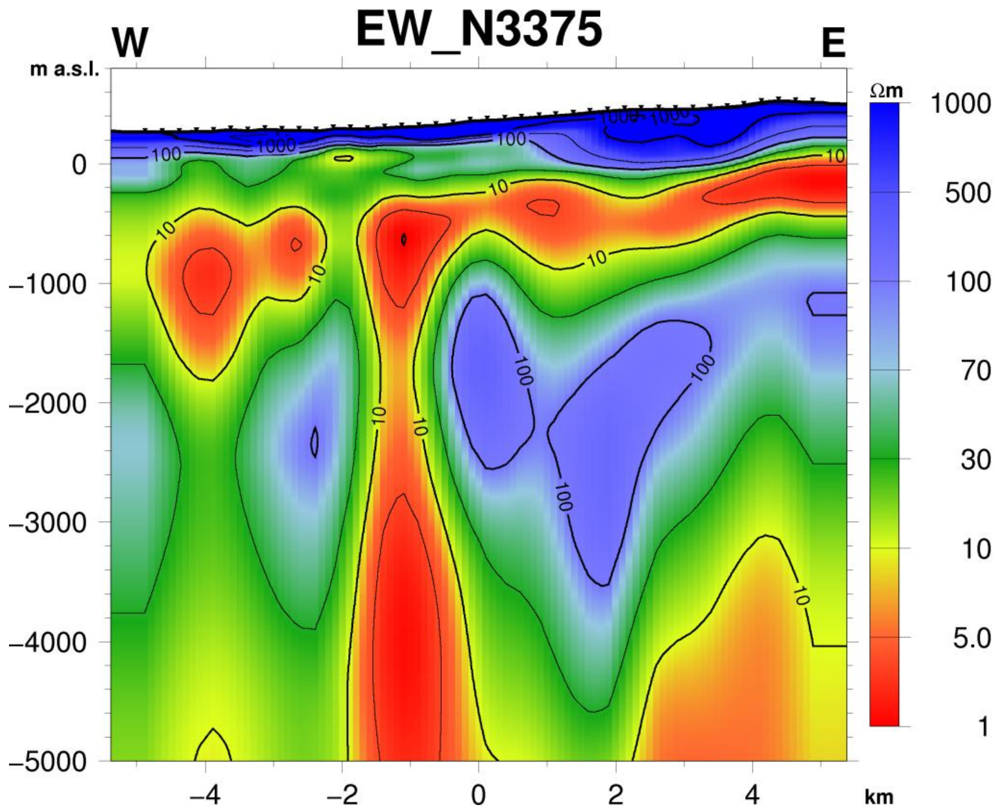

EW_N3375
W
E
m a.s.l.
0
−1000
−2000
−3000
−4000
−5000
−4
−2
0
2
4
km
Ωm
1000
500
100
70
30
10
5.0
1

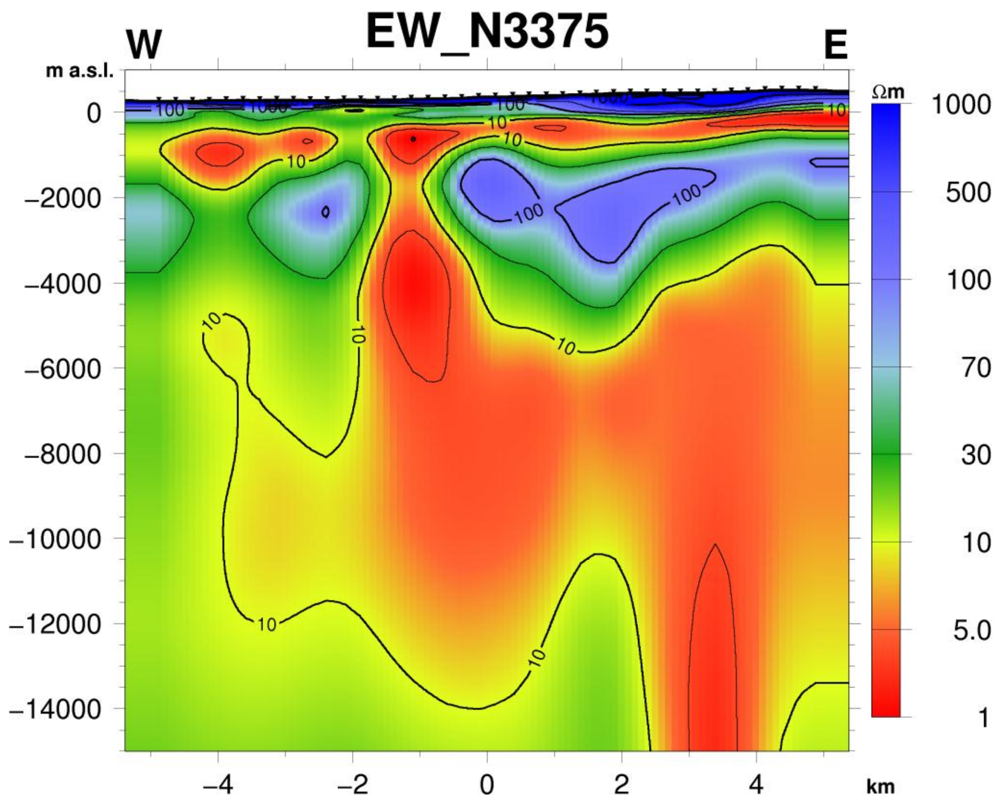

EW_N3375
W
E
m a.s.l.
0
−2000
−4000
−6000
−8000
−10000
−12000
−14000
−4
−2
0
2
4
km
Ωm
1000
500
100
70
30
10
5.0
1

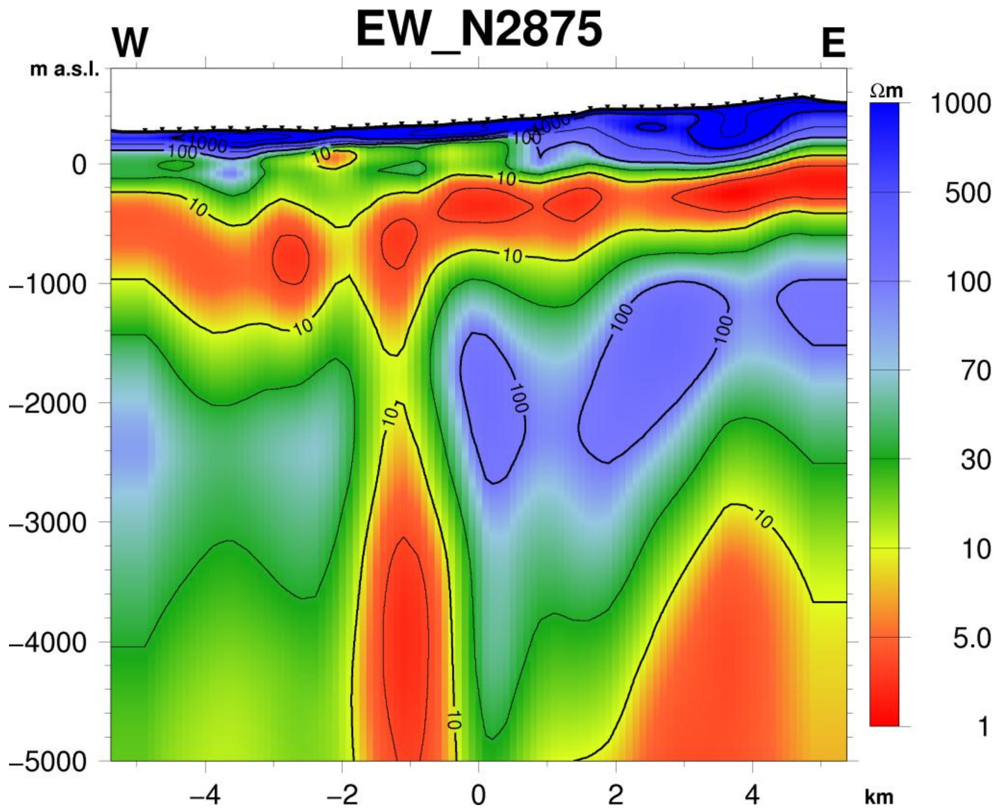
EW_N2875
W
E
m a.s.l.
Ωm
1000
500
100
70
30
10
5.0
1
0
−1000
−2000
−3000
−4000
−5000
−4
−2
0
2
4
km

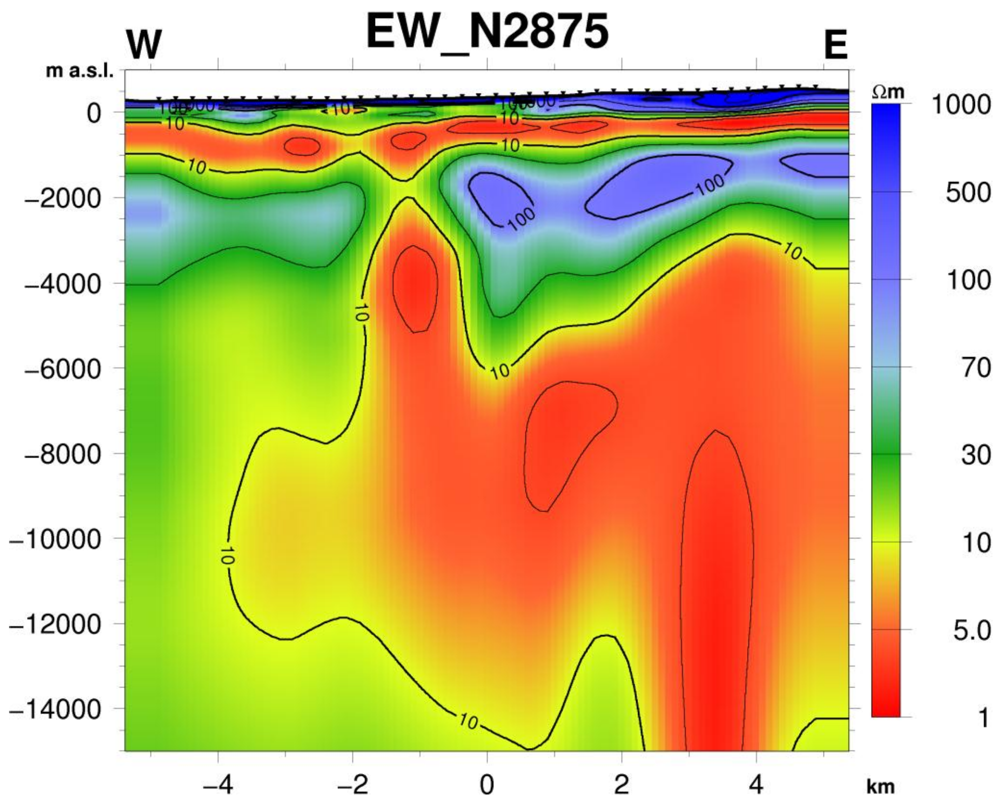
EW_N2875
W
E
m a.s.l.
Ωm
1000
500
100
70
30
10
5.0
1
0
−2000
−4000
−6000
−8000
−10000
−12000
−14000
−4
−2
0
2
4
km

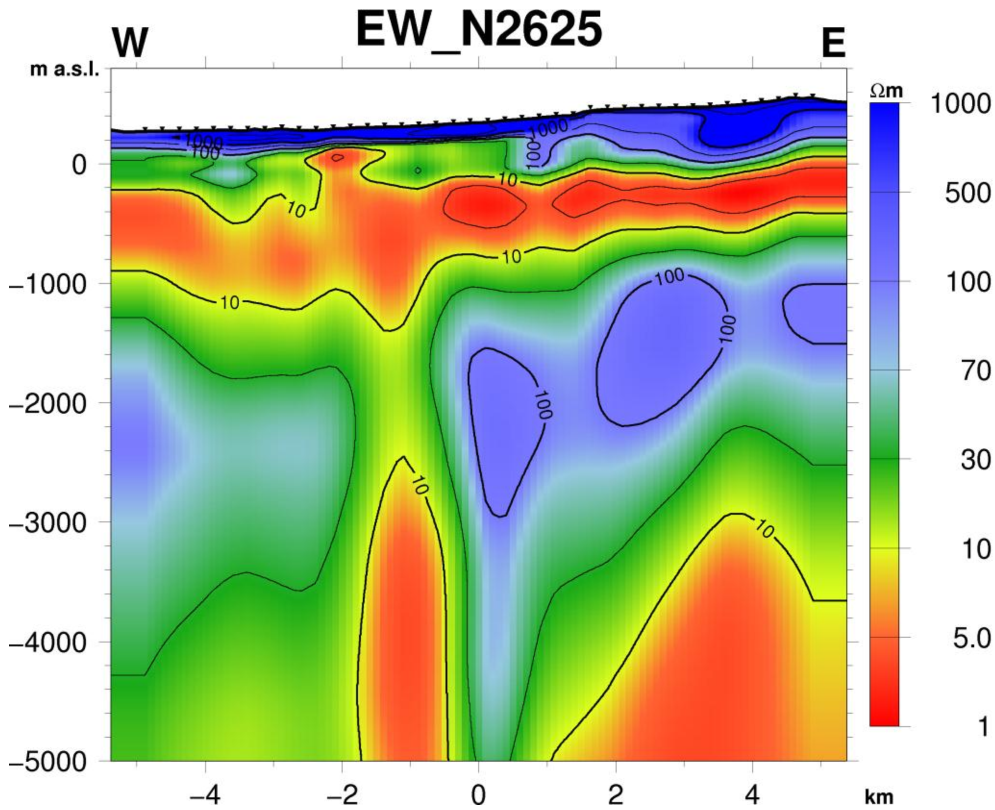
EW_N2625
W
E
m a.s.l.
Ωm
1000
500
100
70
30
10
5.0
1
0
−1000
−2000
−3000
−4000
−5000
−4
−2
0
2
4
km

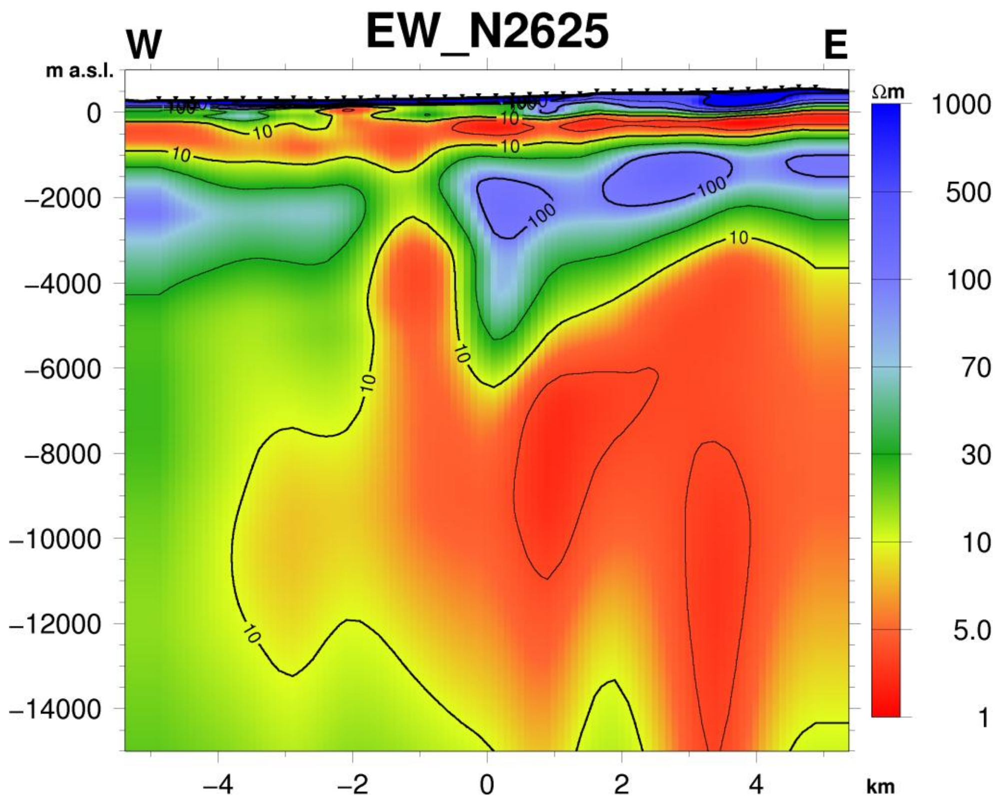
EW_N2625
W
E
m a.s.l.
Ωm
1000
500
100
70
30
10
5.0
1
0
−2000
−4000
−6000
−8000
−10000
−12000
−14000
−4
−2
0
2
4
km

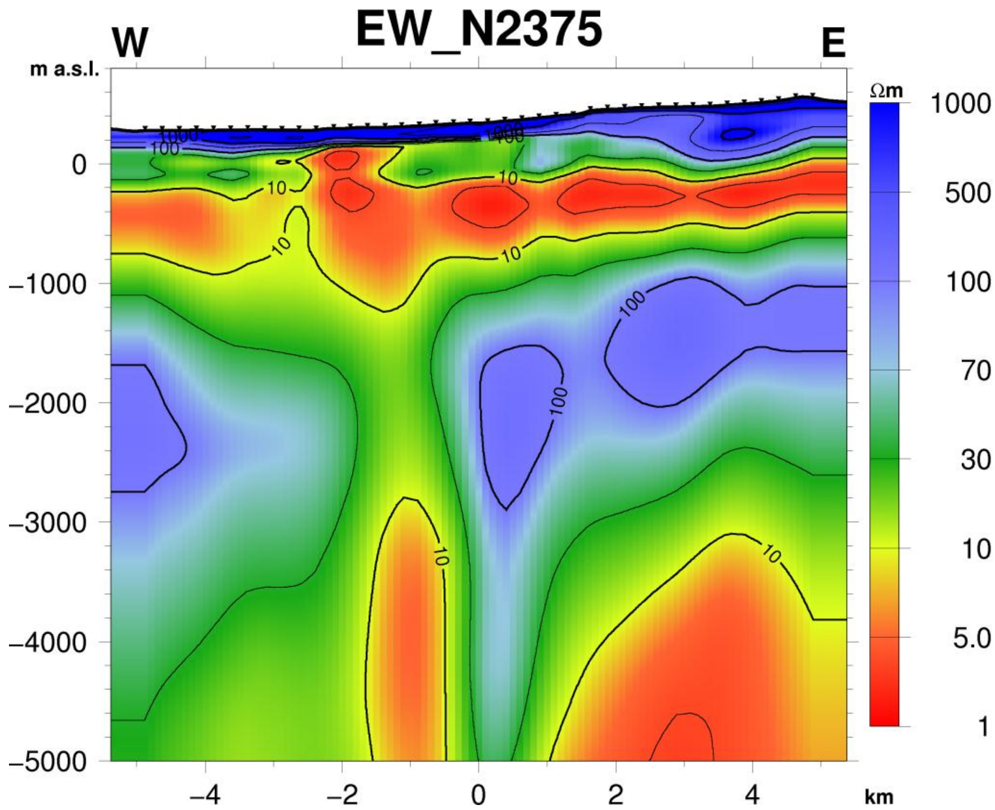
EW_N2375
W
E
m a.s.l.
0
−1000
−2000
−3000
−4000
−5000
−4
−2
0
2
4
km
Ωm
1000
500
100
70
30
10
5.0
1
10
100

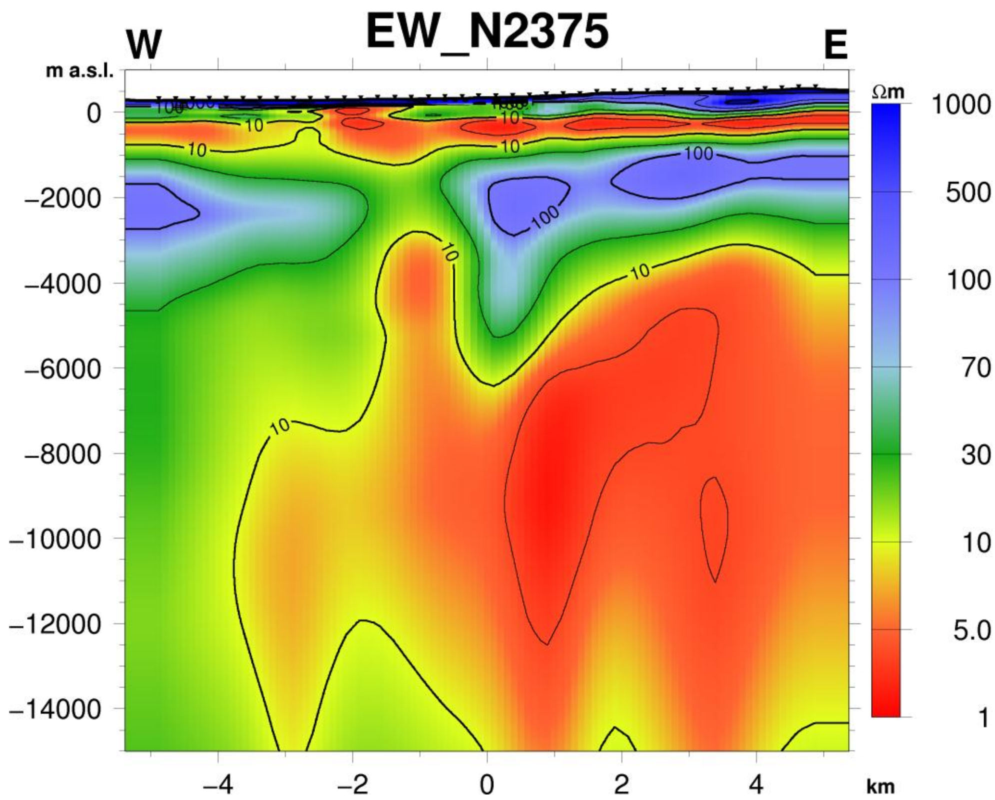
EW_N2375
W
E
m a.s.l.
0
−2000
−4000
−6000
−8000
−10000
−12000
−14000
−4
−2
0
2
4
km
Ωm
1000
500
100
70
30
10
5.0
1
10
100

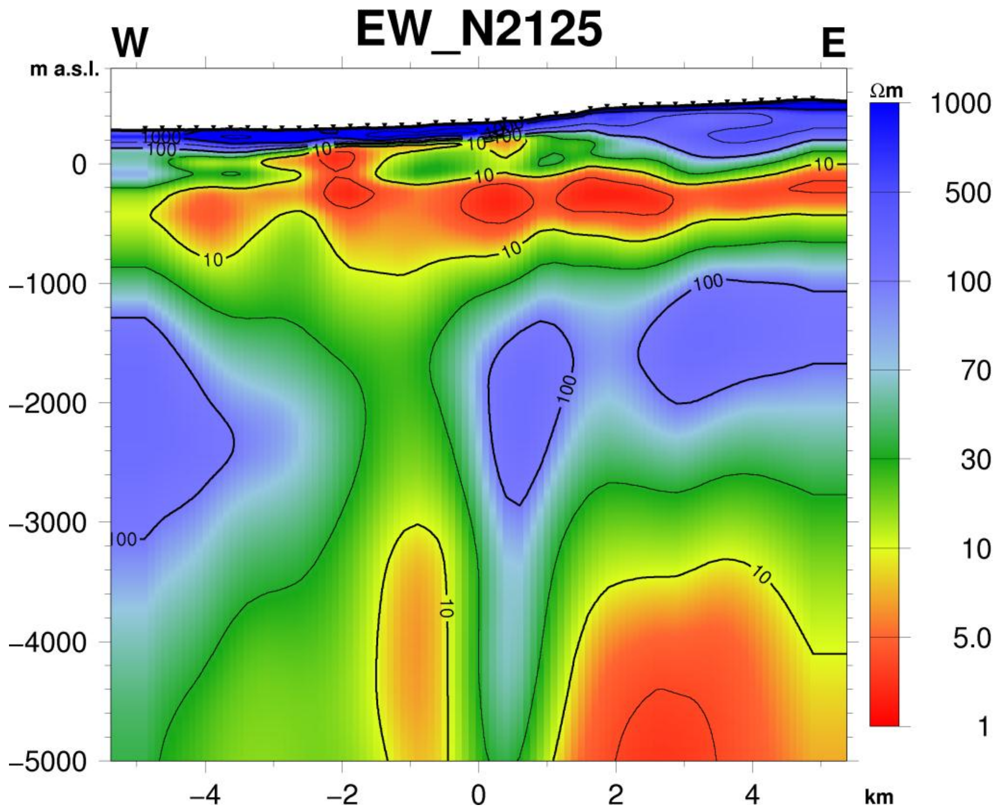

EW_N2125
W
E
m a.s.l.
0
−1000
−2000
−3000
−4000
−5000
−4
−2
0
2
4
km
Ωm
1000
500
100
70
30
10
5.0
1

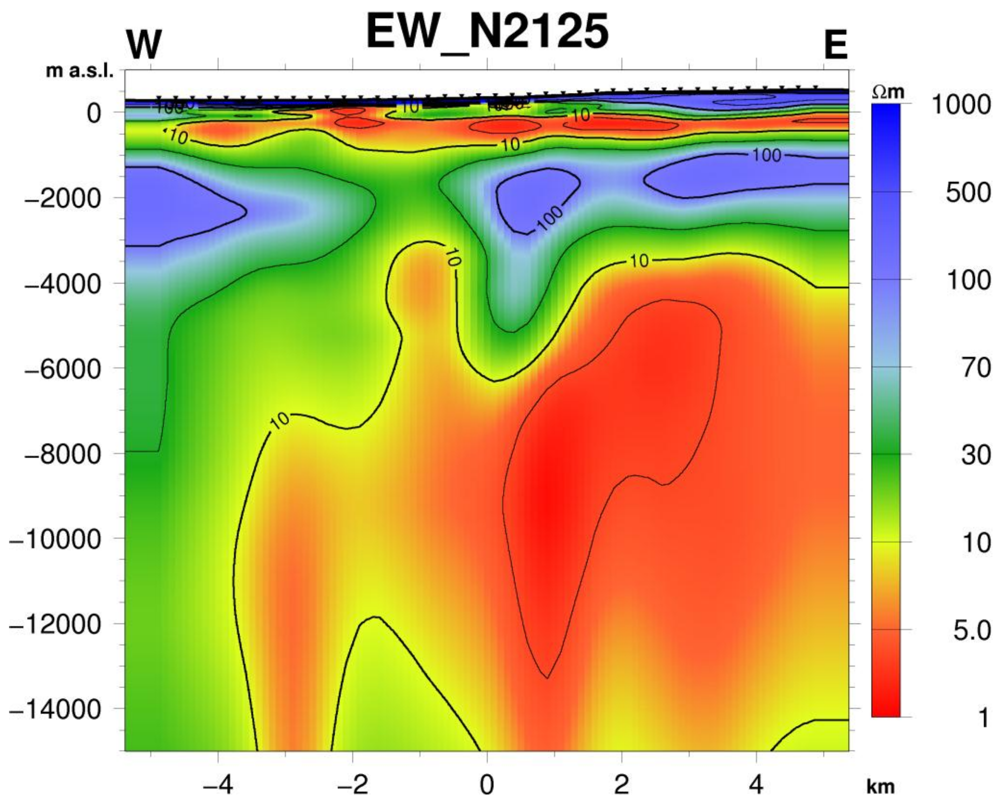

EW_N2125
W
E
m a.s.l.
0
−2000
−4000
−6000
−8000
−10000
−12000
−14000
−4
−2
0
2
4
km
Ωm
1000
500
100
70
30
10
5.0
1

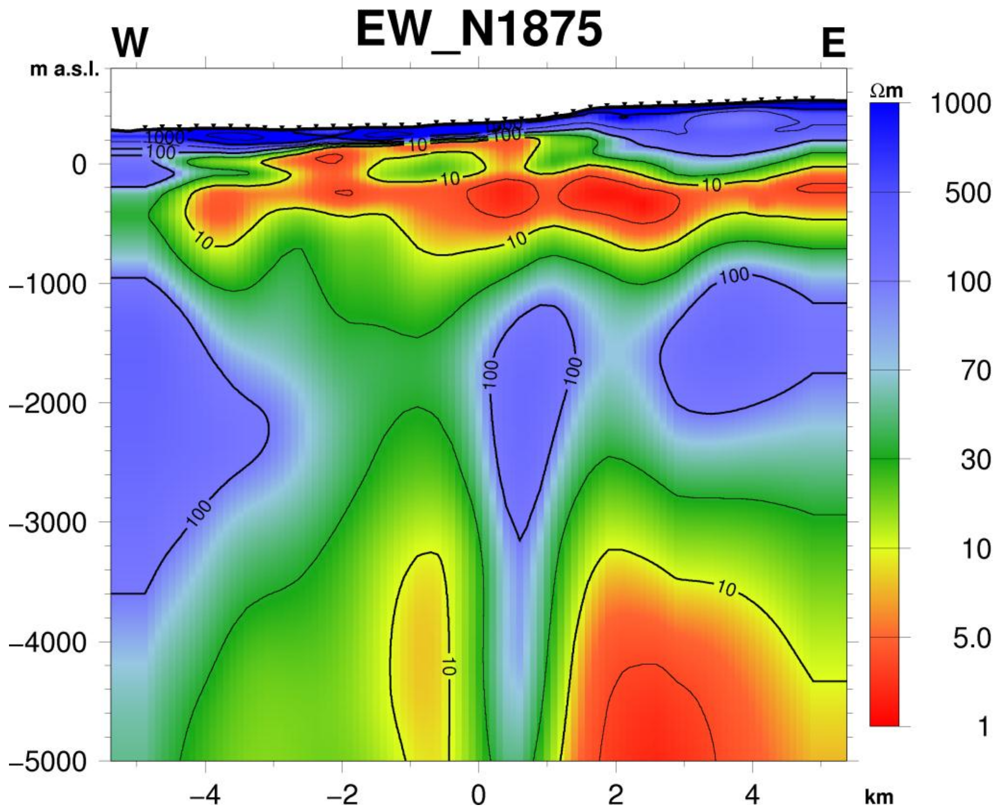
EW_N1875
W
E
m a.s.l.
Ωm
1000
500
100
70
30
10
5.0
1
0
−1000
−2000
−3000
−4000
−5000
−4
−2
0
2
4
km
10
100
1000

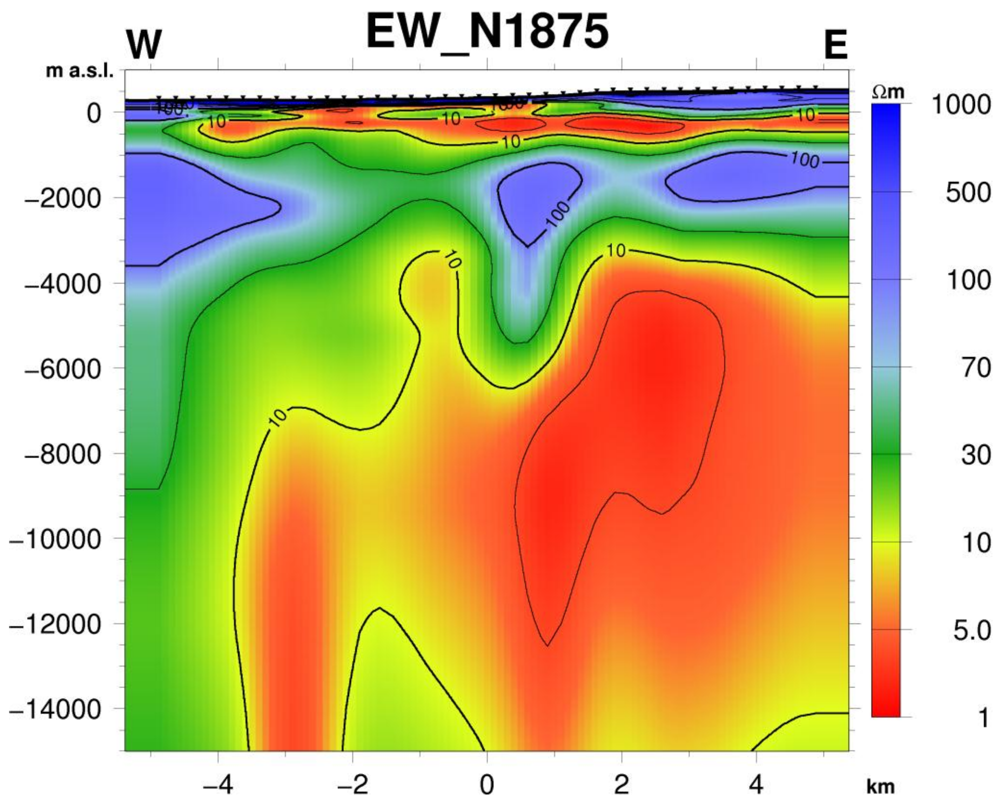
EW_N1875
W
E
m a.s.l.
Ωm
1000
500
100
70
30
10
5.0
1
0
−2000
−4000
−6000
−8000
−10000
−12000
−14000
−4
−2
0
2
4
km
10
100

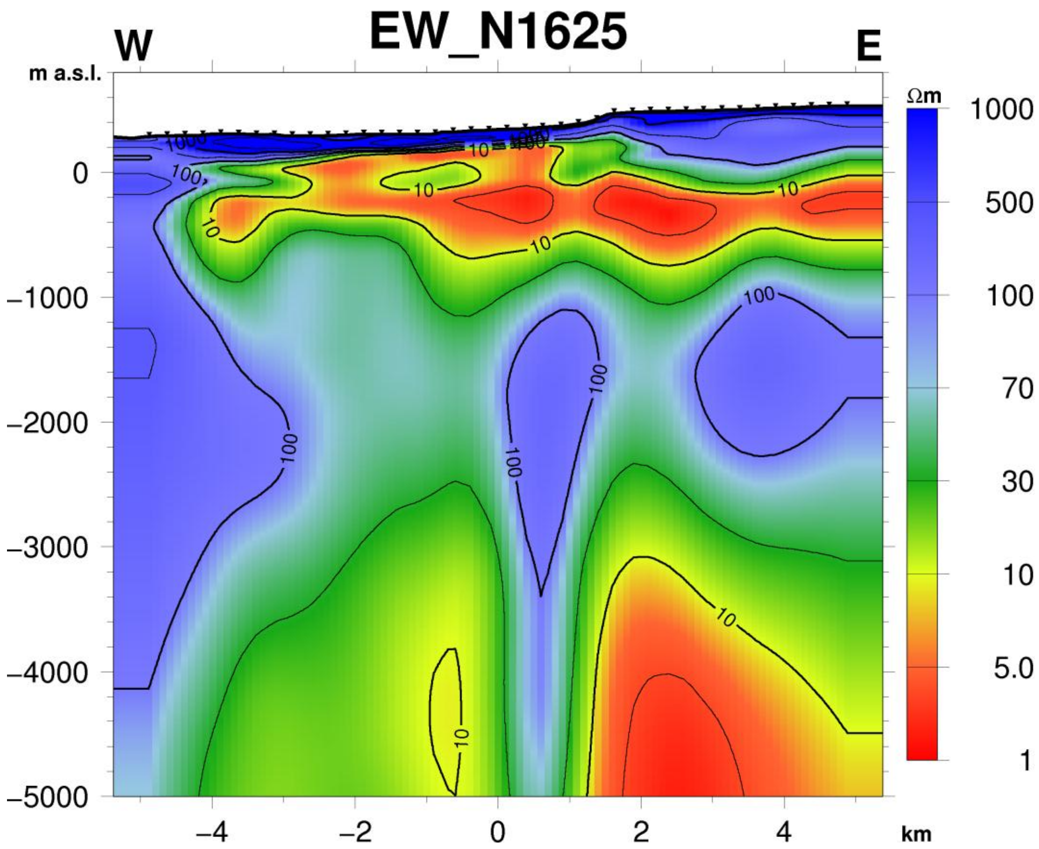
EW_N1625
W
E
m a.s.l.
0
−1000
−2000
−3000
−4000
−5000
−4
−2
0
2
4
km
Ωm
1000
500
100
70
30
10
5.0
1

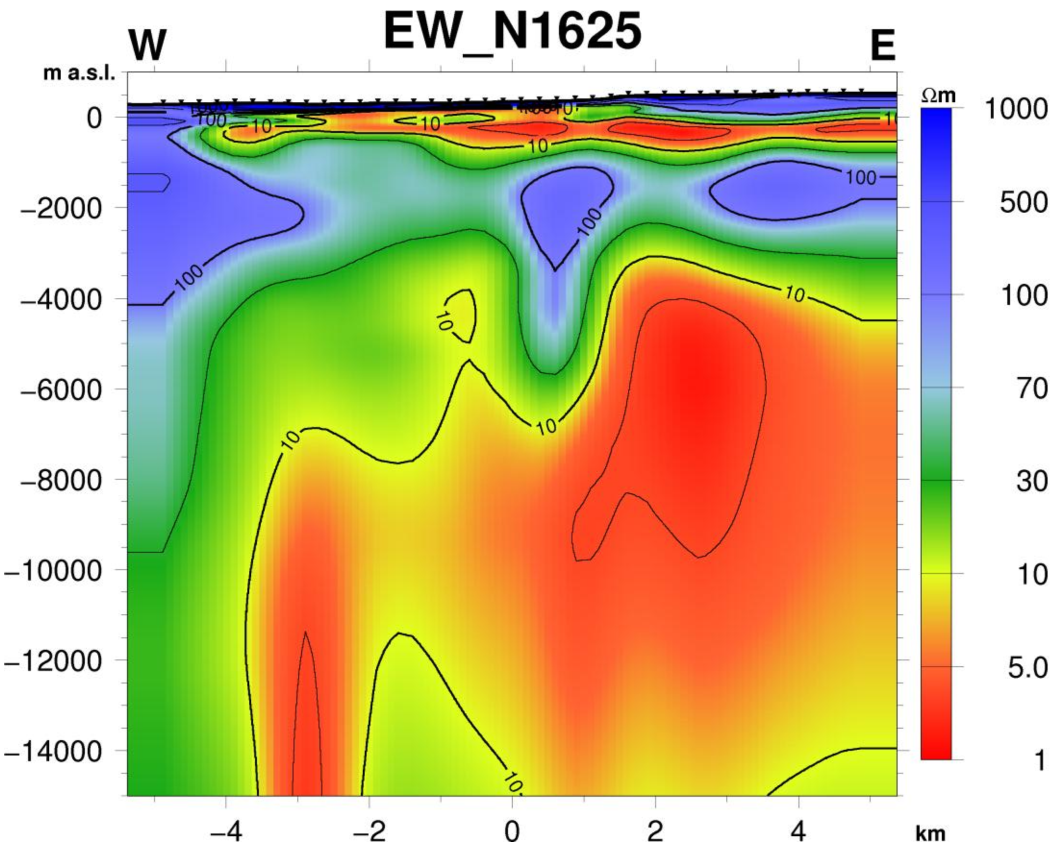
EW_N1625
W
E
m a.s.l.
0
−2000
−4000
−6000
−8000
−10000
−12000
−14000
−4
−2
0
2
4
km
Ωm
1000
500
100
70
30
10
5.0
1

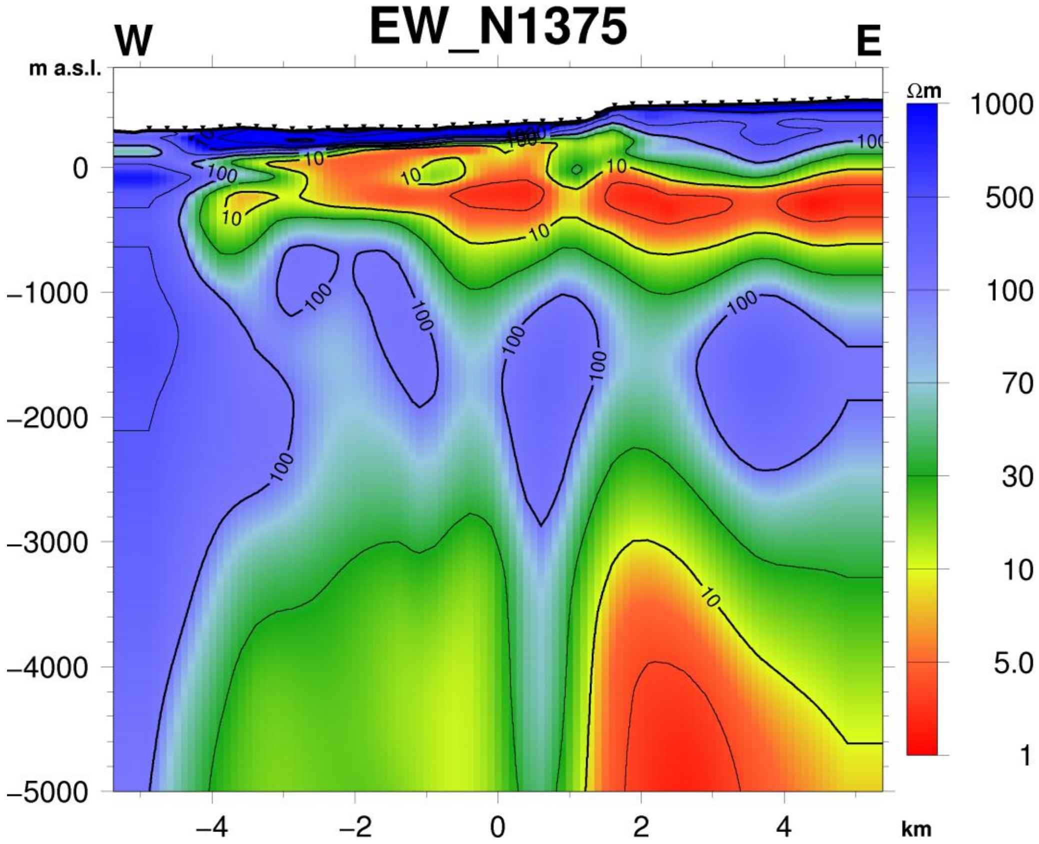

EW_N1375
W
E
m a.s.l.
0
−1000
−2000
−3000
−4000
−5000
−4
−2
0
2
4
km
Ωm
1000
500
100
70
30
10
5.0
1

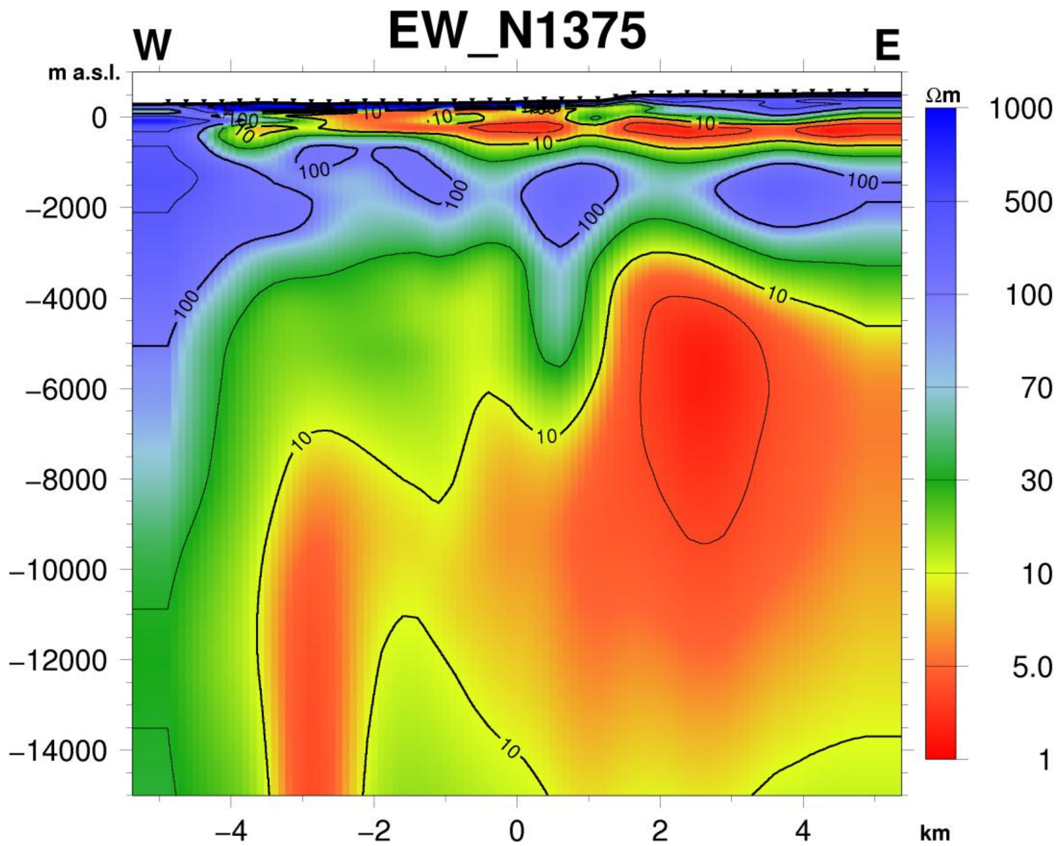

EW_N1375
W
E
m a.s.l.
0
−2000
−4000
−6000
−8000
−10000
−12000
−14000
−4
−2
0
2
4
km
Ωm
1000
500
100
70
30
10
5.0
1

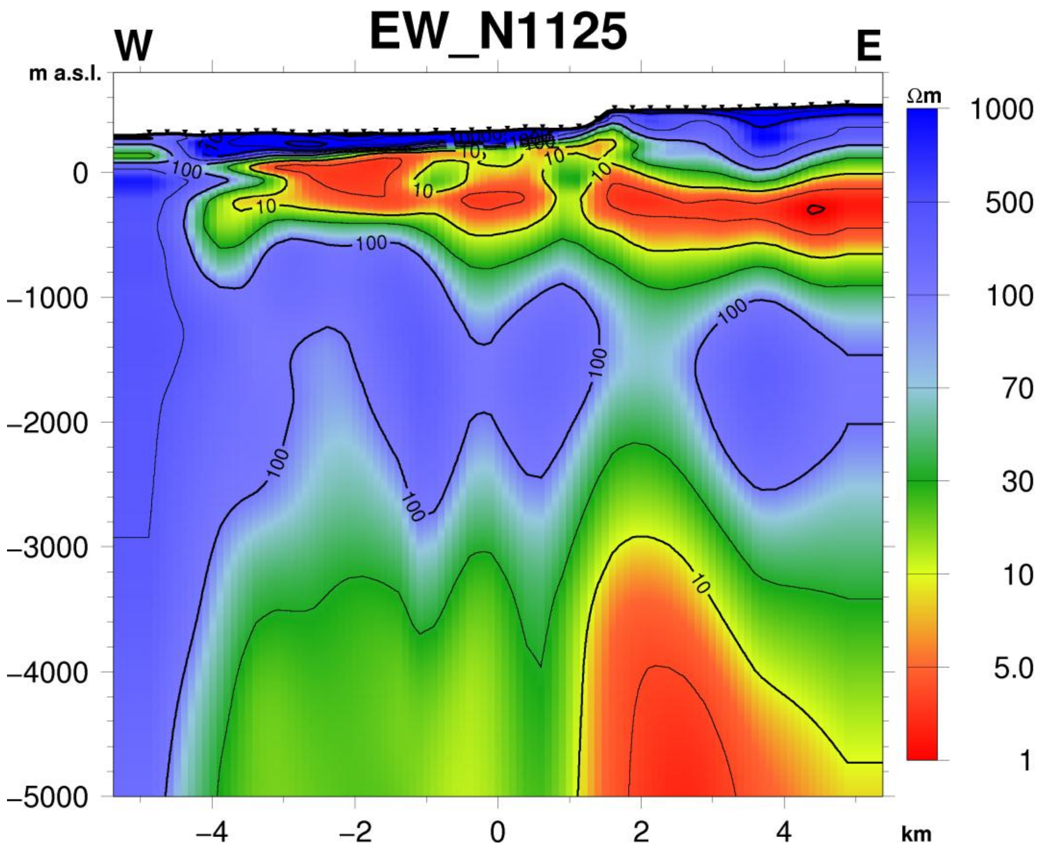

EW_N1125
W
E
m a.s.l.
0
−1000
−2000
−3000
−4000
−5000
−4
−2
0
2
4
km
Ωm
1000
500
100
70
30
10
5.0
1

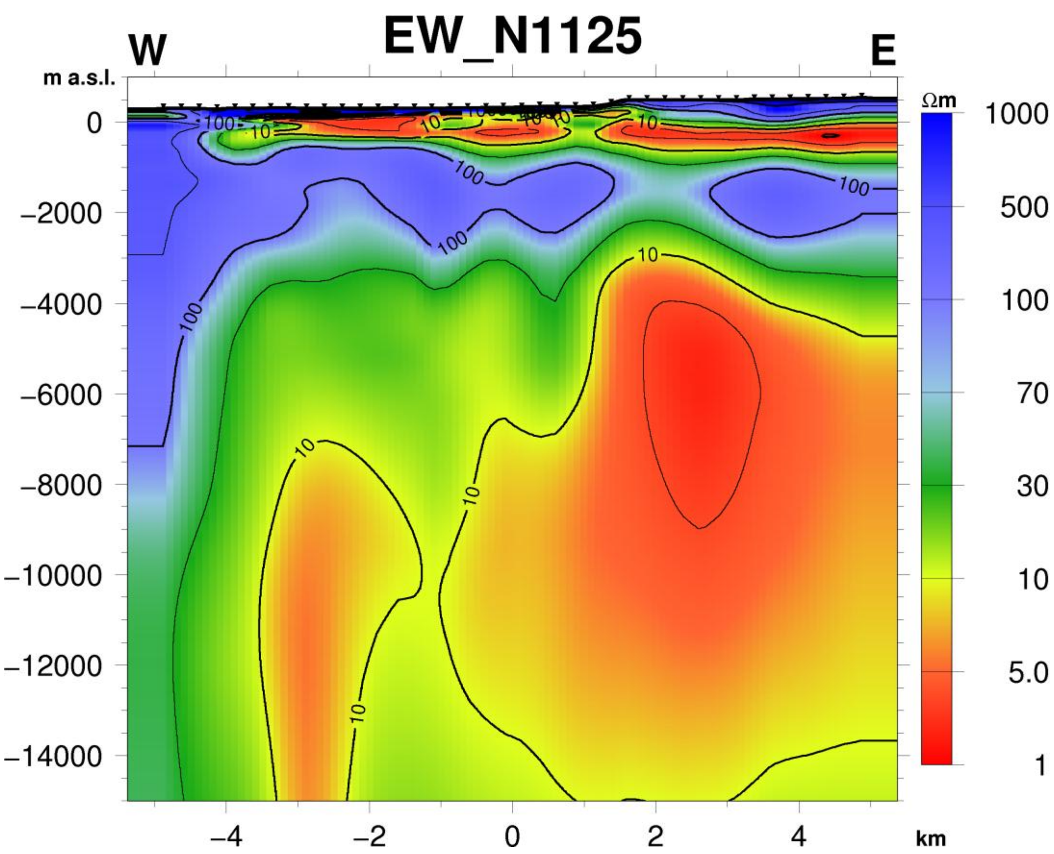

EW_N1125
W
E
m a.s.l.
0
−2000
−4000
−6000
−8000
−10000
−12000
−14000
−4
−2
0
2
4
km
Ωm
1000
500
100
70
30
10
5.0
1

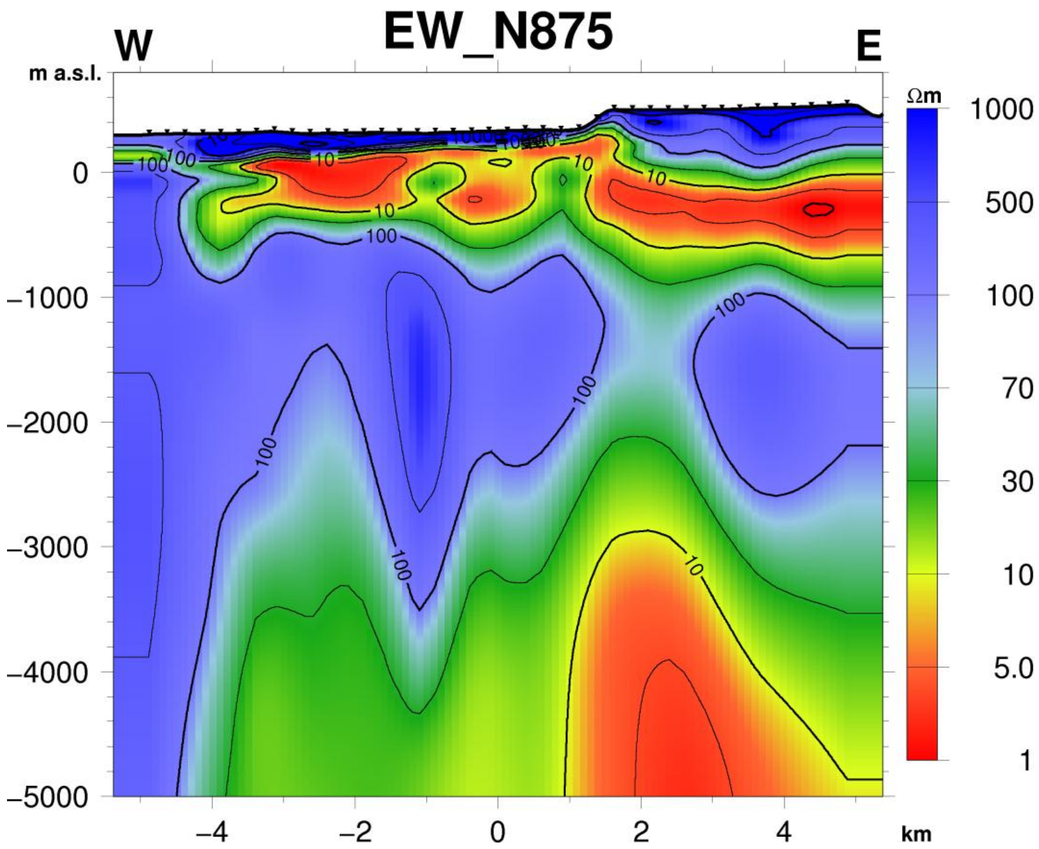

EW_N875
W
E
m a.s.l.
Ωm
1000
500
100
70
30
10
5.0
1
0
−1000
−2000
−3000
−4000
−5000
−4
−2
0
2
4
km

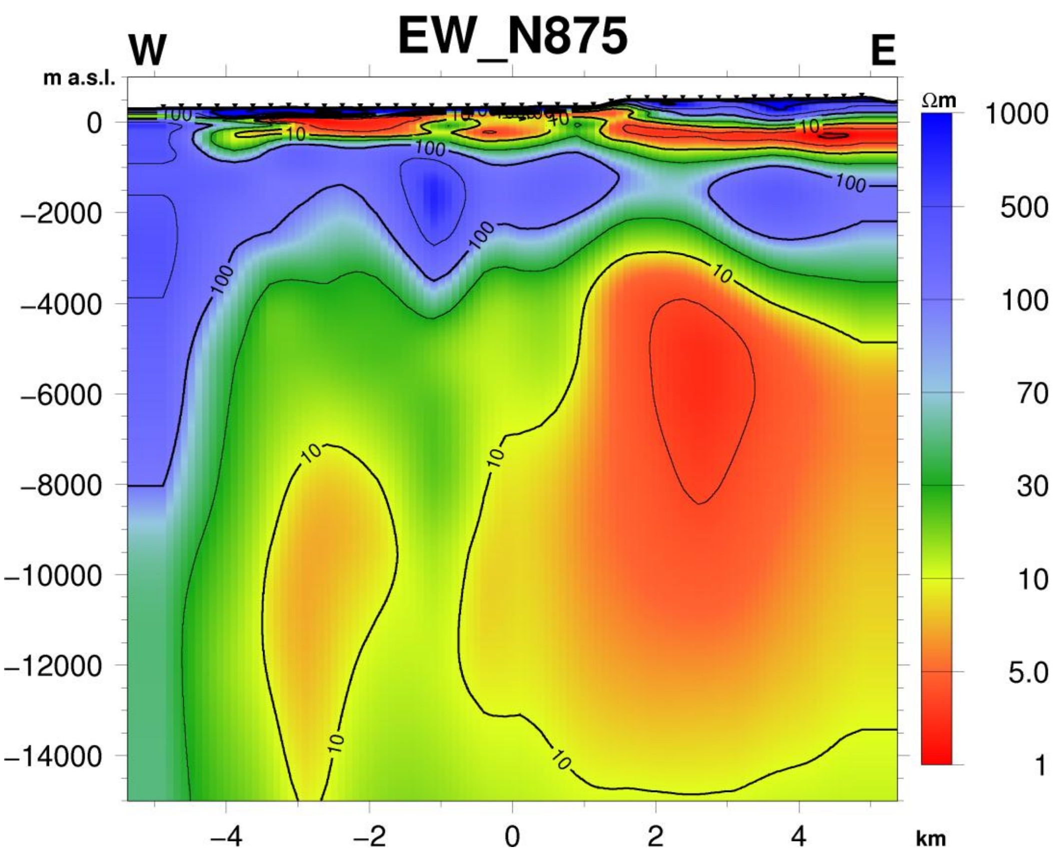

EW_N875
W
E
m a.s.l.
Ωm
1000
500
100
70
30
10
5.0
1
0
−2000
−4000
−6000
−8000
−10000
−12000
−14000
−4
−2
0
2
4
km

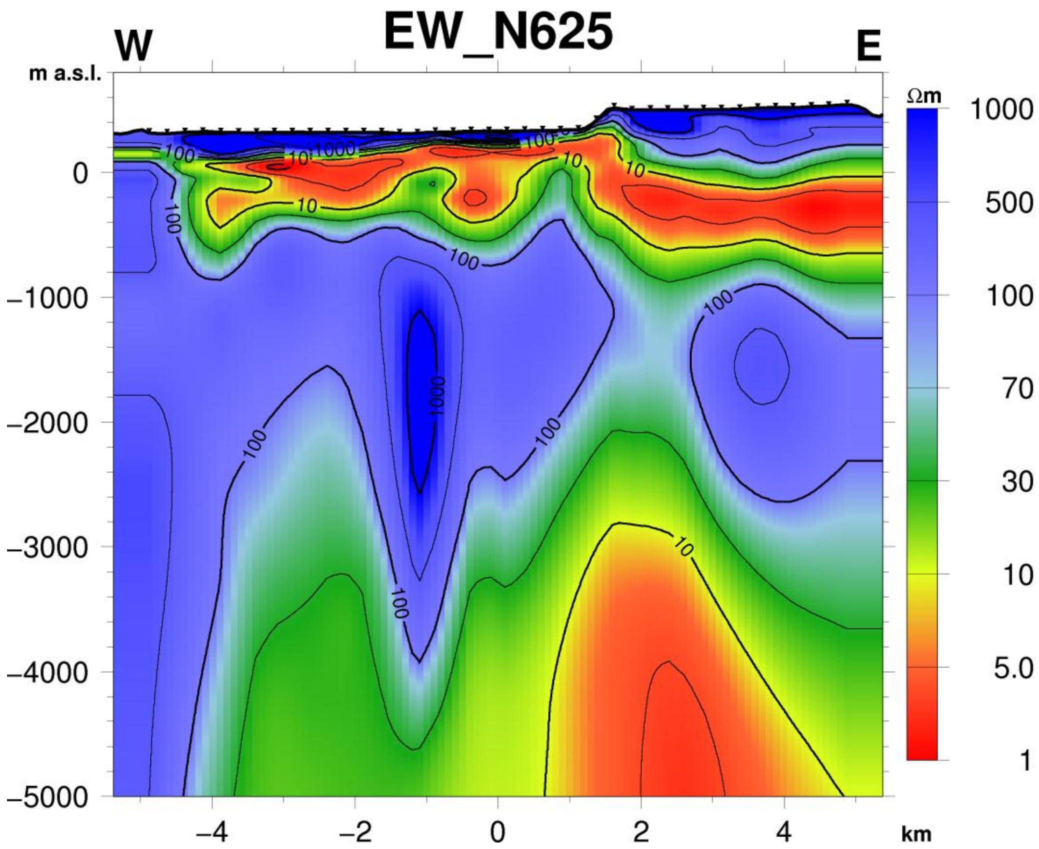
EW_N625
W
E
m a.s.l.
0
−1000
−2000
−3000
−4000
−5000
−4
−2
0
2
4
km
Ωm
1000
500
100
70
30
10
5.0
1

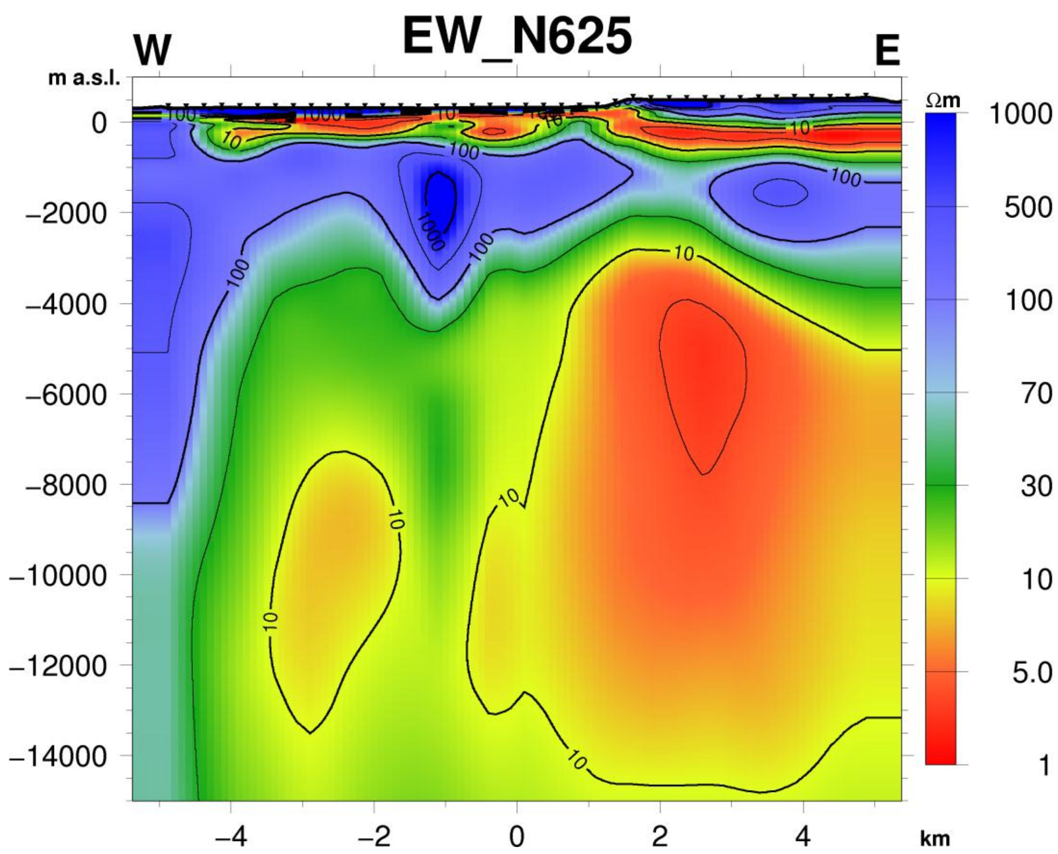
EW_N625
W
E
m a.s.l.
0
−2000
−4000
−6000
−8000
−10000
−12000
−14000
−4
−2
0
2
4
km
Ωm
1000
500
100
70
30
10
5.0
1

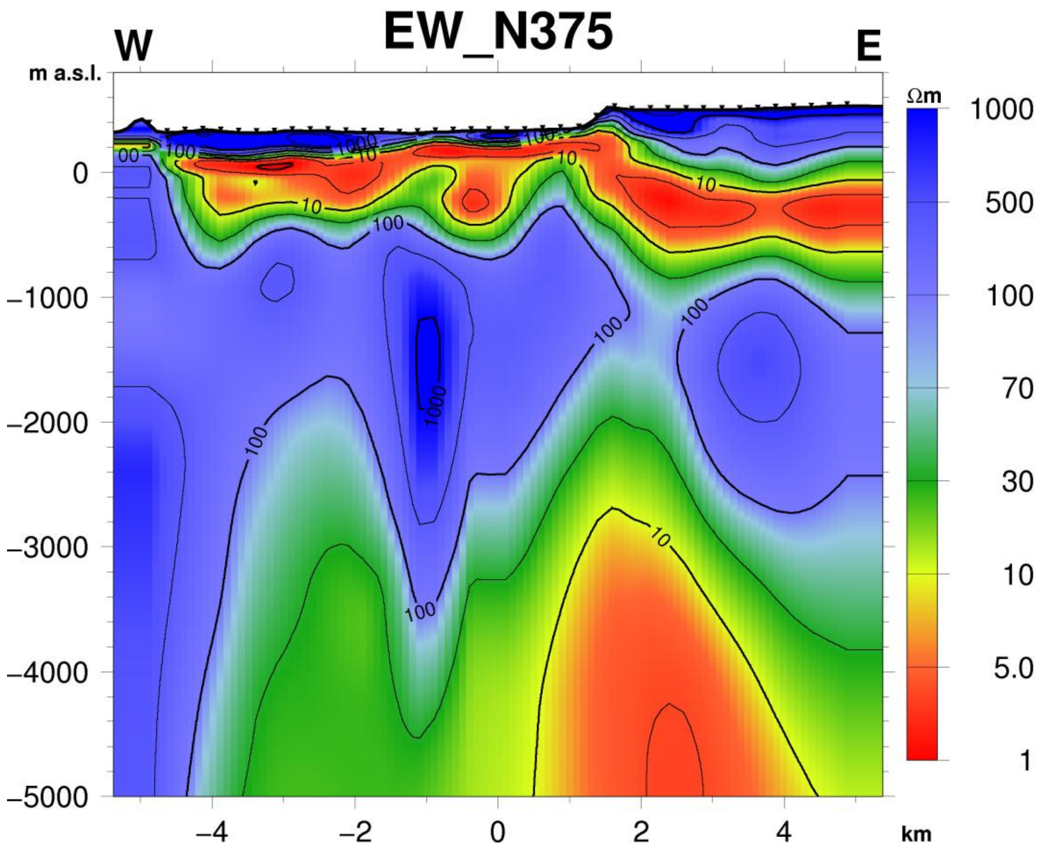
EW_N375
W
E
m a.s.l.
Ωm
km

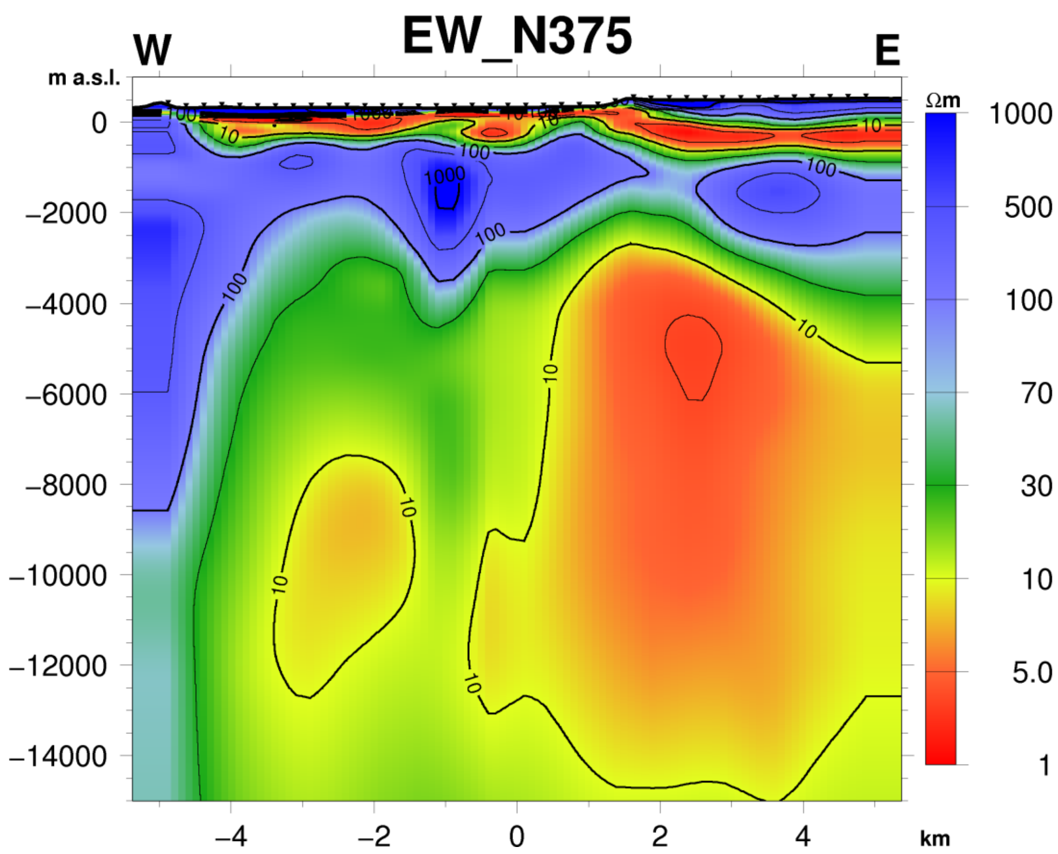
EW_N375
W
E
m a.s.l.
Ωm
km

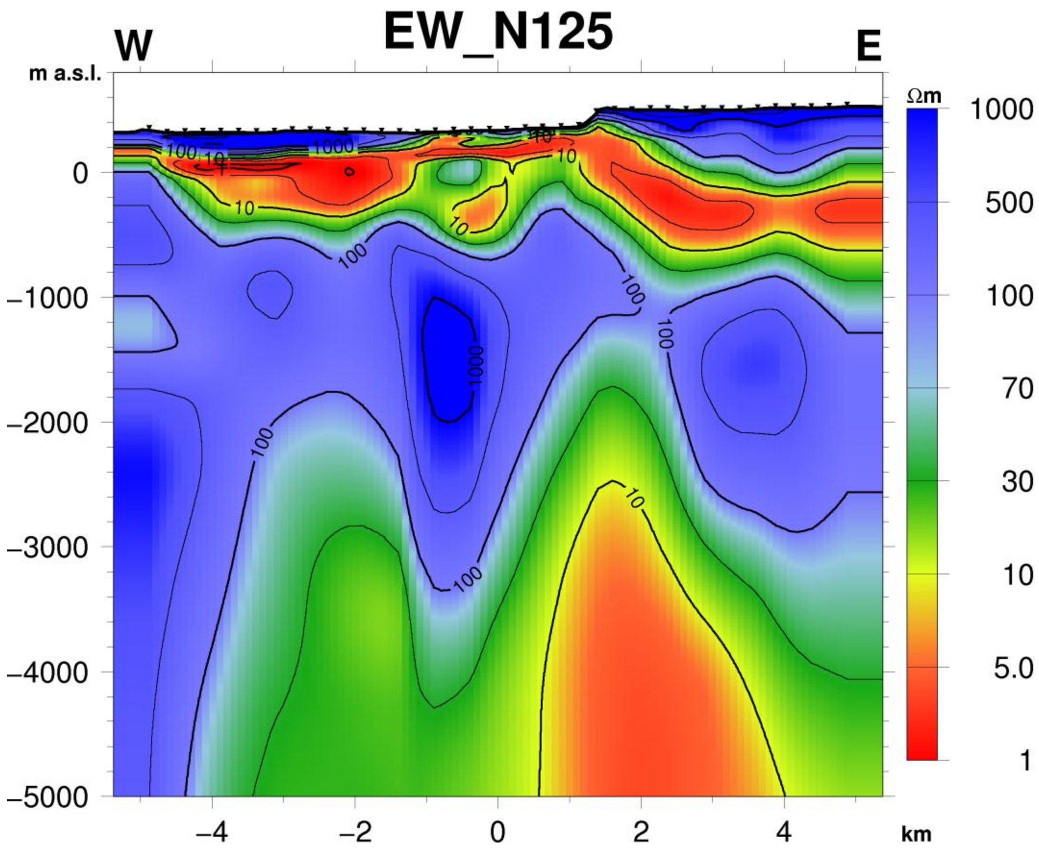
EW_N125
W
E
m a.s.l.
0
–1000
–2000
–3000
–4000
–5000
–4
–2
0
2
4
km
Ωm
1000
500
100
70
30
10
5.0
1

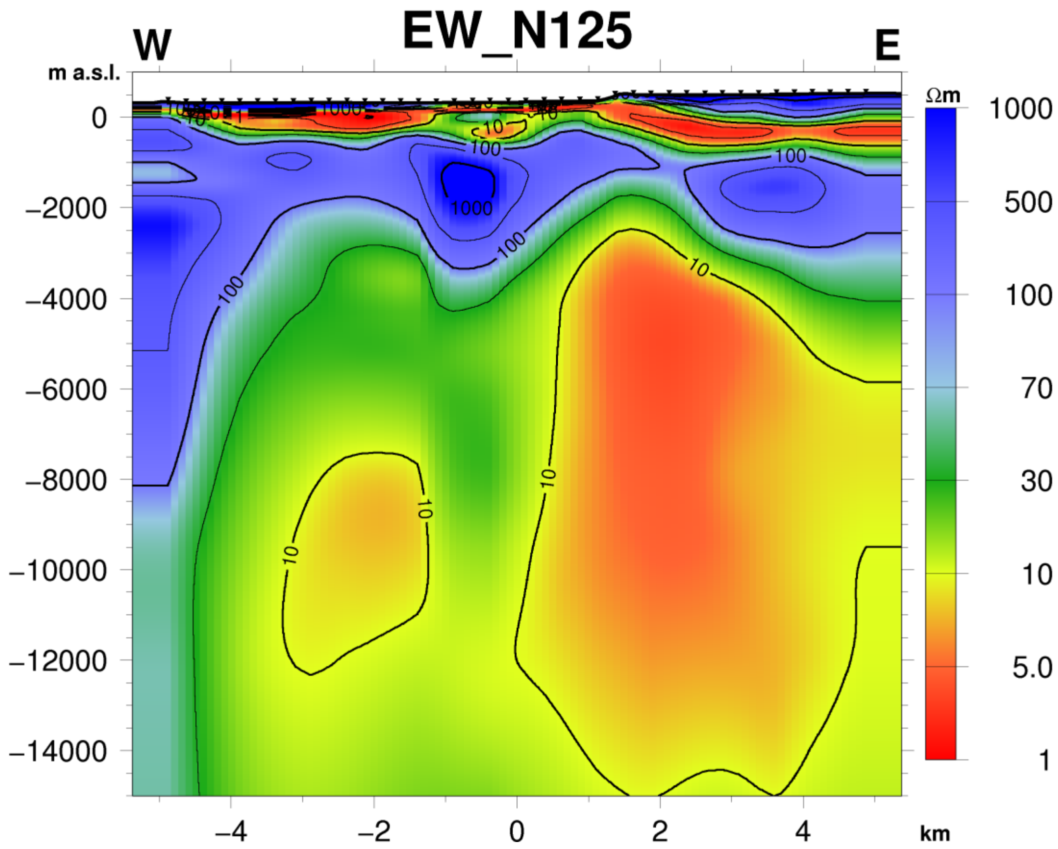
EW_N125
W
E
m a.s.l.
0
–2000
–4000
–6000
–8000
–10000
–12000
–14000
–4
–2
0
2
4
km
Ωm
1000
500
100
70
30
10
5.0
1

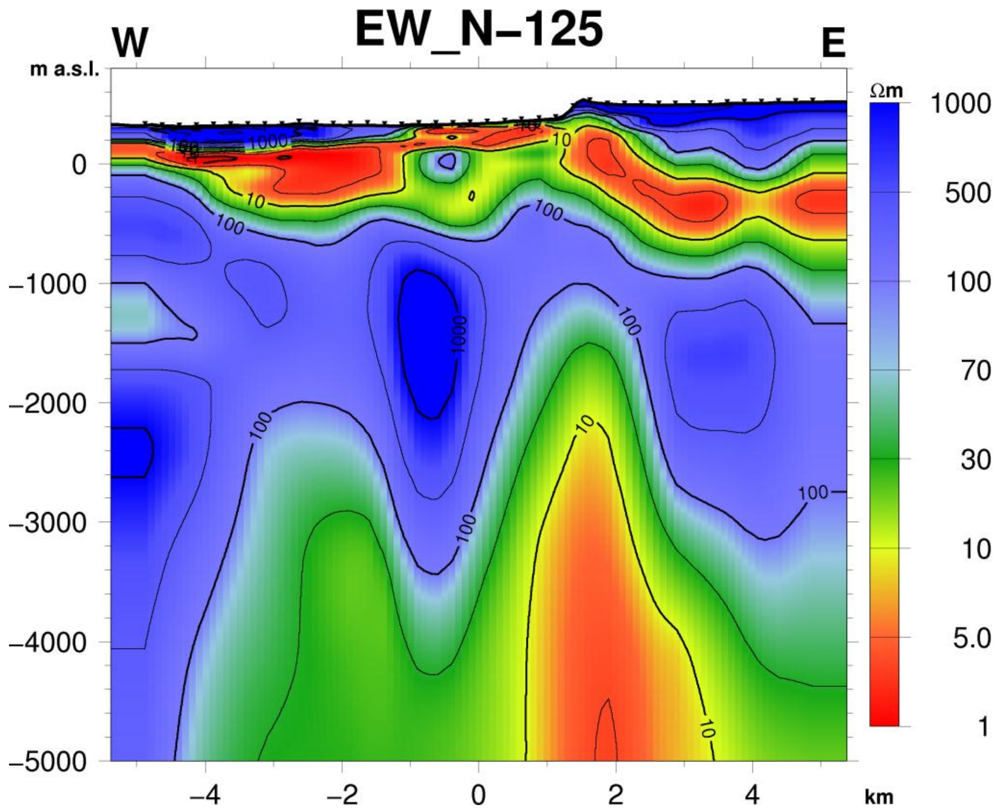
EW_N-125
W
E
m a.s.l.
Ωm
1000
500
100
70
30
10
5.0
1
0
−1000
−2000
−3000
−4000
−5000
−4
−2
0
2
4
km

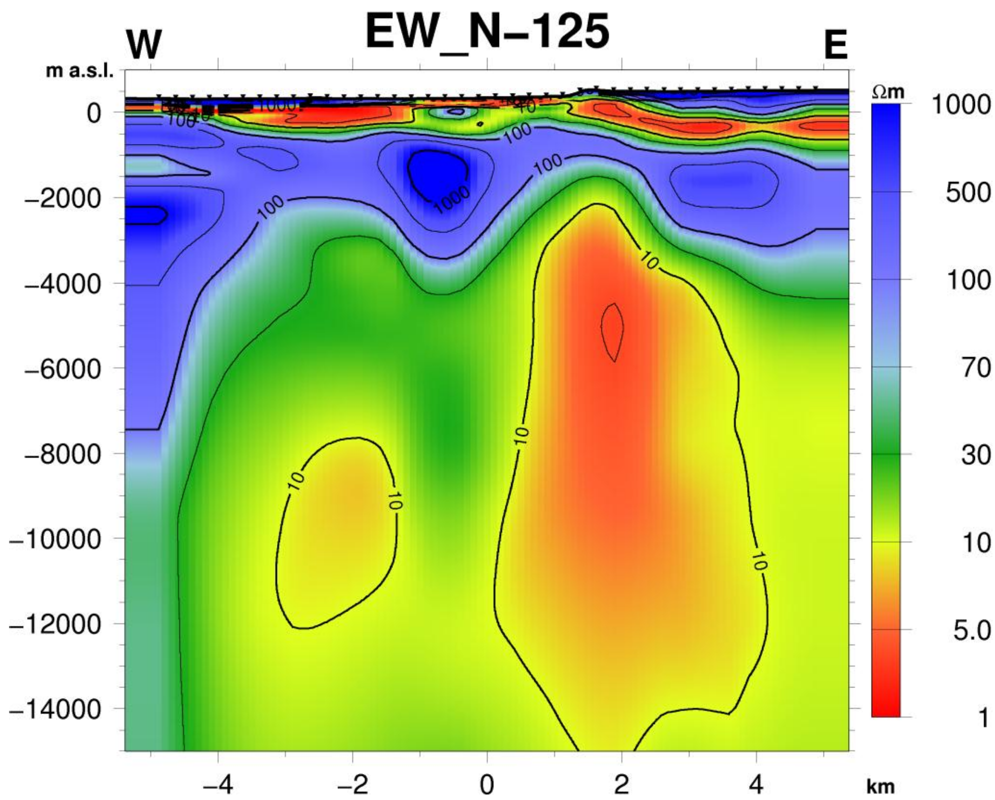
EW_N-125
W
E
m a.s.l.
Ωm
1000
500
100
70
30
10
5.0
1
0
−2000
−4000
−6000
−8000
−10000
−12000
−14000
−4
−2
0
2
4
km

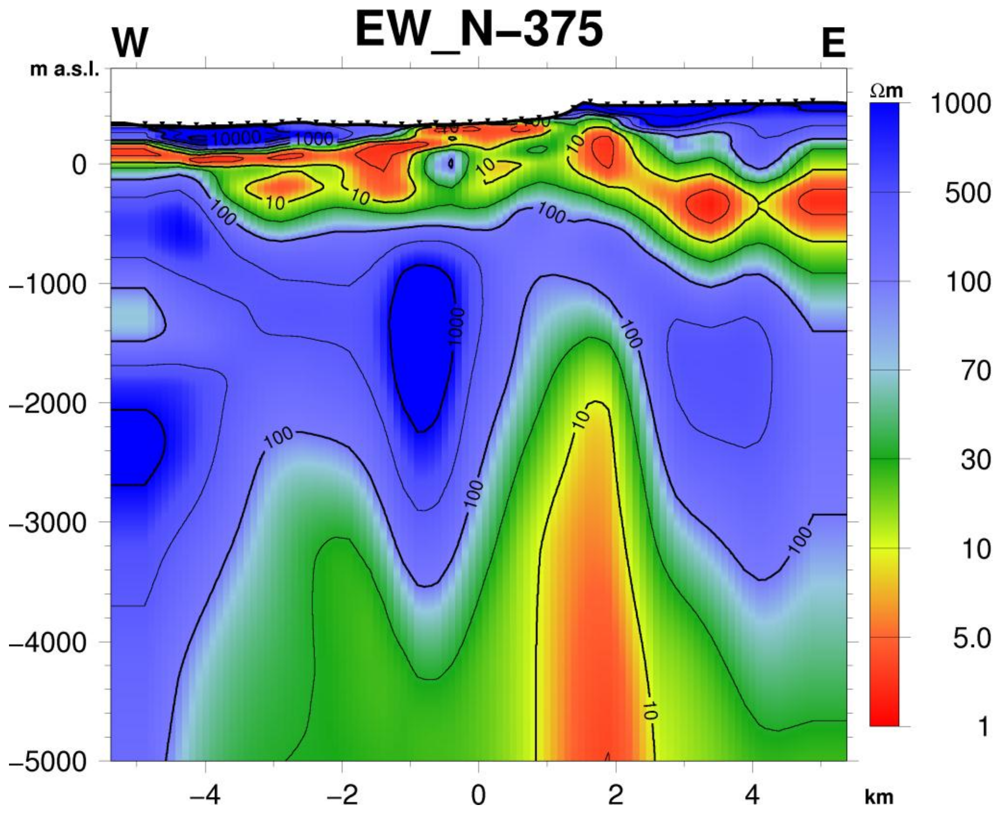
EW_N-375
W
E
m a.s.l.
Ωm
1000
500
100
70
30
10
5.0
1
0
−1000
−2000
−3000
−4000
−5000
−4
−2
0
2
4
km

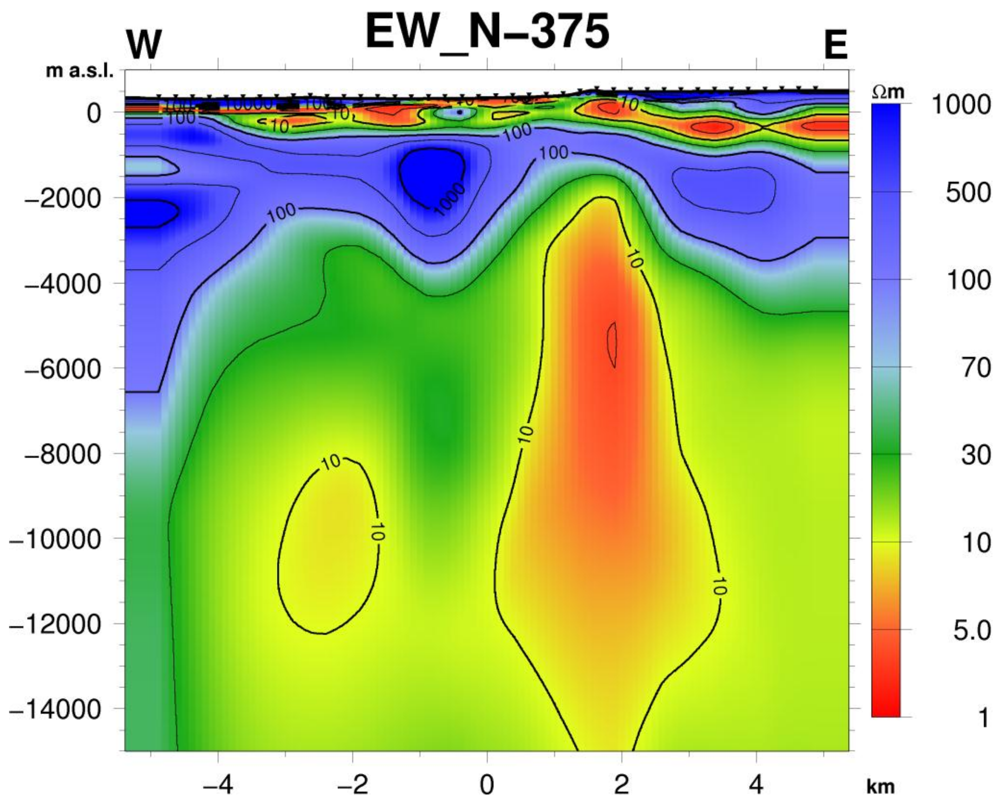
EW_N-375
W
E
m a.s.l.
Ωm
1000
500
100
70
30
10
5.0
1
0
−2000
−4000
−6000
−8000
−10000
−12000
−14000
−4
−2
0
2
4
km

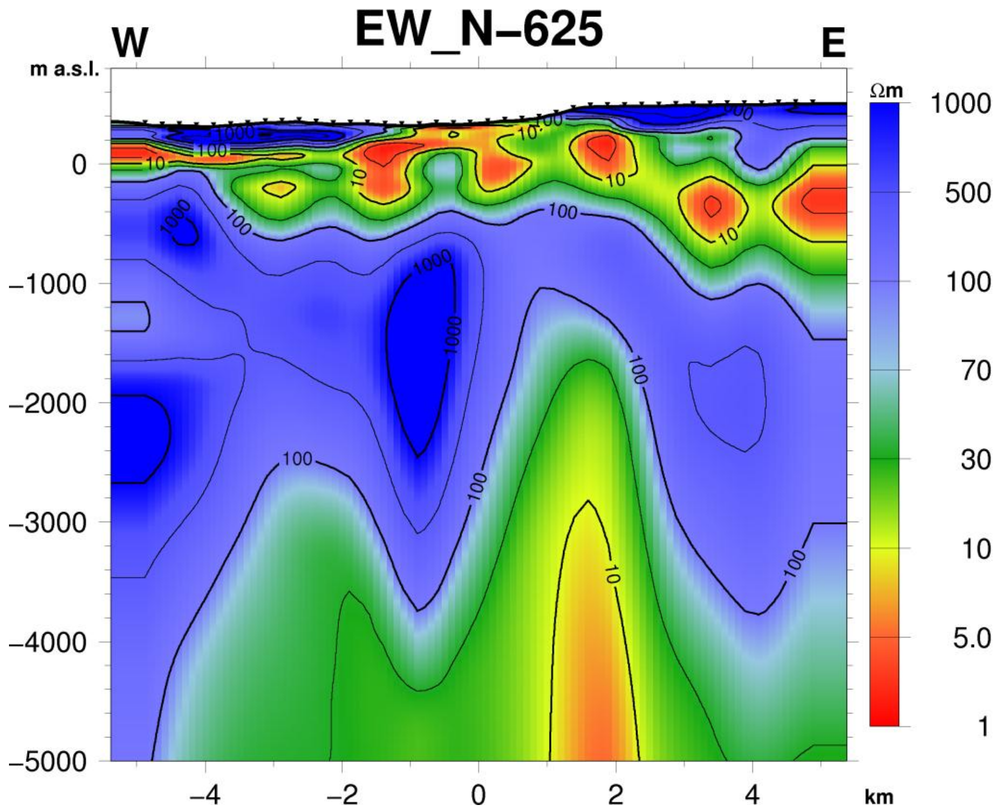

EW_N-625
W
E
m a.s.l.
Ωm
1000
500
100
70
30
10
5.0
1
0
−1000
−2000
−3000
−4000
−5000
−4
−2
0
2
4
km

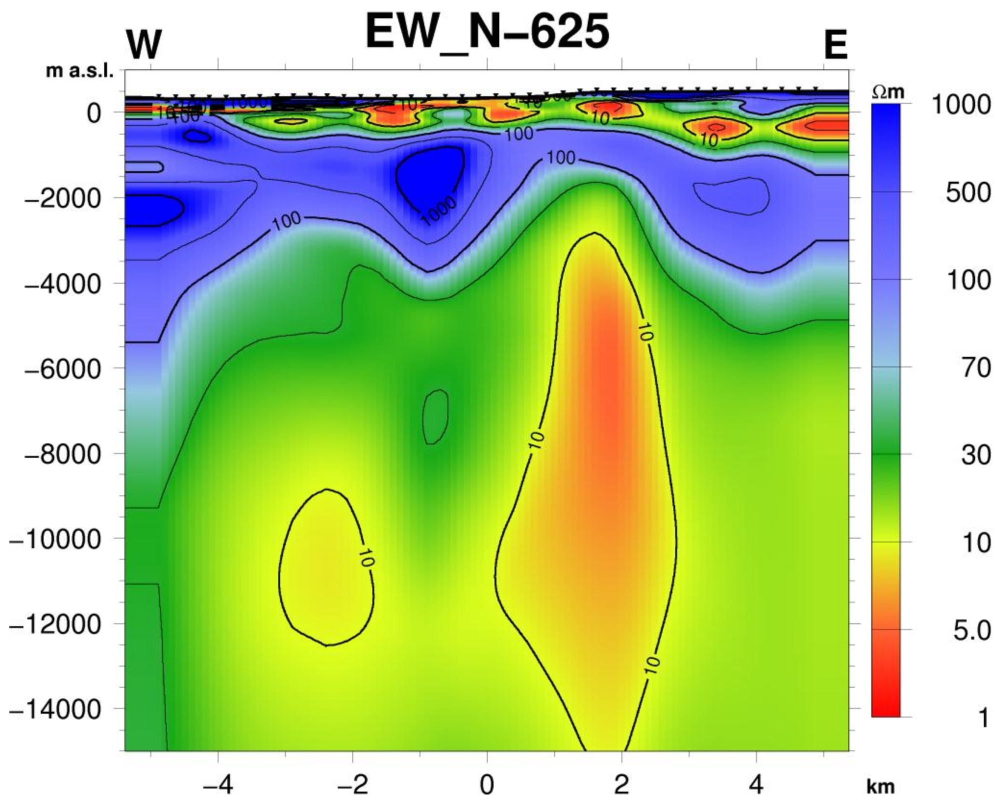

EW_N-625
W
E
m a.s.l.
Ωm
1000
500
100
70
30
10
5.0
1
0
−2000
−4000
−6000
−8000
−10000
−12000
−14000
−4
−2
0
2
4
km

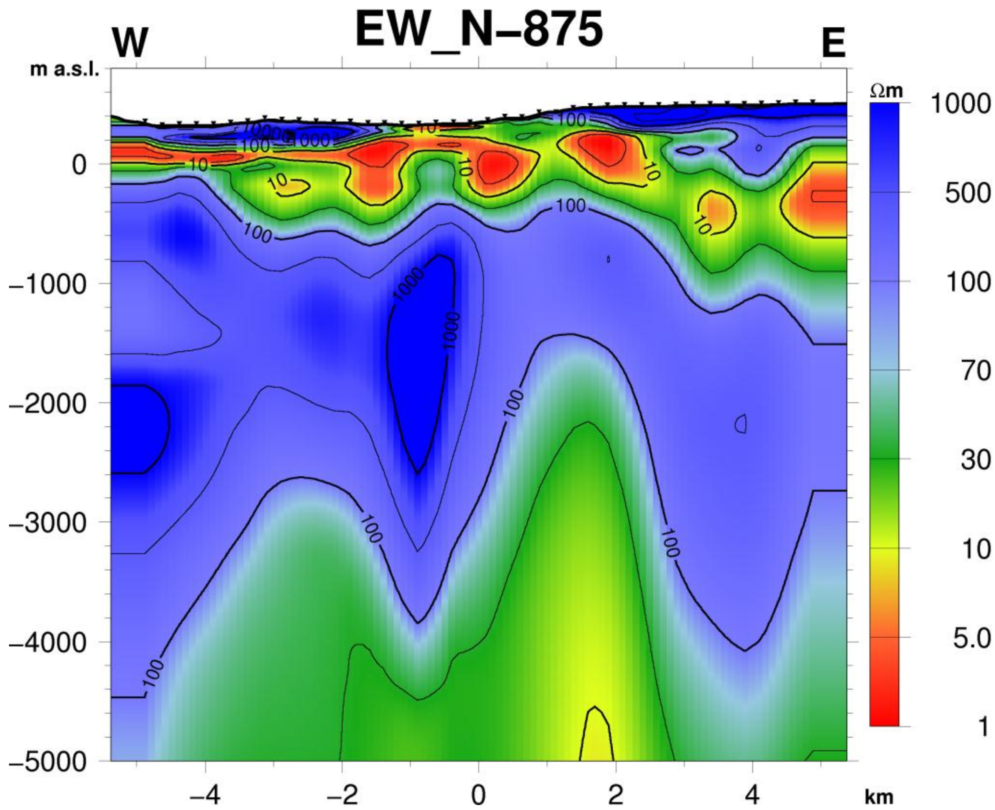

EW_N–875
W
E
m a.s.l.
Ωm
0
−1000
−2000
−3000
−4000
−5000
−4
−2
0
2
4
km
1000
500
100
70
30
10
5.0
1

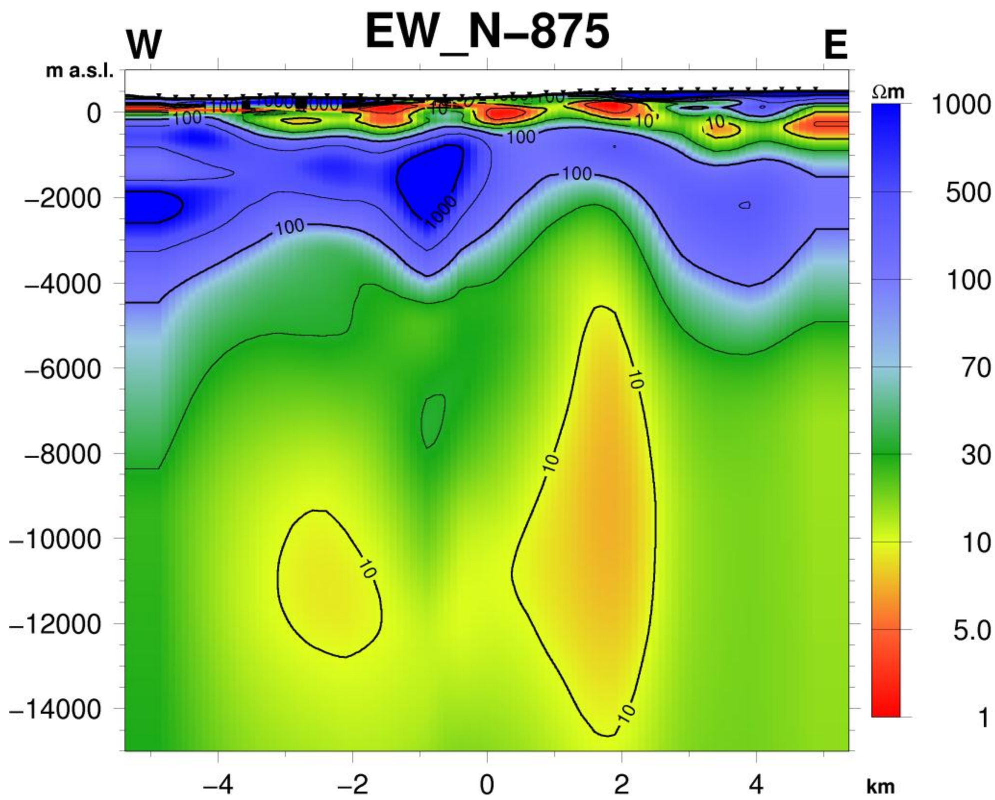

EW_N–875
W
E
m a.s.l.
Ωm
0
−2000
−4000
−6000
−8000
−10000
−12000
−14000
−4
−2
0
2
4
km
1000
500
100
70
30
10
5.0
1

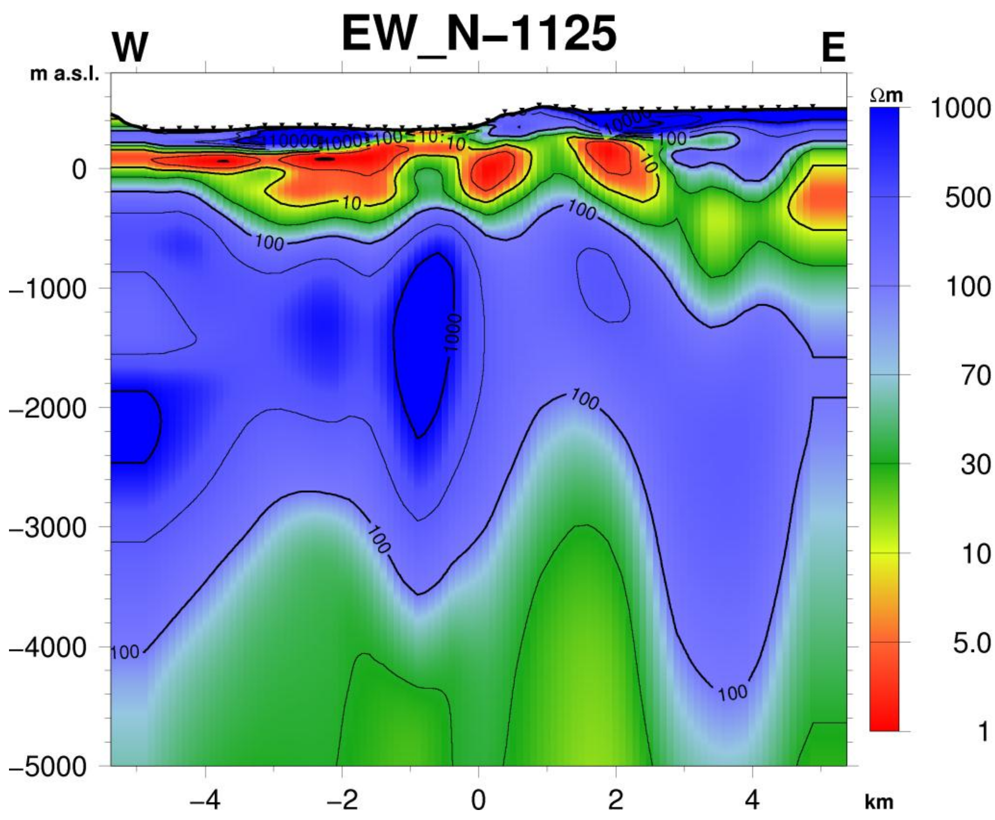

EW_N-1125
W
E
m a.s.l.
0
−1000
−2000
−3000
−4000
−5000
−4
−2
0
2
4
km
Ωm
1000
500
100
70
30
10
5.0
1

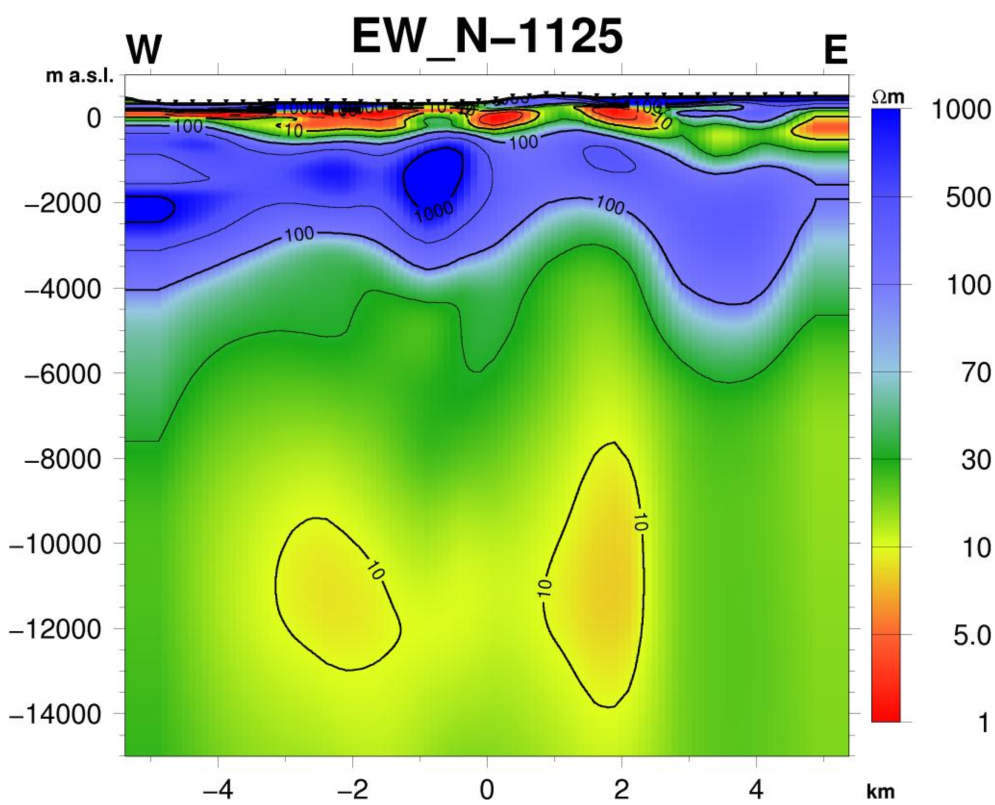

EW_N-1125
W
E
m a.s.l.
0
−2000
−4000
−6000
−8000
−10000
−12000
−14000
−4
−2
0
2
4
km
Ωm
1000
500
100
70
30
10
5.0
1

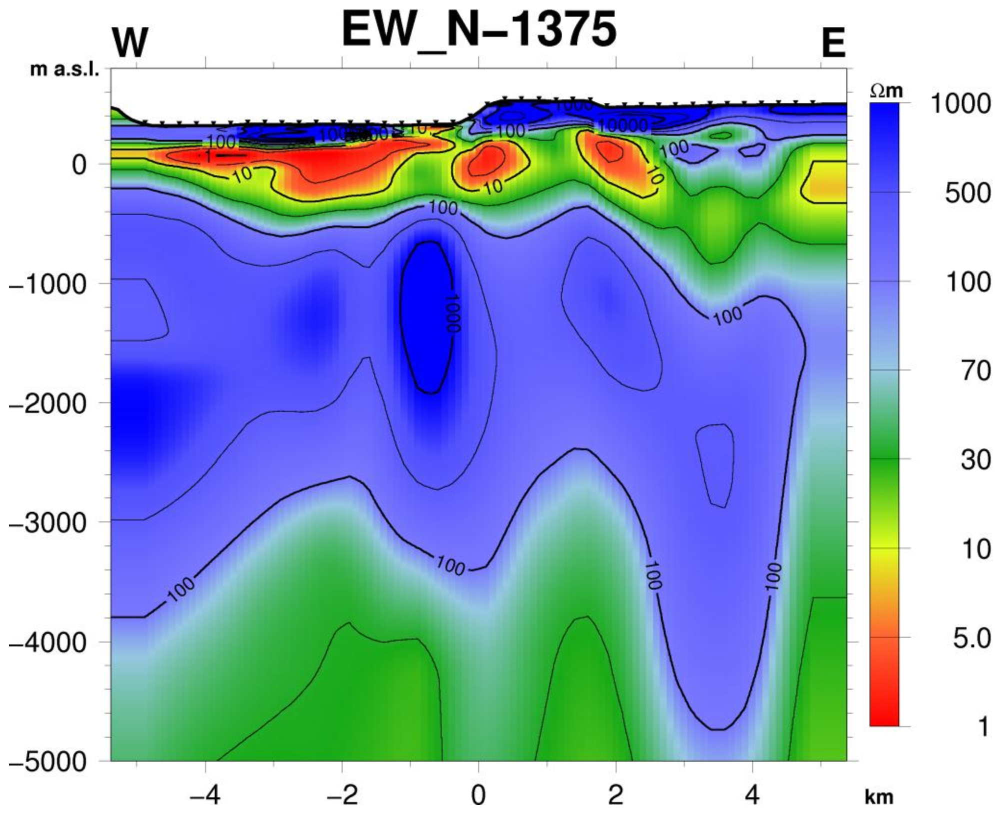
EW_N–1375
W
E
m a.s.l.
Ωm
1000
500
100
70
30
10
5.0
1
0
–1000
–2000
–3000
–4000
–5000
–4
–2
0
2
4
km
100
10
1000

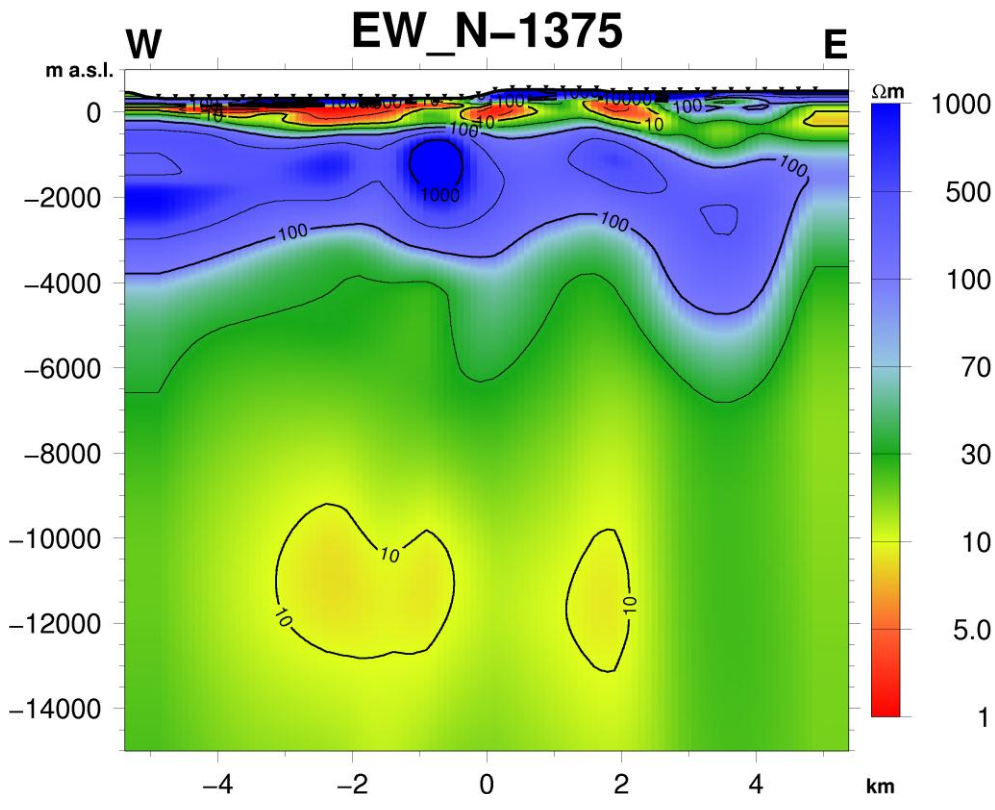
EW_N–1375
W
E
m a.s.l.
Ωm
1000
500
100
70
30
10
5.0
1
0
–2000
–4000
–6000
–8000
–10000
–12000
–14000
–4
–2
0
2
4
km
100
10
1000

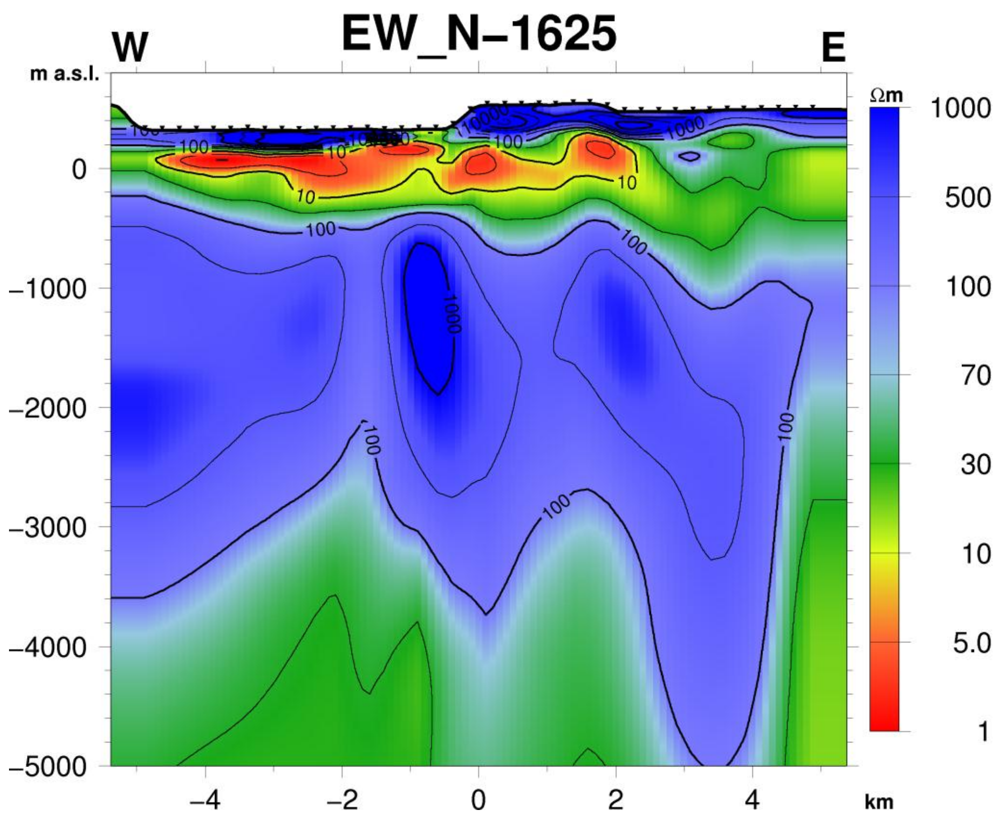
EW_N-1625
W
E
m a.s.l.
0
-1000
-2000
-3000
-4000
-5000
-4
-2
0
2
4
km
Ωm
1000
500
100
70
30
10
5.0
1

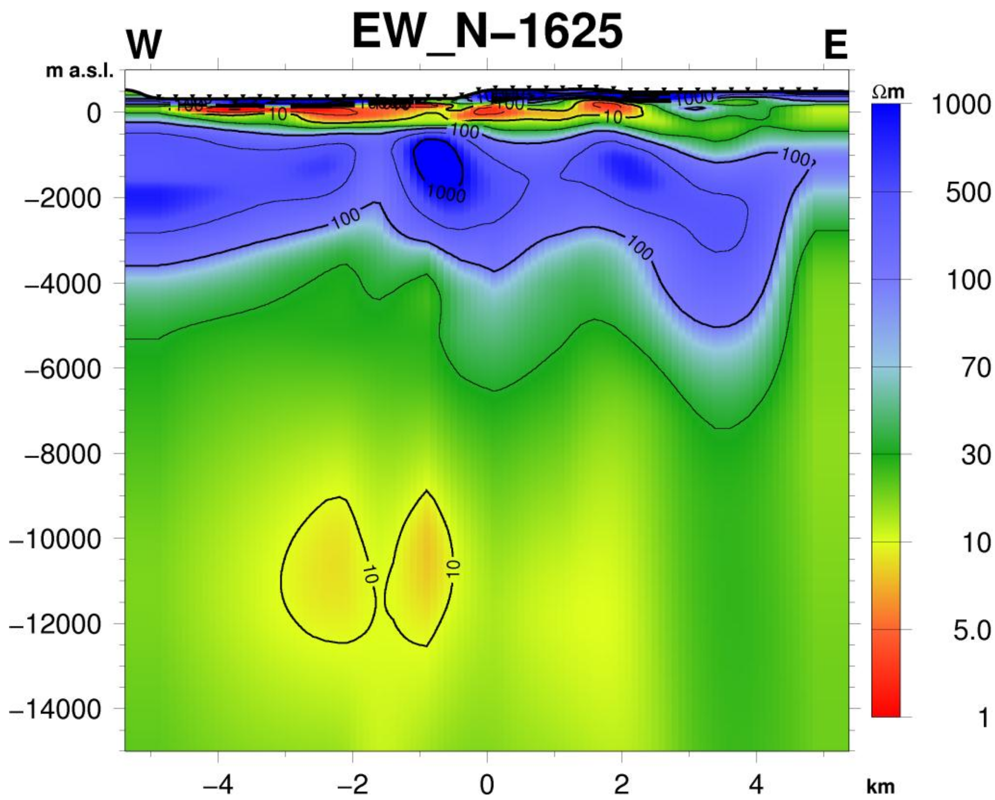
EW_N-1625
W
E
m a.s.l.
0
-2000
-4000
-6000
-8000
-10000
-12000
-14000
-4
-2
0
2
4
km
Ωm
1000
500
100
70
30
10
5.0
1

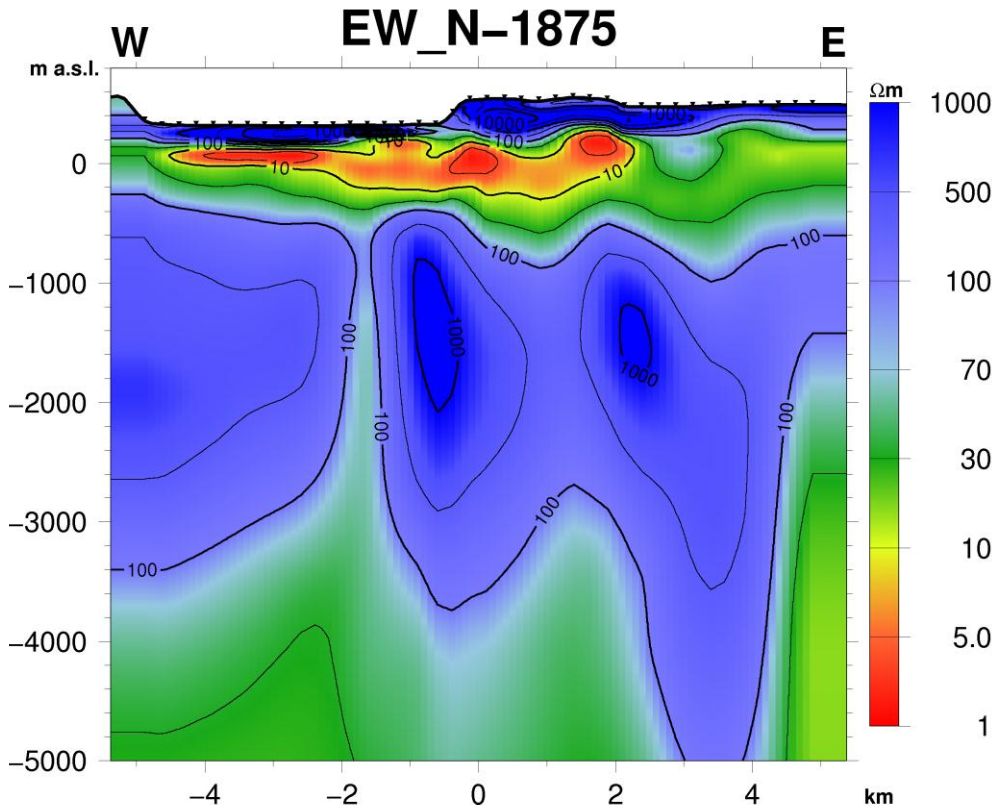

EW_N–1875
W
E
m a.s.l.
0
−1000
−2000
−3000
−4000
−5000
−4
−2
0
2
4
km
Ωm
1000
500
100
70
30
10
5.0
1

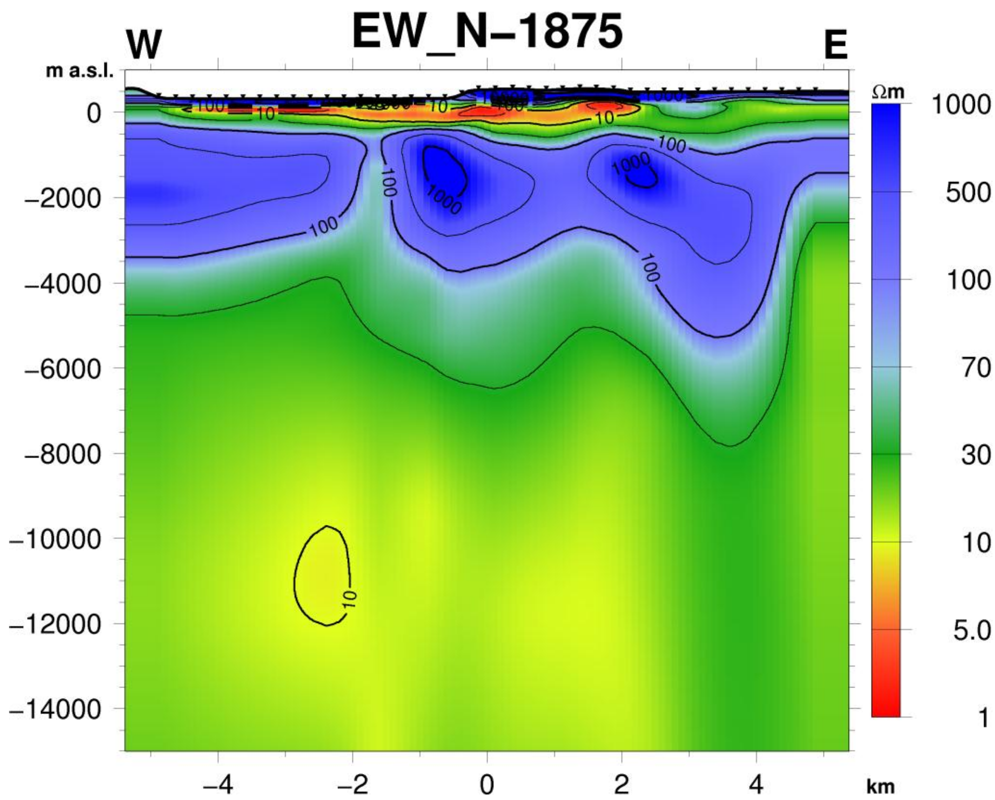

EW_N–1875
W
E
m a.s.l.
0
−2000
−4000
−6000
−8000
−10000
−12000
−14000
−4
−2
0
2
4
km
Ωm
1000
500
100
70
30
10
5.0
1

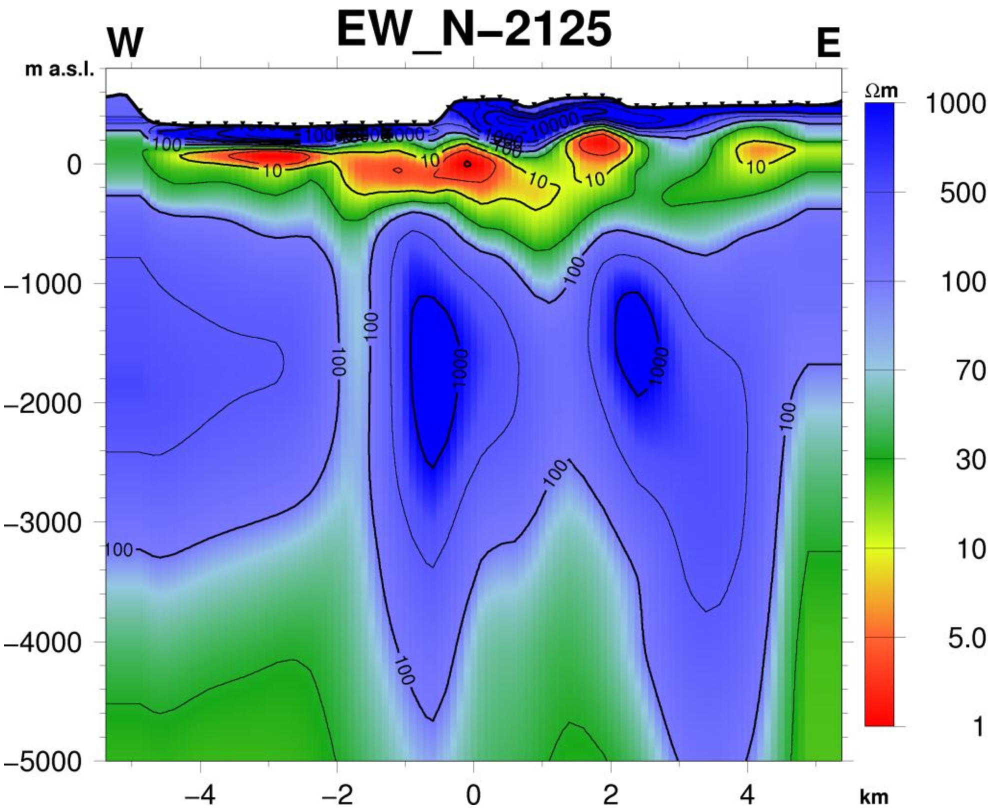

EW_N-2125
W
E
m a.s.l.
0
−1000
−2000
−3000
−4000
−5000
−4
−2
0
2
4
km
Ωm
1000
500
100
70
30
10
5.0
1

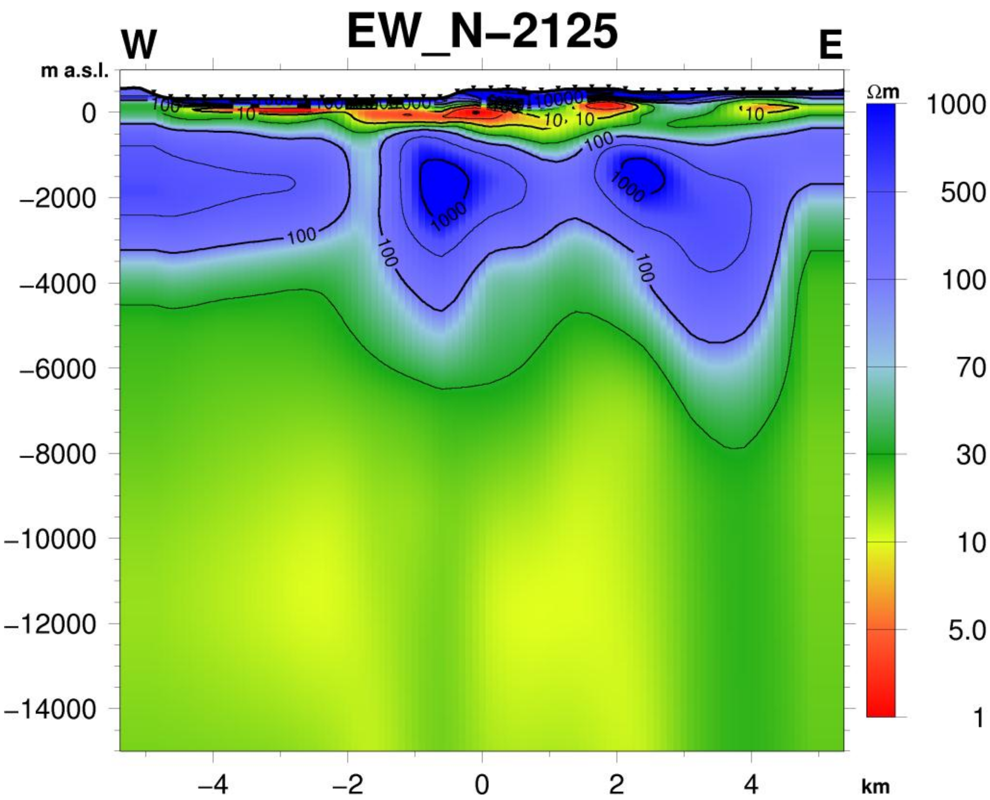

EW_N-2125
W
E
m a.s.l.
0
−2000
−4000
−6000
−8000
−10000
−12000
−14000
−4
−2
0
2
4
km
Ωm
1000
500
100
70
30
10
5.0
1

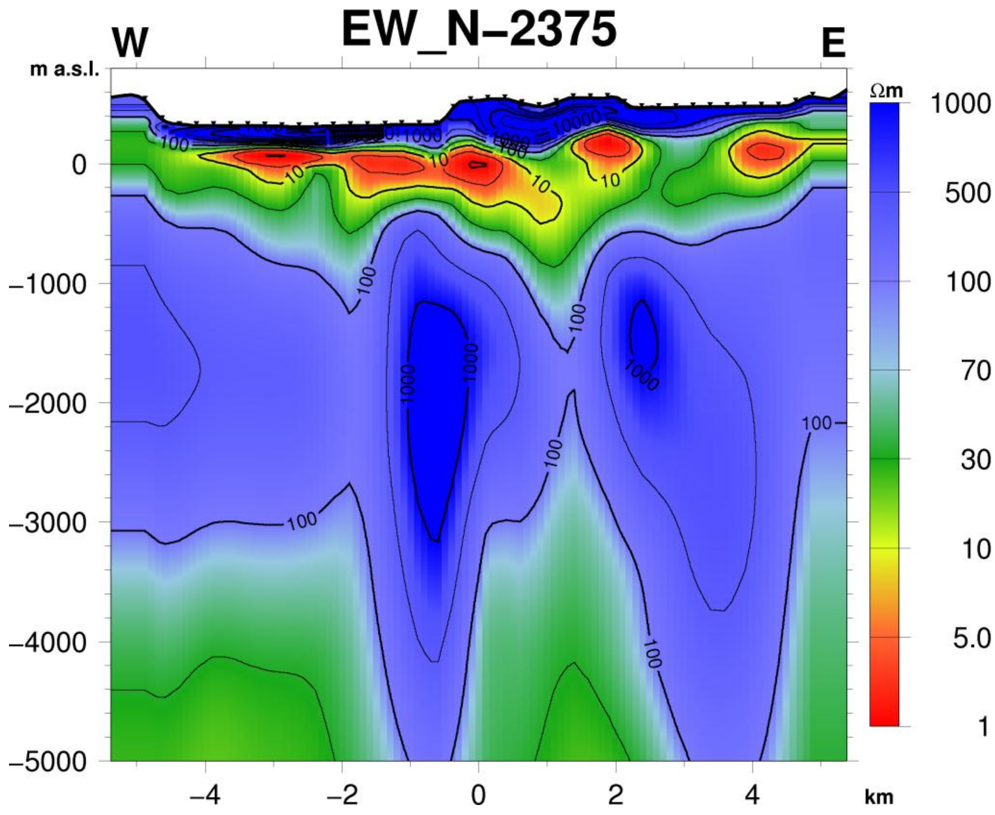
EW_N–2375
W
E
m a.s.l.
Ωm
1000
500
100
70
30
10
5.0
1
0
−1000
−2000
−3000
−4000
−5000
−4
−2
0
2
4
km

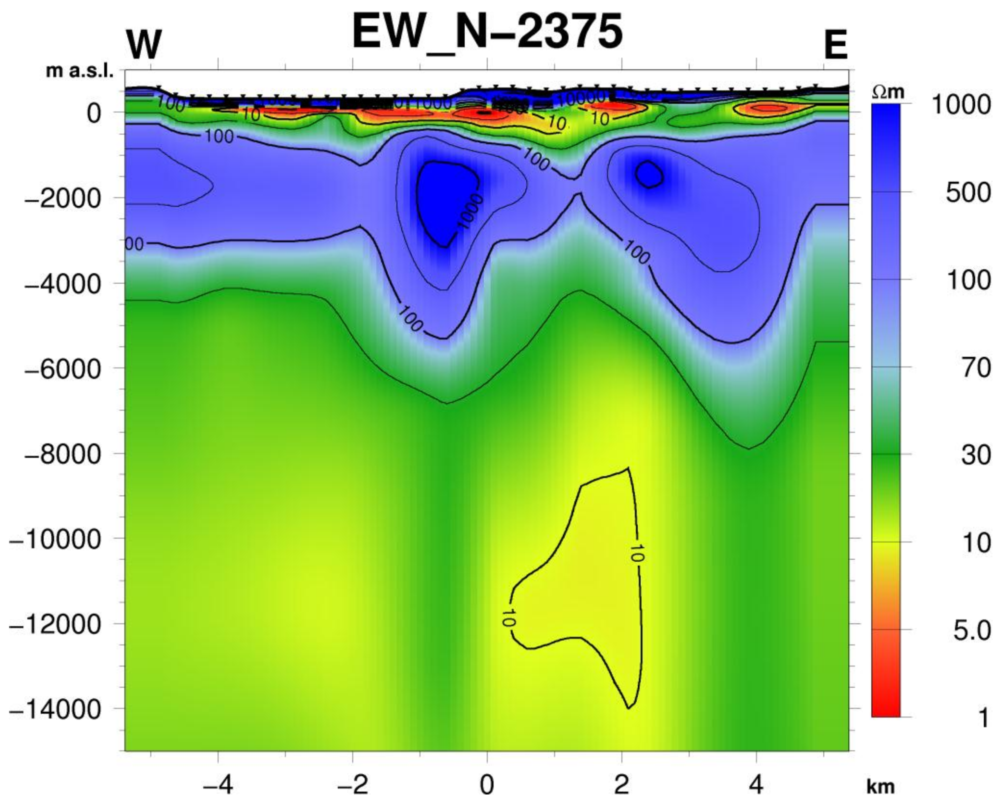
EW_N–2375
W
E
m a.s.l.
Ωm
1000
500
100
70
30
10
5.0
1
0
−2000
−4000
−6000
−8000
−10000
−12000
−14000
−4
−2
0
2
4
km

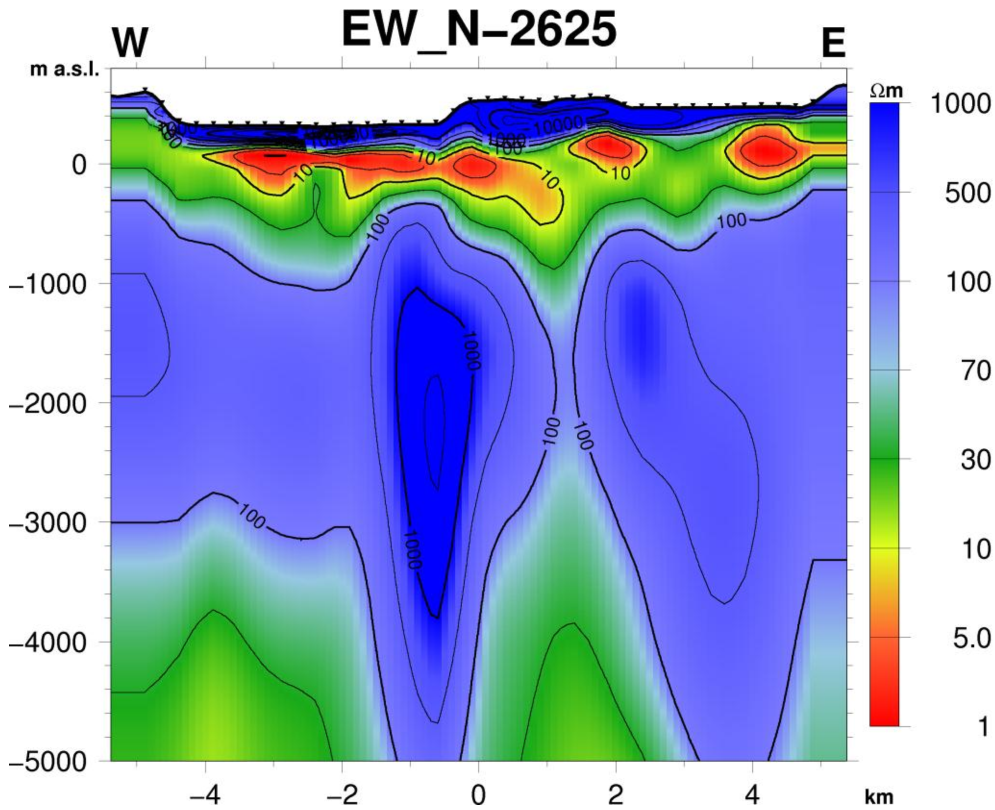
EW_N-2625
W
E
m a.s.l.
0
−1000
−2000
−3000
−4000
−5000
−4
−2
0
2
4
km
Ωm
1000
500
100
70
30
10
5.0
1

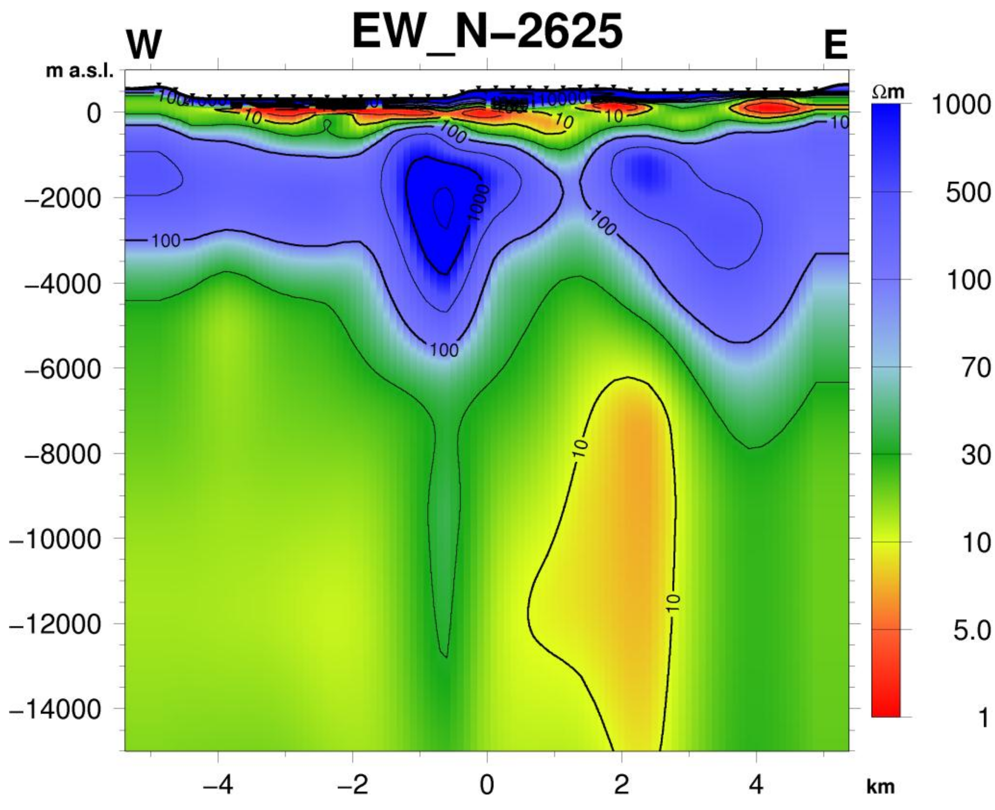
EW_N-2625
W
E
m a.s.l.
0
−2000
−4000
−6000
−8000
−10000
−12000
−14000
−4
−2
0
2
4
km
Ωm
1000
500
100
70
30
10
5.0
1

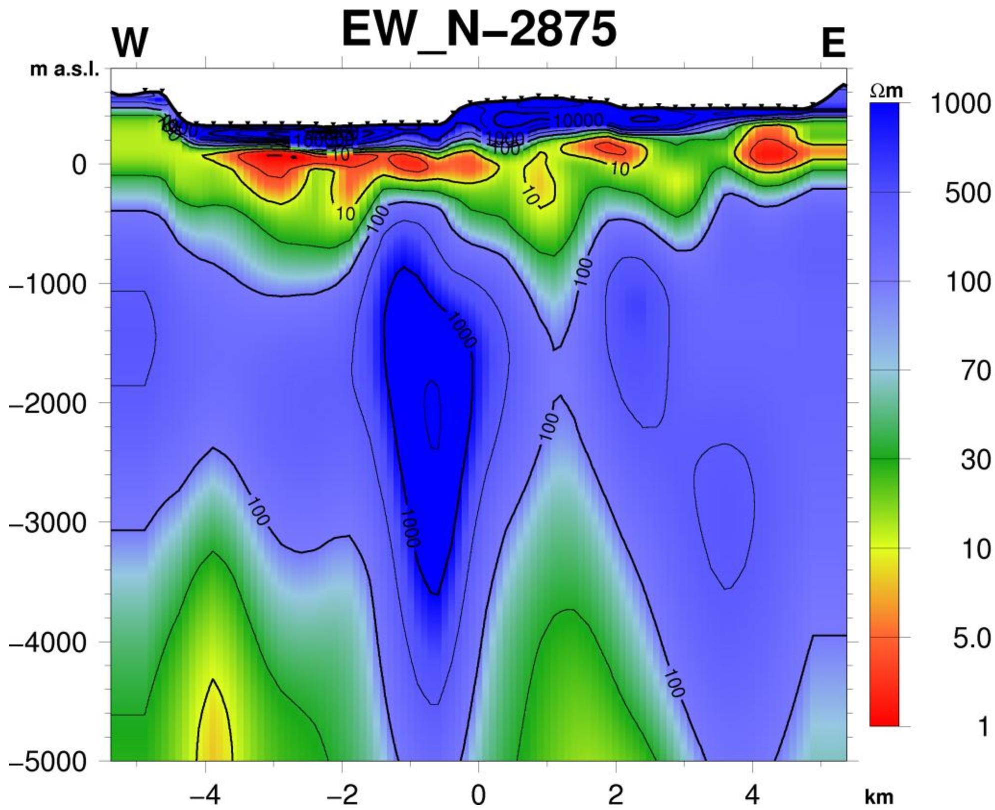
EW_N–2875
W
E
m a.s.l.
0
–1000
–2000
–3000
–4000
–5000
–4
–2
0
2
4
km
Ωm
1000
500
100
70
30
10
5.0
1

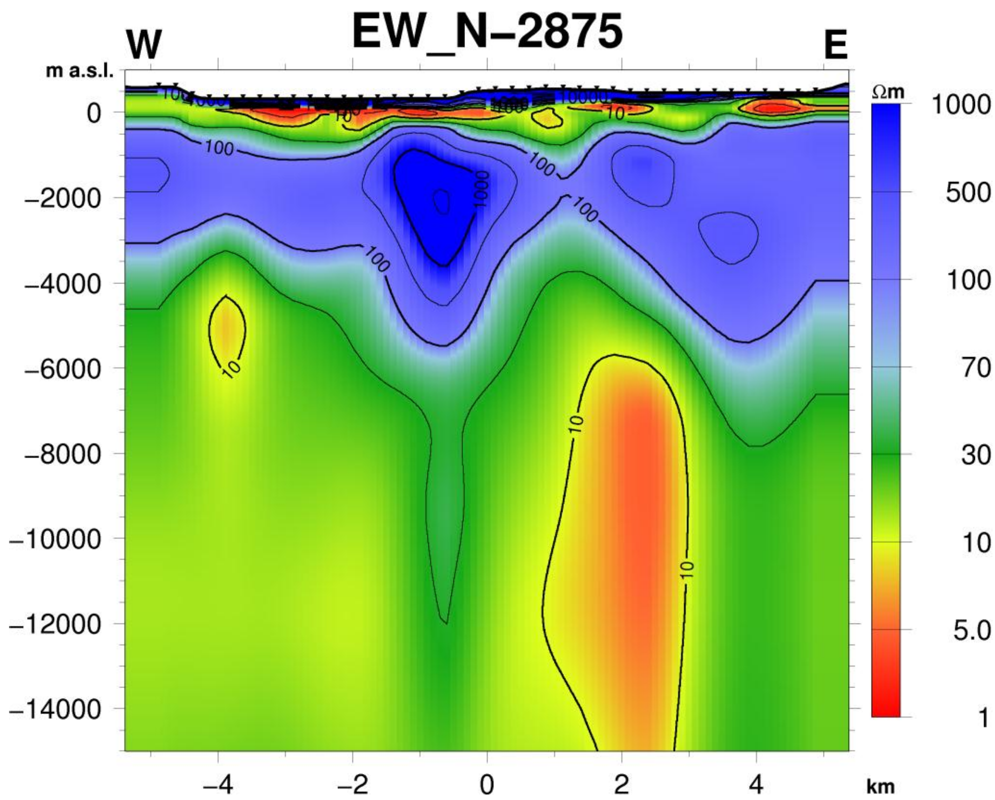
EW_N–2875
W
E
m a.s.l.
0
–2000
–4000
–6000
–8000
–10000
–12000
–14000
–4
–2
0
2
4
km
Ωm
1000
500
100
70
30
10
5.0
1

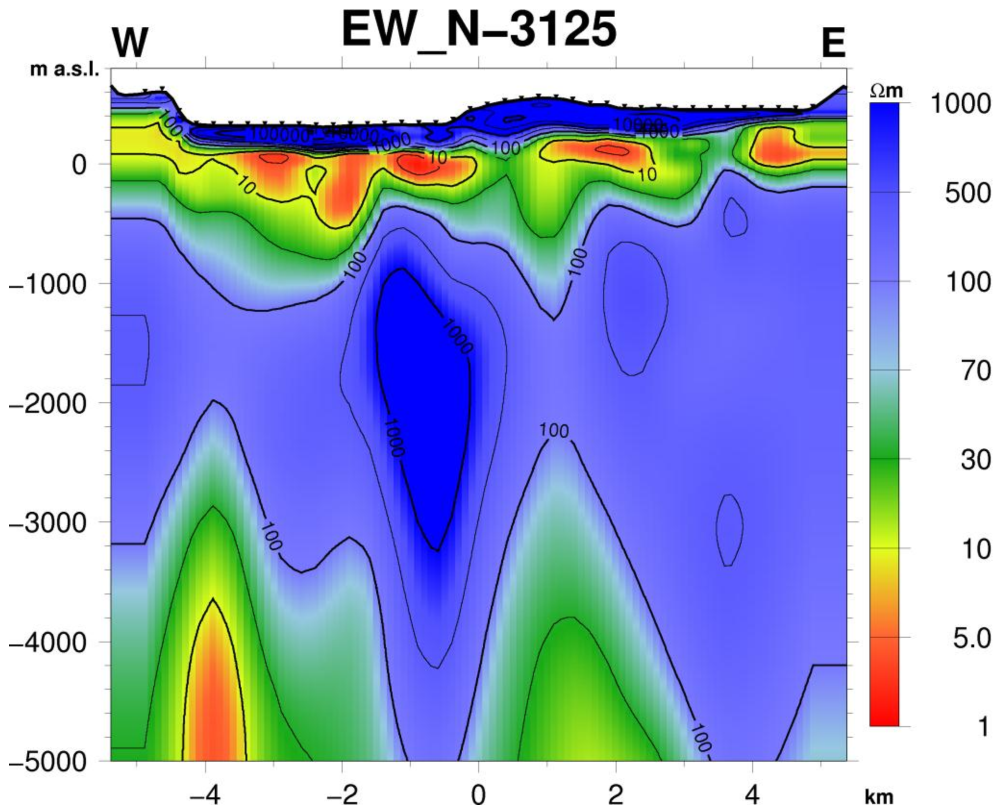
EW_N–3125
W
E
m a.s.l.
Ωm
1000
500
100
70
30
10
5.0
1
0
−1000
−2000
−3000
−4000
−5000
−4
−2
0
2
4
km

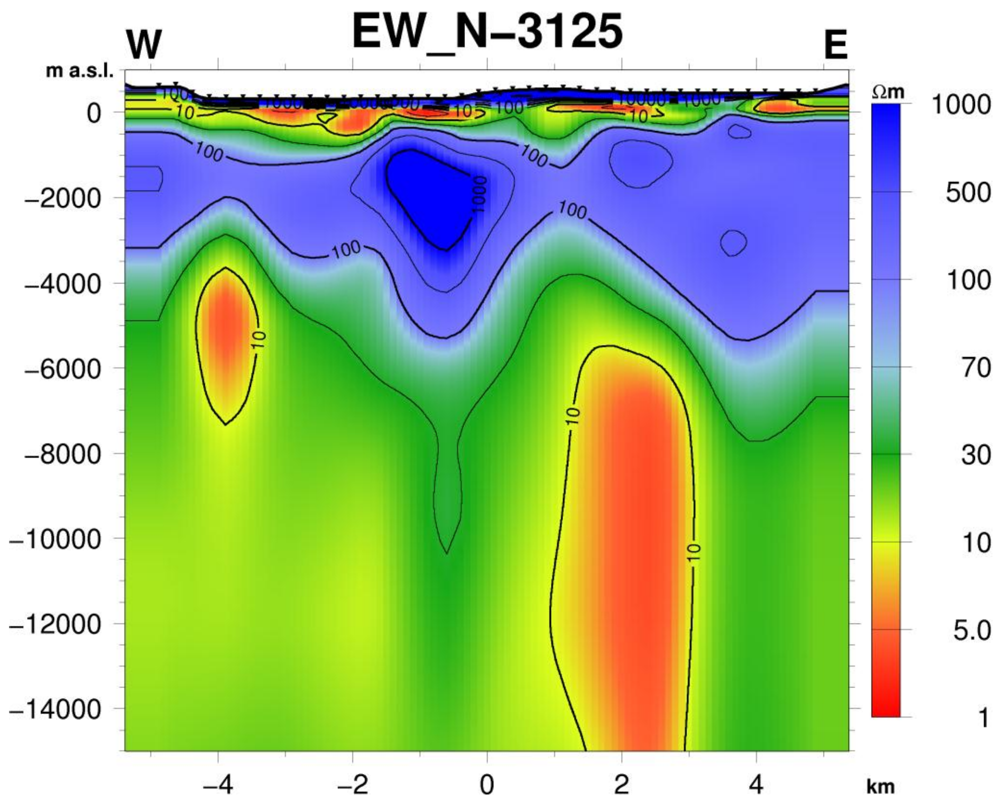
EW_N–3125
W
E
m a.s.l.
Ωm
1000
500
100
70
30
10
5.0
1
0
−2000
−4000
−6000
−8000
−10000
−12000
−14000
−4
−2
0
2
4
km

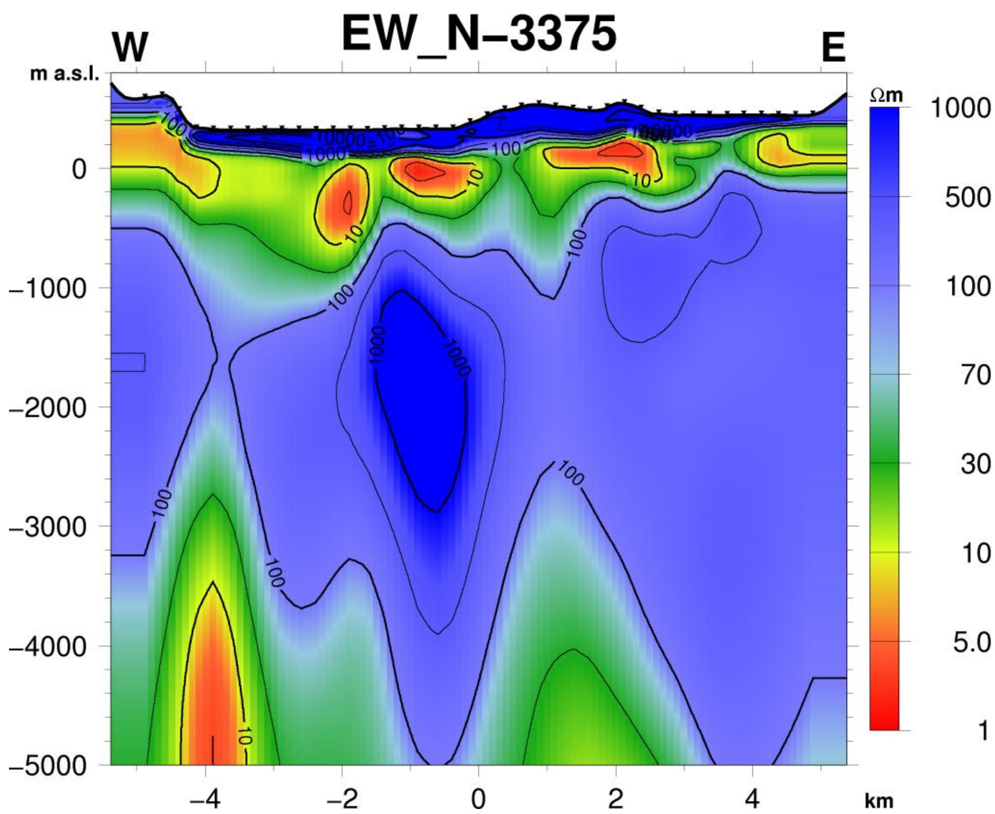

EW_N-3375
W
E
m a.s.l.
Ωm
1000
500
100
70
30
10
5.0
1
0
−1000
−2000
−3000
−4000
−5000
−4
−2
0
2
4
km

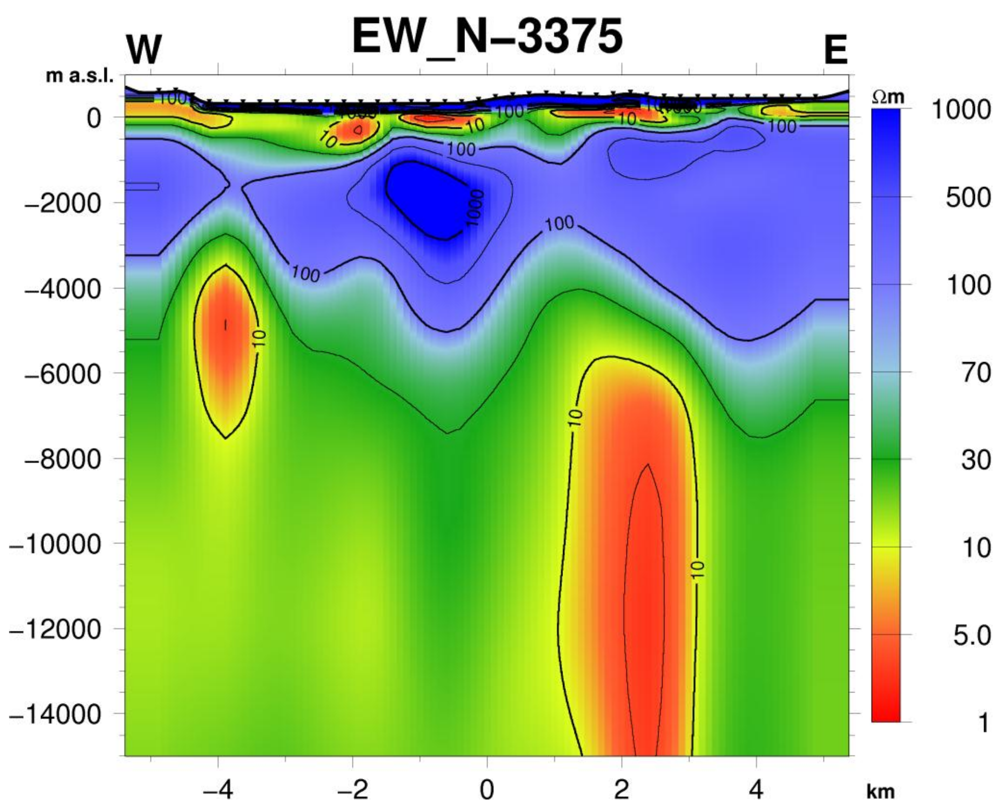

EW_N-3375
W
E
m a.s.l.
Ωm
1000
500
100
70
30
10
5.0
1
0
−2000
−4000
−6000
−8000
−10000
−12000
−14000
−4
−2
0
2
4
km

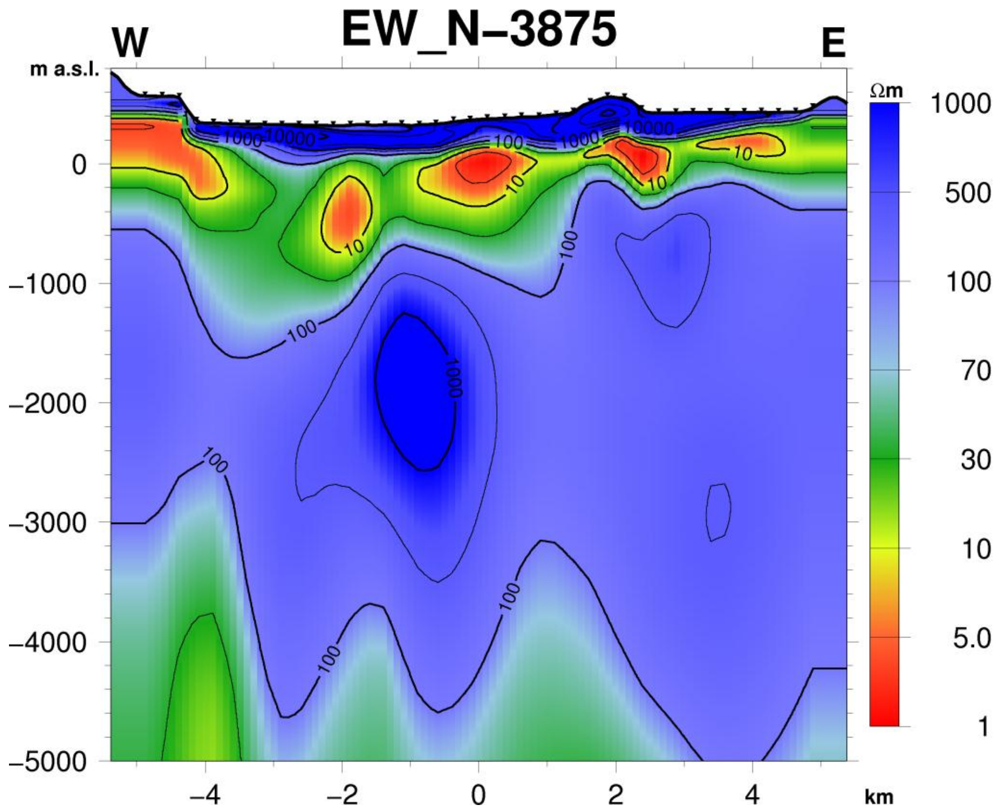
EW_N–3875
W
E
m a.s.l.
Ωm
1000
500
100
70
30
10
5.0
1
0
−1000
−2000
−3000
−4000
−5000
−4
−2
0
2
4
km

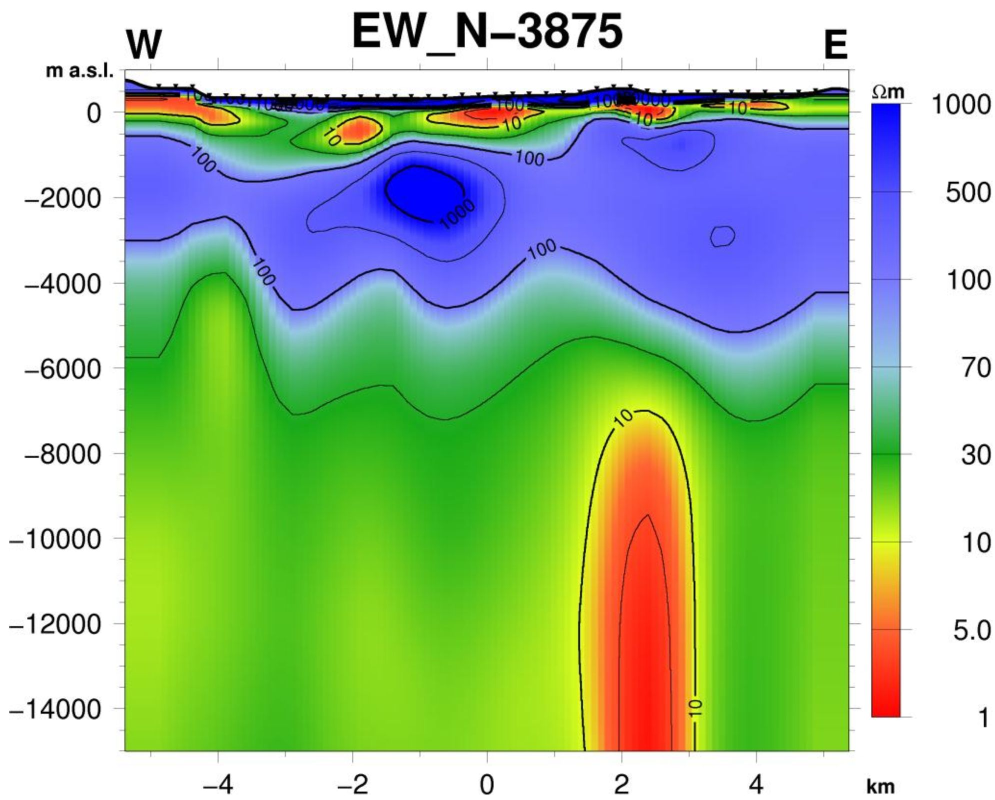
EW_N–3875
W
E
m a.s.l.
Ωm
1000
500
100
70
30
10
5.0
1
0
−2000
−4000
−6000
−8000
−10000
−12000
−14000
−4
−2
0
2
4
km

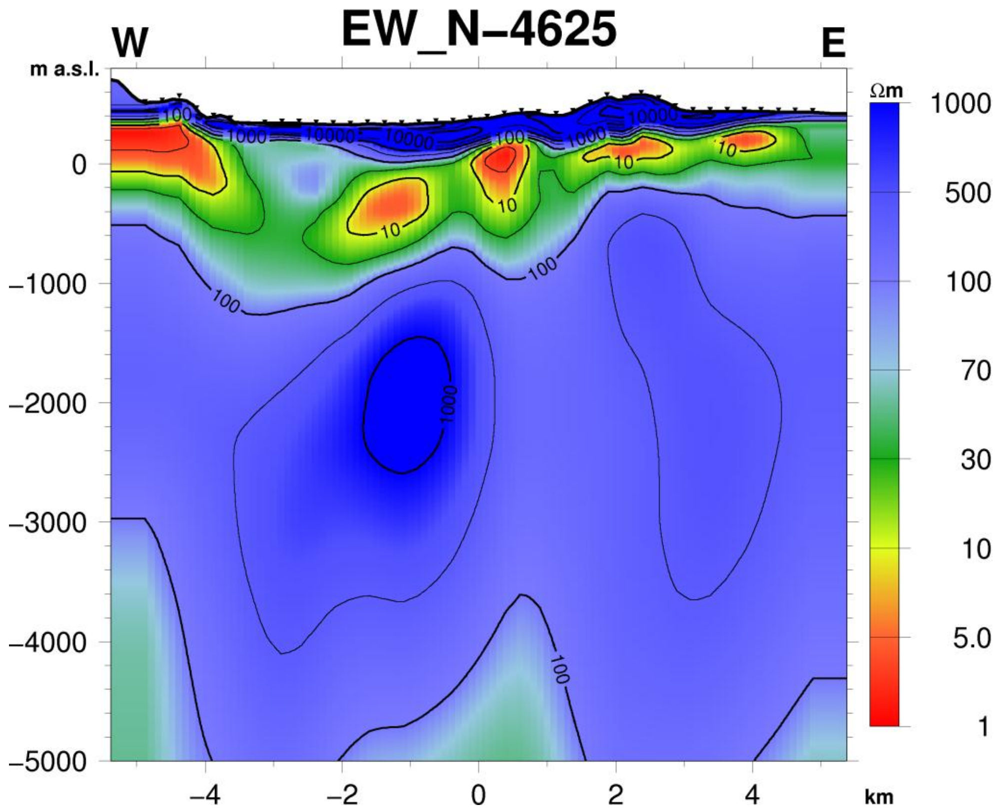

EW_N–4625
W
E
m a.s.l.
Ωm
1000
500
100
70
30
10
5.0
1
0
−1000
−2000
−3000
−4000
−5000
−4
−2
0
2
4
km

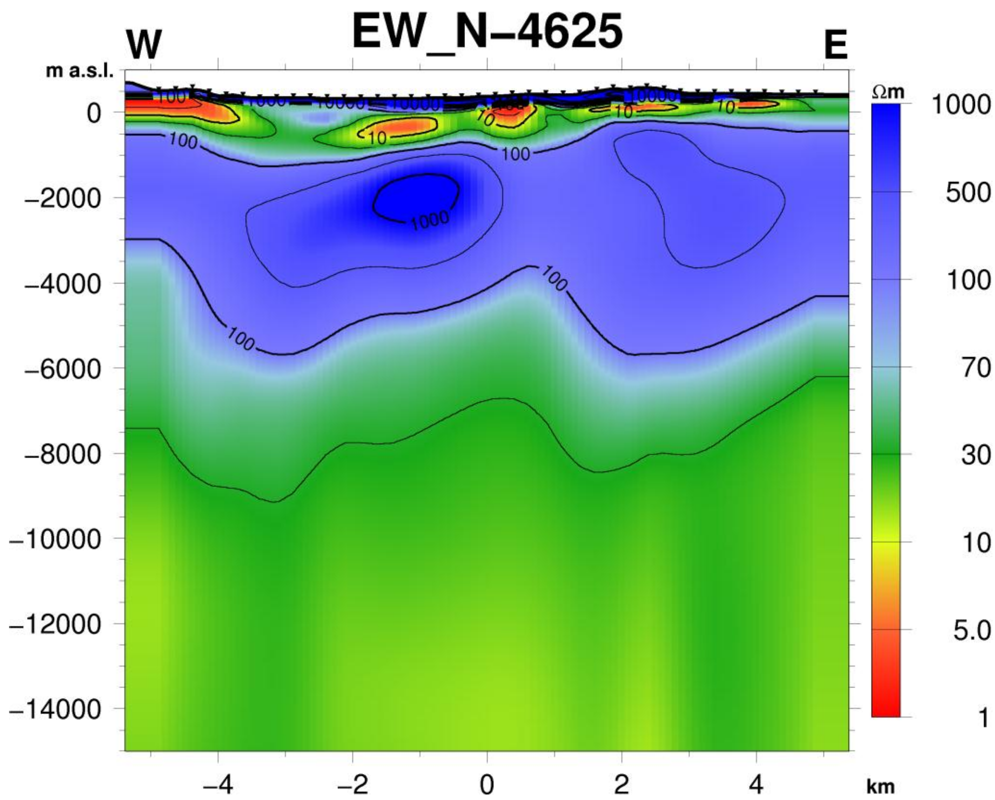

EW_N–4625
W
E
m a.s.l.
Ωm
1000
500
100
70
30
10
5.0
1
0
−2000
−4000
−6000
−8000
−10000
−12000
−14000
−4
−2
0
2
4
km

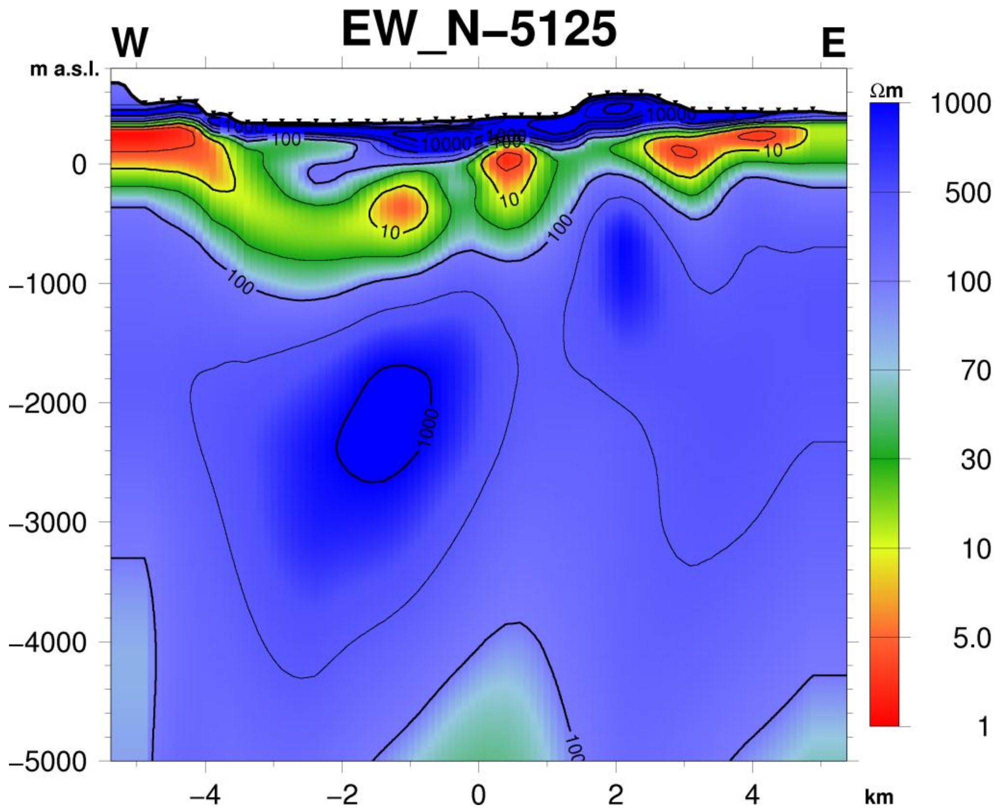
EW_N–5125
W
E
m a.s.l.
0
–1000
–2000
–3000
–4000
–5000
–4
–2
0
2
4
km
Ωm
1000
500
100
70
30
10
5.0
1

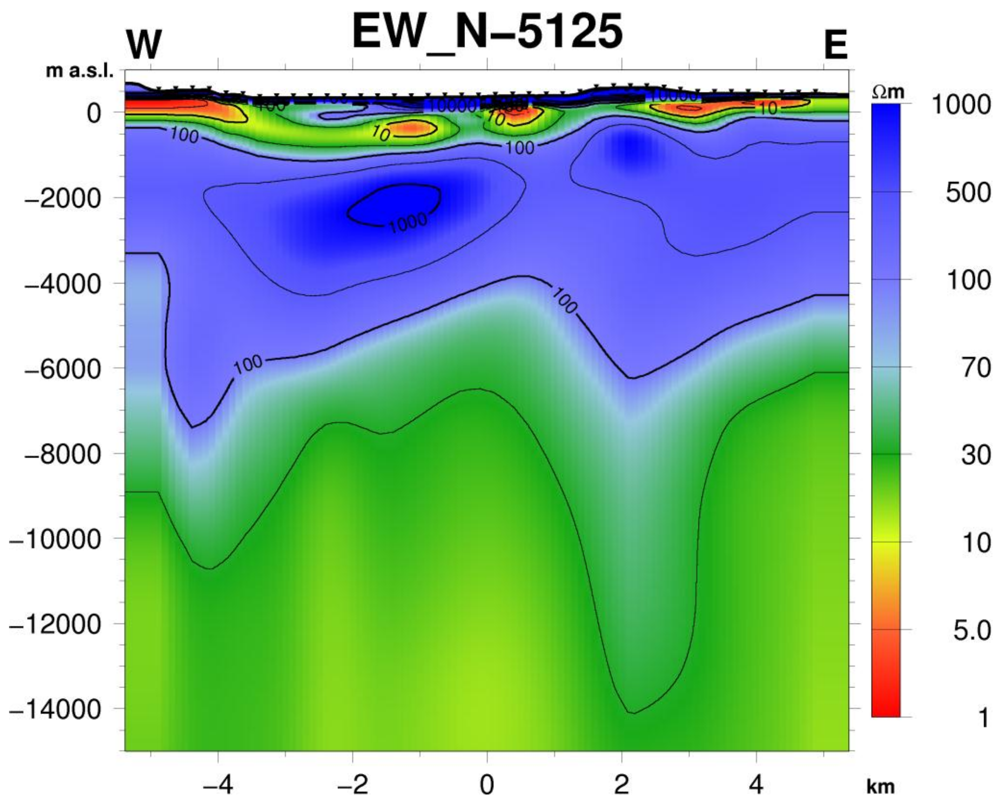
EW_N–5125
W
E
m a.s.l.
0
–2000
–4000
–6000
–8000
–10000
–12000
–14000
–4
–2
0
2
4
km
Ωm
1000
500
100
70
30
10
5.0
1

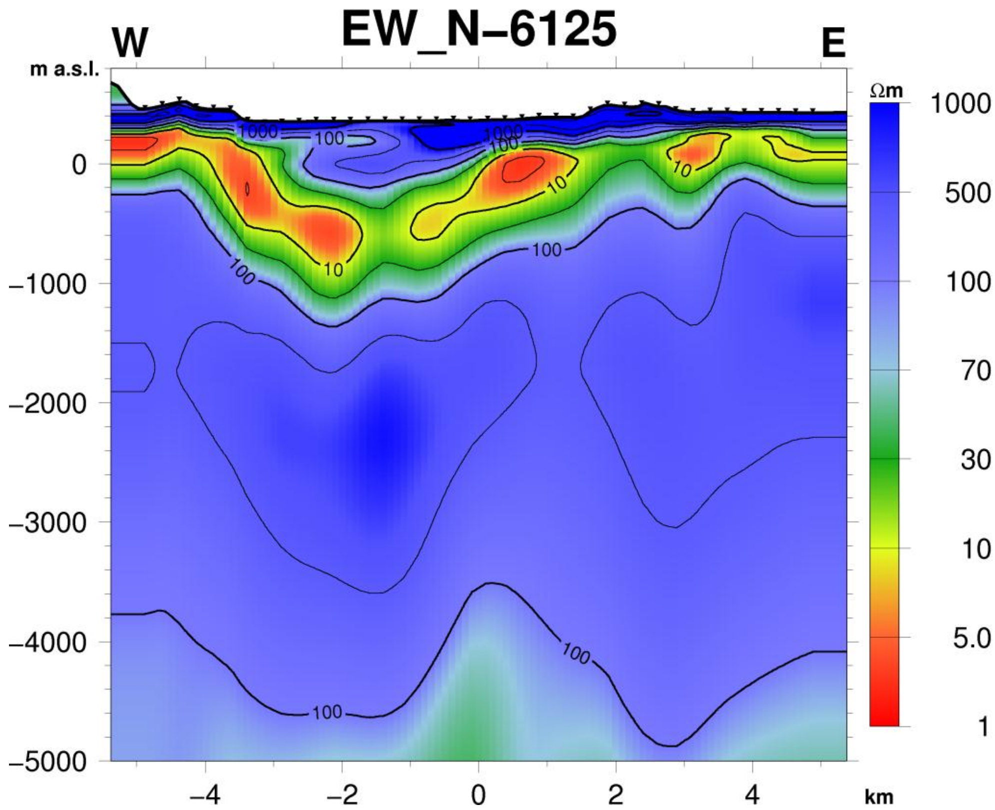

EW_N-6125
W
E
m a.s.l.
Ωm
1000
500
100
70
30
10
5.0
1
0
-1000
-2000
-3000
-4000
-5000
-4
-2
0
2
4
km

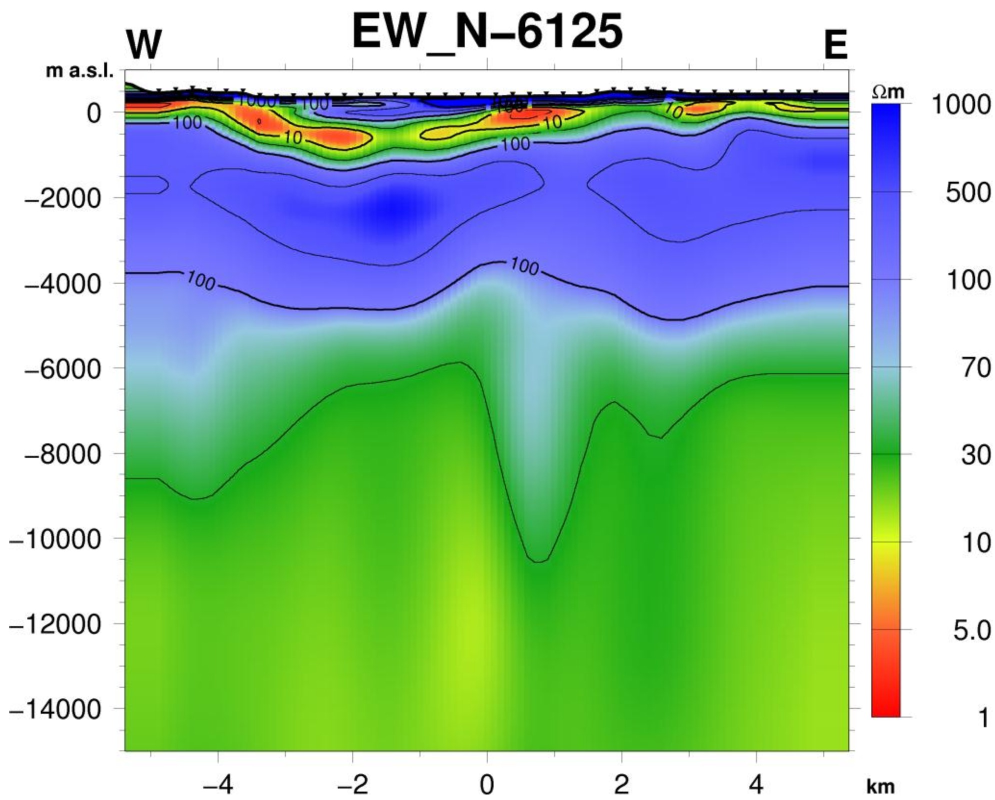

EW_N-6125
W
E
m a.s.l.
Ωm
1000
500
100
70
30
10
5.0
1
0
-2000
-4000
-6000
-8000
-10000
-12000
-14000
-4
-2
0
2
4
km

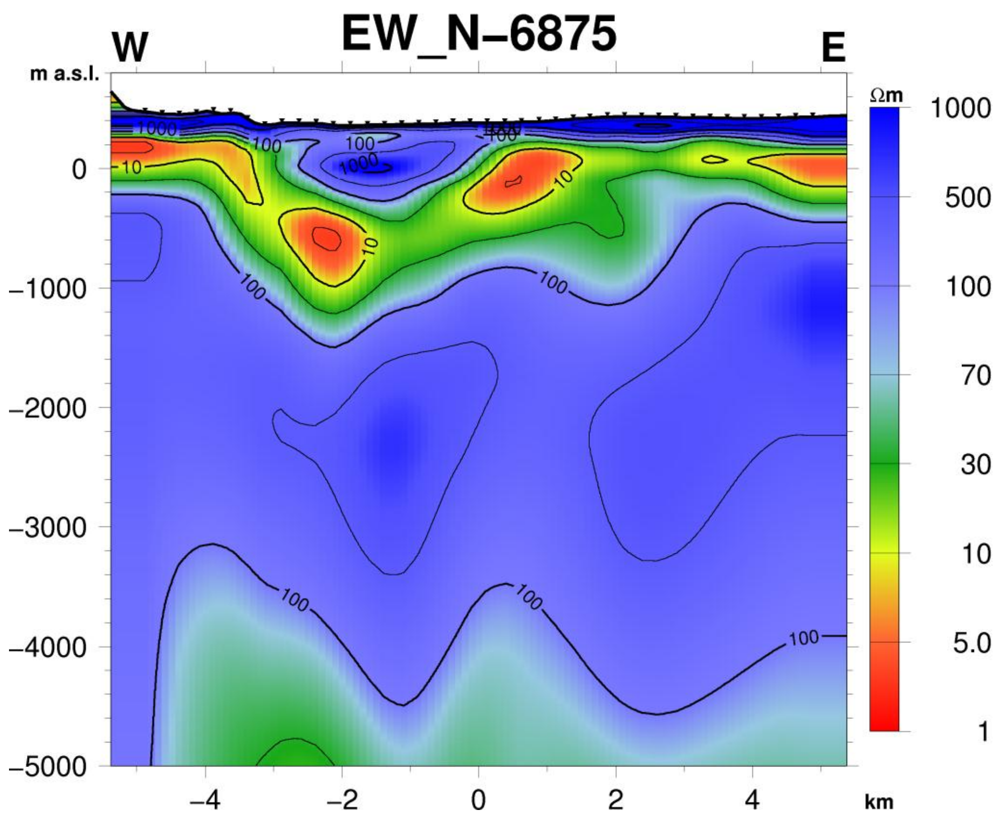
EW_N–6875
W
E
m a.s.l.
Ωm
1000
500
100
70
30
10
5.0
1
km

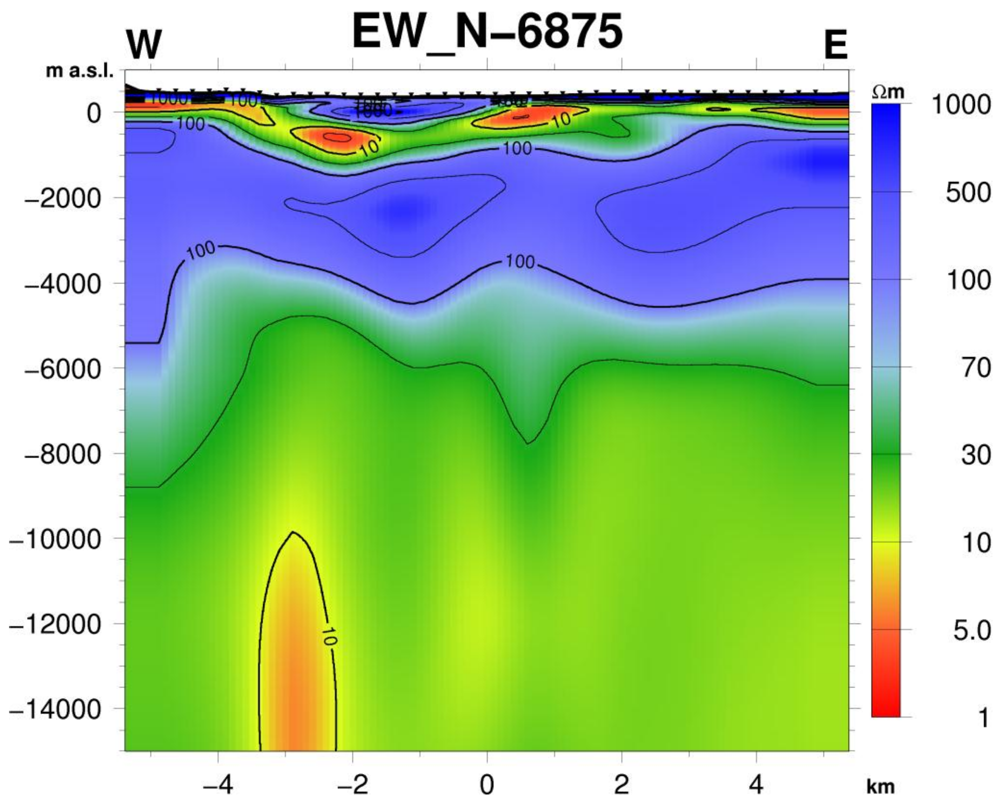
EW_N–6875
W
E
m a.s.l.
Ωm
1000
500
100
70
30
10
5.0
1
km

Appendix 4

Data fit for a 3D model

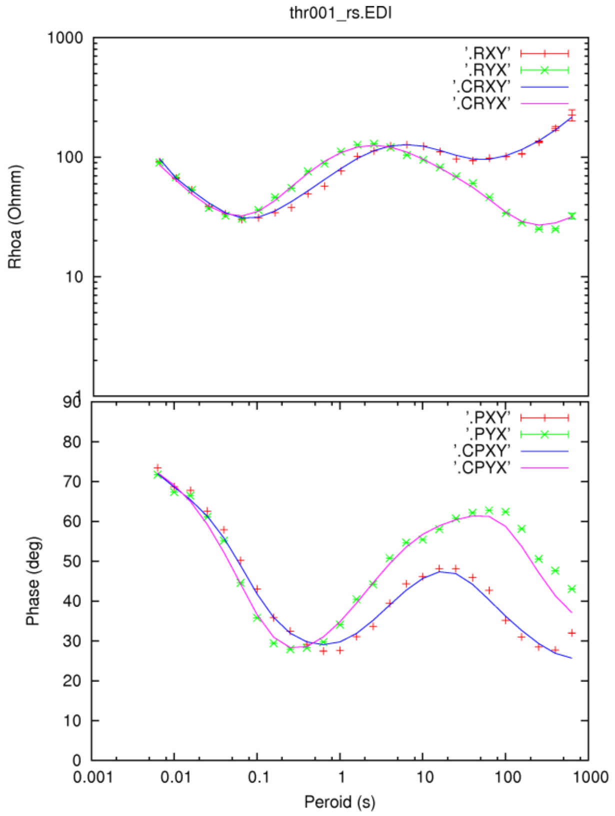
thr001_rs.EDI
'.RXY'
'.RYX'
'.CRXY'
'.CRYX'
Rhoa (Ohmm)
'.PXY'
'.PYX'
'.CPXY'
'.CPYX'
Phase (deg)
Peroid (s)

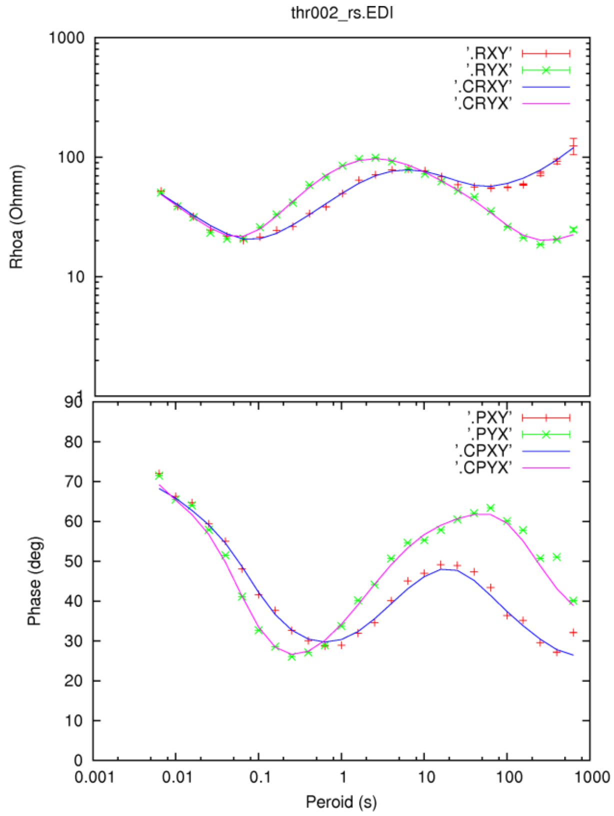
thr002_rs.EDI
'.RXY'
'.RYX'
'.CRXY'
'.CRYX'
Rhoa (Ohmm)
'.PXY'
'.PYX'
'.CPXY'
'.CPYX'
Phase (deg)
Peroid (s)

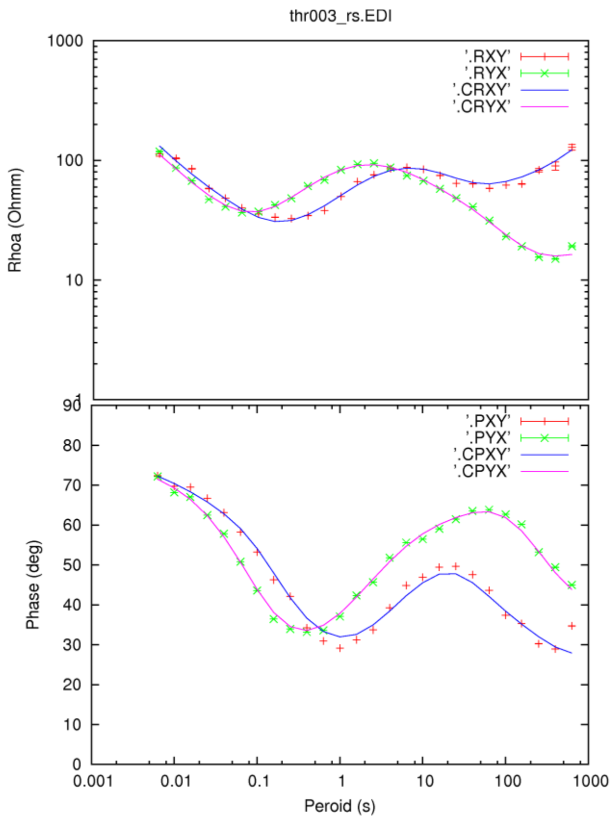
thr003_rs.EDI
'.RXY'
'.RYX'
'.CRXY'
'.CRYX'
Rhoa (Ohmm)
'.PXY'
'.PYX'
'.CPXY'
'.CPYX'
Phase (deg)
Peroid (s)

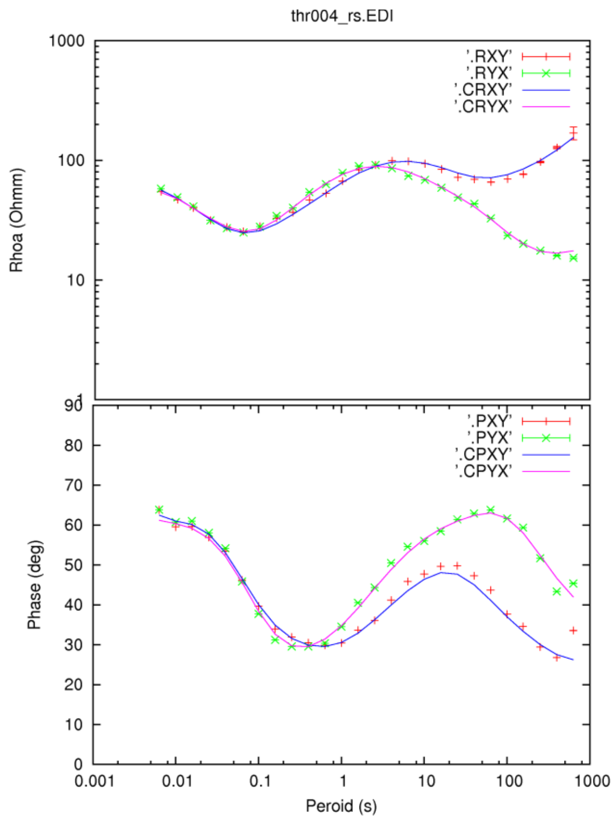
thr004_rs.EDI
'.RXY'
'.RYX'
'.CRXY'
'.CRYX'
Rhoa (Ohmm)
'.PXY'
'.PYX'
'.CPXY'
'.CPYX'
Phase (deg)
Peroid (s)

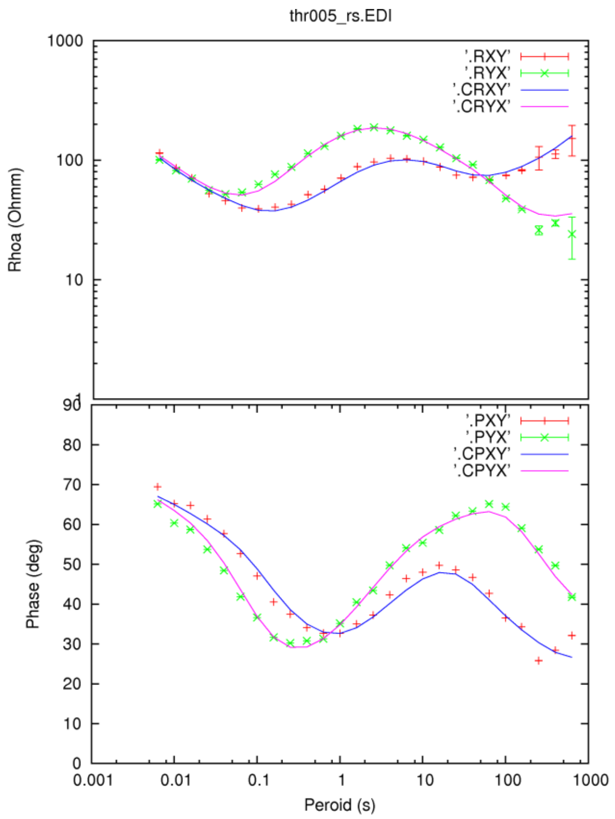
thr005_rs.EDI
Rhoa (Ohmm)
'.RXY'
'.RYX'
'.CRXY'
'.CRYX'
Phase (deg)
'.PXY'
'.PYX'
'.CPXY'
'.CPYX'
Peroid (s)

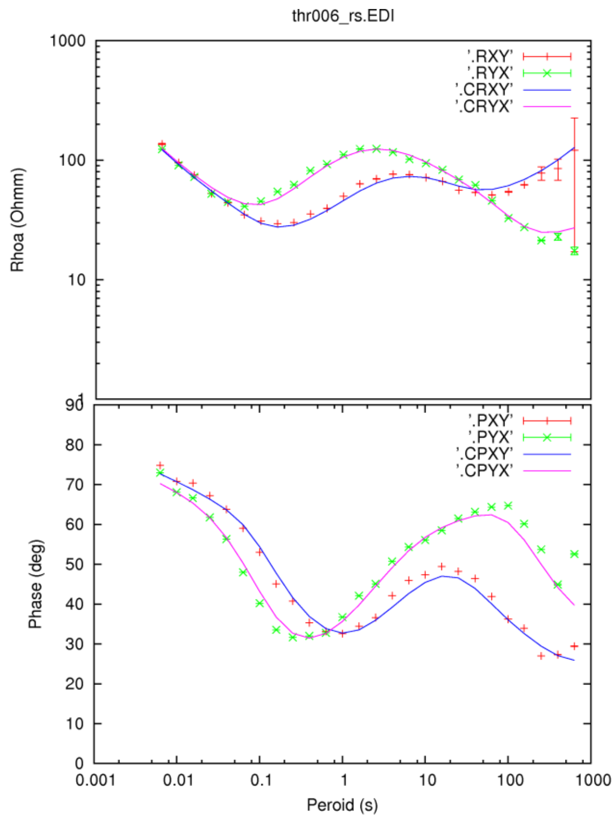
thr006_rs.EDI
Rhoa (Ohmm)
'.RXY'
'.RYX'
'.CRXY'
'.CRYX'
Phase (deg)
'.PXY'
'.PYX'
'.CPXY'
'.CPYX'
Peroid (s)

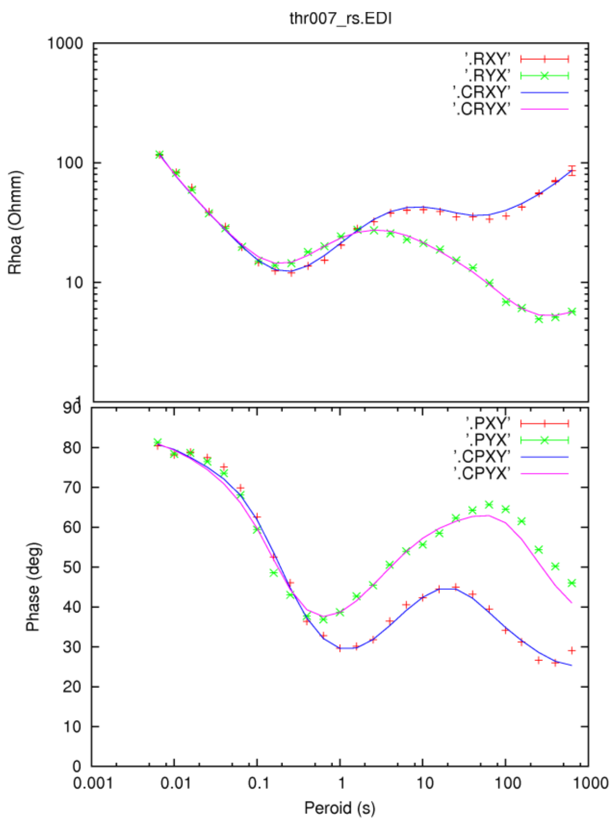
thr007_rs.EDI
Rhoa (Ohmm)
'.RXY'
'.RYX'
'.CRXY'
'.CRYX'
Phase (deg)
'.PXY'
'.PYX'
'.CPXY'
'.CPYX'
Peroid (s)

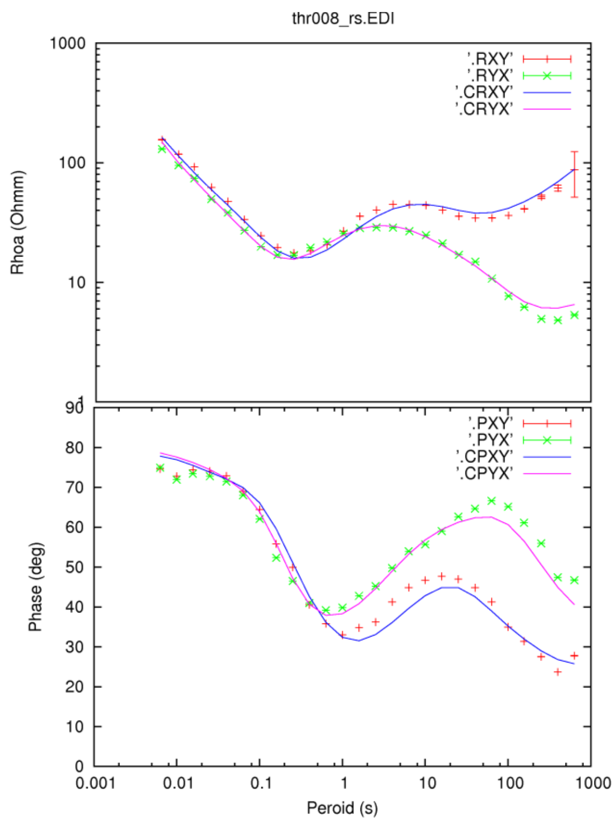
thr008_rs.EDI
Rhoa (Ohmm)
'.RXY'
'.RYX'
'.CRXY'
'.CRYX'
Phase (deg)
'.PXY'
'.PYX'
'.CPXY'
'.CPYX'
Peroid (s)

thr009_rs.EDI

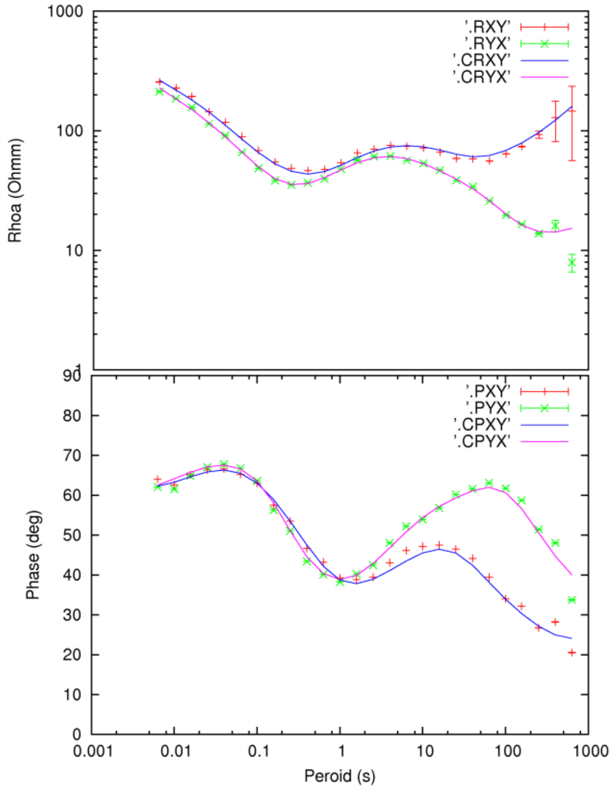

thr010_rs.EDI

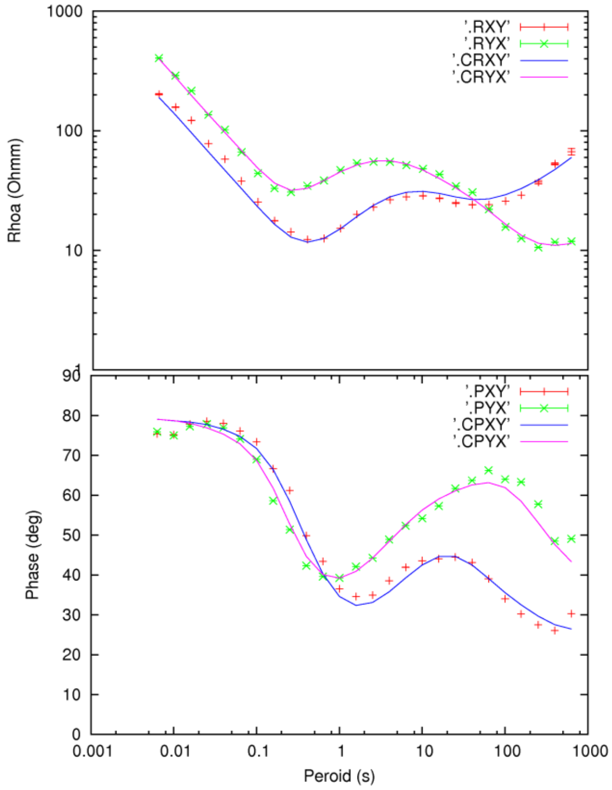

thr011_rs.EDI

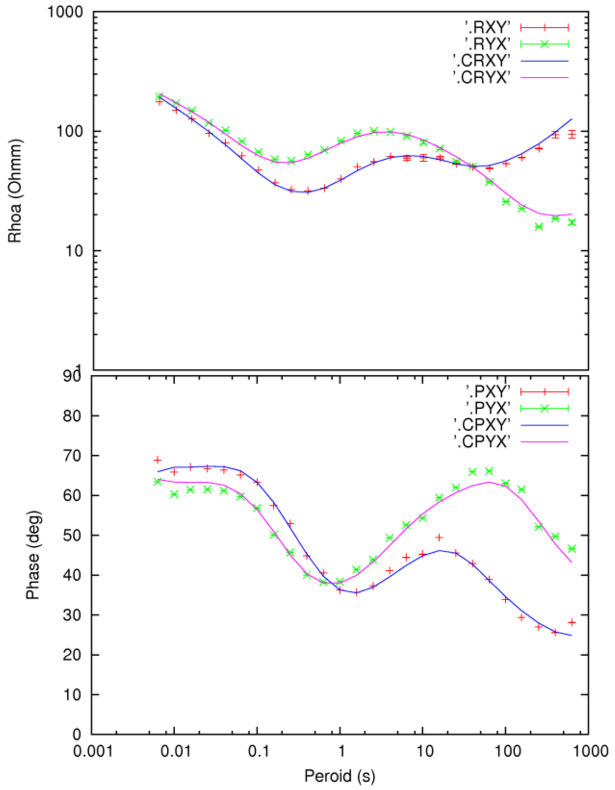

thr012_rs.EDI

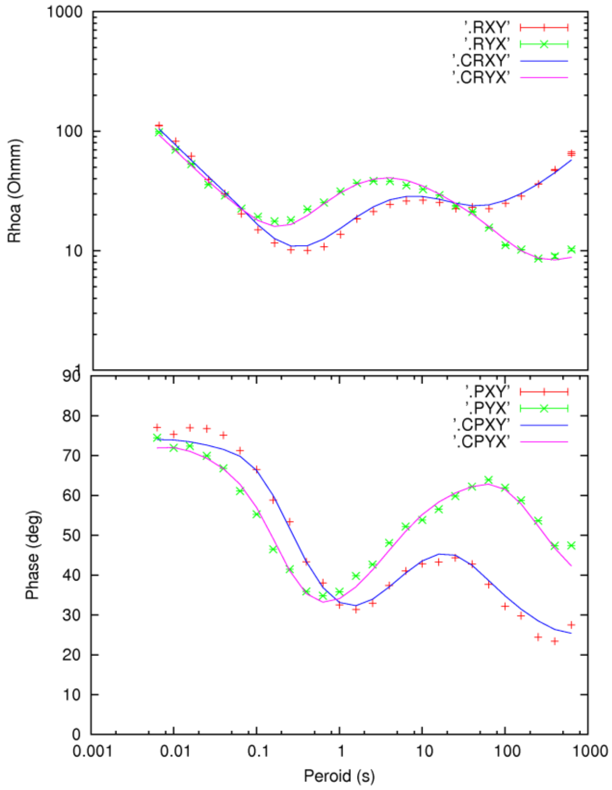

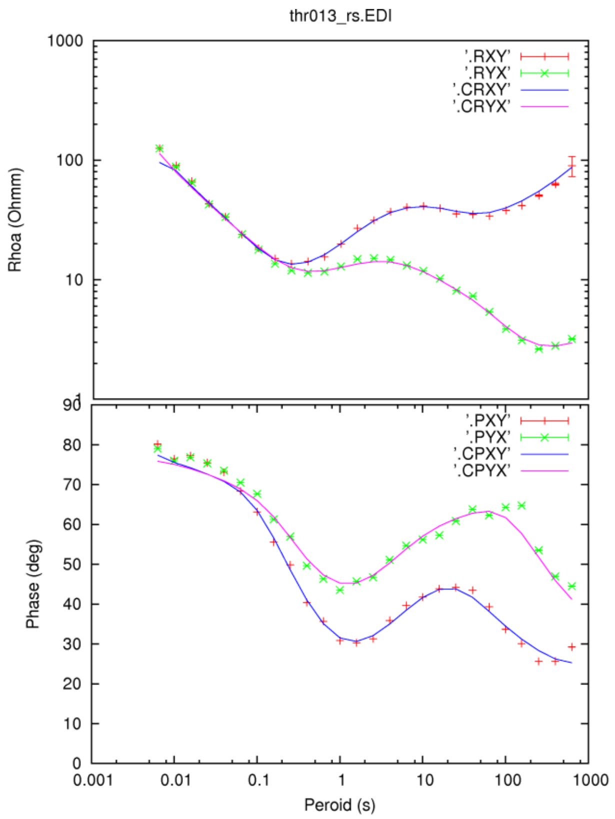
thr013_rs.EDI
'.RXY'
'.RYX'
'.CRXY'
'.CRYX'
Rhoa (Ohmm)
'.PXY'
'.PYX'
'.CPXY'
'.CPYX'
Phase (deg)
Peroid (s)

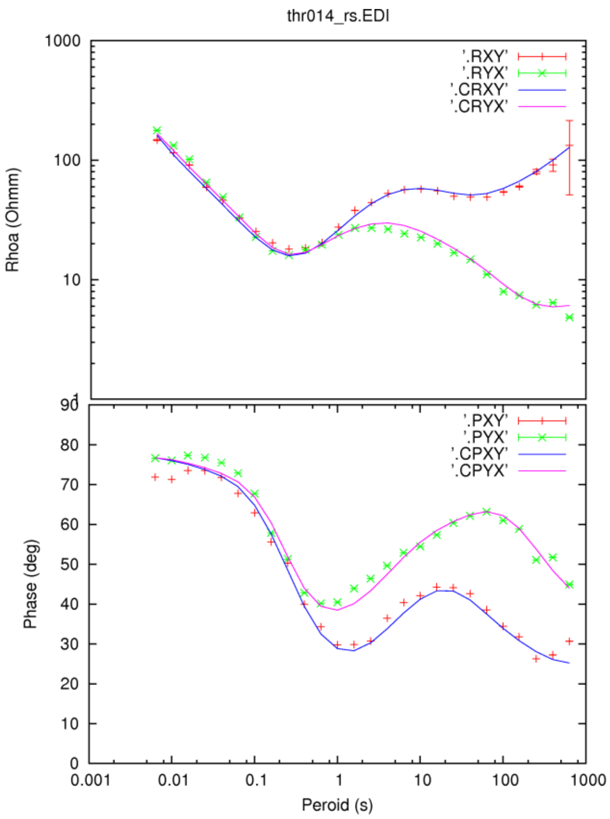
thr014_rs.EDI
'.RXY'
'.RYX'
'.CRXY'
'.CRYX'
Rhoa (Ohmm)
'.PXY'
'.PYX'
'.CPXY'
'.CPYX'
Phase (deg)
Peroid (s)

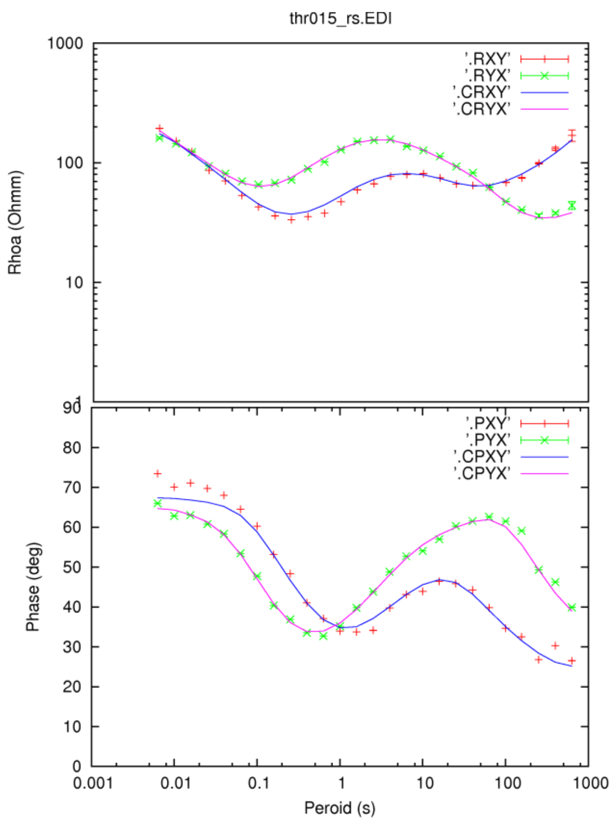
thr015_rs.EDI
'.RXY'
'.RYX'
'.CRXY'
'.CRYX'
Rhoa (Ohmm)
'.PXY'
'.PYX'
'.CPXY'
'.CPYX'
Phase (deg)
Peroid (s)

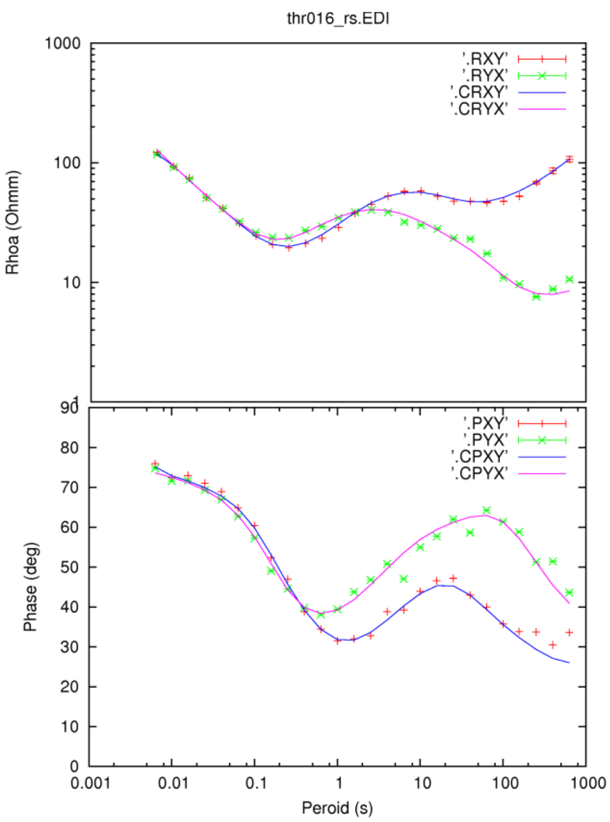
thr016_rs.EDI
'.RXY'
'.RYX'
'.CRXY'
'.CRYX'
Rhoa (Ohmm)
'.PXY'
'.PYX'
'.CPXY'
'.CPYX'
Phase (deg)
Peroid (s)

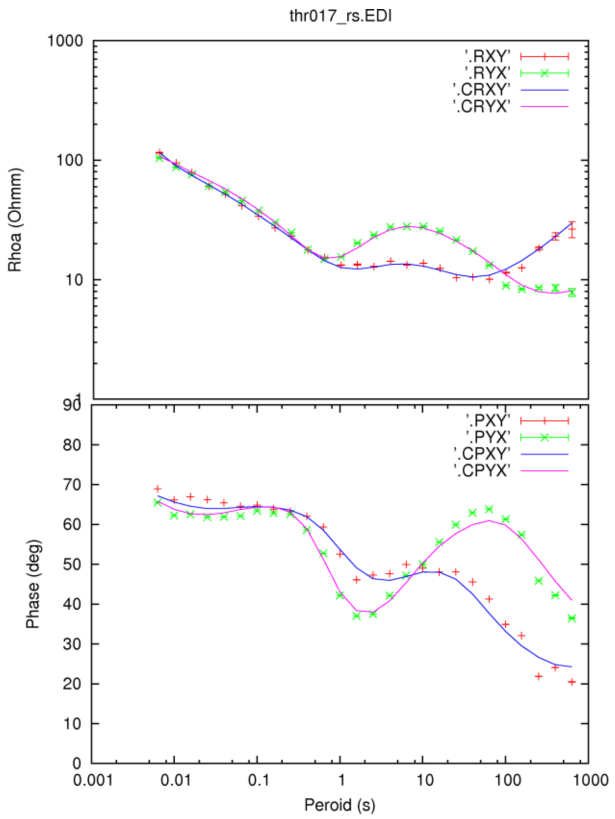
thr017_rs.EDI
'.RXY'
'.RYX'
'.CRXY'
'.CRYX'
Rhoa (Ohmm)
'.PXY'
'.PYX'
'.CPXY'
'.CPYX'
Phase (deg)
Peroid (s)

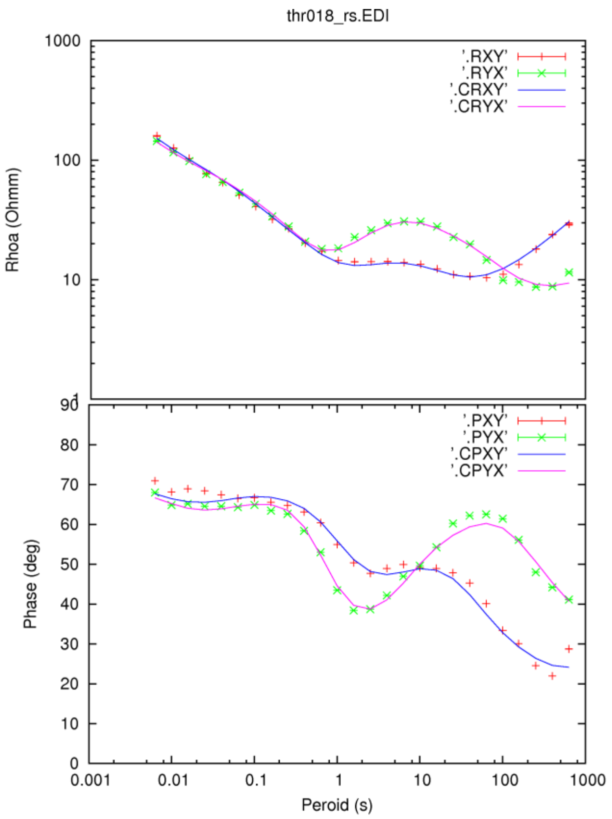
thr018_rs.EDI
'.RXY'
'.RYX'
'.CRXY'
'.CRYX'
Rhoa (Ohmm)
'.PXY'
'.PYX'
'.CPXY'
'.CPYX'
Phase (deg)
Peroid (s)

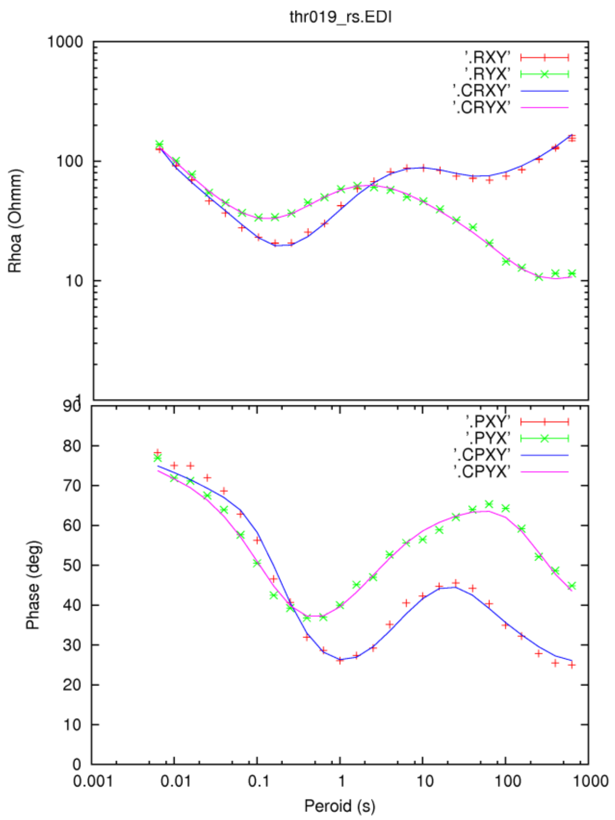
thr019_rs.EDI
'.RXY'
'.RYX'
'.CRXY'
'.CRYX'
Rhoa (Ohmm)
'.PXY'
'.PYX'
'.CPXY'
'.CPYX'
Phase (deg)
Peroid (s)

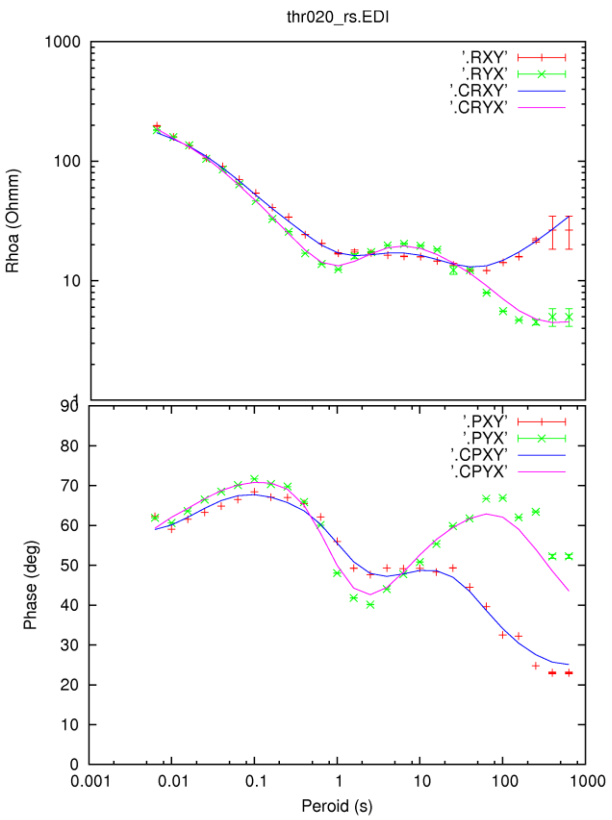
thr020_rs.EDI
'.RXY'
'.RYX'
'.CRXY'
'.CRYX'
Rhoa (Ohmm)
'.PXY'
'.PYX'
'.CPXY'
'.CPYX'
Phase (deg)
Peroid (s)

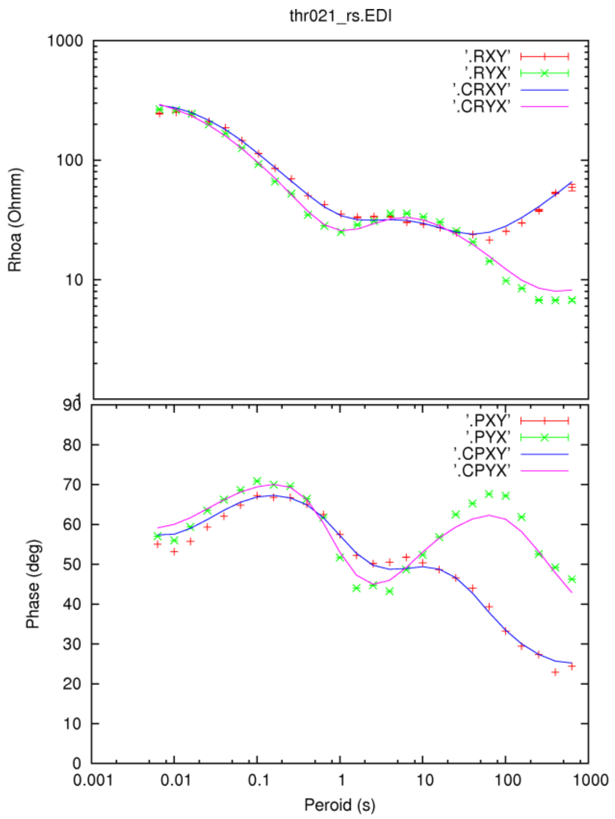
thr021_rs.EDI
1000
100
10
1
Rhoa (Ohmm)
'.RXY'
'.RYX'
'.CRXY'
'.CRYX'
90
80
70
60
50
40
30
20
10
0
Phase (deg)
'.PXY'
'.PYX'
'.CPXY'
'.CPYX'
0.001
0.01
0.1
1
10
100
1000
Peroid (s)

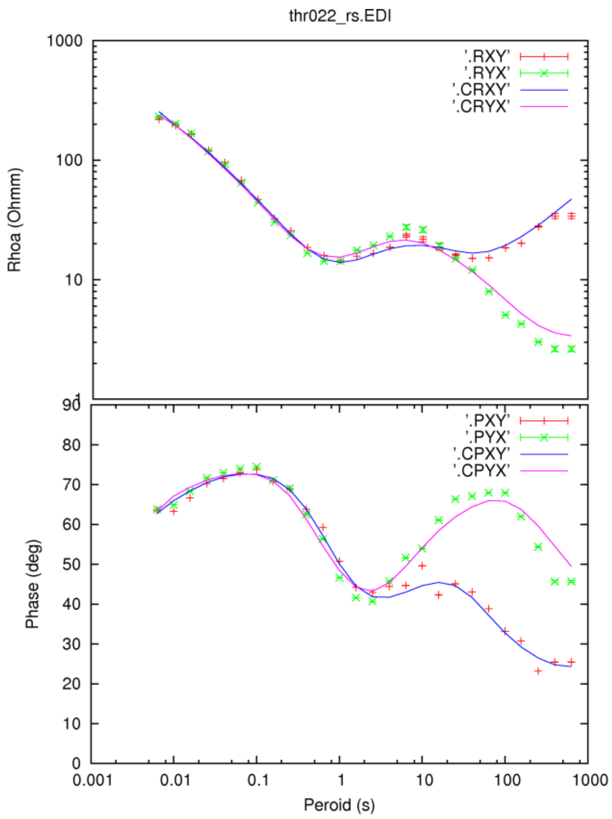
thr022_rs.EDI
1000
100
10
1
Rhoa (Ohmm)
'.RXY'
'.RYX'
'.CRXY'
'.CRYX'
90
80
70
60
50
40
30
20
10
0
Phase (deg)
'.PXY'
'.PYX'
'.CPXY'
'.CPYX'
0.001
0.01
0.1
1
10
100
1000
Peroid (s)

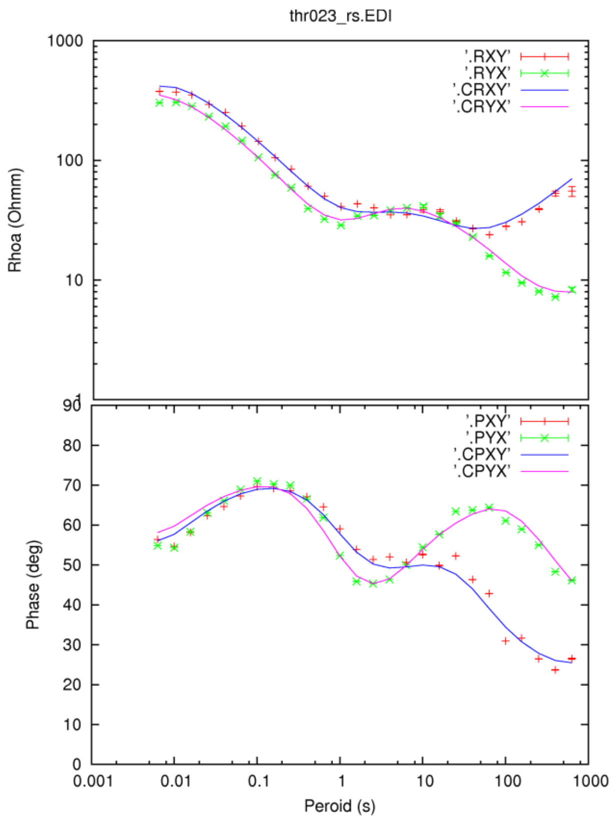
thr023_rs.EDI
1000
100
10
1
Rhoa (Ohmm)
'.RXY'
'.RYX'
'.CRXY'
'.CRYX'
90
80
70
60
50
40
30
20
10
0
Phase (deg)
'.PXY'
'.PYX'
'.CPXY'
'.CPYX'
0.001
0.01
0.1
1
10
100
1000
Peroid (s)

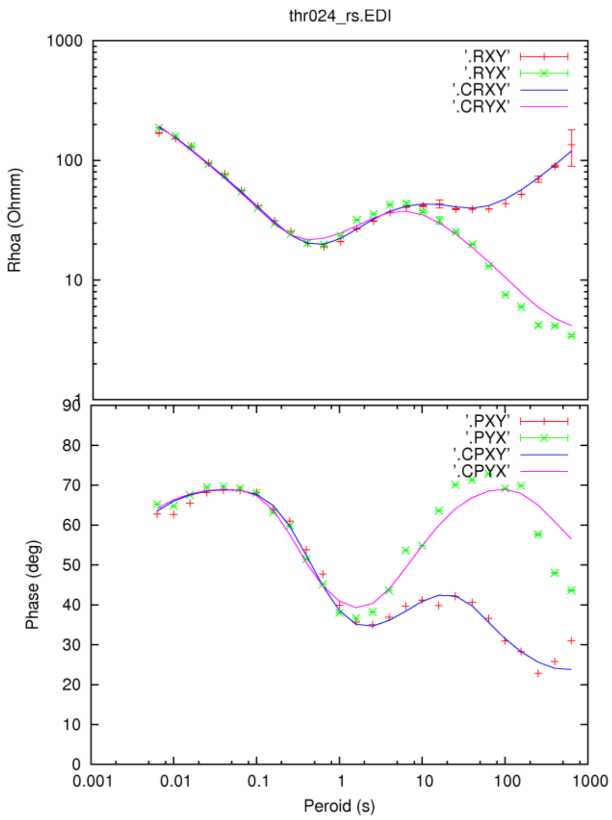
thr024_rs.EDI
1000
100
10
1
Rhoa (Ohmm)
'.RXY'
'.RYX'
'.CRXY'
'.CRYX'
90
80
70
60
50
40
30
20
10
0
Phase (deg)
'.PXY'
'.PYX'
'.CPXY'
'.CPYX'
0.001
0.01
0.1
1
10
100
1000
Peroid (s)

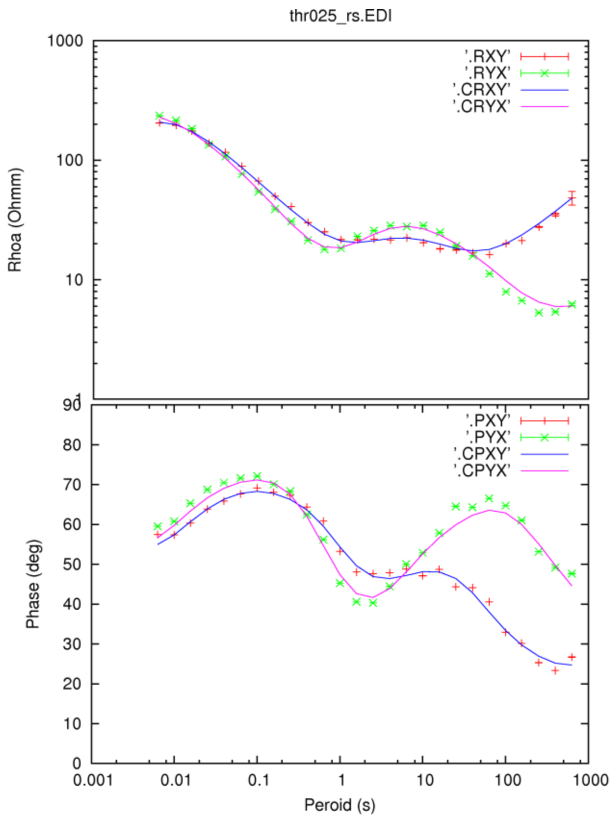
thr025_rs.EDI
'.RXY'
'.RYX'
'.CRXY'
'.CRYX'
Rhoa (Ohmm)
'.PXY'
'.PYX'
'.CPXY'
'.CPYX'
Phase (deg)
Peroid (s)

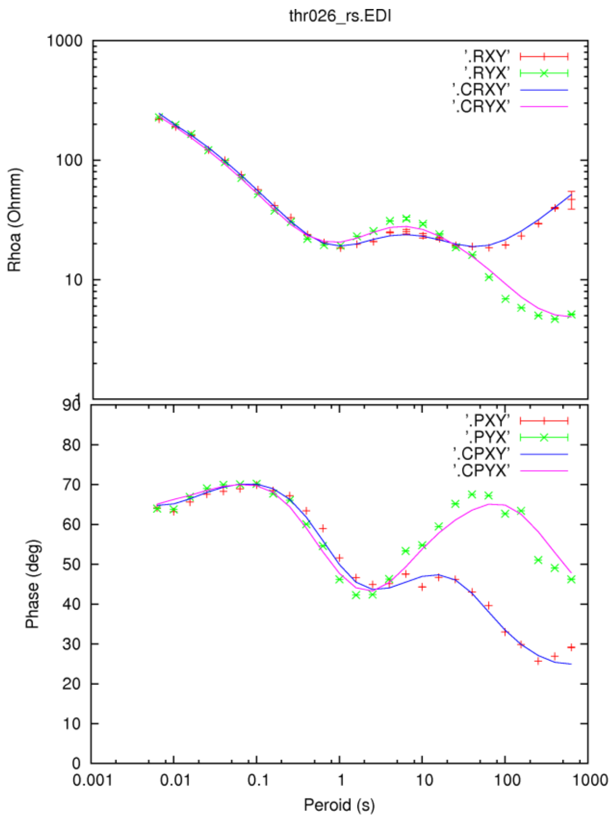
thr026_rs.EDI
'.RXY'
'.RYX'
'.CRXY'
'.CRYX'
Rhoa (Ohmm)
'.PXY'
'.PYX'
'.CPXY'
'.CPYX'
Phase (deg)
Peroid (s)

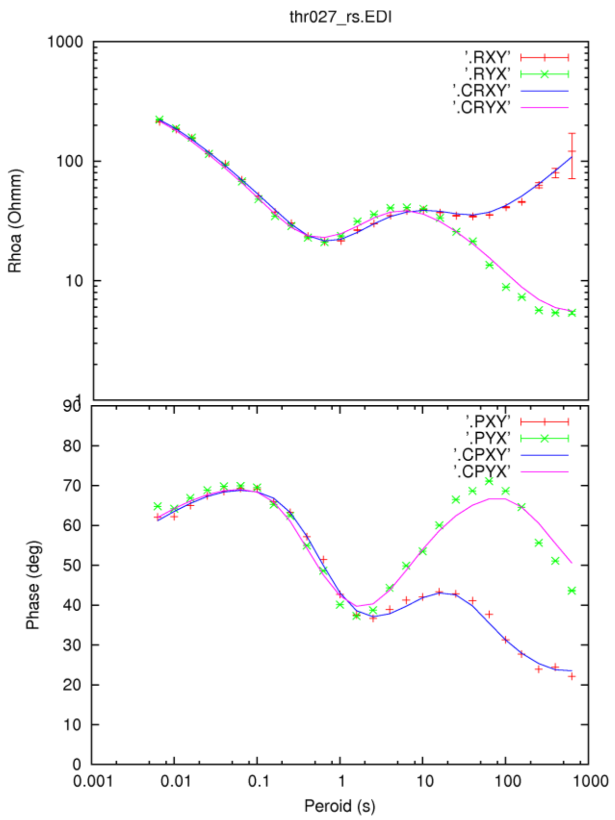
thr027_rs.EDI
'.RXY'
'.RYX'
'.CRXY'
'.CRYX'
Rhoa (Ohmm)
'.PXY'
'.PYX'
'.CPXY'
'.CPYX'
Phase (deg)
Peroid (s)

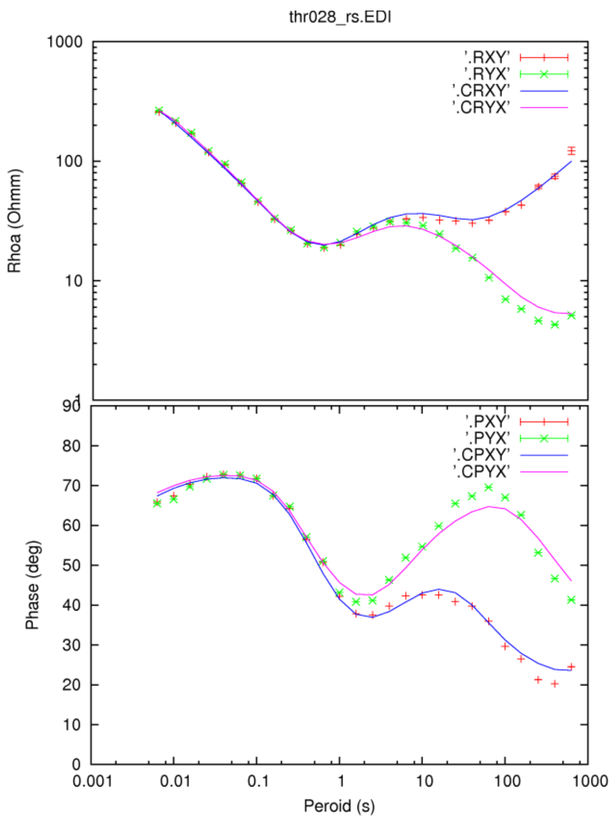
thr028_rs.EDI
'.RXY'
'.RYX'
'.CRXY'
'.CRYX'
Rhoa (Ohmm)
'.PXY'
'.PYX'
'.CPXY'
'.CPYX'
Phase (deg)
Peroid (s)

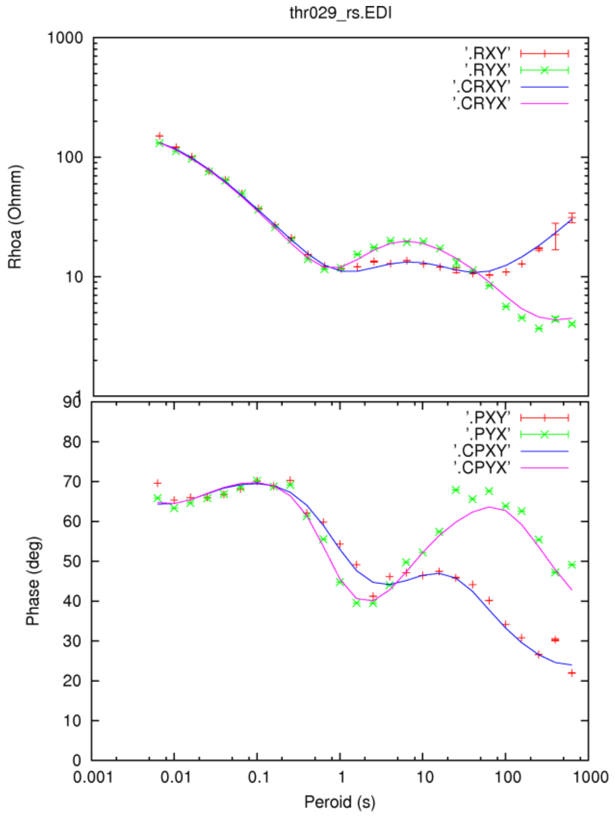
thr029_rs.EDI
'.RXY'
'.RYX'
'.CRXY'
'.CRYX'
Rhoa (Ohmm)
'.PXY'
'.PYX'
'.CPXY'
'.CPYX'
Phase (deg)
Peroid (s)

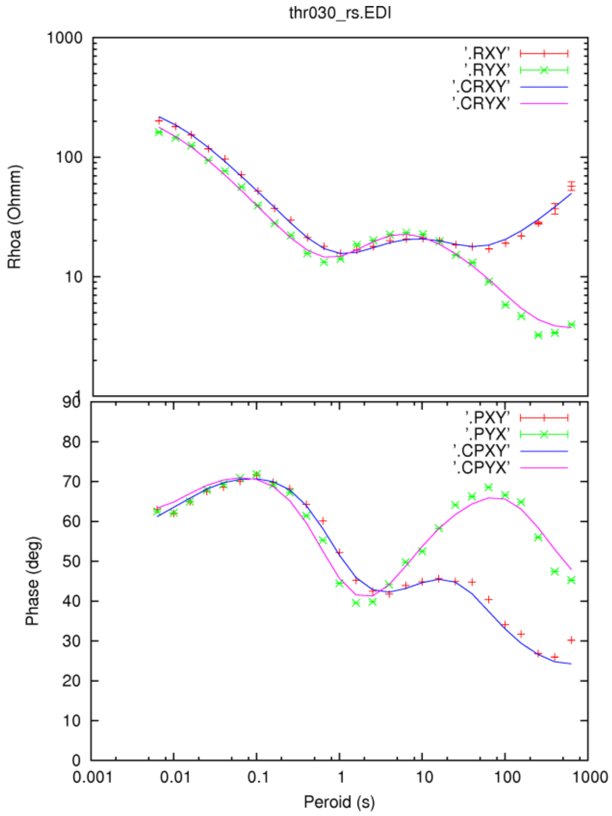
thr030_rs.EDI
'.RXY'
'.RYX'
'.CRXY'
'.CRYX'
Rhoa (Ohmm)
'.PXY'
'.PYX'
'.CPXY'
'.CPYX'
Phase (deg)
Peroid (s)

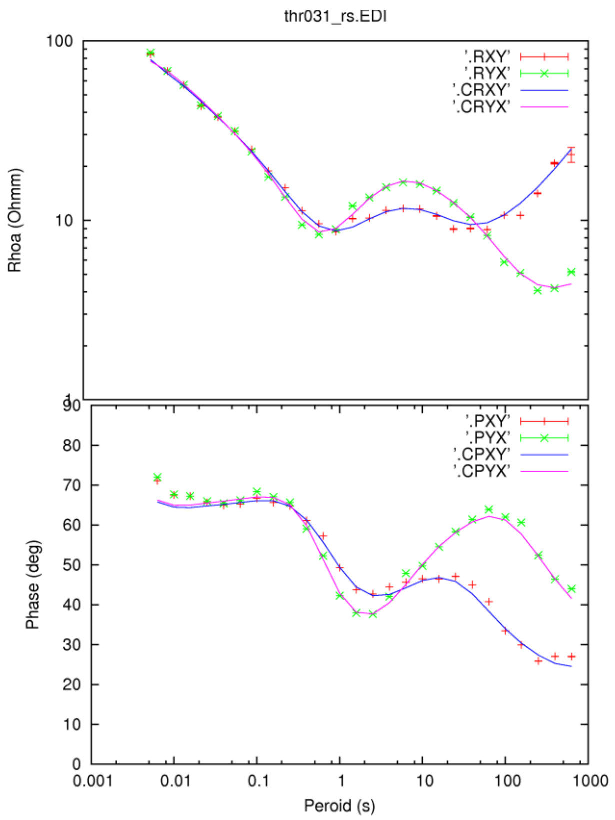
thr031_rs.EDI
'.RXY'
'.RYX'
'.CRXY'
'.CRYX'
Rhoa (Ohmm)
'.PXY'
'.PYX'
'.CPXY'
'.CPYX'
Phase (deg)
Peroid (s)

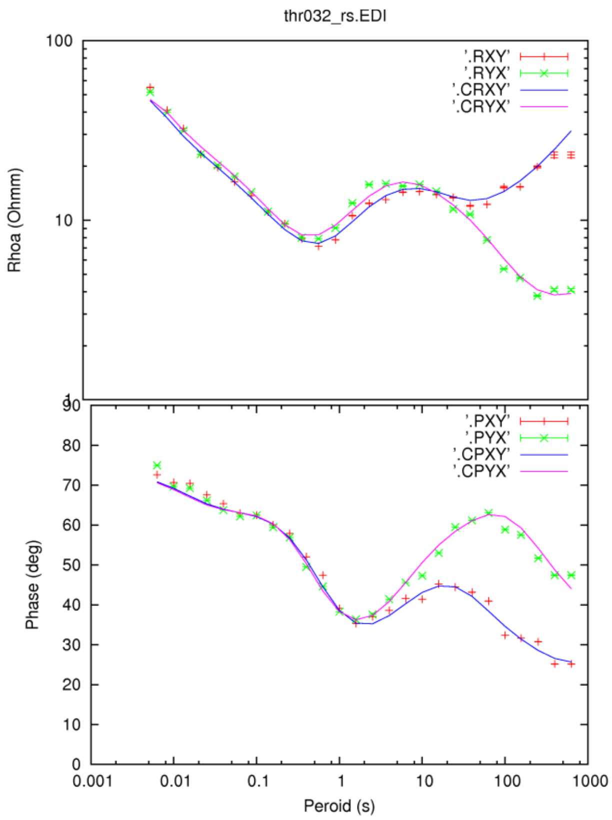
thr032_rs.EDI
'.RXY'
'.RYX'
'.CRXY'
'.CRYX'
Rhoa (Ohmm)
'.PXY'
'.PYX'
'.CPXY'
'.CPYX'
Phase (deg)
Peroid (s)

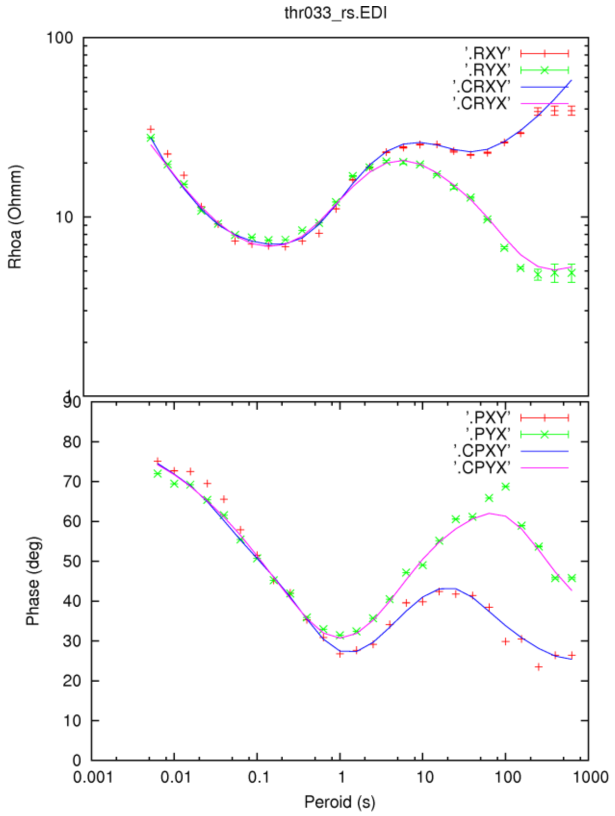
thr033_rs.EDI
Rhoa (Ohmm)
'.RXY'
'.RYX'
'.CRXY'
'.CRYX'
Phase (deg)
'.PXY'
'.PYX'
'.CPXY'
'.CPYX'
Peroid (s)

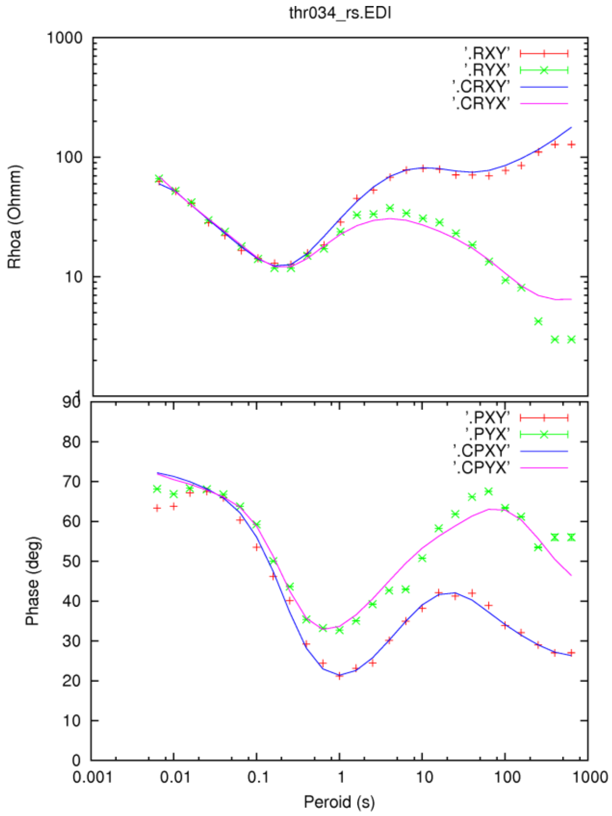
thr034_rs.EDI
Rhoa (Ohmm)
'.RXY'
'.RYX'
'.CRXY'
'.CRYX'
Phase (deg)
'.PXY'
'.PYX'
'.CPXY'
'.CPYX'
Peroid (s)

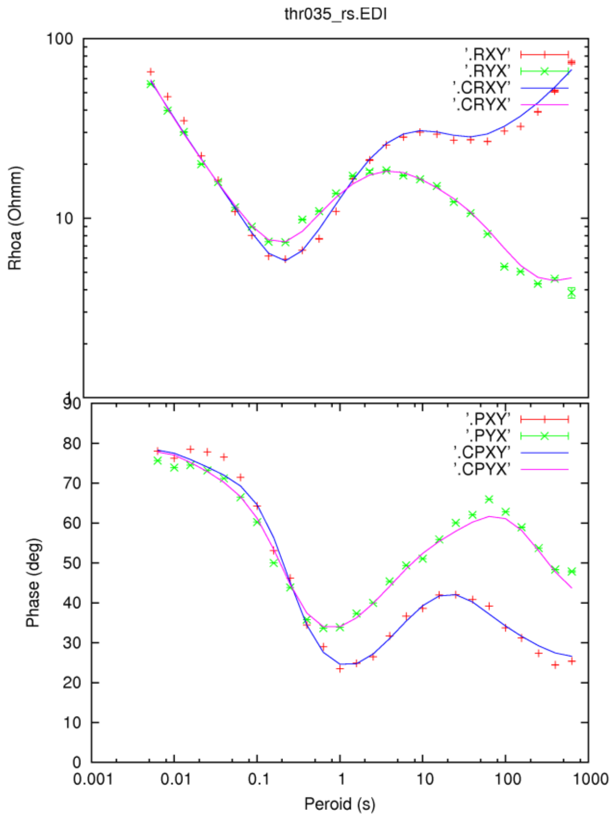
thr035_rs.EDI
Rhoa (Ohmm)
'.RXY'
'.RYX'
'.CRXY'
'.CRYX'
Phase (deg)
'.PXY'
'.PYX'
'.CPXY'
'.CPYX'
Peroid (s)

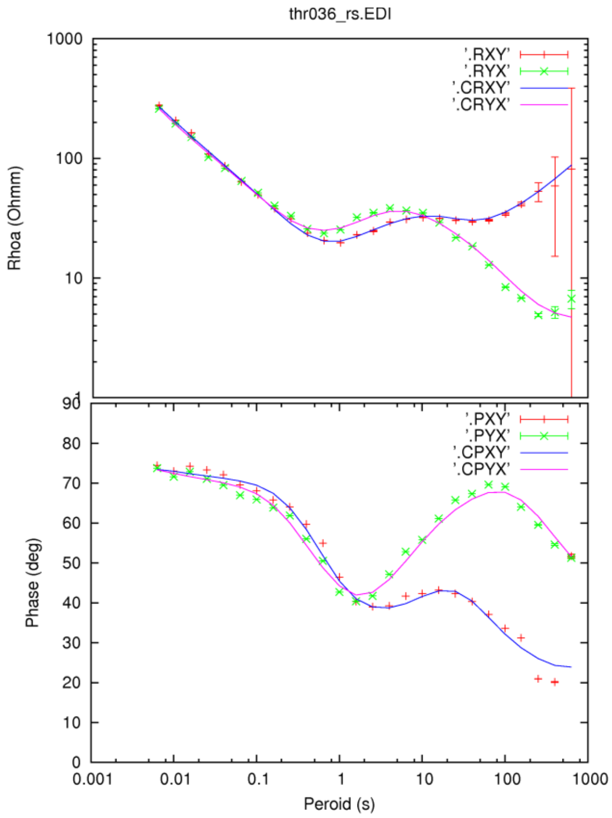
thr036_rs.EDI
Rhoa (Ohmm)
'.RXY'
'.RYX'
'.CRXY'
'.CRYX'
Phase (deg)
'.PXY'
'.PYX'
'.CPXY'
'.CPYX'
Peroid (s)

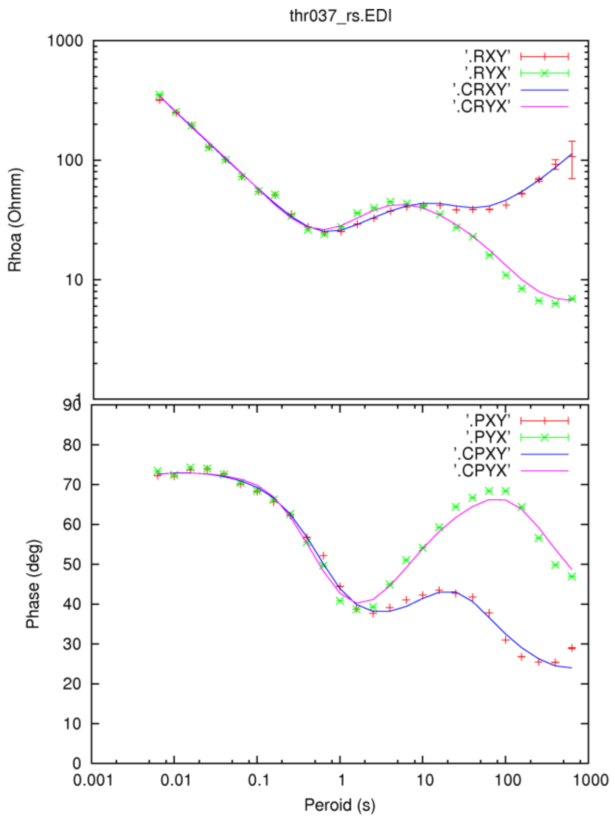
thr037_rs.EDI
'.RXY'
'.RYX'
'.CRXY'
'.CRYX'
Rhoa (Ohmm)
'.PXY'
'.PYX'
'.CPXY'
'.CPYX'
Phase (deg)
Peroid (s)

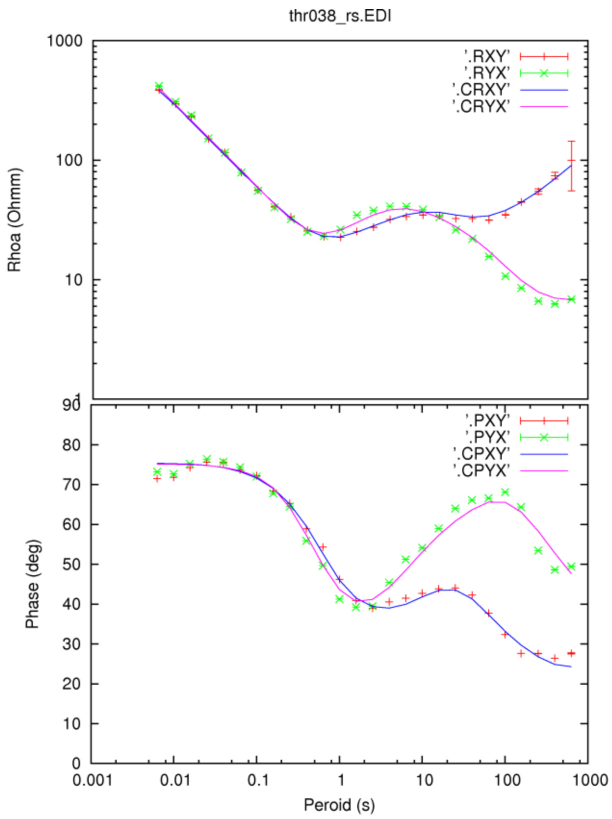
thr038_rs.EDI
'.RXY'
'.RYX'
'.CRXY'
'.CRYX'
Rhoa (Ohmm)
'.PXY'
'.PYX'
'.CPXY'
'.CPYX'
Phase (deg)
Peroid (s)

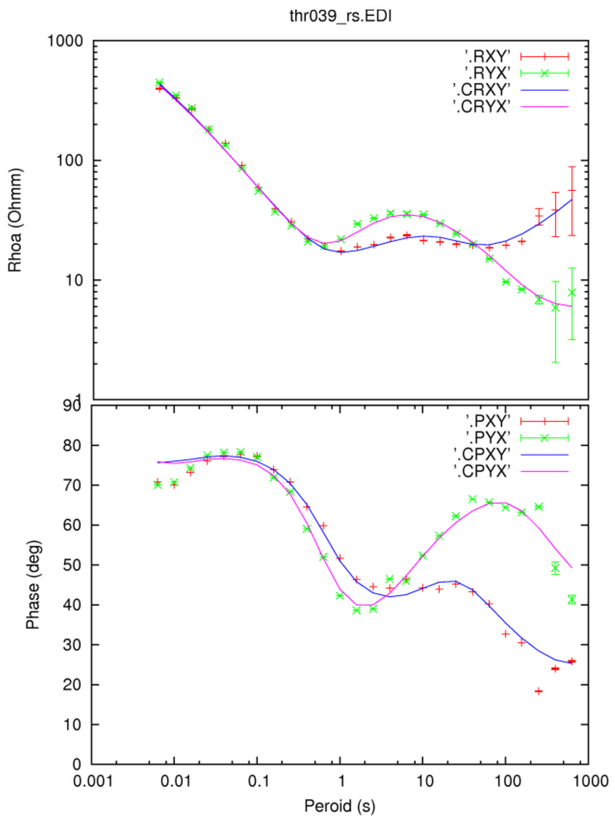
thr039_rs.EDI
'.RXY'
'.RYX'
'.CRXY'
'.CRYX'
Rhoa (Ohmm)
'.PXY'
'.PYX'
'.CPXY'
'.CPYX'
Phase (deg)
Peroid (s)

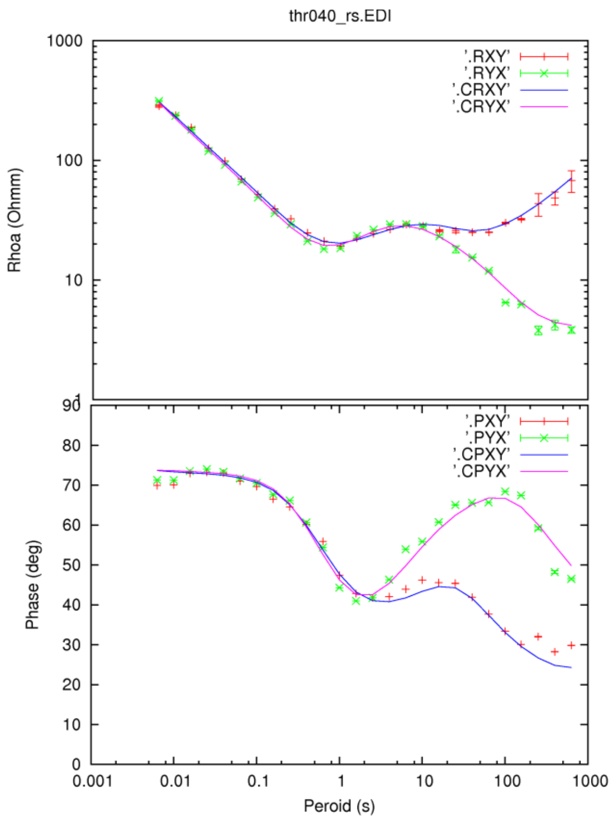
thr040_rs.EDI
'.RXY'
'.RYX'
'.CRXY'
'.CRYX'
Rhoa (Ohmm)
'.PXY'
'.PYX'
'.CPXY'
'.CPYX'
Phase (deg)
Peroid (s)

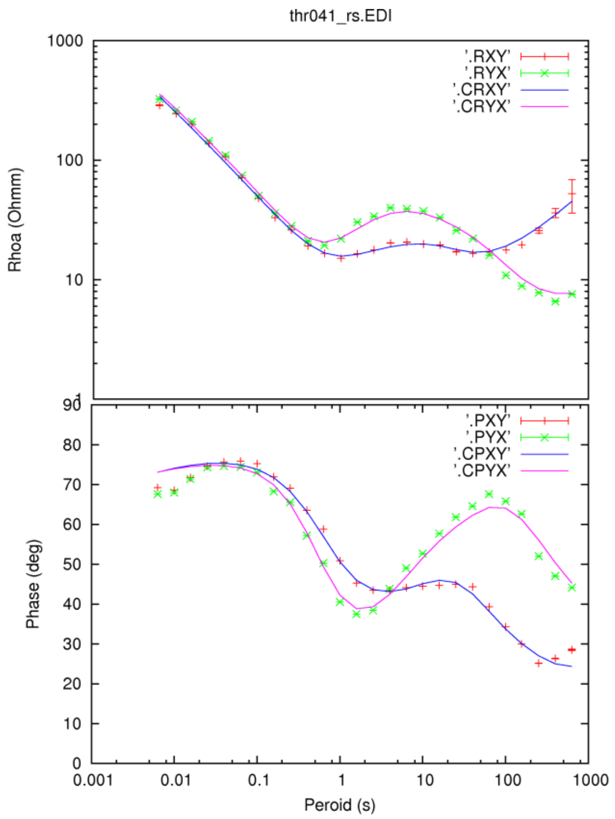
thr041_rs.EDI
'.RXY'
'.RYX'
'.CRXY'
'.CRYX'
'.PXY'
'.PYX'
'.CPXY'
'.CPYX'
Rhoa (Ohmm)
Phase (deg)
Peroid (s)

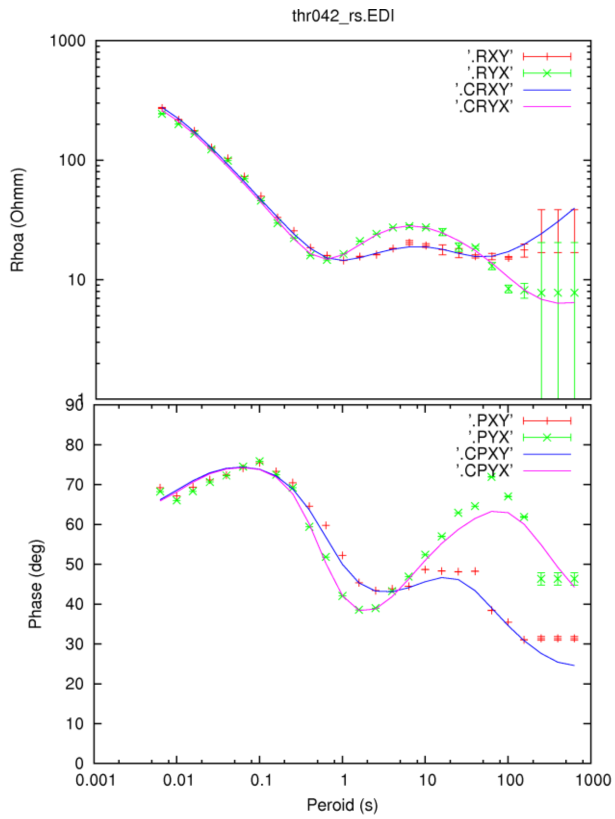
thr042_rs.EDI
'.RXY'
'.RYX'
'.CRXY'
'.CRYX'
'.PXY'
'.PYX'
'.CPXY'
'.CPYX'
Rhoa (Ohmm)
Phase (deg)
Peroid (s)

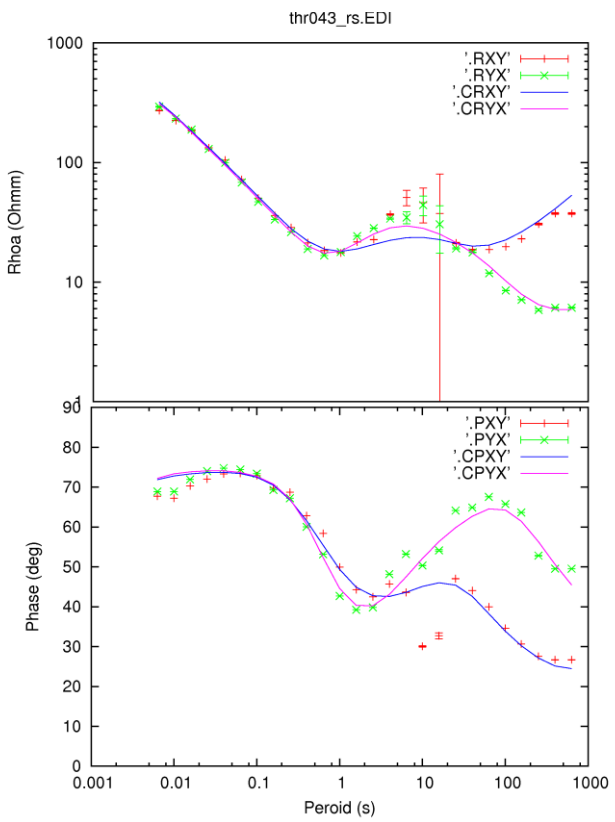
thr043_rs.EDI
'.RXY'
'.RYX'
'.CRXY'
'.CRYX'
'.PXY'
'.PYX'
'.CPXY'
'.CPYX'
Rhoa (Ohmm)
Phase (deg)
Peroid (s)

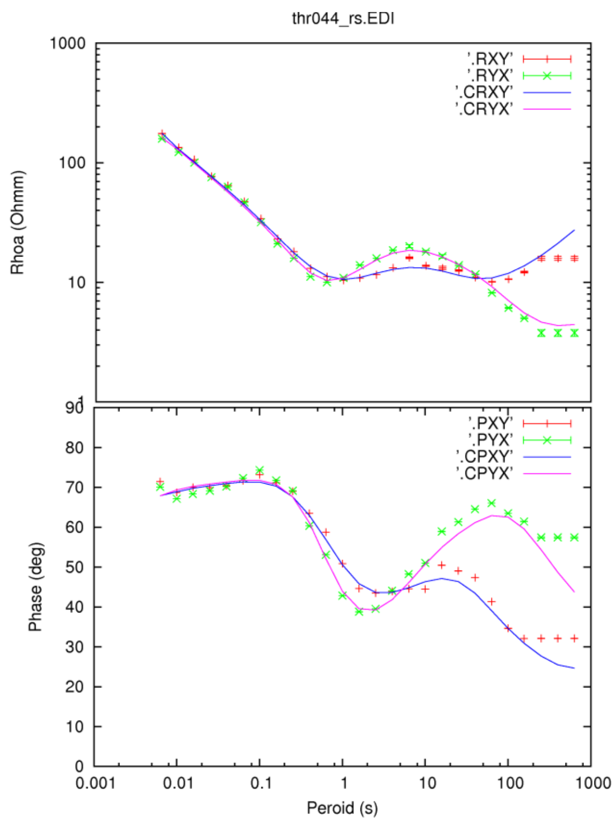
thr044_rs.EDI
'.RXY'
'.RYX'
'.CRXY'
'.CRYX'
'.PXY'
'.PYX'
'.CPXY'
'.CPYX'
Rhoa (Ohmm)
Phase (deg)
Peroid (s)

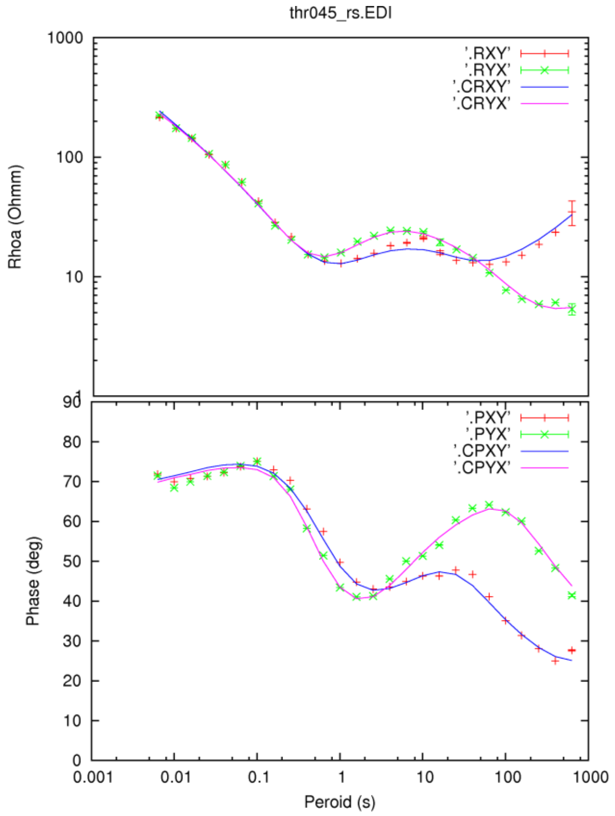
thr045_rs.EDI
Rhoa (Ohmm)
Phase (deg)
Peroid (s)
'.RXY'
'.RYX'
'.CRXY'
'.CRYX'
'.PXY'
'.PYX'
'.CPXY'
'.CPYX'

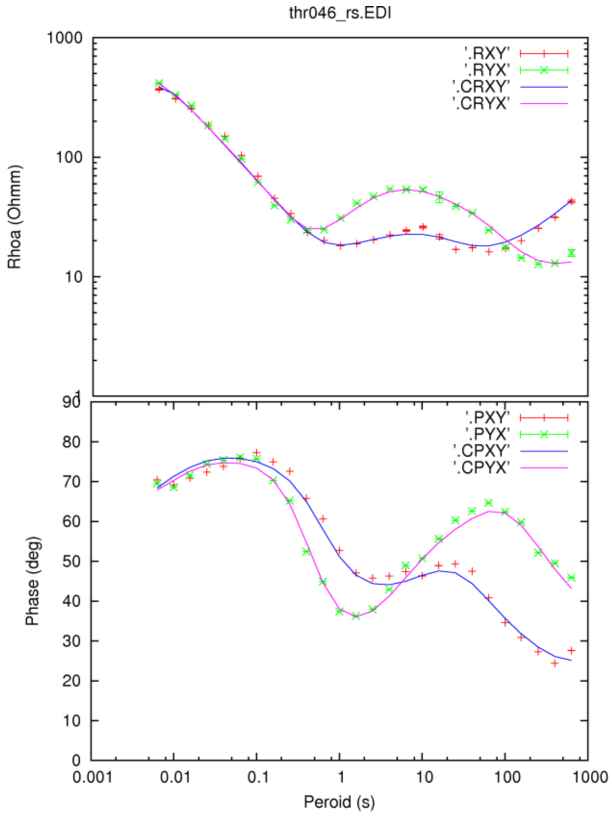
thr046_rs.EDI
Rhoa (Ohmm)
Phase (deg)
Peroid (s)
'.RXY'
'.RYX'
'.CRXY'
'.CRYX'
'.PXY'
'.PYX'
'.CPXY'
'.CPYX'

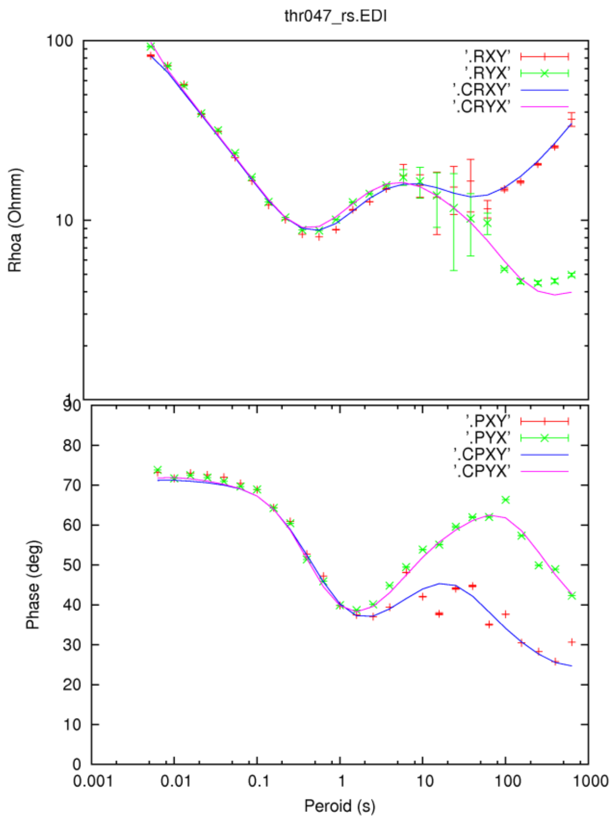
thr047_rs.EDI
Rhoa (Ohmm)
Phase (deg)
Peroid (s)
'.RXY'
'.RYX'
'.CRXY'
'.CRYX'
'.PXY'
'.PYX'
'.CPXY'
'.CPYX'

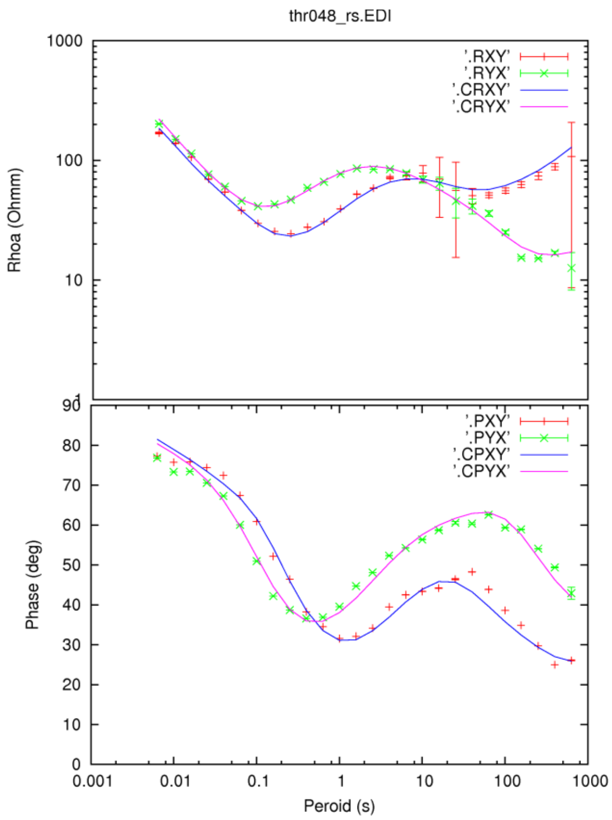
thr048_rs.EDI
Rhoa (Ohmm)
Phase (deg)
Peroid (s)
'.RXY'
'.RYX'
'.CRXY'
'.CRYX'
'.PXY'
'.PYX'
'.CPXY'
'.CPYX'

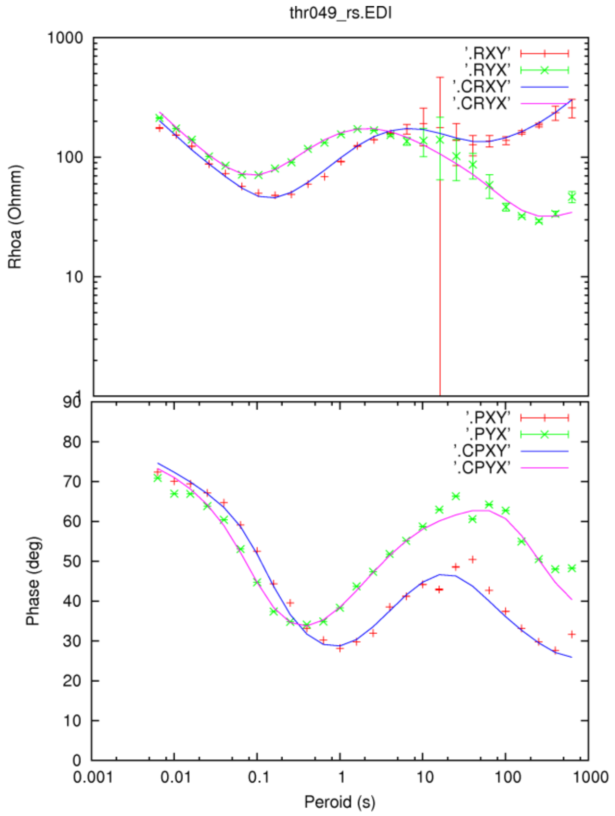
thr049_rs.EDI
Rhoa (Ohmm)
'.RXY'
'.RYX'
'.CRXY'
'.CRYX'
Phase (deg)
'.PXY'
'.PYX'
'.CPXY'
'.CPYX'
Peroid (s)

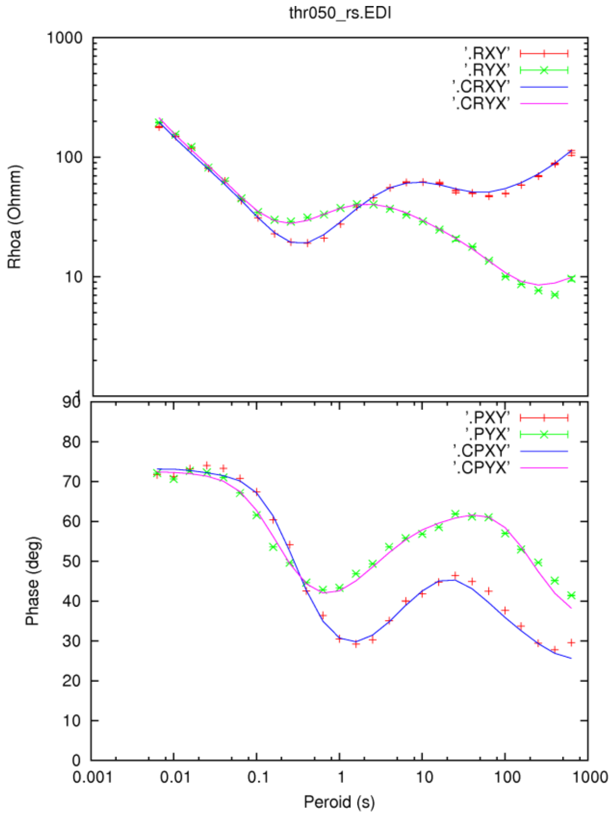
thr050_rs.EDI
Rhoa (Ohmm)
'.RXY'
'.RYX'
'.CRXY'
'.CRYX'
Phase (deg)
'.PXY'
'.PYX'
'.CPXY'
'.CPYX'
Peroid (s)

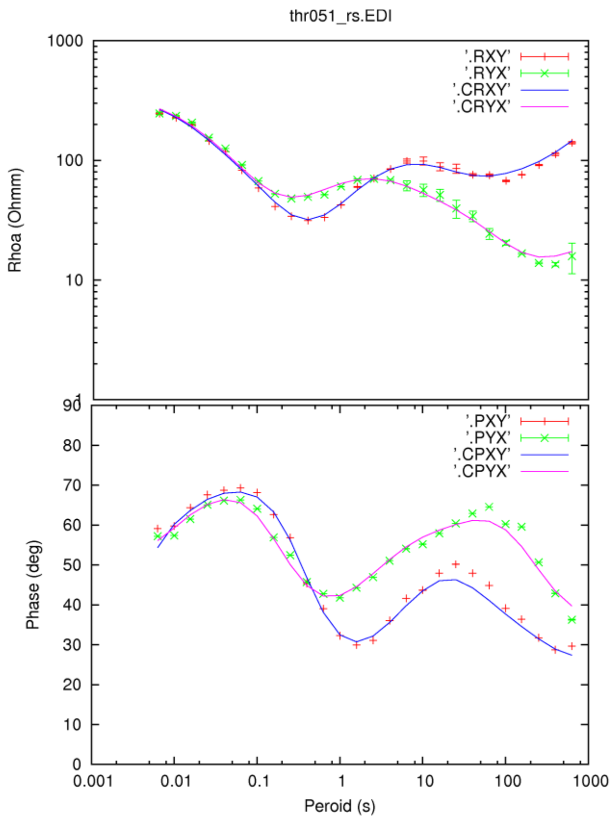
thr051_rs.EDI
Rhoa (Ohmm)
'.RXY'
'.RYX'
'.CRXY'
'.CRYX'
Phase (deg)
'.PXY'
'.PYX'
'.CPXY'
'.CPYX'
Peroid (s)

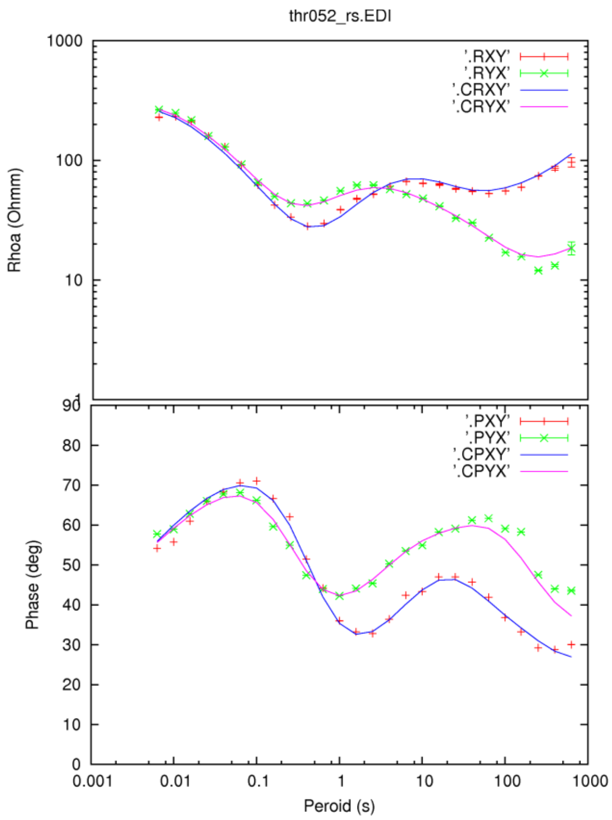
thr052_rs.EDI
Rhoa (Ohmm)
'.RXY'
'.RYX'
'.CRXY'
'.CRYX'
Phase (deg)
'.PXY'
'.PYX'
'.CPXY'
'.CPYX'
Peroid (s)

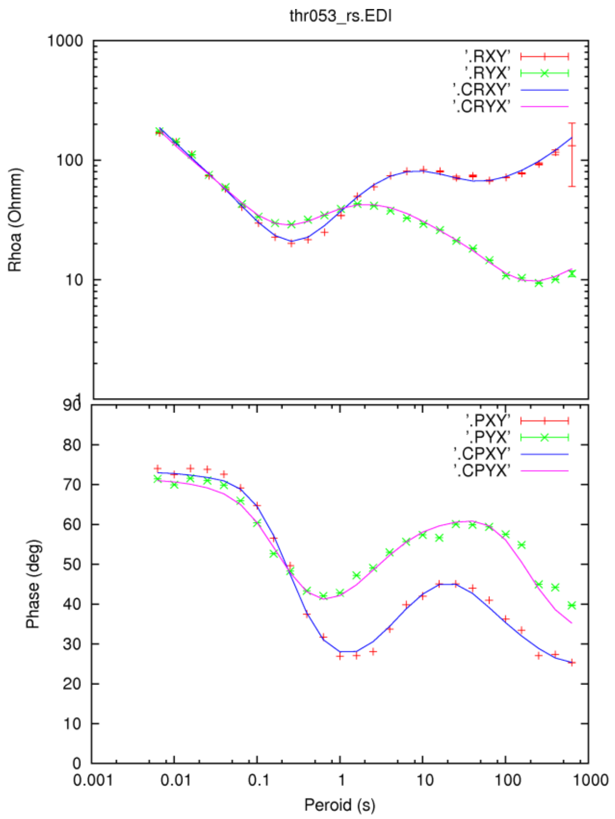
thr053_rs.EDI
Rhoa (Ohmm)
'.RXY'
'.RYX'
'.CRXY'
'.CRYX'
Phase (deg)
'.PXY'
'.PYX'
'.CPXY'
'.CPYX'
Peroid (s)

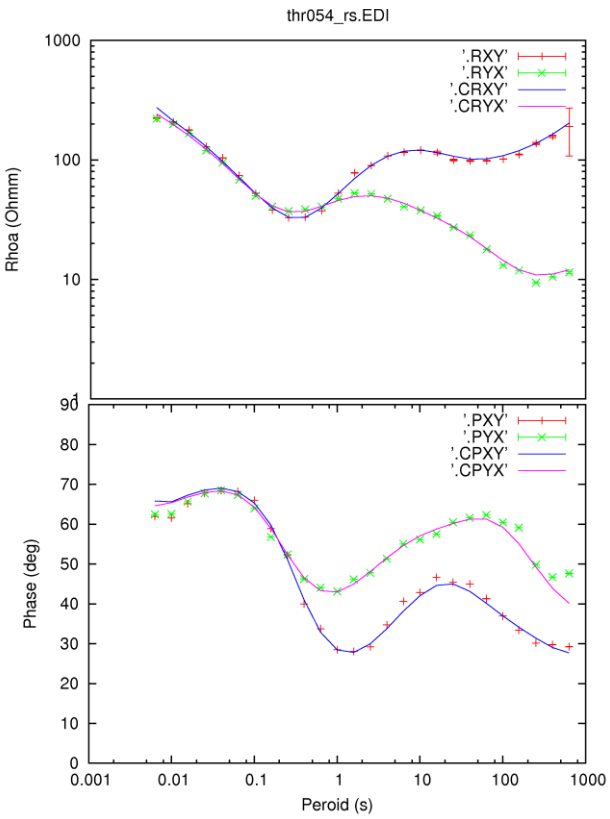
thr054_rs.EDI
Rhoa (Ohmm)
'.RXY'
'.RYX'
'.CRXY'
'.CRYX'
Phase (deg)
'.PXY'
'.PYX'
'.CPXY'
'.CPYX'
Peroid (s)

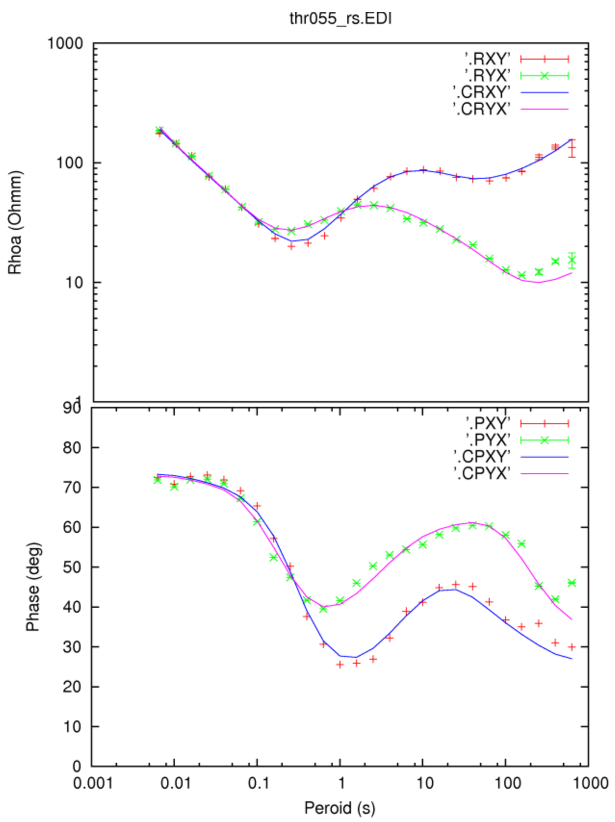
thr055_rs.EDI
Rhoa (Ohmm)
'.RXY'
'.RYX'
'.CRXY'
'.CRYX'
Phase (deg)
'.PXY'
'.PYX'
'.CPXY'
'.CPYX'
Peroid (s)

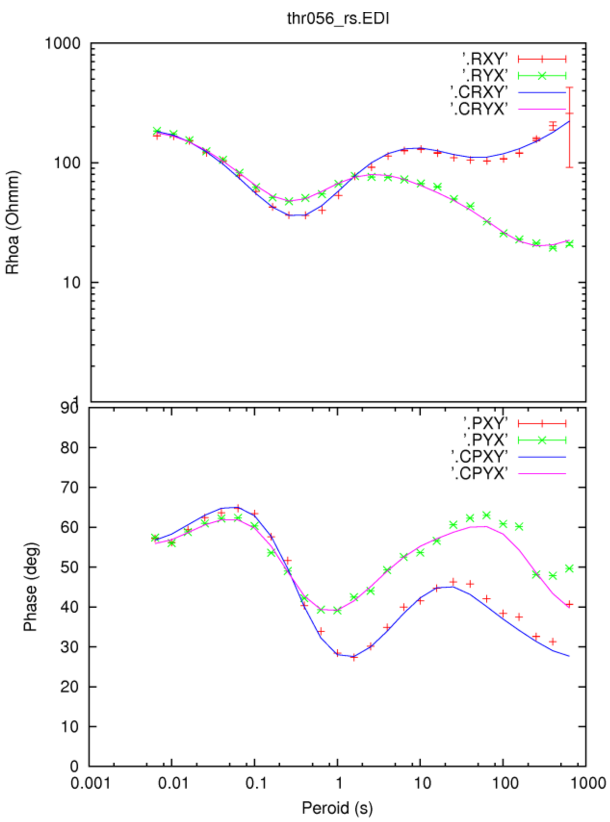
thr056_rs.EDI
Rhoa (Ohmm)
'.RXY'
'.RYX'
'.CRXY'
'.CRYX'
Phase (deg)
'.PXY'
'.PYX'
'.CPXY'
'.CPYX'
Peroid (s)

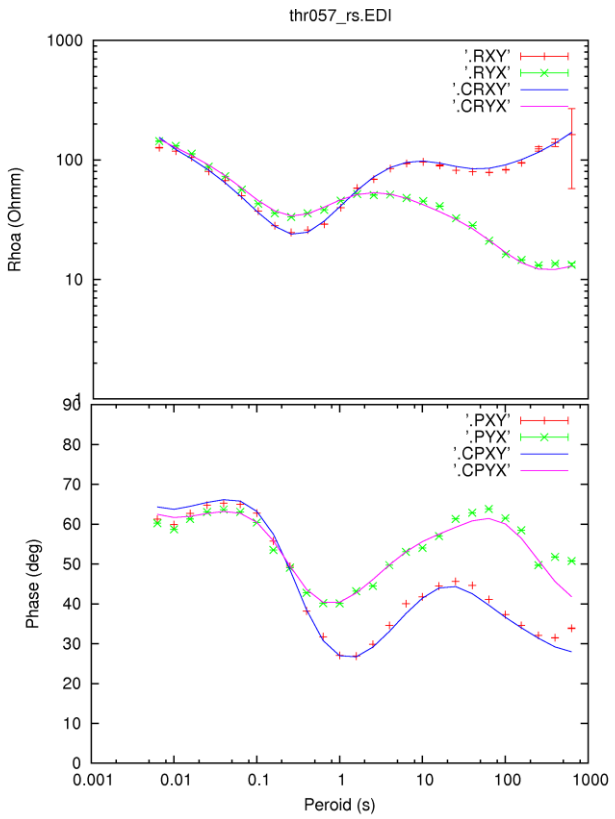
thr057_rs.EDI
Rhoa (Ohmm)
'.RXY'
'.RYX'
'.CRXY'
'.CRYX'
Phase (deg)
'.PXY'
'.PYX'
'.CPXY'
'.CPYX'
Peroid (s)

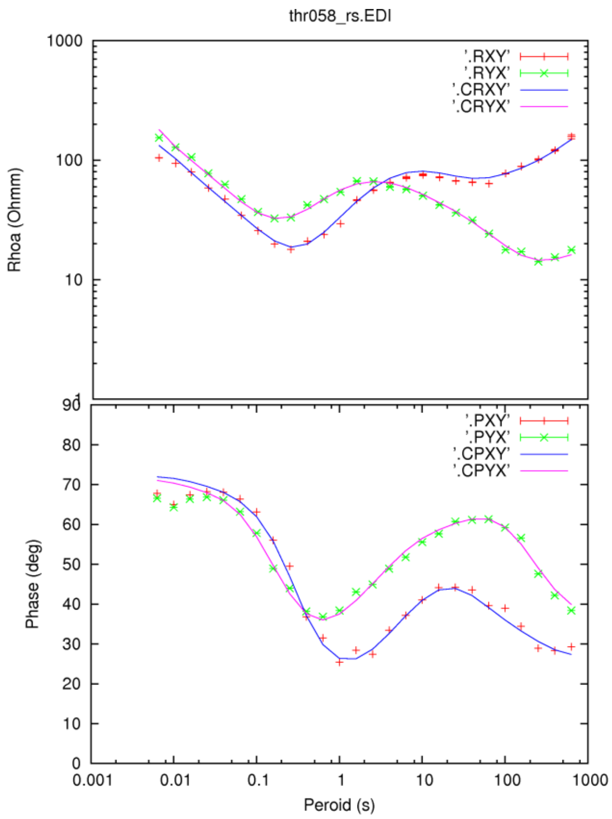
thr058_rs.EDI
Rhoa (Ohmm)
'.RXY'
'.RYX'
'.CRXY'
'.CRYX'
Phase (deg)
'.PXY'
'.PYX'
'.CPXY'
'.CPYX'
Peroid (s)

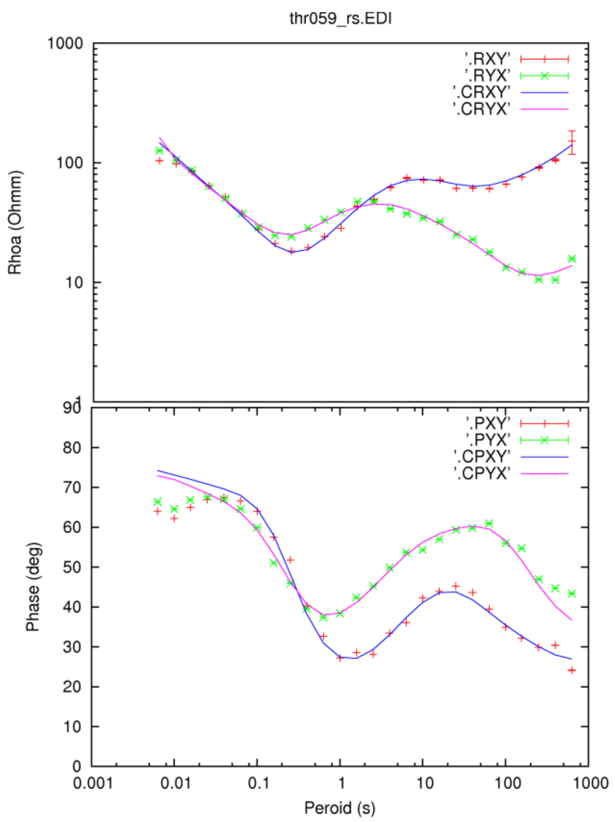
thr059_rs.EDI
Rhoa (Ohmm)
'.RXY'
'.RYX'
'.CRXY'
'.CRYX'
Phase (deg)
'.PXY'
'.PYX'
'.CPXY'
'.CPYX'
Peroid (s)

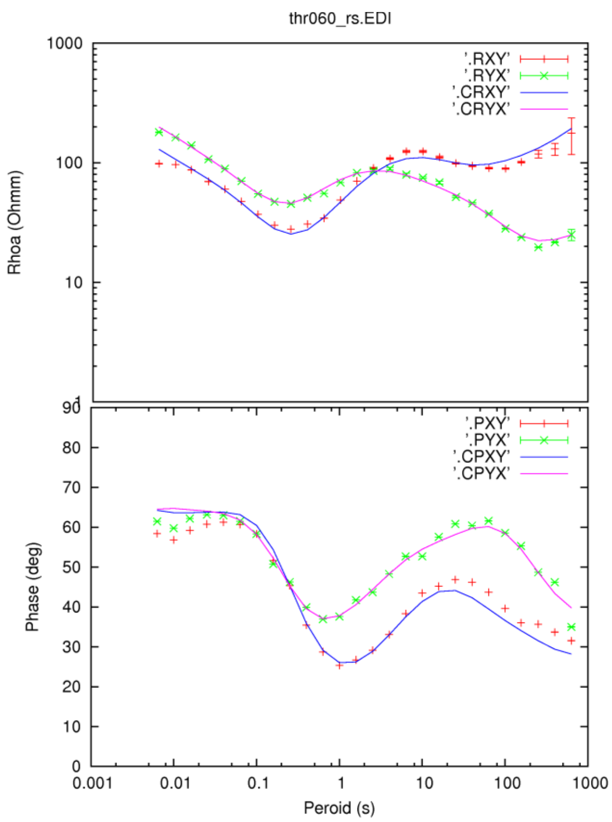
thr060_rs.EDI
Rhoa (Ohmm)
'.RXY'
'.RYX'
'.CRXY'
'.CRYX'
Phase (deg)
'.PXY'
'.PYX'
'.CPXY'
'.CPYX'
Peroid (s)

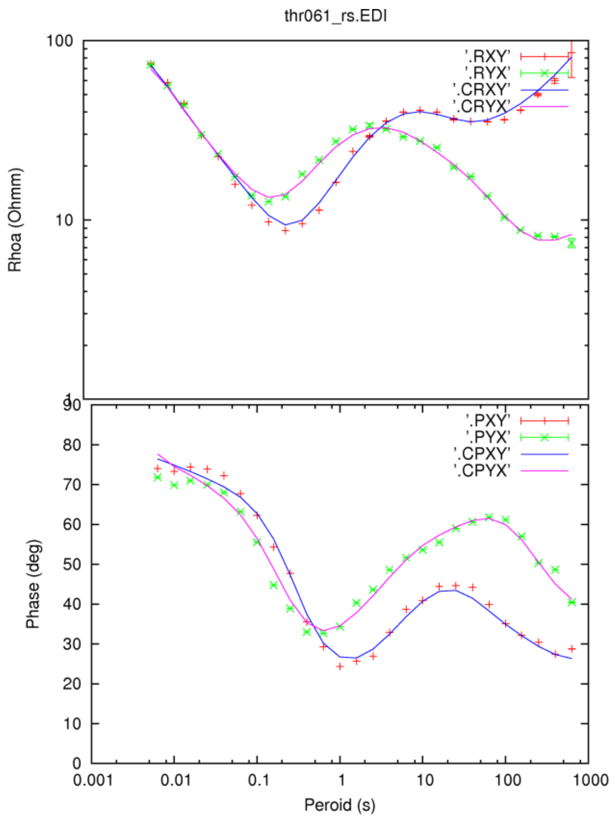
thr061_rs.EDI
Rhoa (Ohmm)
'.RXY'
'.RYX'
'.CRXY'
'.CRYX'
Phase (deg)
'.PXY'
'.PYX'
'.CPXY'
'.CPYX'
Peroid (s)

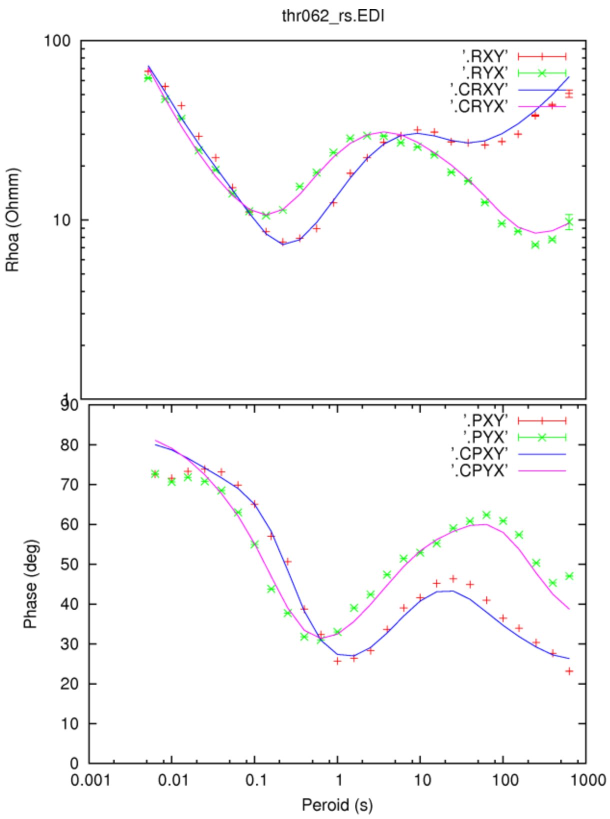
thr062_rs.EDI
Rhoa (Ohmm)
'.RXY'
'.RYX'
'.CRXY'
'.CRYX'
Phase (deg)
'.PXY'
'.PYX'
'.CPXY'
'.CPYX'
Peroid (s)

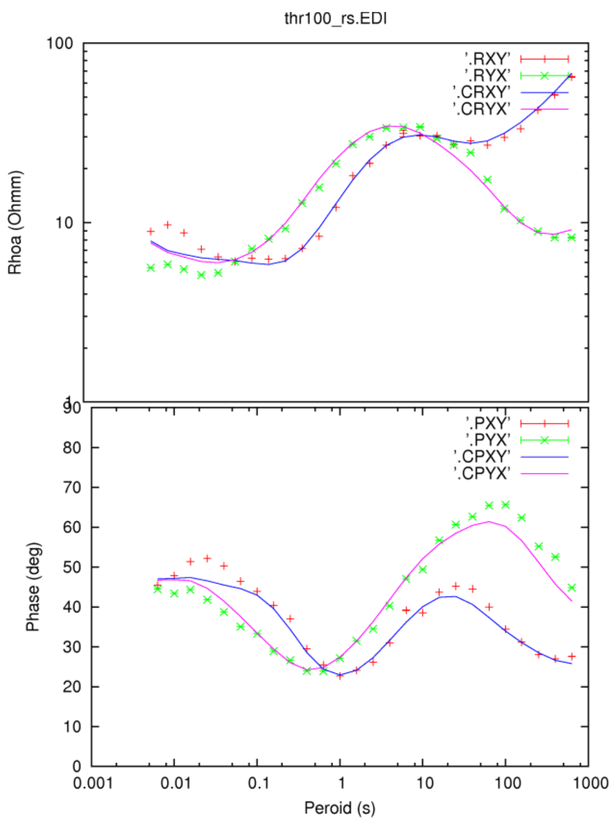
thr100_rs.EDI
Rhoa (Ohmm)
'.RXY'
'.RYX'
'.CRXY'
'.CRYX'
Phase (deg)
'.PXY'
'.PYX'
'.CPXY'
'.CPYX'
Peroid (s)

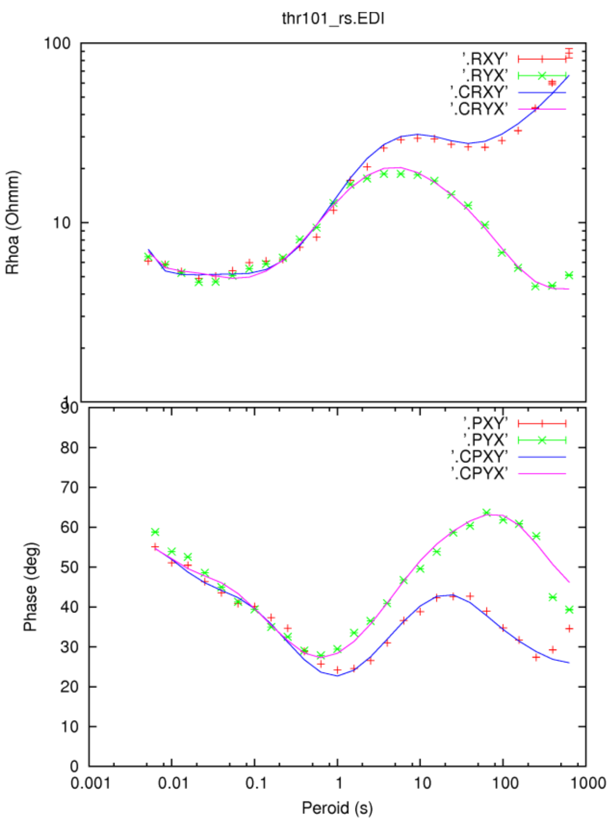
thr101_rs.EDI
Rhoa (Ohmm)
'.RXY'
'.RYX'
'.CRXY'
'.CRYX'
Phase (deg)
'.PXY'
'.PYX'
'.CPXY'
'.CPYX'
Peroid (s)

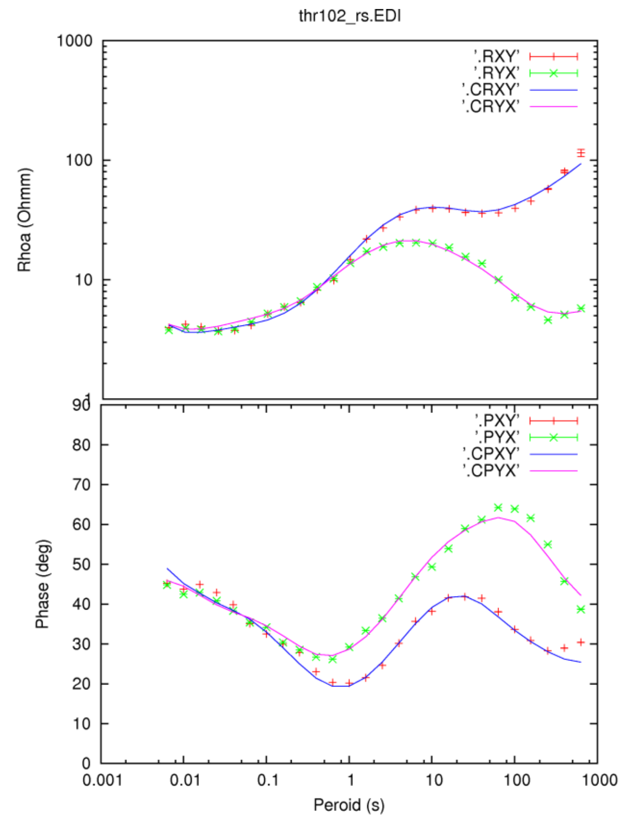
thr102_rs.EDI
'.RXY'
'.RYX'
'.CRXY'
'.CRYX'
Rhoa (Ohmm)
'.PXY'
'.PYX'
'.CPXY'
'.CPYX'
Phase (deg)
Peroid (s)

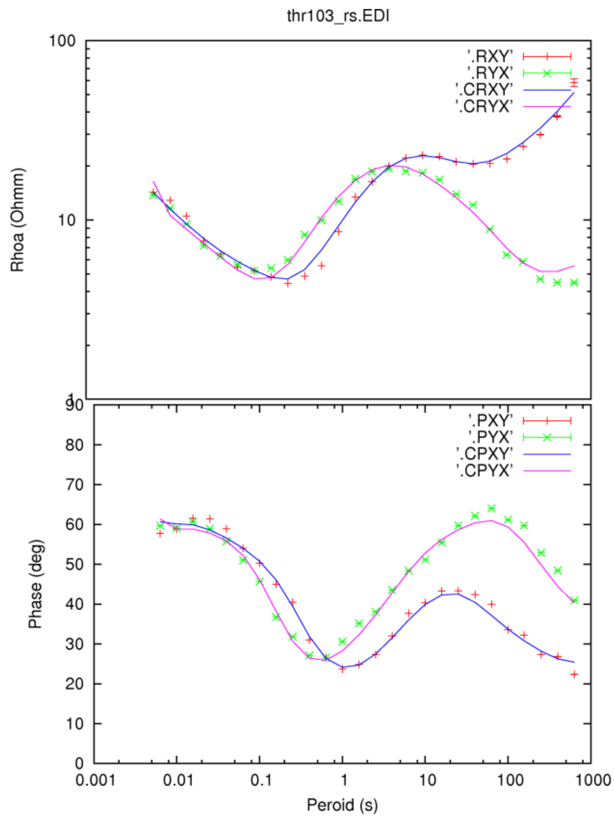
thr103_rs.EDI
'.RXY'
'.RYX'
'.CRXY'
'.CRYX'
Rhoa (Ohmm)
'.PXY'
'.PYX'
'.CPXY'
'.CPYX'
Phase (deg)
Peroid (s)

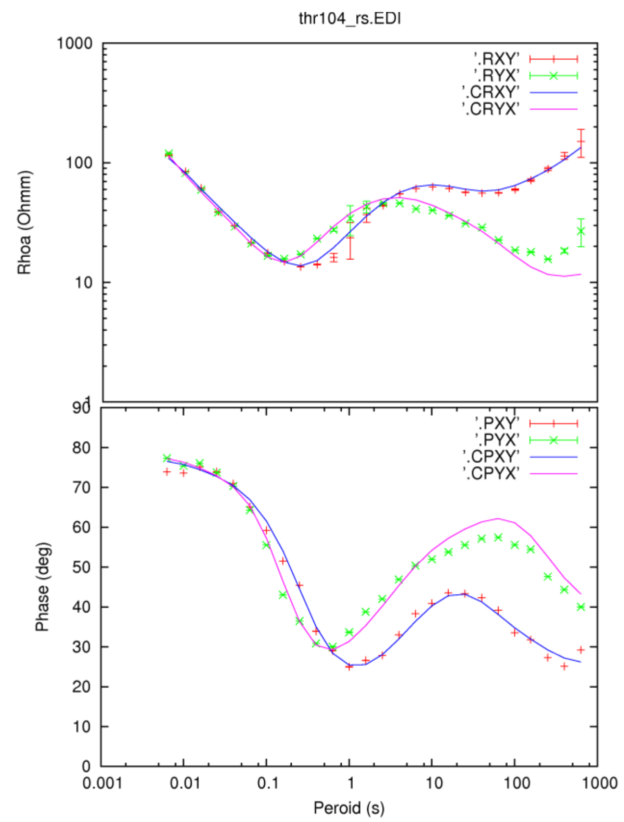
thr104_rs.EDI
'.RXY'
'.RYX'
'.CRXY'
'.CRYX'
Rhoa (Ohmm)
'.PXY'
'.PYX'
'.CPXY'
'.CPYX'
Phase (deg)
Peroid (s)

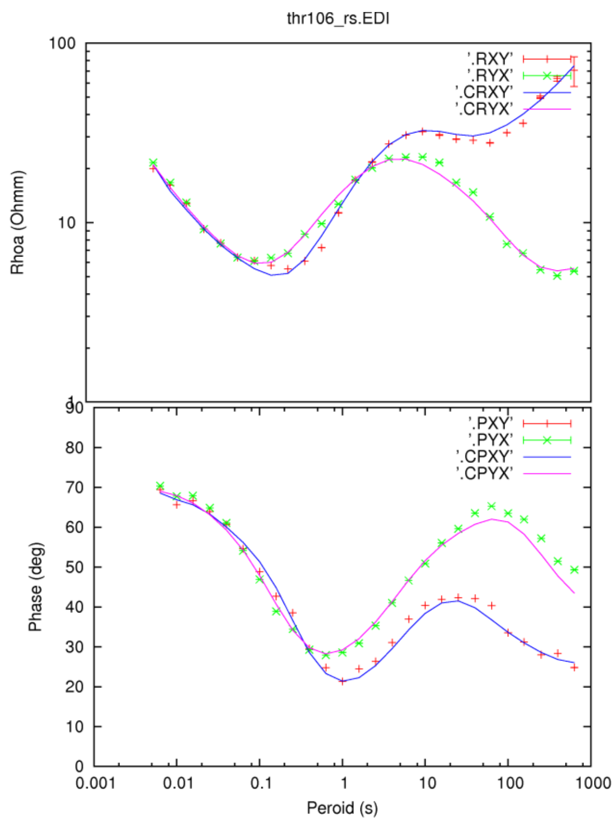
thr106_rs.EDI
'.RXY'
'.RYX'
'.CRXY'
'.CRYX'
Rhoa (Ohmm)
'.PXY'
'.PYX'
'.CPXY'
'.CPYX'
Phase (deg)
Peroid (s)

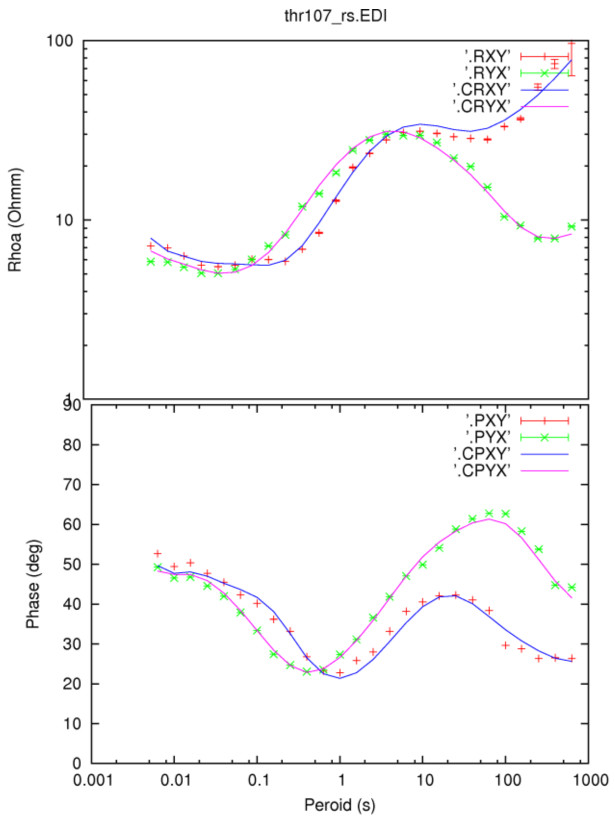
thr107_rs.EDI
'.RXY'
'.RYX'
'.CRXY'
'.CRYX'
Rhoa (Ohmm)
'.PXY'
'.PYX'
'.CPXY'
'.CPYX'
Phase (deg)
Peroid (s)

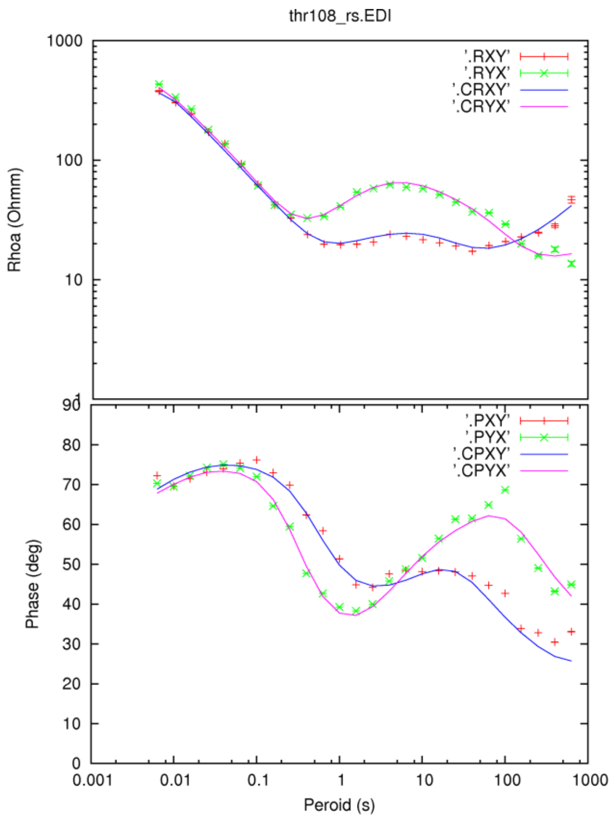
thr108_rs.EDI
'.RXY'
'.RYX'
'.CRXY'
'.CRYX'
Rhoa (Ohmm)
'.PXY'
'.PYX'
'.CPXY'
'.CPYX'
Phase (deg)
Peroid (s)

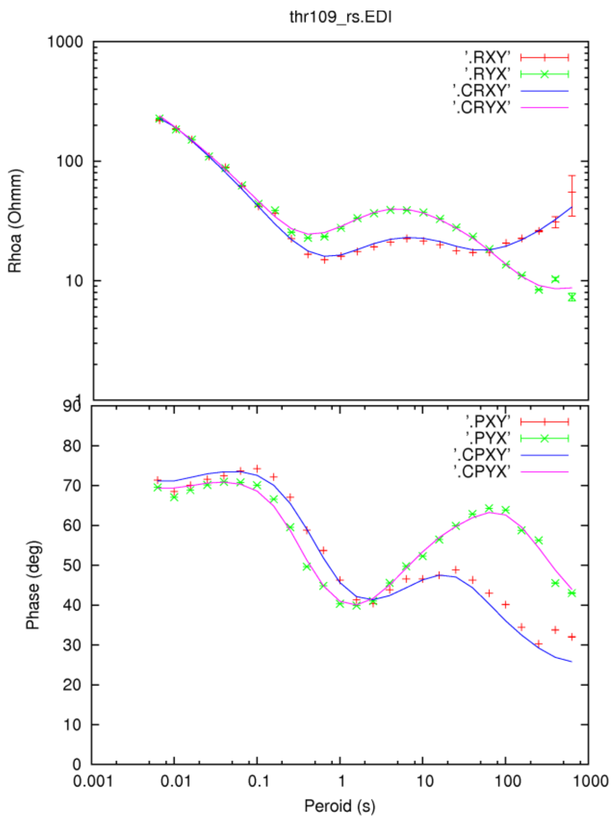
thr109_rs.EDI
'.RXY'
'.RYX'
'.CRXY'
'.CRYX'
Rhoa (Ohmm)
'.PXY'
'.PYX'
'.CPXY'
'.CPYX'
Phase (deg)
Peroid (s)

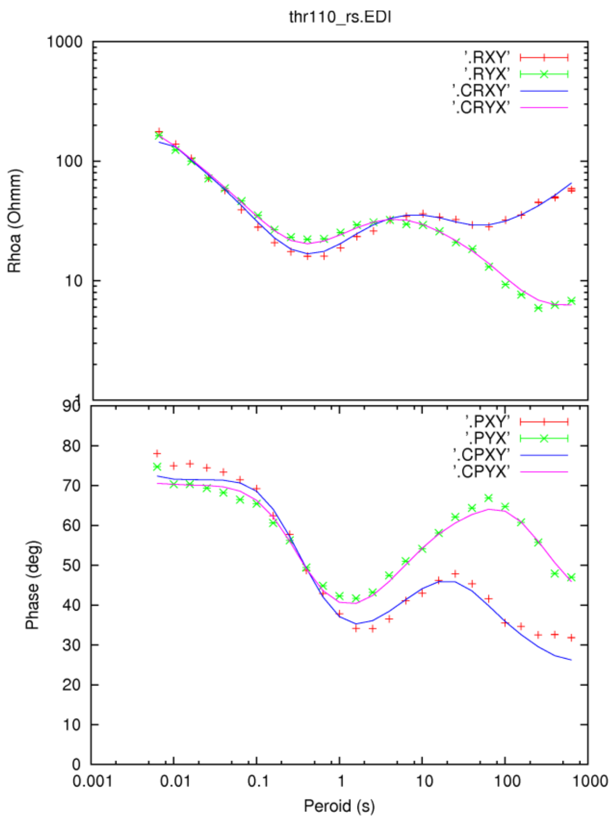
thr110_rs.EDI
'.RXY'
'.RYX'
'.CRXY'
'.CRYX'
Rhoa (Ohmm)
'.PXY'
'.PYX'
'.CPXY'
'.CPYX'
Phase (deg)
Peroid (s)

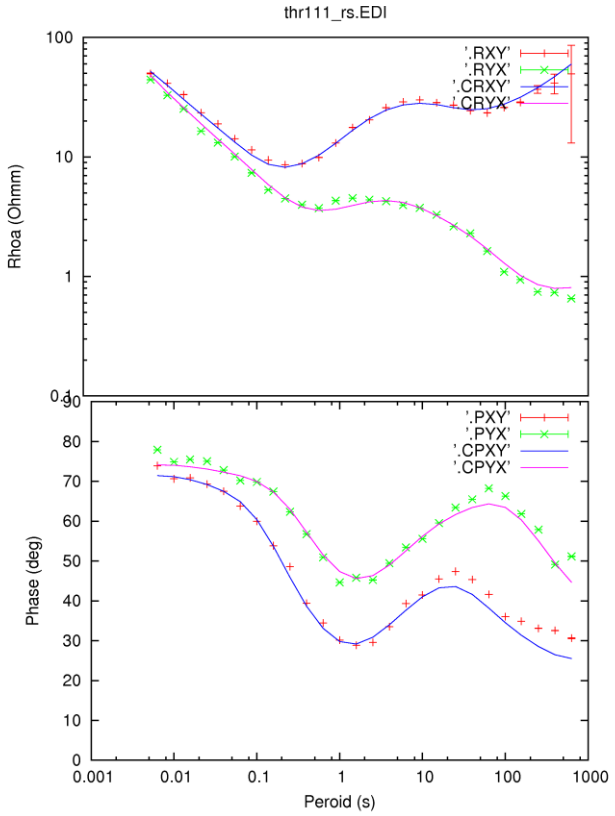
thr111_rs.EDI
'.RXY'
'.RYX'
'.CRXY'
'.CRYX'
Rhoa (Ohmm)
'.PXY'
'.PYX'
'.CPXY'
'.CPYX'
Phase (deg)
Peroid (s)

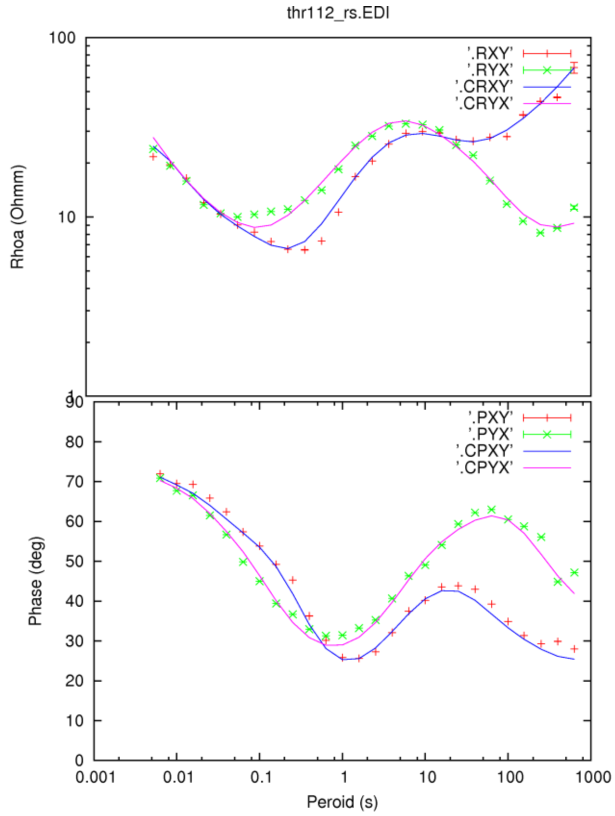
thr112_rs.EDI
'.RXY'
'.RYX'
'.CRXY'
'.CRYX'
Rhoa (Ohmm)
'.PXY'
'.PYX'
'.CPXY'
'.CPYX'
Phase (deg)
Peroid (s)

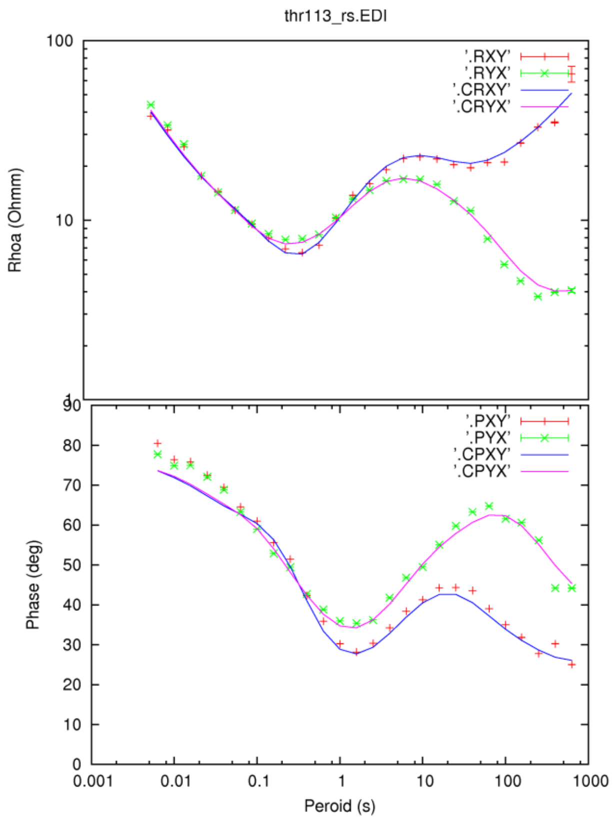
thr113_rs.EDI
'.RXY'
'.RYX'
'.CRXY'
'.CRYX'
Rhoa (Ohmm)
'.PXY'
'.PYX'
'.CPXY'
'.CPYX'
Phase (deg)
Peroid (s)

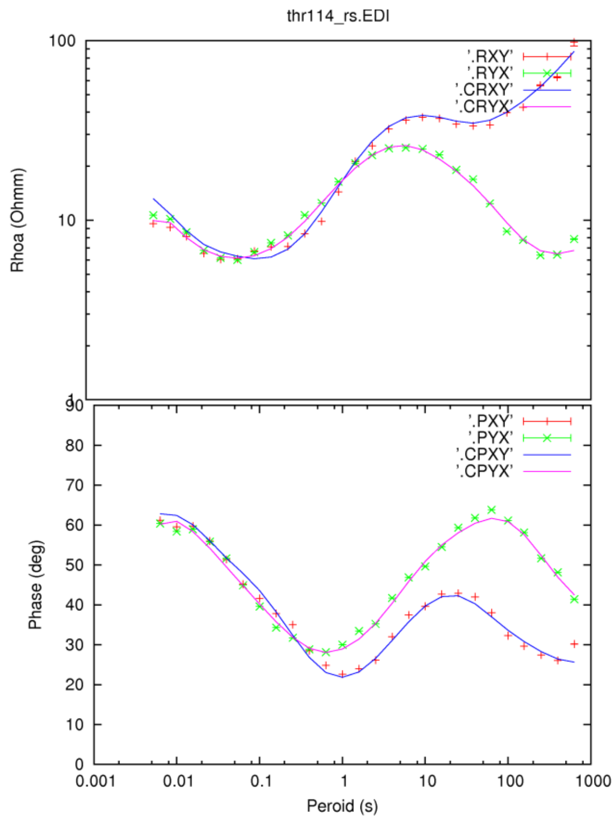
thr114_rs.EDI
'.RXY'
'.RYX'
'.CRXY'
'.CRYX'
Rhoa (Ohmm)
'.PXY'
'.PYX'
'.CPXY'
'.CPYX'
Phase (deg)
Peroid (s)

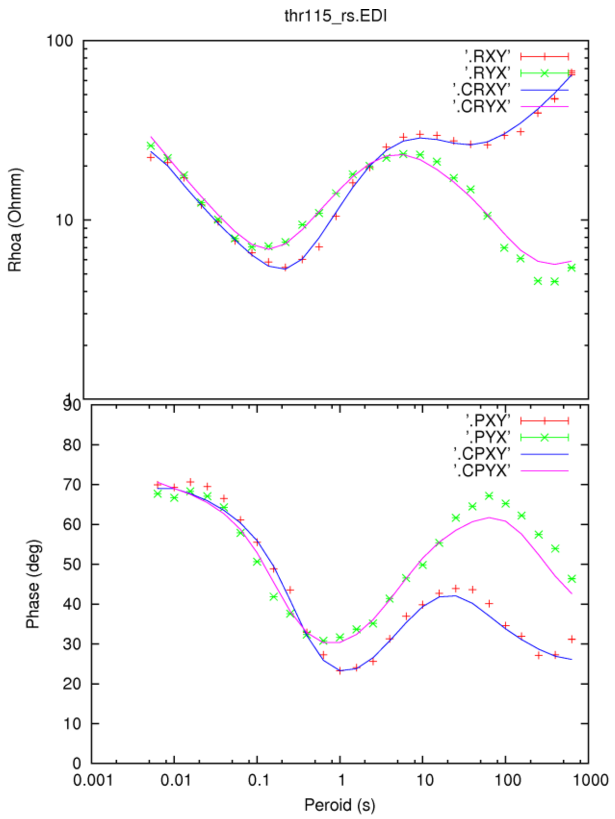
thr115_rs.EDI
Rhoa (Ohmm)
Phase (deg)
'.RXY'
'.RYX'
'.CRXY'
'.CRYX'
'.PXY'
'.PYX'
'.CPXY'
'.CPYX'
Peroid (s)

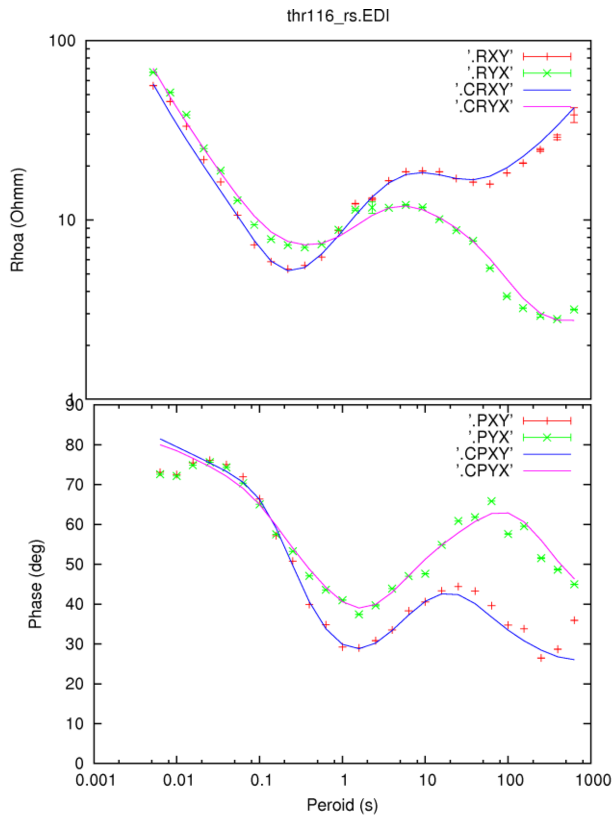
thr116_rs.EDI
Rhoa (Ohmm)
Phase (deg)
'.RXY'
'.RYX'
'.CRXY'
'.CRYX'
'.PXY'
'.PYX'
'.CPXY'
'.CPYX'
Peroid (s)

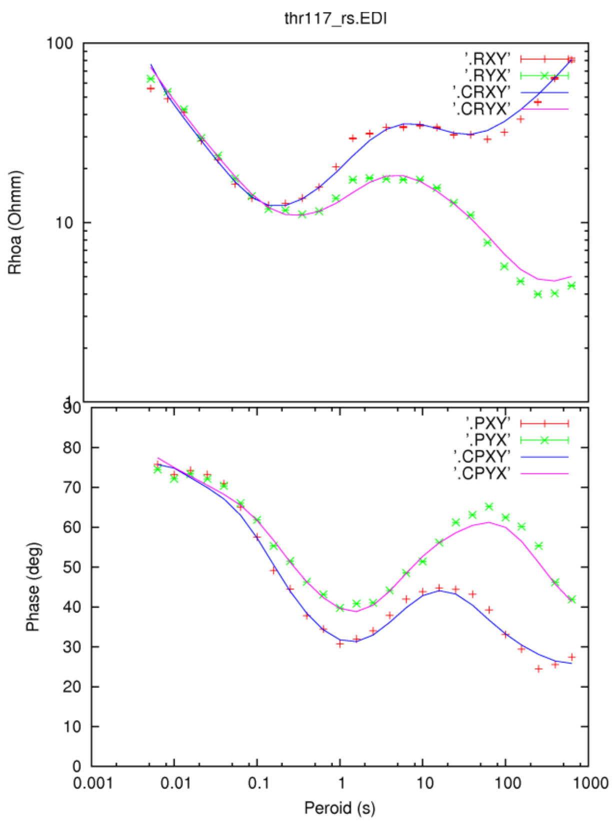
thr117_rs.EDI
Rhoa (Ohmm)
Phase (deg)
'.RXY'
'.RYX'
'.CRXY'
'.CRYX'
'.PXY'
'.PYX'
'.CPXY'
'.CPYX'
Peroid (s)

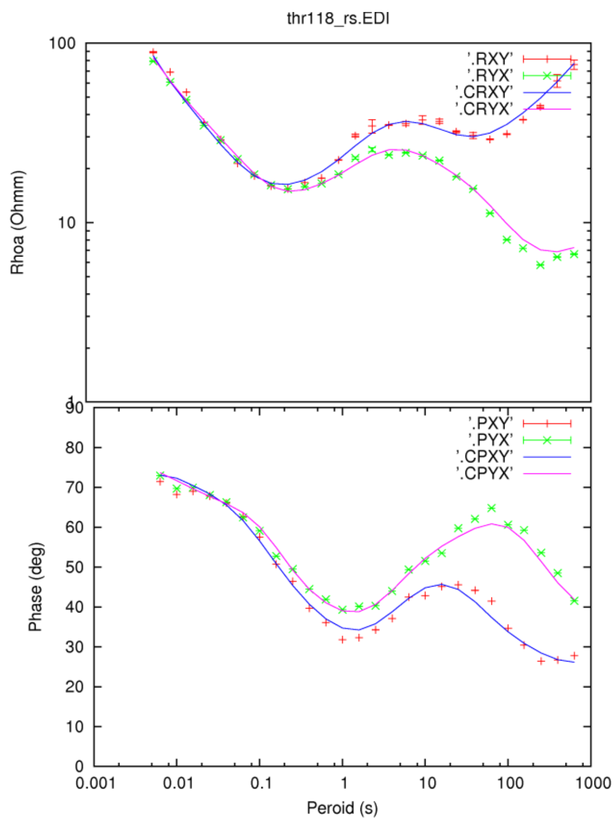
thr118_rs.EDI
Rhoa (Ohmm)
Phase (deg)
'.RXY'
'.RYX'
'.CRXY'
'.CRYX'
'.PXY'
'.PYX'
'.CPXY'
'.CPYX'
Peroid (s)

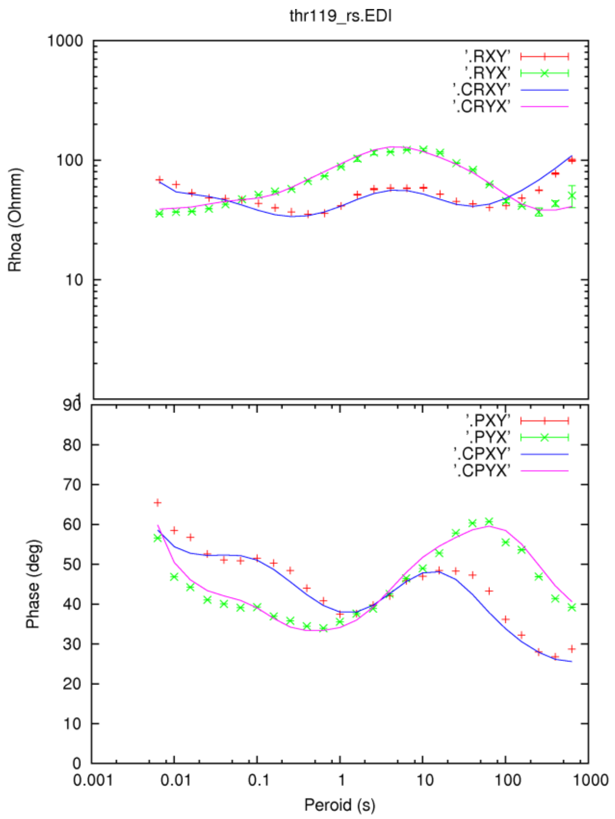
thr119_rs.EDI
'.RXY'
'.RYX'
'.CRXY'
'.CRYX'
Rhoa (Ohmm)
1000
100
10
1
'.PXY'
'.PYX'
'.CPXY'
'.CPYX'
Phase (deg)
90
80
70
60
50
40
30
20
10
0
0.001
0.01
0.1
1
10
100
1000
Peroid (s)

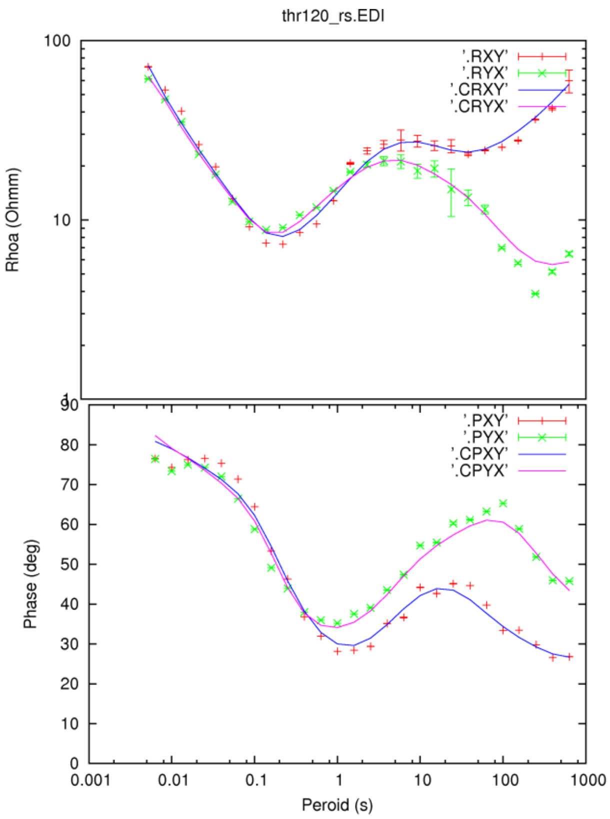
thr120_rs.EDI
'.RXY'
'.RYX'
'.CRXY'
'.CRYX'
Rhoa (Ohmm)
100
10
1
'.PXY'
'.PYX'
'.CPXY'
'.CPYX'
Phase (deg)
90
80
70
60
50
40
30
20
10
0
0.001
0.01
0.1
1
10
100
1000
Peroid (s)

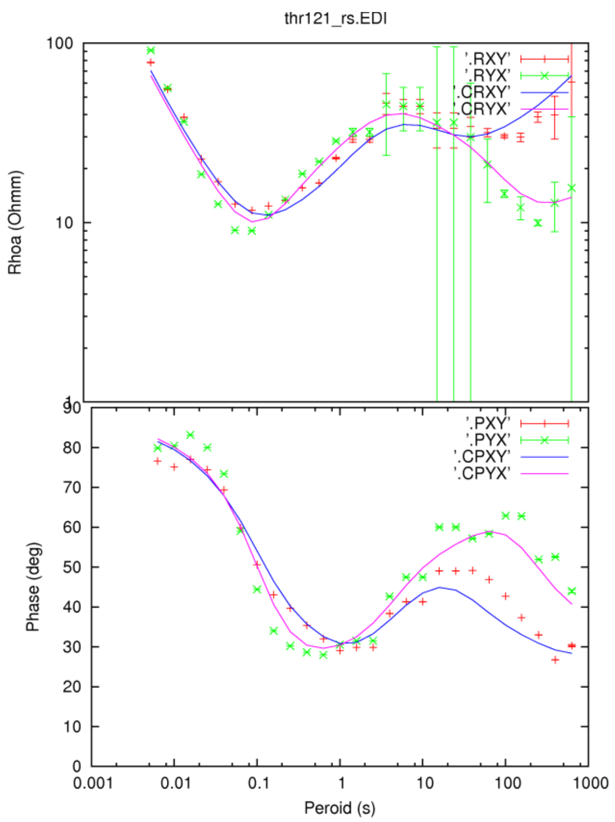
thr121_rs.EDI
'.RXY'
'.RYX'
'.CRXY'
'.CRYX'
Rhoa (Ohmm)
100
10
1
'.PXY'
'.PYX'
'.CPXY'
'.CPYX'
Phase (deg)
90
80
70
60
50
40
30
20
10
0
0.001
0.01
0.1
1
10
100
1000
Peroid (s)

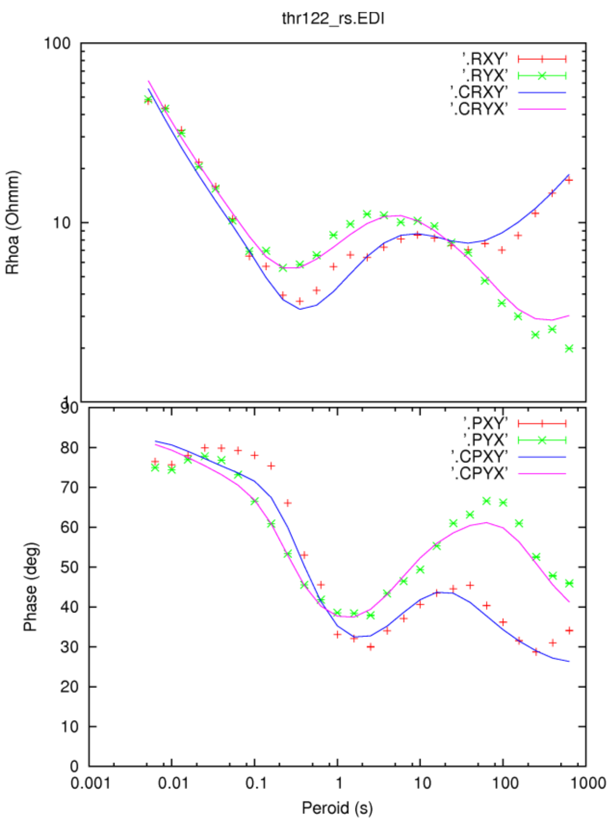
thr122_rs.EDI
'.RXY'
'.RYX'
'.CRXY'
'.CRYX'
Rhoa (Ohmm)
100
10
1
'.PXY'
'.PYX'
'.CPXY'
'.CPYX'
Phase (deg)
90
80
70
60
50
40
30
20
10
0
0.001
0.01
0.1
1
10
100
1000
Peroid (s)

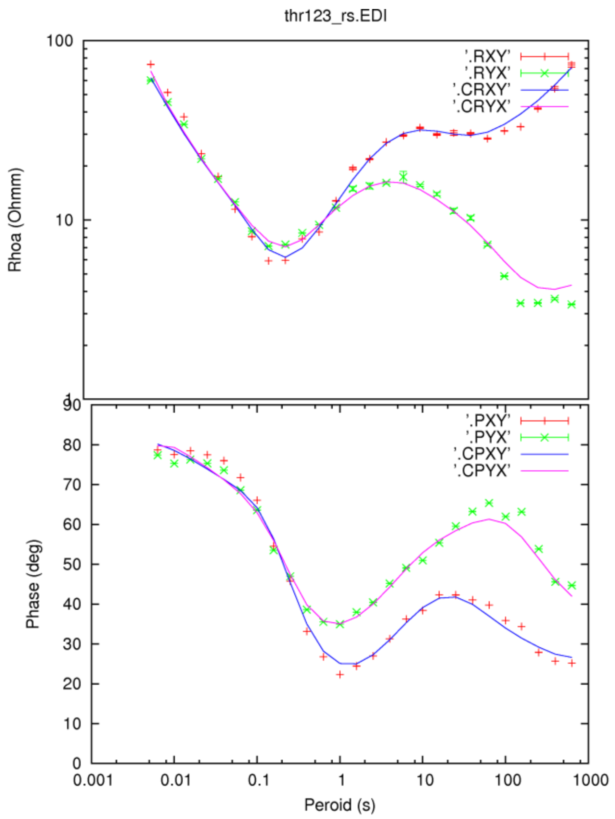
thr123_rs.EDI
'.RXY'
'.RYX'
'.CRXY'
'.CRYX'
Rhoa (Ohmm)
'.PXY'
'.PYX'
'.CPXY'
'.CPYX'
Phase (deg)
Peroid (s)

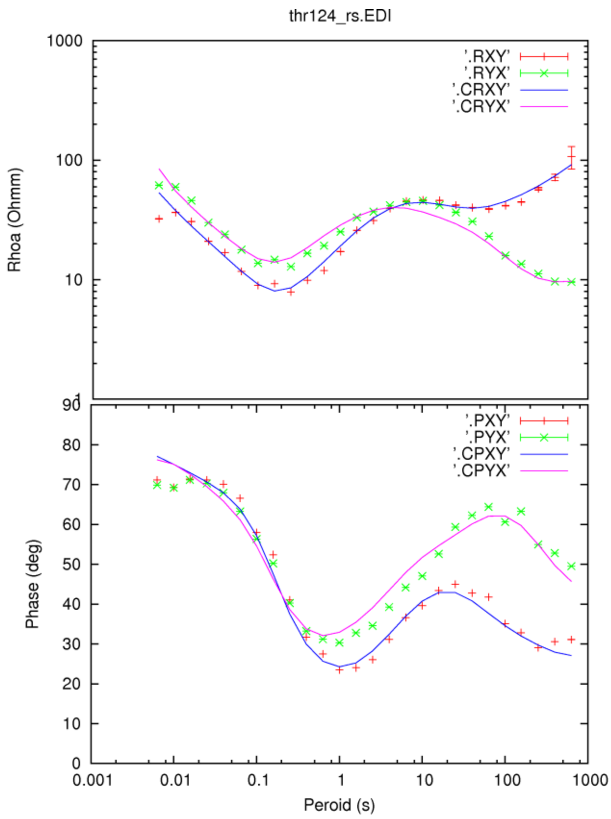
thr124_rs.EDI
'.RXY'
'.RYX'
'.CRXY'
'.CRYX'
Rhoa (Ohmm)
'.PXY'
'.PYX'
'.CPXY'
'.CPYX'
Phase (deg)
Peroid (s)

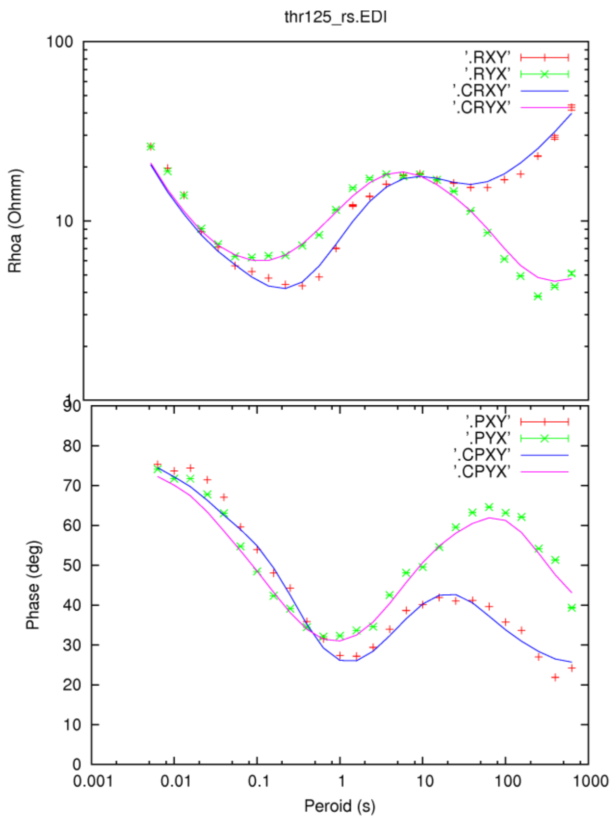
thr125_rs.EDI
'.RXY'
'.RYX'
'.CRXY'
'.CRYX'
Rhoa (Ohmm)
'.PXY'
'.PYX'
'.CPXY'
'.CPYX'
Phase (deg)
Peroid (s)

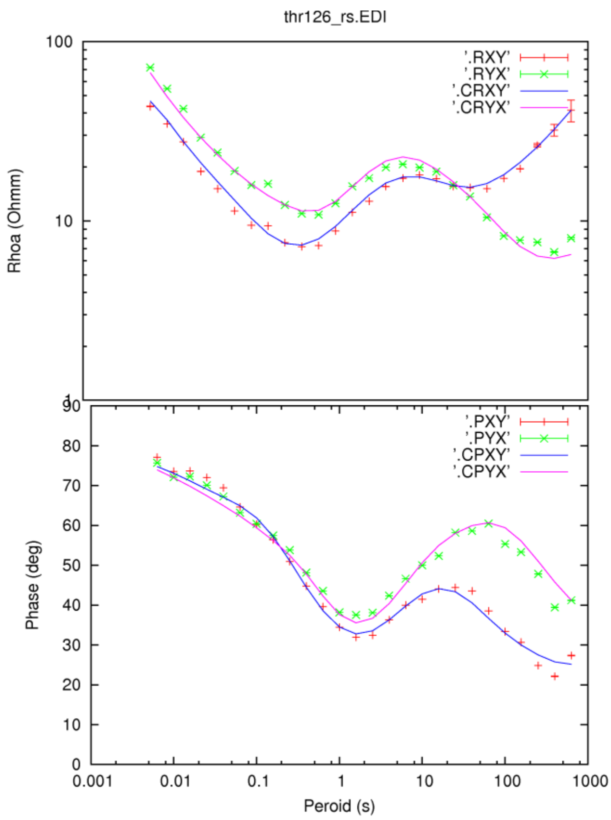
thr126_rs.EDI
'.RXY'
'.RYX'
'.CRXY'
'.CRYX'
Rhoa (Ohmm)
'.PXY'
'.PYX'
'.CPXY'
'.CPYX'
Phase (deg)
Peroid (s)

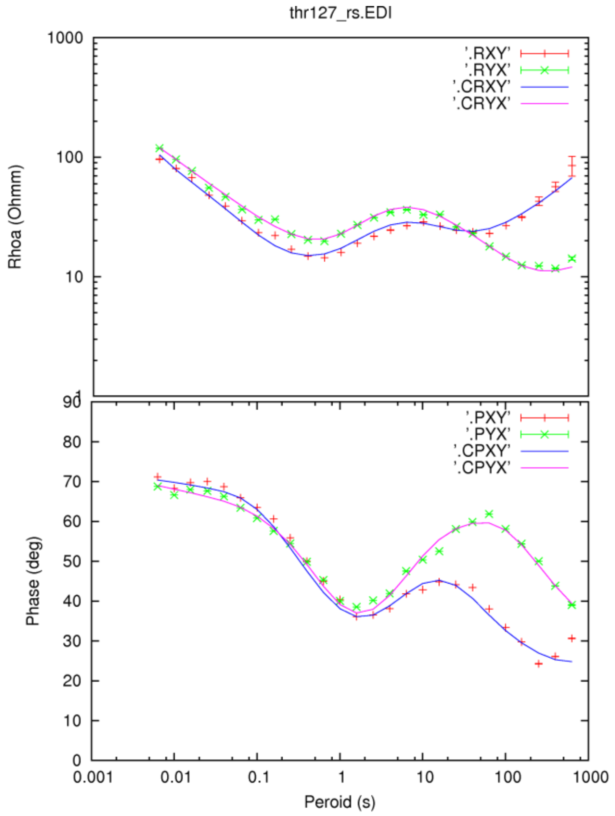
thr127_rs.EDI
Rhoa (Ohmm)
Phase (deg)
Peroid (s)
'.RXY'
'.RYX'
'.CRXY'
'.CRYX'
'.PXY'
'.PYX'
'.CPXY'
'.CPYX'

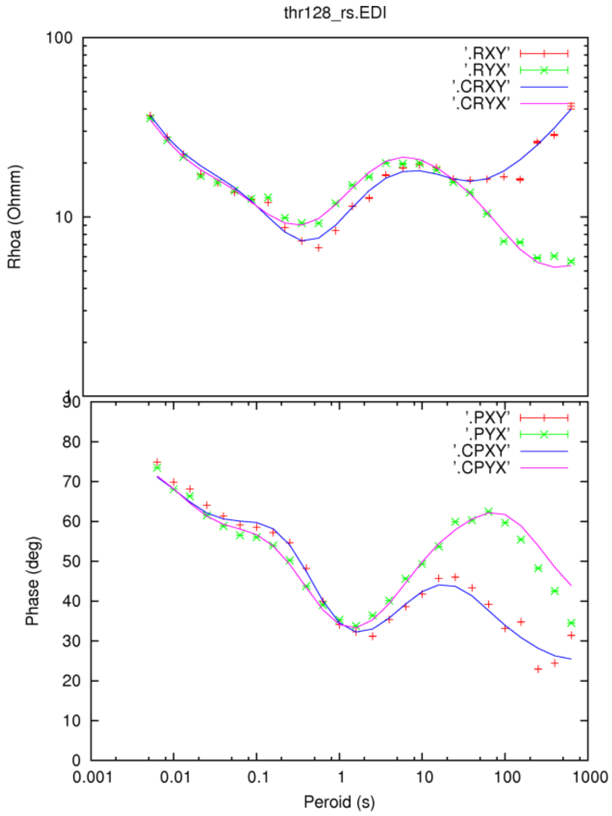
thr128_rs.EDI
Rhoa (Ohmm)
Phase (deg)
Peroid (s)
'.RXY'
'.RYX'
'.CRXY'
'.CRYX'
'.PXY'
'.PYX'
'.CPXY'
'.CPYX'

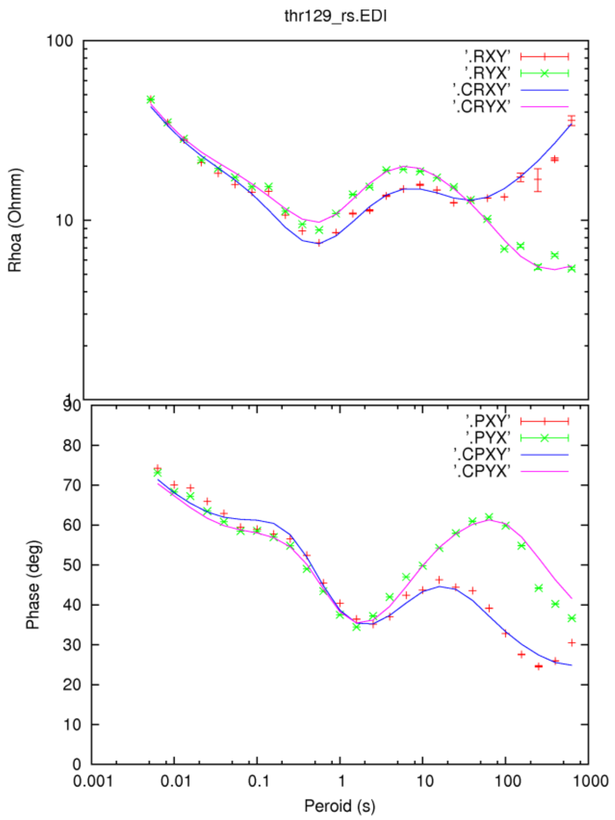
thr129_rs.EDI
Rhoa (Ohmm)
Phase (deg)
Peroid (s)
'.RXY'
'.RYX'
'.CRXY'
'.CRYX'
'.PXY'
'.PYX'
'.CPXY'
'.CPYX'

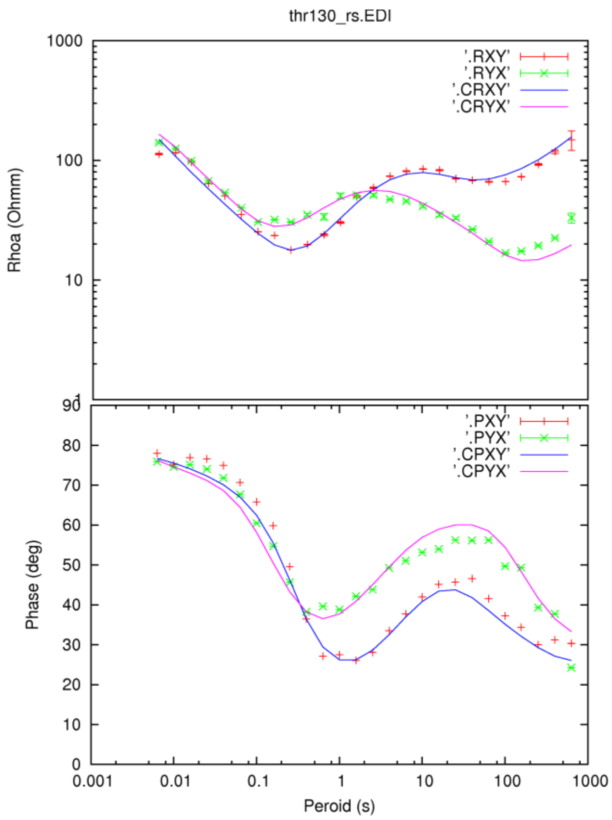
thr130_rs.EDI
Rhoa (Ohmm)
Phase (deg)
Peroid (s)
'.RXY'
'.RYX'
'.CRXY'
'.CRYX'
'.PXY'
'.PYX'
'.CPXY'
'.CPYX'

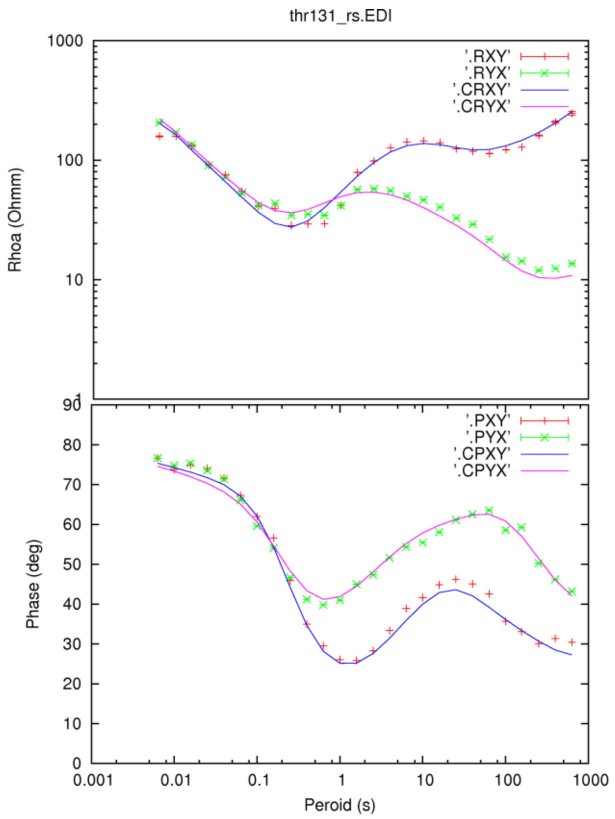
thr131_rs.EDI
'.RXY'
'.RYX'
'.CRXY'
'.CRYX'
Rhoa (Ohmm)
'.PXY'
'.PYX'
'.CPXY'
'.CPYX'
Phase (deg)
Peroid (s)

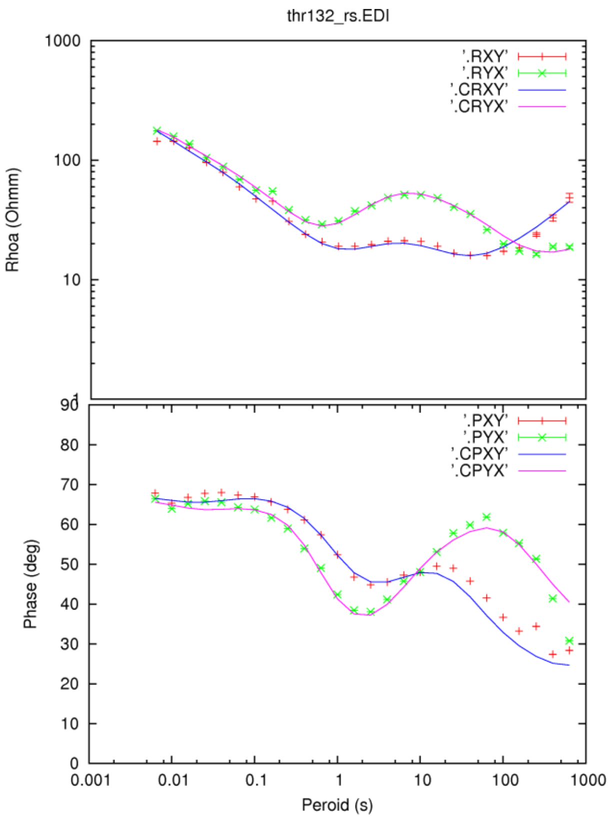
thr132_rs.EDI
'.RXY'
'.RYX'
'.CRXY'
'.CRYX'
Rhoa (Ohmm)
'.PXY'
'.PYX'
'.CPXY'
'.CPYX'
Phase (deg)
Peroid (s)

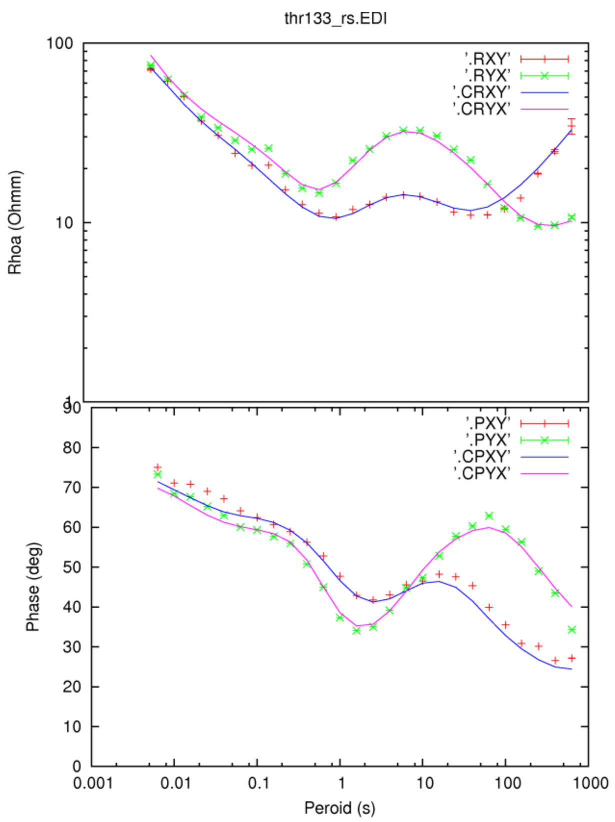
thr133_rs.EDI
'.RXY'
'.RYX'
'.CRXY'
'.CRYX'
Rhoa (Ohmm)
'.PXY'
'.PYX'
'.CPXY'
'.CPYX'
Phase (deg)
Peroid (s)

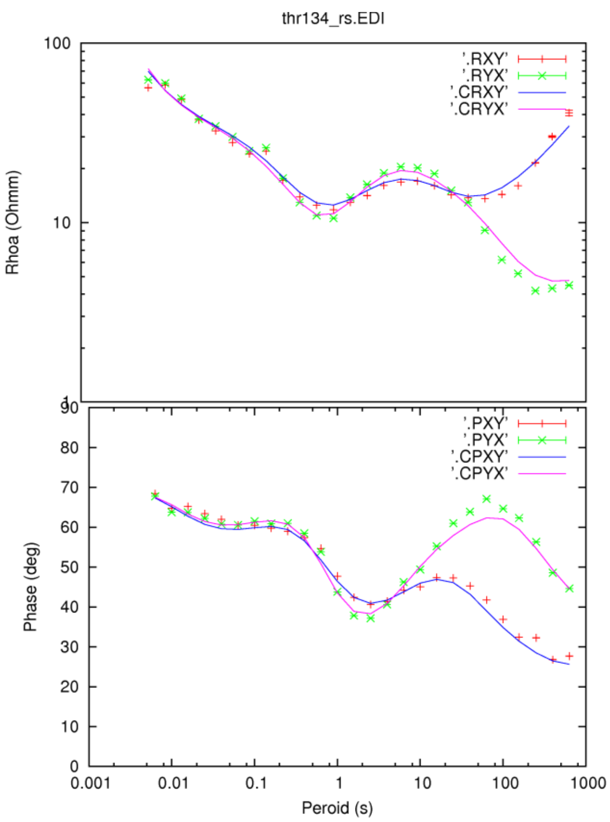
thr134_rs.EDI
'.RXY'
'.RYX'
'.CRXY'
'.CRYX'
Rhoa (Ohmm)
'.PXY'
'.PYX'
'.CPXY'
'.CPYX'
Phase (deg)
Peroid (s)

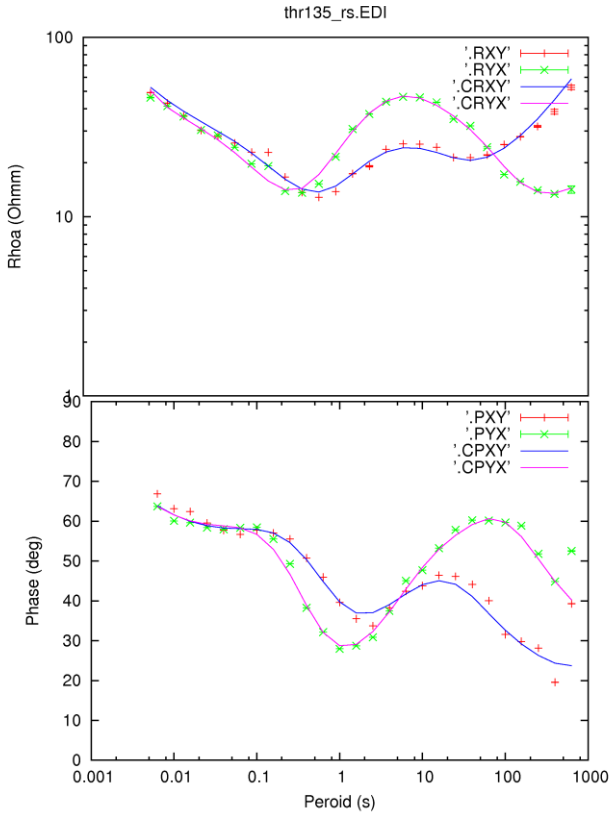
thr135_rs.EDI
Rhoa (Ohmm)
'.RXY'
'.RYX'
'.CRXY'
'.CRYX'
Phase (deg)
'.PXY'
'.PYX'
'.CPXY'
'.CPYX'
Peroid (s)

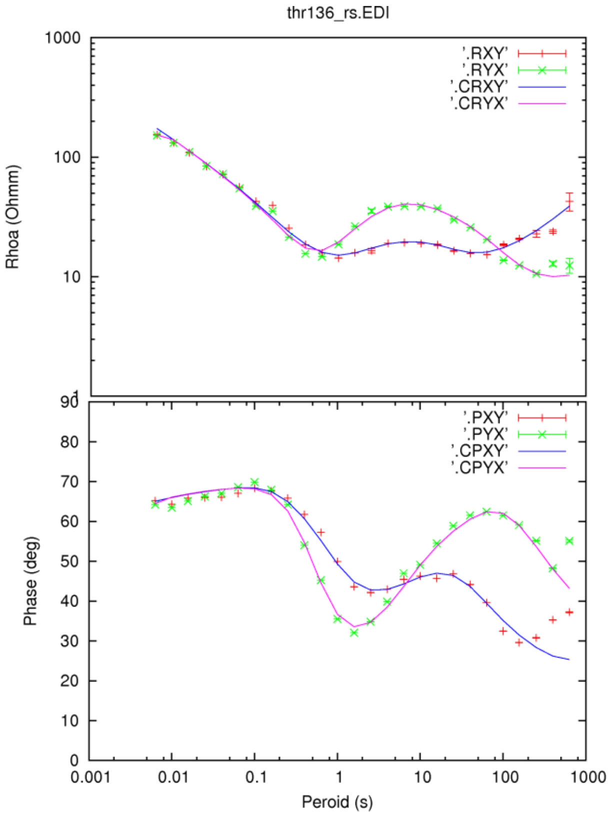
thr136_rs.EDI
Rhoa (Ohmm)
'.RXY'
'.RYX'
'.CRXY'
'.CRYX'
Phase (deg)
'.PXY'
'.PYX'
'.CPXY'
'.CPYX'
Peroid (s)

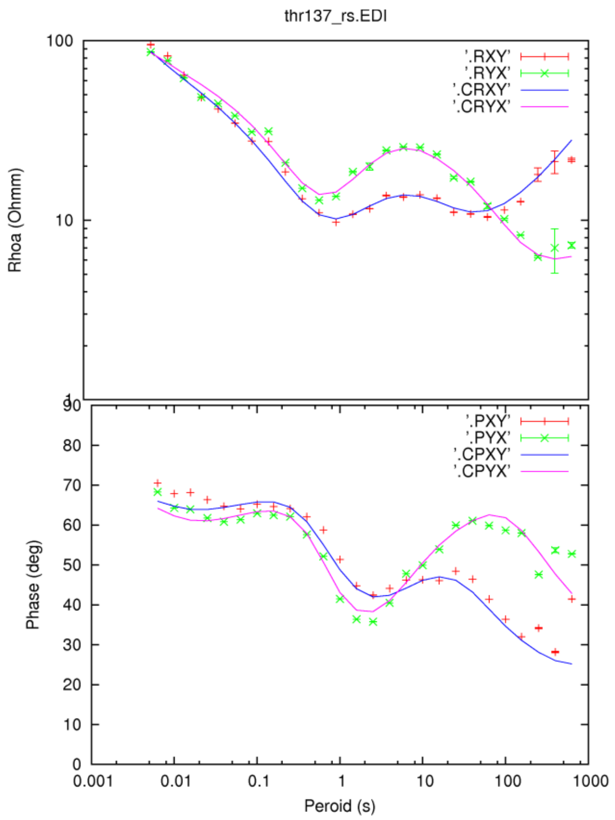
thr137_rs.EDI
Rhoa (Ohmm)
'.RXY'
'.RYX'
'.CRXY'
'.CRYX'
Phase (deg)
'.PXY'
'.PYX'
'.CPXY'
'.CPYX'
Peroid (s)

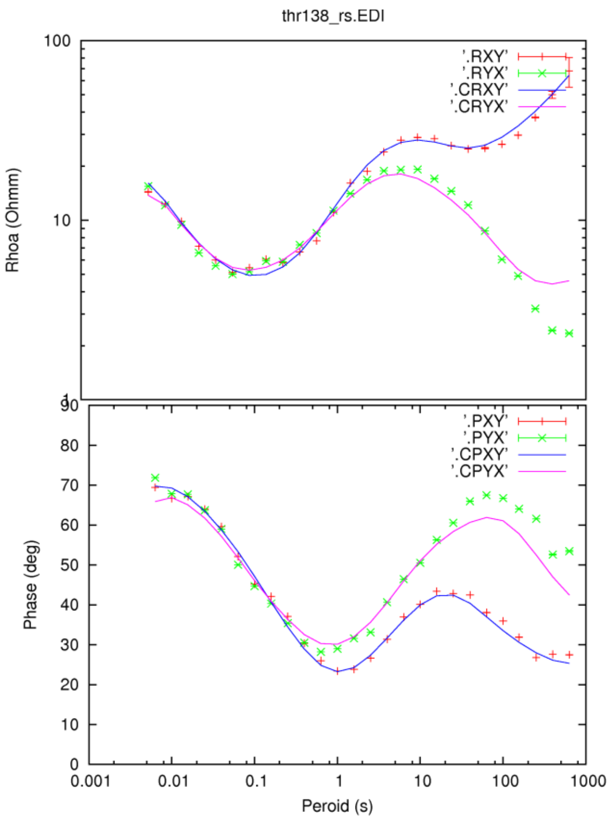
thr138_rs.EDI
Rhoa (Ohmm)
'.RXY'
'.RYX'
'.CRXY'
'.CRYX'
Phase (deg)
'.PXY'
'.PYX'
'.CPXY'
'.CPYX'
Peroid (s)

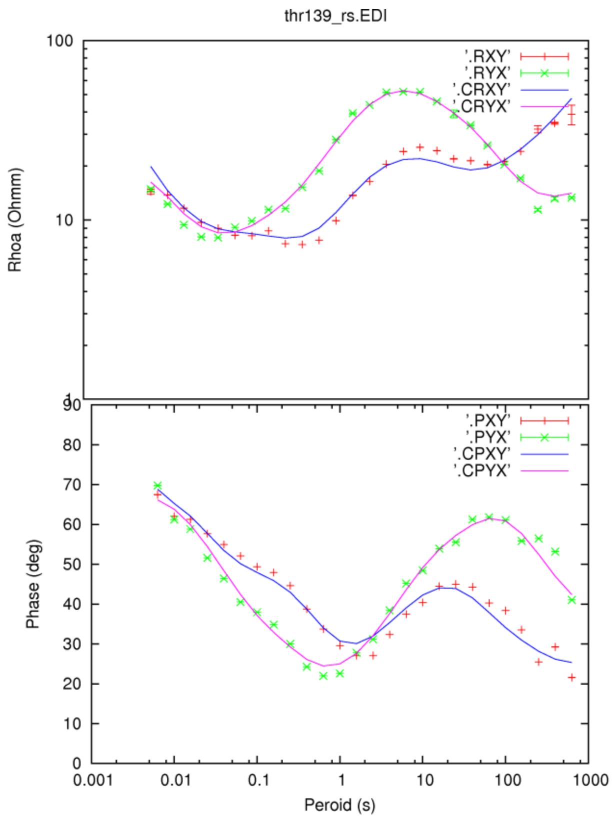

thr139_rs.EDI
100
10
1
Rhoa (Ohmm)
'.RXY'
'.RYX'
'.CRXY'
'.CRYX'
90
80
70
60
50
40
30
20
10
0
Phase (deg)
'.PXY'
'.PYX'
'.CPXY'
'.CPYX'
0.001
0.01
0.1
1
10
100
1000
Peroid (s)